Development of Robust Multiphase Equilibrium Calculation Algorithms for Complex Reservoir Fluids Containing Asphaltene

by

Zhuo Chen

A thesis submitted in partial fulfillment of the requirements for the degree of

Doctor of Philosophy

in

Petroleum Engineering

Department of Civil and Environmental Engineering
University of Alberta

ABSTRACT

Multiphase equilibria, including three-phase vapor-liquid-asphaltene (VLS) equilibria and four-phase vapor-liquid-aqueous-asphaltene (VLAS) equilibria, can appear during enhanced oil recovery (EOR) processes. Robust multiphase equilibrium calculation algorithms are important techniques in reservoir simulations to better simulate such EOR processes. However, developing such robust algorithms can be challenging since convergence problems are frequently encountered during multiphase equilibrium calculations. In this research, we intend to develop a suite of robust multiphase equilibrium calculation algorithms dedicated to VLS and VLAS equilibria.

There are different thermodynamic models that have been proposed to model asphaltene precipitation. The simplest model is the pure solid model, in which asphaltene is considered as a solid phase that only contains asphaltene. With this assumption, we first develop a robust and efficient three-phase VLS equilibrium calculation algorithm based on the recent work by Li and Li (2019). The results show that our algorithm is able to predict asphaltene precipitation under different pressure/temperature conditions and the injection of different gases. However, asphaltene may behave like a highly-dense liquid phase, especially at high temperatures. Therefore, we subsequently modify our algorithm based on a so-called free-asphaltene assumption, in which the asphaltene phase is considered as a pure liquid phase. The findings indicate that, compared with the outcomes derived from the solid assumption, those obtained from the free-asphaltene assumption are more consistent with experimental observations.

In fact, the asphaltene phase is not an entirely pure phase. To further increase the accuracy of the three-phase equilibrium calculations, we aim to extend the trust-region-based three-phase VLL equilibrium calculation algorithm to conduct three-phase VLS equilibrium calculations. In such

an algorithm, the asphaltene phase is considered as a liquid phase containing both asphaltene and other oil components. However, it is a challenging task to properly identify different kinds of two-phase equilibria that can possibly appear in the three-phase equilibrium calculations. Since the composition of the asphaltene phase or the low-density liquid phase is dominated either by the asphaltene component or a gaseous solvent component, we further develop a VL/LL and VL/LA phase boundary tracking algorithm, in which the mole fraction of the most dominant component in such phases is used as an indicator to track the VL/LL and VL/LA phase boundaries. It can be concluded from the calculated results that the predicted VL/LS and VL/LL two-phase boundaries show smooth behavior and intersect with the VL_1L_2 three-phase region's apex, supporting the idea of an extended three-phase region. Besides, our prediction results align well with that predicted by Bennett and Schmidt (2017), validating the accuracy of this new method.

In addition to three-phase VLS equilibria, four-phase VLAS equilibria can also occur when the reservoir fluid contains a substantial amount of water. Based on the proposed trust-region-based three-phase VLS equilibrium calculation algorithm, we further aim to develop a four-phase VLAS equilibrium calculation algorithm. The algorithm is validated by comparing the calculated asphaltene precipitation amount during CO_2 injections with and without water and experimental data. Once validated, this method is applied to forecast asphaltene behavior under different pressures and temperatures, as well as to generate *PT* and *Px* phase diagrams. Observations reveal that the presence of water increases the area of asphaltene precipitation in the *Px* diagrams, implying that water may facilitate asphaltene precipitation during the CO_2 flooding process. Nevertheless, water overall seems to diminish the peak amount of the precipitated asphaltene.

PREFACE

A version of **Chapter 2** has been published as Chen, Z., Zhou, Y., Li, H., 2022. A review of phase behavior mechanisms of CO_2 EOR and storage in subsurface formations. *Ind. Eng. Chem. Res.* 61 (29), 10298-10318. Chen, Z. is responsible for the manuscript composition, data collection, formal analysis, investigation, writing – original draft, writing – review & editing, visualization, and funding acquisition. Zhou, Y. is responsible for the manuscript composition and data collection. Li, H. is the supervisory author and gets involved in the manuscript composition, formal analysis, investigation, writing – original draft, writing – review & editing, visualization and funding acquisition.

A version of **Chapter 3** has been published as Chen, Z., Li, R., Li, H., 2021. An improved vapor-liquid-asphaltene three-phase equilibrium computation algorithm. *Fluid Phase Equilibr.* 537, 113004–113016. Chen, Z. is responsible for the conceptualization, methodology, validation, formal analysis, investigation, writing – original draft, writing – review & editing, visualization, and funding acquisition. Li, R. is responsible for the methodology, formal analysis, investigation, and writing – review & editing. Li, H. is the supervisory author and gets involved in the conceptualization, methodology, validation, formal analysis, writing – review & editing, supervision, project administration, and funding acquisition.

A version of **Chapter 4** has been published as Chen, Z., Li, R., Li, H., 2022. A new vapor-liquid-asphaltene three-phase equilibrium computation algorithm based on the free-asphaltene assumption. *Fluid Phase Equilibr.* 556,1–14. Chen, Z. is responsible for the conceptualization, methodology, validation, formal analysis, investigation, writing – original draft, writing – review & editing, visualization, and funding acquisition. Li, R. is responsible for the methodology, formal

analysis, investigation, and writing – review & editing. Li, H. is the supervisory author and gets involved in the conceptualization, methodology, validation, formal analysis, writing – review & editing, supervision, project administration, and funding acquisition.

A version of **Chapter 5** has been published as Chen, Z., Xu L., Zhou, Y., Li, R., Li, H., 2022. A robust and efficient algorithm for vapor-liquid-equilibrium/liquid-liquid-equilibrium (VLE/LLE) phase boundary tracking. *Chem. Eng. Sci.* 266, 118286–118301. Chen, Z. is responsible for the conceptualization, methodology, validation, formal analysis, investigation, writing – original draft, writing – review & editing, visualization, and funding acquisition. Xu, L. is responsible for the theoretical development, simulation results, analysis, and manuscript composition. Zhou, Y. is responsible for the theoretical development, simulation results, and analysis. Li, R. is responsible for the methodology, formal analysis, investigation, and writing – review & editing. Li, H. is the supervisory author and gets involved in the conceptualization, methodology, validation, formal analysis, writing – review & editing, supervision, project administration, and funding acquisition.

A version of **Chapter 6** is submitted to *Applied Thermal Engineering* for possible publication on Oct 21, 2023. Chen, Z. is responsible for the conceptualization, methodology, formal analysis, investigation, writing – original draft, writing – review & editing, visualization. Wang Q. is responsible for conceptualization, methodology, formal analysis, investigation, writing – review & editing. Zhang J. is responsible for conceptualization, methodology, formal analysis, investigation, writing – review & editing; Li, S. is responsible for conceptualization, methodology, formal analysis, investigation and visualization. Zhou, Y. is responsible for conceptualization, methodology, formal analysis, investigation, writing – review & editing and visualization. Li, R. is responsible for the conceptualization, methodology, formal analysis, writing – review & editing. Jiang, L. is responsible for the formal analysis and writing – review & editing. Li, H. is the

supervisory author and gets involved in the conceptualization, methodology, validation, formal analysis, writing – review & editing, supervision, project administration, and funding acquisition.

Chapter 1 summarizes the research background, problem statement, research objectives, and thesis structure. **Chapter 7** summarizes the conclusions reached in this thesis as well as the recommendations for future research. **Chapters 1** and **7** are originally written by Zhuo Chen and have never been published elsewhere.

DEDICATION

This dissertation is dedicated to my dearest parents: Mrs. Zhenhua Zhao and Mr. Lingquan Chen.

ACKNOWLEDGMENTS

I would like to express my sincere appreciation to my supervisor Dr. Huazhou (Andy) Li for his dedication to my PhD education. I am also grateful to Dr. Hongbo Zeng, Dr. Zhehui Jin, Dr. Tayfun Babadagli., and Dr. Nobuo Maeda for serving as my examination committee members as well as providing constructive comments and suggestions.

I would also like to thank the following individuals or organizations for their support during my Ph.D. program:

- The past and present group members in Dr. Li's research group.
- Natural Sciences and Engineering Research Council (NSERC) for one Discovery Grant to Dr. Li.
- China Scholarship Council (CSC) for the financial support.
- All my friends in Edmonton for their friendship.

TABLE OF CONTENTS

LIST OF TABLES

LIST OF FIGURES

CHAPTER 1 INTRODUCTION

1.1. Research Background

In most compositional simulators, only two-phase vapor-liquid (VL) equilibrium calculations are conducted since VL two-phase equilibrium is the most common type of equilibria during the oil and gas production process. However, multiphase equilibria are also frequently encountered in petroleum engineering applications. Asphaltene phase is one of the most common third phase that can appear due to the change of pressure and temperature or the introduction of various gases during the gas flooding and carbon capture, utilization and storage (CCUS) processes (Angle *et al.*, 2006; Chen *et al.*, 2022). The precipitation of asphaltene in the pipeline can result in tubing plugging, while the asphaltene precipitation in the reservoirs can cause alteration of some key petrophysical properties like permeability and wettability. Therefore, the study of asphaltene precipitation has garnered substantial interest within the oil and gas industry (Creek, 2005; Punnapala and Vargas, 2013). Figure 1 shows the schematic of possible phase equilibria that could be encountered in multiphase equilibrium calculations considering asphaltene precipitation. As shown in Figure 1-1, five kinds of possible phase equilibria are considered in three-phase equilibrium calculations, while twelve kinds of possible phase equilibria are considered in four-phase equilibrium calculations. A compositional simulator that can consider multiphase equilibria is thus required to precisely capture the actual multiphase flow, possibly helping propose engineering procedures that can avoid the flow assurance problem involving asphaltene precipitation.

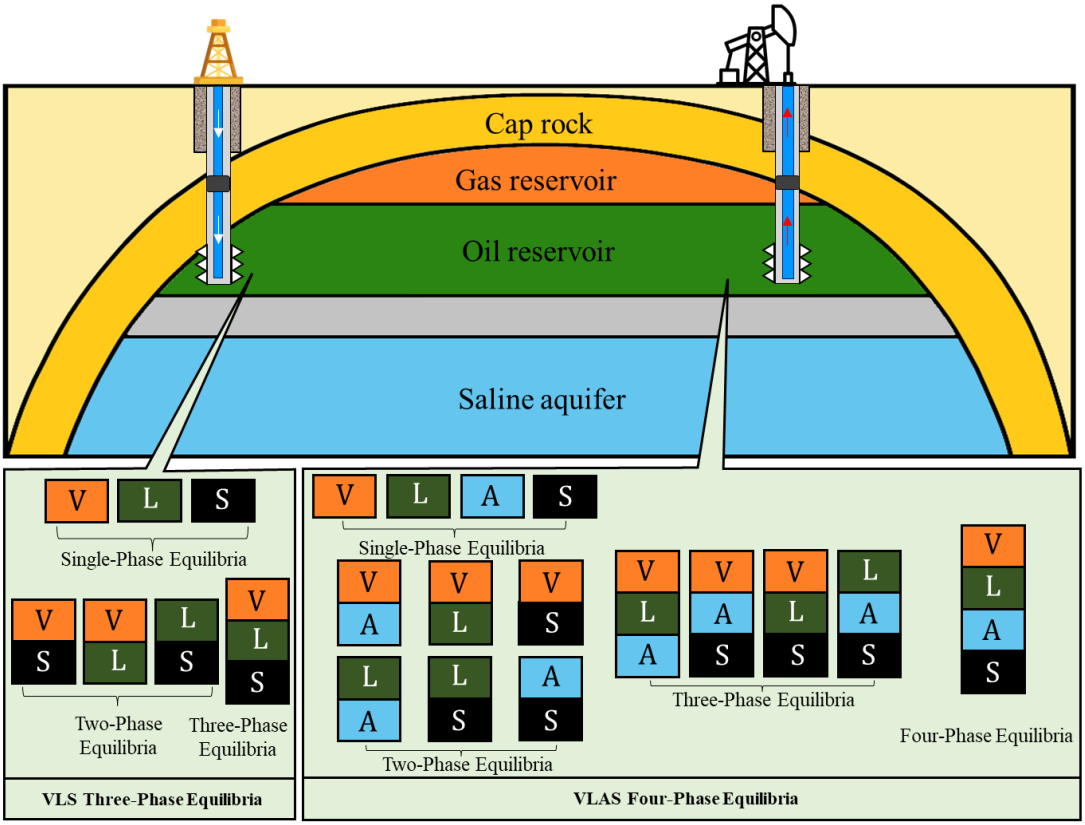

Figure 1-1 Schematic of possible phase equilibria that could be encountered in multiphase equilibria calculations considering asphaltene precipitation. V: vapor phase; L: liquid phase; A: aqueous phase; S: solid phase (Chen *et al*., 2022).

In addition to the commonly-observed three-phase VLS equilibrium, the vapor-liquid-liquid (VL_1L_2) three-phase equilibrium is another phase equilibrium that can appear during CO_2 flooding operations (Pan *et al.*, 2015; Pasqualette *et al.*, 2020). The presence of the L_1 and L_2 liquid phases, where L_1 is a denser liquid phase and L_2 is a lighter liquid phase enriched with gaseous components (Li *et al.*, 2013), can substantially influence the oil recovery efficiency by altering the relative permeability curves (Badamchi-Zadeh *et al.*, 2009a; Badamchi-Zadeh *et al.*, 2009b; Li *et al.*, 2013; Simon *et al.*, 1978). This complexity makes it imperative to develop robust and precise algorithms capable of accurately representing the VL_1L_2 three-phase equilibria in reservoir fluids, along with forecasting the pressure-temperature (*PT*) and pressure-composition (*Px*) phase diagrams. However, a significant challenge lies in the accurate identification of the three possible two-phase

equilibria—specifically, the VL (or VL_1) equilibrium, the VS (or VL_2) equilibrium, and the LS (or L_1L_2) equilibrium. Accurately determining these equilibria is critical for calculating the key in-situ multiphase flow properties such as relative permeability and capillary pressure (Bennett and Schmidt, 2017). Although various phase-identification techniques exist, their effective application to asphaltic oil systems, especially in capturing VL/LS phase boundaries, remains elusive. Furthermore, the identification of such boundaries often still depends on time-consuming point-by-point phase equilibrium calculations.

During the CO_2 flooding process, water will be injected into reservoirs to increase reservoir pressures. With the presence of an asphaltene phase and an aqueous phase, up to four phases (i.e., a vapor phase, an oleic phase, an asphaltene phase, and an aqueous phase) can coexist at a given thermodynamic equilibrium. In 1999, Srivastava *et al.* (Srivastava *et al.*, 1999) experimentally investigated the effect of water on the amount of asphaltene precipitation. Their findings suggest that brine seems to exert a minor impact on asphaltene precipitation (Srivastava *et al.*, 1999). Despite of numerous endeavors made to develop algorithms for calculating three-phase VLS and VLA equilibria, the detailed impact of brine on the asphaltene-precipitation onsets and the amount of precipitated asphaltene remains uncertain. Furthermore, the available data points demonstrating the influence of water presence on asphaltene precipitation levels are limited in scope.

1.2.Modeling Approaches

Numerous thermodynamic models have been developed to predict asphaltene precipitation, which can be broadly categorized into two groups: colloidal theory-based models and solubility theory-based models. Each theory offers a distinct perspective on how asphaltenes exist in crude oil. Models grounded in colloidal theory suggest that asphaltene particles are present as solid particles in suspension, with resins adhering to their surface (Nellensteyn, 1938). The inadequate presence

of resins to peptize the asphaltene is believed to lead to the attraction and subsequent aggregation of asphaltene particles (Nellensteyn, 1938). The solubility theory approach, which is established on regular solution theory or equation of state (EOS), assumes that asphaltene is soluble in crude oil and precipitates once its solubility drops beneath a specific value (Nellensteyn, 1938). Thermodynamic operations (such as gas injection or the alterations of pressure/temperature conditions) disrupt the phase equilibrium of the oil mixture, and lead to phase separation due to the changes in the solubility of the liquid or the asphaltene phases. A deeper dive into each approach and the accompanying models are given below.

1.2.1.Colloidal Approach

Models based on the colloidal theory propose that asphaltene particles are presented as colloidal suspensions that are peptized by resins in the crude oil (Nellensteyn, 1938). Once asphaltenes precipitate, the process is irreversible (Nellensteyn, 1938). Over the years, the colloidal nature of asphaltene has been rigorously investigated (Escobedo and Mansoori, 1997; Leontaritis and Mansoori, 1992; Mansoori, 1996; Park and Mansoori, 1988a, 1988b; Yaseen and Mansoori, 2018a, 2018b). Nellensteyn (1933) was the pioneer of the colloidal approach, which was subsequently expanded upon by Pfeiffer and Saal (1940). Central to this approach is the idea that a specific quantity of resin is essential to stabilize the asphaltene molecules within crude oil, which leads to the introduction of the concept of critical micelle concentration (CMC). A lack of resin will cause the mutual attraction of colloids and lead to the formation of micelle (Leontaritis and Mansoori, 1992). Notable models stemming from this perspective include those of Leontaritis and Mansoori (1988), Victorov and Firoozabadi (1996), and Pan and Firoozabadi (2000). However, colloidal-based asphaltene precipitation models require the fitting of many parameters (Punnapala and Vargas, 2013). Moreover, experimental studies show that the dispersion forces have a more

pronounced influence on phase behavior of asphaltene than the polar forces (Boek *et al.*, 2009; Buckley *et al.*, 1998; Czarnecki, 2009; Goual, 2009), which contradicts the applicability of the colloidal theory in describing the asphaltene precipitation phenomenon.

1.2.2.Solubility Theory Approach

The solubility approach divides crude oil into asphaltene and non-asphaltene components and views the asphaltene precipitation as a reversible process. Models employing this approach, which are often based on the solubility parameter concept, are routinely utilized to predict asphaltene precipitation. Notable models in this domain are the Flory-Huggins polymer solution theory, Scott-Magat theory, and regular solution theory (Flory, 1942; Hildebrand, 1919; Huggins, 1941; Scatchard, 1931; Scott and Magat, 1945). The models based on the Flory-Huggins theory and regular solution theory postulate uniform asphaltene properties and structure. In contrast, the Scott-Magat theory allows for a uniform structure of asphaltene but accommodates the polydispersity of asphaltenes by accounting for variations in molecular weight. The simplicity of the regular solution theory has inspired the development of a lot of models built on similar principles (Alboudwarej *et al.*, 2003; Andersen and Speight, 1999; Cimino *et al.*, 1995; Correra and Merino-Garcia, 2007; De Boer *et al.*, 1995; Gonzalez *et al.*, 2012; Kawanaka *et al.*, 1991; Kraiwattanawong *et al.*, 2007; Wang and Buckley, 2001; Wang *et al.*, 2004; Yarranton and Masliyah, 1996). However, this theory has its shortcomings. Specifically, it overlooks molecular interplays due to polarity, free volume combination, and the effects of pressure—unless pressure impacts are integrated using an EOS. The model also relies heavily on empirical correlations to consider the effect of temperature on variables such as density, solubility parameters, and mass distribution. Another notable limitation is the requirement to tune a lot of parameters to calibrate the model with experimental data since

the component solubility parameters cannot be quantified in a natural manner. Additionally, these models are unsuitable for vapor-liquid phase equilibrium calculations (Vargas *et al.*, 2009).

The EOS-based solubility models benefit from their applicability across diverse thermodynamic scenarios and are not limited to predicting asphaltene precipitation boundaries, which makes them a suitable choice for modeling the phase behavior of reservoir fluids containing asphaltenes. The cubic EOS (CEOS)-based solid model is widely used due to its simplicity and good agreement with the experimental results (Darabi *et al.*, 2014; Fazelipour, 2011; Kohse *et al.*, 2000; Kord and Ayatollahi, 2012; Nghiem *et al.*, 1993; Nguele *et al.*, 2016; Qin *et al.*, 2000; Zanganeh *et al.*, 2015). Nghiem *et al.* (Nghiem *et al.*, 1993) developed a thermodynamic model for isothermal asphaltene precipitation predictions. This framework visualizes the asphaltene phase as a pure solid phase, with the heaviest component in crude oil being segregated into precipitating and non-precipitating components. These components possess identical critical properties and acentric factors but have different binary interaction parameters (BIPs) with other components. However, this model does not consider the effect of temperature. To address this issue, Kohse *et al.* (Kohse *et al.*, 2000) formulated a solid model considering temperature and pressure effects on asphaltene precipitation. By adjusting two distinct parameters based on asphaltene onset pressures from laboratory studies, the model shows a commendable match with the experimental results across different temperature and pressure scenarios. Another popular CEOS-based approach to model asphaltene precipitation is proposed by Pedersen *et al.* (Pedersen *et al.*, 2006), in which the asphaltene phase is considered as a high-density liquid phase that is dominated by the asphaltene component, and the asphaltene precipitation can be modeled as a traditional separation between the low-density liquid phase and the high-density liquid phase.

The cubic plus association (CPA) EOS represents an advancement of the CEOS, incorporating extra terms to characterize the self-association among asphaltene molecules as well as the cross-association between asphaltenes and resins. Over the past decade, asphaltene precipitation models grounded on the CPA EOS have been rigorously investigated [37–43] and are showing encouraging outcomes. However, these models demand additional tuning parameters for each associating component [44]. The Statistical Associating Fluid Theory (SAFT) [45] and the Perturbed-Chain SAFT (PC-SAFT) [46] are also sophisticated EOS models. The PC-SAFT model stands out for its ability to predict phase behaviors, especially in complex polymers. Given the similarities between asphaltenes and large, heavy molecular compounds, this model has also been investigated for its ability to predict the phase behavior of asphaltene-rich oils [3, 5, 36, 47–56]. Although asphaltene precipitation models based on SAFT EOSs demonstrate commendable modeling capabilities, [57, 58], they still have much greater computational demands compared to the conventional CEOSs, even when speed-up procedures are employed [57].

Research has also been carried out to evaluate the performance of CEOS, CPA EOS and SAFT/PC-SAFT EOS in predicting asphaltene precipitation. A recent study by Leekumjorn *et al.* (2020) utilized CEOS, CPA EOS and PC-SAFT EOS to forecast the onset of asphaltene precipitation in 14 oil samples, and the prediction results are compared with experimental data. The study revealed that using CEOS allows for the development of a model to simulate fluid asphaltene behavior in most instances by merely adjusting the critical temperature of the asphaltene component to match the experimental data. For reservoir fluids with high asphaltene content, additional fine-tuning might be necessary; however, the optimized parameters serve as an excellent starting point. While the CPA and PC-SAFT EOSs could achieve similar accuracy, they demanded significantly more

computational resources and offered no advantages over the simpler CEOS. Moreover, the parameter tuning processes of CPA and PC-SAFT EOSs have proved to be much more complex.

1.3.Problem Statement

There are still several unresolved technical challenges concerning the robustness of multiphase equilibrium calculations and the construction of phase envelopes involving asphaltene precipitation. This dissertation primarily addresses the following issues:

- During the three-phase VLS equilibrium calculations, the conventional three-phase flash calculation algorithm may not converge to the correct solutions. One reason is that multiple stationary points may appear on the Gibbs free-energy surface in a three-phase equilibrium calculation. When the possible three phases contain an asphaltene phase, one of the stationary points may appear near the boundary of the Gibbs free-energy surface (Li and Li, 2019). The initial estimates of the equilibrium ratios used in the existing stability test algorithms may fail to identify this kind of stationary points. In order to avoid this problem, the asphaltene phase can be considered as a pure phase. Although Li and Li (2019) have proposed an algorithm to conduct the three-phase VLS equilibrium calculations by assuming asphaltene phase is a pure solid phase, the effect of temperature is ignored in their algorithm. Therefore, a robust and efficient three-phase VLS equilibrium calculation algorithm, which can be used to predict asphaltene precipitation under different pressure/temperature conditions and with different gas injections based on the solid assumption, is still required.
- At elevated temperatures, the asphaltene phase tends to behave like a highly-dense liquid phase rather than solid particles. Thus, a free-asphaltene assumption should be used, in which the asphaltene phase is treated as a liquid phase composed solely of asphaltene.

Moreover, a robust three-phase VLS equilibrium calculation algorithm based on such an assumption is also needed.

- In traditional phase equilibrium calculations, we normally find solutions by combining the successive substitution iteration (SSI) method with Newton's method. However, this method may fail in the three-phase VLS equilibrium calculations based on the assumption that the asphaltene phase is a highly-dense liquid phase that contains not only asphaltene component but also other substances. This requires us to introduce a more robust algorithm (e.g., the trust-region method) to tackle such convergence difficulties.
- When constructing *PT* and *Px* phase diagrams, the VL/LS and VL/LL boundaries often receive little attention. Although the traditional phase identification method can be used to identify such boundaries, the process is time-consuming, and the results can be of low accuracy. We are still lacking an efficient algorithm to accurately track the VL/LS and VL/LL phase boundaries.
- Water can frequently appear during the oil and gas production process. With the presence of an asphaltene phase and an aqueous phase, up to four phases (i.e., a vapor phase, a hydrocarbon phase, an asphaltene phase, and an aqueous phase) can coexist at a given thermodynamic equilibrium. However, the absence of robust four-phase VLAS equilibrium computation algorithms leaves the influence of water on asphaltene precipitation ambiguous.

1.4.Research Objectives

The general objective of this research is to develop more efficient and robust algorithms to conduct multiphase equilibrium calculations considering asphaltene precipitation for reservoir fluids. The

EOS model used in this research is Peng-Robinson (PR) EOS (Peng and Robinson, 1976). In order to accomplish this task, the short-term and long-term objectives are provided as follows:

Short-term objectives:

- Develop a robust three-phase VLS equilibrium calculation algorithm where single-phase, two-phase, and three-phase VLS equilibria can be considered based on the pure solid assumption.
- Develop a three-phase VLS equilibrium calculation algorithm that can handle single-phase, two-phase, and three-phase VLS equilibria based on the free-asphaltene assumption (i.e., the asphaltene phase is considered as a pure liquid phase).
- In cases where the free-asphaltene assumption and the pure solid assumption do not hold, extend the trust-region-based three-phase VLL equilibrium calculation algorithm to conduct three-phase VLS equilibrium calculations.
- Propose a VL/LL and VL/LS phase boundary tracking method and develop an algorithm based on such a method to automatically track the VL/LL and VL/LS phase boundaries.
- Develop a four-phase VLAS equilibrium calculation algorithm where single-phase, two-phase, three-phase and four-phase VLAS equilibria can be considered, and implement this algorithm to study the effect of water on asphaltene precipitation.

Long-term objective:

- Integrate the developed algorithms to the reservoir and wellbore simulators to help us better simulate the various EOR processes that involve these complex phase equilibria.

1.5.Hypothesis

Three hypotheses are considered in this thesis. The first one is that applying the pure solid assumption and the free-asphaltene assumption can help develop robust and efficient three-phase VLS equilibrium calculation algorithms. The second hypothesis is that the asphaltene phase can be treated as a heavy liquid phase that contains not only asphaltene component but also other components from the reservoir fluids, and thus the three-phase VLS equilibrium calculations and four-phase VLAS equilibrium calculations can be conducted by using the recently developed trust-region-based three-phase VLL equilibrium calculation algorithm. The third hypothesis is that the dominant component in the solvent-rich liquid phase or the asphaltene rich-phase can be used as an indicator to track the VL/LL and VL/LS phase boundaries.

1.6.Thesis Structure

This thesis is a paper-based thesis and a total of seven chapters are presented and organized as follows:

Chapter 1 introduces the basic research background, as well as the problem statement and the major research objectives. In **Chapter 2**, a review of the phase behavior mechanisms associated with CO_2 storage in subsurface formations, including asphaltene precipitation, is performed. Both the experimental studies and the modeling studies are included in this review. In **Chapter 3**, a robust three-phase VLS equilibrium calculation algorithm is developed by considering asphaltene phase as a solid phase. In order to avoid convergence problems, the modified initialization methods developed by Li and Li (2019) are applied to both stability tests and flash calculations. In **Chapter 4**, a three-phase VLS precipitation algorithm is proposed based on the free-asphaltene assumption. This approach facilitates easy detection of the asphaltene phase by contrasting the asphaltene component's fugacity across asphaltene and non-asphaltene phases, negating the need for an

additional thermodynamic model. **Chapter 5** introduces an innovative phase-boundary tracking technique designed to accurately identify the VL/LS and VL/LL two-phase boundaries within pressure-temperature and pressure-composition phase diagrams. To ensure the accuracy and efficiency of the phase boundary tracking algorithm, we utilize a reliable numerical solution method known as Brent's method (Brent, 1971). In **Chapter 6**, a four-phase VLAS equilibrium calculation algorithm is presented, in which single-phase, two-phase, three-phase and four-phase VLAS equilibria can be considered. The effects of water on asphaltene precipitation onsets and asphaltene precipitation amounts are studied in detail. Finally, **Chapter 7** summarizes the conclusions obtained from the thesis research and the recommendations for future work.

References

Alboudwarej, H., Akbarzadeh, K., Beck, J., Svrcek, W.Y., Yarranton, H.W., 2003. Regular solution model for asphaltene precipitation from bitumens and solvents. AIChE Journal 49, 2948-2956.

Andersen, S.I., Speight, J.G., 1999. Thermodynamic models for asphaltene solubility and precipitation. Journal of Petroleum Science and Engineering 22, 53-66.

Angle, C.W., Long, Y., Hamza, H., Lue, L., 2006. Precipitation of asphaltenes from solvent-diluted heavy oil and thermodynamic properties of solvent-diluted heavy oil solutions. Fuel 85, 492-506.

Badamchi-Zadeh, A., Yarranton, H., Maini, B.B., Satyro, M., 2009a. Phase behaviour and physical property measurements for VAPEX solvents: part II. propane, carbon dioxide and Athabasca bitumen. Journal of Canadian Petroleum Technology 48, 57-65.

Badamchi-Zadeh, A., Yarranton, H., Svrcek, W., Maini, B., 2009b. Phase behaviour and physical property measurements for VAPEX solvents: Part I. Propane and Athabasca bitumen. Journal of Canadian Petroleum Technology 48, 54-61.

Bennett, J., Schmidt, K.A., 2017. Comparison of phase identification methods used in oil industry flow simulations. Energy & Fuels 31, 3370-3379.

Boek, E.S., Yakovlev, D.S., Headen, T.F., 2009. Quantitative molecular representation of asphaltenes and molecular dynamics simulation of their aggregation. Energy & Fuels 23, 1209-1219.

Brent, R.P., 1971. An algorithm with guaranteed convergence for finding a zero of a function. The Computer Journal 14, 422-425.

Buckley, J., Hirasaki, G., Liu, Y., Von Drasek, S., Wang, J., Gill, B., 1998. Asphaltene precipitation and solvent properties of crude oils. Petroleum Science and Technology 16, 251-285.

Chen, Z., Zhou, Y., Li, H., 2022. A review of phase behavior mechanisms of CO_2 EOR and storage in subsurface formations. Industrial & Engineering Chemistry Research 61, 10298-10318.

Cimino, R., Correra, S., Sacomani, P., Carniani, C., 1995. Thermodynamic modelling for prediction of asphaltene deposition in live oils, SPE International Symposium on Oilfield Chemistry. OnePetro.

Correra, S., Merino-Garcia, D., 2007. Simplifying the thermodynamic modeling of asphaltenes in upstream operations. Energy & Fuels 21, 1243-1247.

Creek, J.L., 2005. Freedom of action in the state of asphaltenes: Escape from conventional wisdom. Energy & Fuels 19, 1212-1224.

Czarnecki, J., 2009. Stabilization of water in crude oil emulsions. Part 2. Energy & Fuels 23, 1253-1257.

Darabi, H., Shirdel, M., Kalaei, M.H., Sepehrnoori, K., 2014. Aspects of modeling asphaltene deposition in a compositional coupled wellbore/reservoir simulator, SPE Improved Oil Recovery Symposium. OnePetro.

De Boer, R., Leerlooyer, K., Eigner, M., Van Bergen, A., 1995. Screening of crude oils for asphalt precipitation: theory, practice, and the selection of inhibitors. SPE Production & Facilities 10, 55-61.

Fazelipour, W., 2011. Predicting asphaltene precipitation in oilfields via the technology of compositional reservoir simulation, SPE International Symposium on Oilfield Chemistry. OnePetro.

Flory, P.J., 1942. Thermodynamics of high polymer solutions. The Journal of Chemical Physics 10, 51-61.

Gonzalez, D.L., Vargas, F.M., Mahmoodaghdam, E., Lim, F., Joshi, N., 2012. Asphaltene stability prediction based on dead oil properties: Experimental evaluation. Energy & Fuels 26, 6218-6227.

Goual, L., 2009. Impedance spectroscopy of petroleum fluids at low frequency. Energy & Fuels 23, 2090-2094.

Hildebrand, J.H., 1919. Solubility. III. Relative values of internal pressures and their practical application. Journal of the American Chemical Society 41, 1067-1080.

Huggins, M.L., 1941. Solutions of long chain compounds. The Journal of Chemical Physics 9, 440-440.

Kawanaka, S., Park, S.J., Mansoori, G.A., 1991. Organic deposition from reservoir fluids: a thermodynamic predictive technique. SPE Reservoir Engineering 6, 185-192.

Kohse, B.F., Nghiem, L.X., Maeda, H., Ohno, K., 2000. Modelling phase behaviour including the effect of pressure and temperature on asphaltene precipitation, SPE Asia Pacific Oil and Gas Conference and Exhibition. OnePetro.

Kord, S., Ayatollahi, S., 2012. Asphaltene precipitation in live crude oil during natural depletion: Experimental investigation and modeling. Fluid Phase Equilibria 336, 63-70.

Kraiwattanawong, K., Fogler, H.S., Gharfeh, S.G., Singh, P., Thomason, W.H., Chavadej, S., 2007. Thermodynamic solubility models to predict asphaltene instability in live crude oils. Energy & Fuels 21, 1248-1255.

Leekumjorn, S., Risum, R. B., Sørensen, H., Krejbjerg, K., 2020. Asphaltene modeling with cubic and more complex equations of state, Abu Dhabi International Petroleum Exhibition & Conference. OnePetro.

Li, H., Yang, D., Li, X., 2013. Determination of three-phase boundaries of solvent(s)–CO_2–heavy oil systems under reservoir conditions. Energy & Fuels 27, 145-153.

Li, R., Li, H., 2019. Robust three-phase vapor–liquid–asphaltene equilibrium calculation algorithm for isothermal CO_2 flooding applications. Industrial & Engineering Chemistry Research 58, 15666-15680.

Michelsen, M.L., 1982a. The isothermal flash problem. Part I. Stability. Fluid Phase Equilibria 9, 1-19.

Michelsen, M.L., 1982b. The isothermal flash problem. Part II. Phase-split calculation. Fluid Phase Equilibria 9, 21-40.

Nellensteyn, F., 1938. The colloidal structure of bitumens. The Science of Petroleum 4, 401.

Nghiem, L.X., Hassam, M., Nutakki, R., George, A., 1993. Efficient modelling of asphaltene precipitation, SPE Annual Technical Conference and Exhibition. OnePetro.

Nguele, R., Ghulami, M.R., Sasaki, K., Said-Al Salim, H., Widiatmojo, A., Sugai, Y., Nakano, M., 2016. Asphaltene aggregation in crude oils during supercritical gas injection. Energy & Fuels 30, 1266-1278.

Pan, H., Chen, Y., Sheffield, J., Chang, Y.-B., Zhou, D., 2015. Phase-behavior modeling and flow simulation for low-temperature CO_2 injection. SPE Reservoir Evaluation & Engineering 18, 250-263.

Pan, H., Firoozabadi, A., 1996. A thermodynamic micellization model for asphaltene precipitation: Part 1: Micellar size and growth, SPE Annual Technical Conference and Exhibition. Onepetro.

Pasqualette, M.d.A., Carneiro, J.N., Johansen, S.T., Løvfall, B.T., Fonseca, R., Ciambelli, J.R., 2020. A numerical assessment of carbon-dioxide-rich two-phase flows with dense phases in offshore production pipelines. SPE Journal 25, 712-731.

Pedersen, K.S., Christensen, P.L., Shaikh, J.A., Christensen, P.L., 2006. Phase Behavior of Petroleum Reservoir Fluids. CRC Press.

Peng, D.-Y., Robinson, D.B., 1976. A new two-constant equation of state. Industrial & Engineering Chemistry Fundamentals 15, 59-64.

Punnapala, S., Vargas, F.M., 2013. Revisiting the PC-SAFT characterization procedure for an improved asphaltene precipitation prediction. Fuel 108, 417-429.

Qin, X., Wang, P., Sepehrnoori, K., Pope, G.A., 2000. Modeling asphaltene precipitation in reservoir simulation. Industrial & Engineering Chemistry Research 39, 2644-2654.

Scatchard, G., 1931. Equilibria in non-electrolyte solutions in relation to the vapor pressures and densities of the components. Chemical Reviews 8, 321-333.

Scott, R.L., Magat, M., 1945. The thermodynamics of high-polymer solutions: I. The free energy of mixing of solvents and polymers of heterogeneous distribution. The Journal of Chemical Physics 13, 172-177.

Simon, R., Rosman, A., Zana, E., 1978. Phase-behavior properties of CO_2-reservoir oil systems. SPE Journal 18, 20-26.

Srivastava, R., Huang, S., Dong, M., 1999. Asphaltene deposition during CO_2 flooding. SPE Production & Facilities 14, 235-245.

Vargas, F.M., Gonzalez, D.L., Hirasaki, G.J., Chapman, W.G., 2009. Modeling asphaltene phase behavior in crude oil systems using the perturbed chain form of the statistical associating fluid theory (PC-SAFT) equation of state. Energy & Fuels 23, 1140-1146.

Victorov, A.I., Firoozabadi, A., 1996. Thermodynamic micellization model of asphaltene precipitation from petroleum fluids. AIChE Journal 42, 1753-1764.

Wang, J., Buckley, J., 2001. A two-component solubility model of the onset of asphaltene flocculation in crude oils. Energy & Fuels 15, 1004-1012.

Wang, J., Buckley, J., Burke, N., Creek, J., 2004. A practical method for anticipating asphaltene problems. SPE Production & Facilities 19, 152-160.

Wu, J., Prausnitz, J.M., Firoozabadi, A., 1998. Molecular-thermodynamic framework for asphaltene-oil equilibria. AIChE Journal 44, 1188-1199.

Yarranton, H.W., Masliyah, J.H., 1996. Molar mass distribution and solubility modeling of asphaltenes. AIChE Journal 42, 3533-3543.

Zanganeh, P., Dashti, H., Ayatollahi, S., 2015. Visual investigation and modeling of asphaltene precipitation and deposition during CO_2 miscible injection into oil reservoirs. Fuel 160, 132-139.

CHAPTER 2 A REVIEW OF PHASE BEHAVIOR MECHANISMS OF CO_2 EOR AND STORAGE IN SUBSURFACE FORMATIONS

A version of this chapter has been published in *Industrial & Engineering Chemistry Research*.

Abstract

The emissions of CO_2 have been recognized as the main cause of climate change. As an important strategy being used to reduce the CO_2 concentration in the atmosphere, carbon capture, utilization and storage (CCUS) has attracted significant attention in recent years. Geological formations, including depleted oil and gas reservoirs, aquifers and saline aquifers, are popular CO_2 storage options. During the process of CO_2 storage in subsurface formations, the interactions between CO_2 and formation fluids must be considered as they could greatly affect the CO_2 trapping mechanisms and CO_2 storage capacity. In this paper, we give a brief review of the phase behavior mechanisms associated with CO_2 storage in subsurface formations. Two different CO_2-storage strategies are considered in this paper: CO_2 storage in saline aquifers and CO_2 storage in oil reservoirs. Multiphase equilibria, including two-phase, three-phase, and four-phase equilibria can be observed during CO_2 injection into underground formations. Both the experimental and modeling studies on the related phase behavior mechanisms are included in this review. We also introduce some recently developed robust algorithms for the multiphase equilibria calculations, which could be essential for the design of the CO_2 storage process and prediction of CO_2 storage capacity.

Keywords: CCUS, CO_2 storage, Phase behavior, Two-phase equilibria, Three-phase equilibria, Four-phase equilibria.

2.1. Introduction

Global warming caused by the high emission of CO_2 has become a growing concern of human society. Carbon capture, utilization and storage (CCUS) has been proven to be an efficient way to mitigate climate change due to CO_2 emissions[1]. According to the International Energy Agency (IEA)[2], CCUS can reduce global CO_2 emissions by 19% before 2050 while being cost-effective, which makes CCUS an important technique for achieving carbon neutrality.

CO_2 injection into subsurface formations is a technical option to reduce the concentration of CO_2 in the atmosphere[3]. In order to achieve long-term and stable CO_2 storage, it is a prerequisite to first understand different CO_2 storage mechanisms. There are mainly four CO_2 trapping mechanisms in subsurface formations: structural trapping, residual trapping, solubility trapping and mineral trapping[1]. Structural trapping is the primary CO_2 trapping mechanism, in which the injected CO_2 will be trapped below the impermeable cap rock (normally shale) due to the buoyancy effect[4]. This process highly relies on the small pore sizes of the caprock, which could provide sufficiently high capillary pressure to prevent the trapped CO_2 from moving upwards[4]. As time goes on, secondary trapping mechanisms, including residual trapping, solubility trapping and mineral trapping, will replace structural trapping and dominate CO_2 storage[5]. Compared with primary trapping, secondary trapping is more stable. Even if the primary trapping fails, secondary trapping could still store a considerable amount of CO_2[5]. Residual trapping is an important secondary trapping method due to its large CO_2 storage capacity. In residual trapping, the injected CO_2 flows through the pores of rocks and replaces the formation fluids[5]. Eventually, the formation fluids will become disconnected and trap CO_2 in pores due to the capillary force[1, 5]. The value of the capillary force is proportional to the interfacial tension (IFT), which is one of the most important phase behavior properties. Thus, the consideration of phase behavior of the CO_2-formation fluids mixtures can be

important since it could greatly affect the structural trapping and the residual trapping of CO_2 in subsurface formations.

At larger time scales, the injected CO_2 will be either dissolved in formation fluids, which is called solubility trapping, or precipitated in solid minerals, which is called mineral trapping. Solubility trapping and mineral trapping are considered as much safer CO_2 storage mechanisms since the injected CO_2 exists as a liquid or solid phase rather than a free phase[6]. Mineral trapping is considered the safest CO_2 trapping mechanism as CO_2 will be stored in solid minerals[7]. However, mineral trapping usually happens on a very long timescale (more than 1000 years), which exceeds the time frame of most research[7]. Compared with mineral trapping, solubility trapping can happen much sooner. Nevertheless, complex phase changes are involved in the solubility trapping mechanism, and they must be addressed to accurately predict the CO_2 storage capacity and evaluate the safety of CO_2 storage.

Although there are already some reviews focusing on the CO_2 trapping mechanisms, the considerations of CO_2 storage from the perspective of phase behavior are still missing. Figure 2-1 shows the schematic of the possible phase equilibria encountered during the process of CO_2 storage in subsurface formations. It can be seen in Figure 2-1 that there are different types of two-phase, three-phase and four-phase equilibria that are relevant to the CO_2 storage process. The interactions between CO_2 and formation fluids can greatly affect the CO_2 trapping mechanisms and CO_2 storage efficiency. In this paper, a comprehensive review of the phase behavior mechanisms associated with CO_2 storage in different subsurface formations is conducted from both experimental and modeling perspectives. This review is divided into three major parts: phase behavior measurements and modeling for CO_2-water/brine mixtures (Section 2), phase behavior

measurements and modeling for CO_2-oil mixtures (Section 3), and multiphase equilibrium computation algorithms (Section 4). A brief summary is given at the end of this paper.

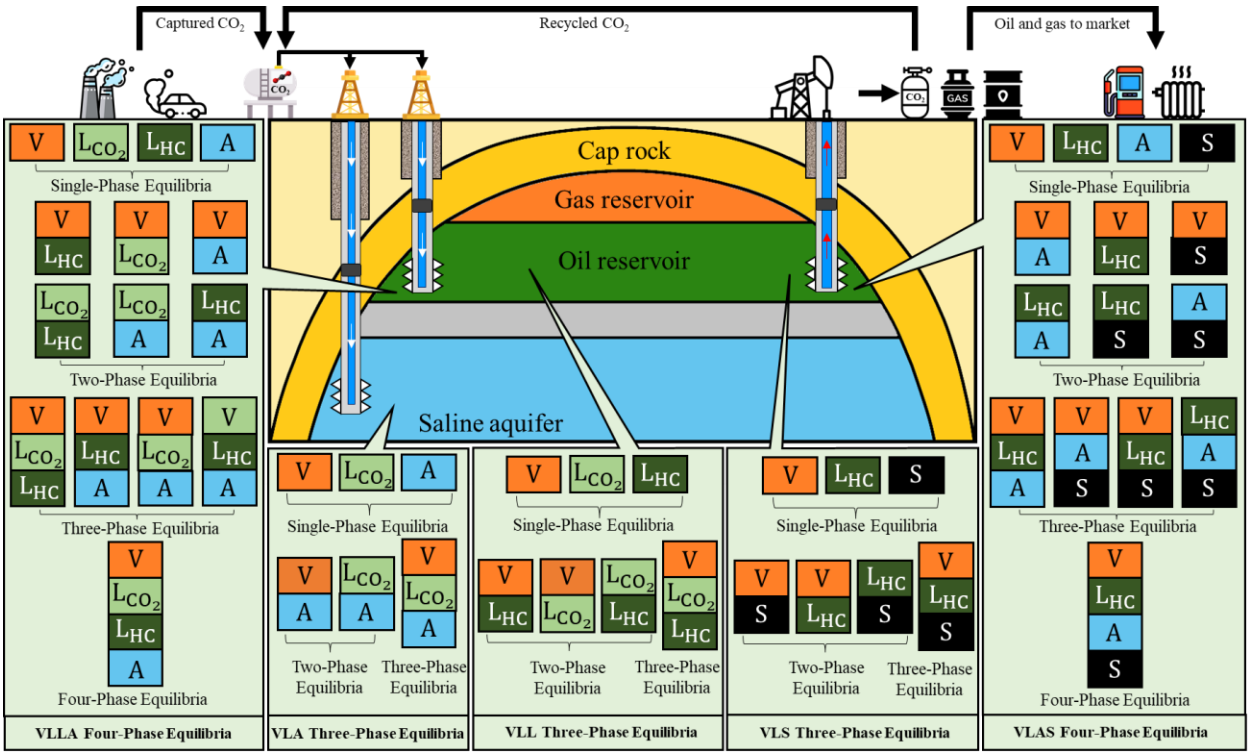

Fig. 2-1 Schematic of the possible phase equilibria encountered during the process of CO_2 storage in subsurface formations. V: vapor phase; L_{HC}: hydrocarbon-rich liquid phase; L_{CO2}: CO_2-rich liquid phase; A: aqueous phase; S: asphaltene phase. We thank flaticon.com for providing 10 icons that are used to create the drawing here.

2.2. Phase Behavior Measurements and Modeling for CO_2-Water/Brine Mixtures

The storage of CO_2 in water formations and brine formations are known as promising options to mitigate the effect of CO_2 on climate change due to their large CO_2 storage capacity[1]. However, it should be noted that the solubility of CO_2 in water/brine is generally less than 6%, and will be further decreased by rising temperatures or increasing salinities[1]. Besides, most aquifers are regional and do not have the impermeable cap rocks to prevent CO_2 from leaking[8]. In addition, since most pore spaces in aquifers are occupied by water, the pressure will build up fast in aquifers due to the injection of CO_2, which may fracture the formations and lead to the leakage of CO_2[1, 8].

The injected CO_2 mainly exists in three different phases in aquifers: free gas phase, residual gas phase and dissolved phase. Among these phases, the residual gas phase and the dissolved phase are more favorable as CO_2 in the residual and dissolved phases are less likely to leak[9]. Therefore, in order to evaluate the efficiency and capacity of CO_2 storage, it is of great importance to have a good understanding of the phase behavior of CO_2-water/brine mixtures. It can be seen from Figure 2-1 that three types of phase equilibria can be encountered for CO_2-water or CO_2-brine mixtures: single-phase equilibria, two-phase VA equilibria, two-phase $L_{CO2}A$ equilibria, and $VL_{CO2}A$ three-phase equilibria. Figure 2-2 shows the effect of temperature, pressure and molality on the solubility of CO_2 in brine. It can be concluded from Figure 2-2 (a) that in general, the CO_2 solubility in brine increases with pressure at a fixed temperature, but decreases with the temperature at a fixed pressure. However, this trend of variation will change if the temperature and pressure come close to the phase-transition boundary. On the other hand, it can be seen from Figure 2-2 (b) that the increase in salt concentrations leads to a lower CO_2 solubility. In this section, we review the efforts that have been made towards experimental measurements or modeling studies about the phase behavior of CO_2-water/brine mixtures.

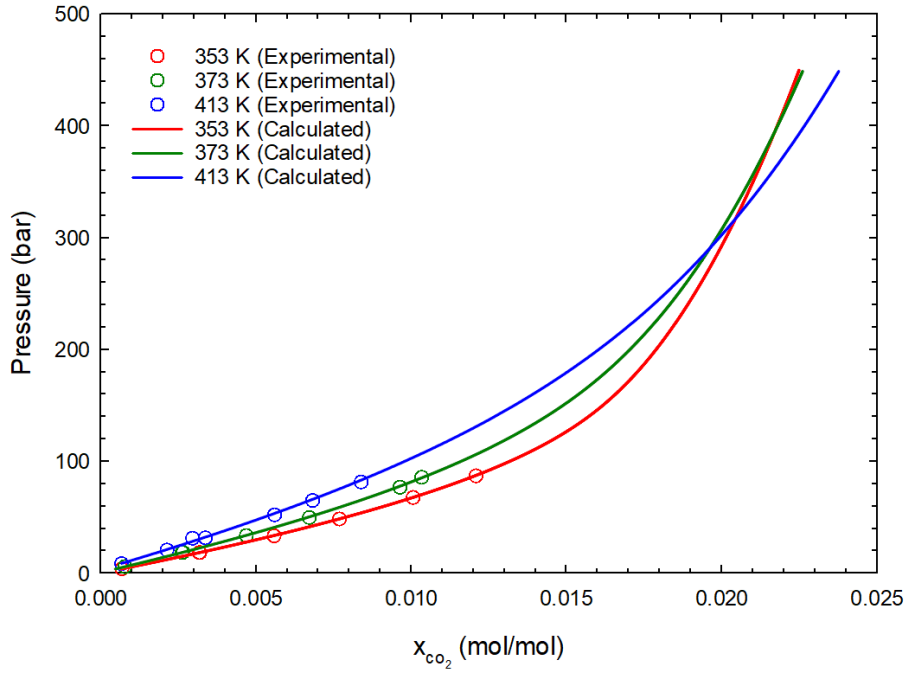

(a)

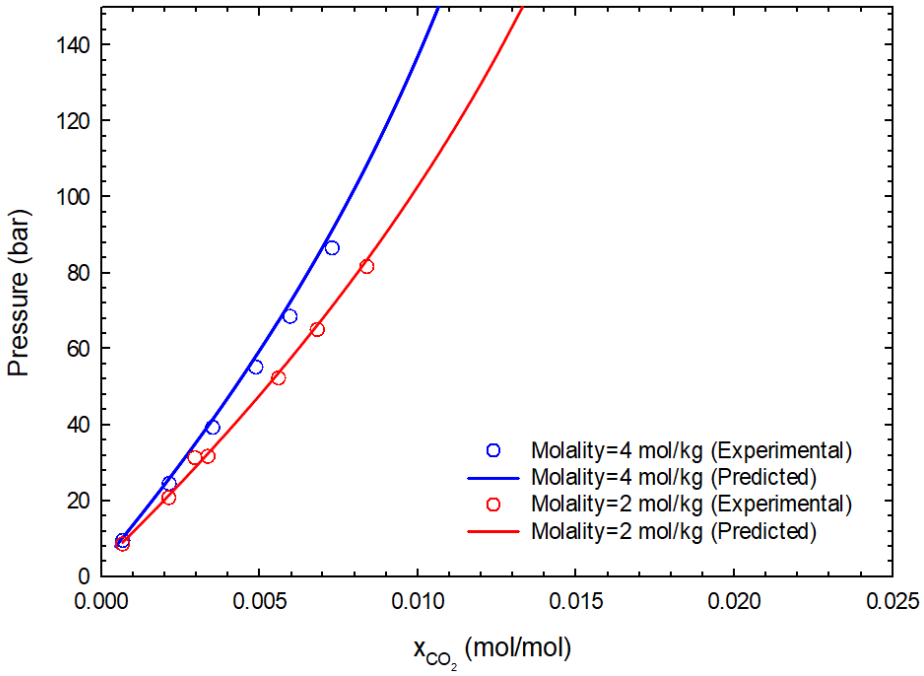

(b)

Fig. 2-2 Effect of temperature, pressure and molality on the solubility of CO_2 in KCl water solutions: (a) Effect of temperature and pressure on the solubility of CO_2 in 2 mol/kg KCl water solution; (b) Effect of molality on the solubility of CO_2 in KCl water solutions. Calculations are conducted using Sun's method[10]. Experimental data are obtained from the literature[11].

2.2.1. Phase Behavior Measurements for CO_2-Water/Brine Mixtures

2.2.1.1. Phase Behavior Measurements for CO_2-Water Mixtures

Supporting Information, Table S1 shows an overview of the experimental studies on the CO_2-water mixtures that measured the equilibrium phase compositions of different phases in the range of 273.15 K-642.15 K and 0.07 bar-1291.9 bar, including 1730 data points. Such experiments are normally conducted using either volumetric expansion, water trapping, gas chromatography, synthetic method, Raman spectroscopy or calorimetric technique[12]. Most of the collected data are compared with previous studies by the authors to check the reliability of their measurements. There are also some review studies focusing on the interaction between CO_2 and water at the low-pressure range[13], the solubilities of CO_2 in water at the temperature up to critical point[14], the mutual solubilities of CO_2 and water in different phases[15], and the equilibrium phase compositions at relatively high temperatures and pressures[16-18]. The quality of the experimental data in the literature is evaluated by Aasen *et al*.[19]. The data set of Drummond[20] covers the largest temperature range (303.85 K-621.65 K), while the data set of Takenouchi and Kennedy[21] covers the largest pressure range (100 bar-1500 bar). It can be concluded from Table S1 that sufficient experimental studies have been conducted to measure the solubilities of CO_2 in water. However, the composition of the CO_2-enriched phase is still not well-characterized experimentally. Accurate measurements of the vapor phase composition are still required at different pressure/temperature conditions.

2.2.1.2. Phase Behavior Measurements for CO_2/Brine Mixtures

Compared with the CO_2-water mixtures, the CO_2-brine mixtures are more common in the CO_2 storage and sequestration processes in subterranean and submarine formations. The solubility data of CO_2 in aqueous solutions of different salts is of immense importance for more accurate estimations of CO_2 storage capacity due to solubility trapping. Supporting Information, Table S2

summarizes the solubility data of CO_2 in NaCl, KCl, $MgCl_2$, $CaCl_2$, Na_2SO_4, K_2SO_4 and $MgSO_4$ aqueous solutions in the range of 273.15 K-723.15 K and 0.04 bar-2500.00 bar. There are 3316 data points in total. NaCl salt is the most commonly seen salt in saline aquifers, and hence the CO_2 solubilities in NaCl solutions have attracted most interest from researchers. Up to now, the experimental data of the CO_2 solubilities in NaCl aqueous solutions is available with the NaCl concentration close to the saturation concentration. In Table S2, we collect the CO_2 solubility data in NaCl aqueous solutions with NaCl concentrations between 0.001 mol/kg and 7.234 mol/kg. The data set of Drummond[20] covers the largest temperature range (292.85 K-673.15 K) of the CO_2 solubility in NaCl aqueous solution, while the data set of Deng *et al.*[22] covers that of the largest pressure range (500 bar-2500 bar). The number of studies focusing on other salts is significantly smaller than that on NaCl. In Table S2, we also include the CO_2 solubilities in 0.001 mol/kg-5.000 mol/kg KCl aqueous solutions, 0.100 mol/kg -6.335 mol/kg $MgCl_2$ aqueous solutions, 0.100 mol/kg-10.272 mol/kg $CaCl_2$ aqueous solutions, 0.010 mol/kg-3.254 mol/kg Na_2SO_4 aqueous solutions, 0.010 mol/kg-0.493 mol/kg K_2SO_4 aqueous solutions and 0.009 mol/kg-4.003 mol/kg $MgSO_4$ aqueous solutions. More experimental data of CO_2 solubility in sulfate aqueous solutions at high pressure/temperature conditions are still required to further enrich the understanding of the phase behavior of CO_2-sulfate brine mixtures. It can be also concluded that a saline aquifer with a lower salt concentration can potentially help to store more CO_2 via the solubility trapping mechanism.

The experimental data of CO_2 solubilities in mixed-salt solutions are relatively rare. In Table 2-1, we summarize CO_2 solubilities in 7 different mixed-salt solutions at 297.00 K-424.67 K and 1.01 bar-383.30 bar, including 308 data points. The concentration of different salts in their aqueous solutions are also shown in Table 2-1. We note that more experimental works need to be conducted

to obtain more CO_2 solubility data in mixed-salt solutions. These data will help develop, as well as validate, thermodynamic models dedicated to CO_2/brine mixtures.

Table 2-1 Phase behavior measurements on CO_2-water-mixed salt mixtures.

	Year	Temperature (K)	Pressure (bar)	Salt	Salt Concentration (mol/kg H_2O)		N_p
Yasunishi *et al.*[23]	1979	298.15	1.01	$KCl+CaCl_2$	KCl	0.107-4.969	15
					$CaCl_2$	0.109-3.317	
				$NaCl+Na_2SO_4$	NaCl	0.058-1.710	15
					Na_2SO_4	0.067-1.606	
				NaCl+KCl	NaCl	0.135-3.987	15
					KCl	0.138- 4.021	
				$NaCl+MgSO_4$	NaCl	0.066-1.807	15
					$MgSO_4$	0.066-1.974	
				$NaCl+KCl+CaCl_2$	NaCl	0.097-2.522	17
					KCl	0.196-2.629	
					$CaCl_2$	0.098-2.096	
Liu *et al.*[24]	2011	308.15-328.15	13.40-158.50	$NaCl+KCl+CaCl_2$	NaCl	0.291-0.857	75
					KCl	0.228-0.672	
					$CaCl_2$	0.153-0.451	
		318.15	15.40-383.30	NaCl+KCl	NaCl	0.901	8
					KCl	0.706	
		318.15	14.40-35.80	$NaCl+CaCl_2$	NaCl	0.901	8
					$CaCl_2$	0.474	
		318.15	13.60-39.30	$KCl+CaCl_2$	KCl	0.706	8
					$CaCl_2$	0.474	
Tong *et al.*[25]	2013	308.90-424.67	11.07-171.60	NaCl+KCl	NaCl	0.910	14
					KCl	0.143	
Jacob and Saylor[26]	2016	297.00	48.20-141.20	$NaCl+KCl+CaCl_2+MgCl_2$	NaCl	0.101-1.521	84
					KCl	0.047-0.102	
					$CaCl_2$	0.101-0.353	

					$MgCl_2$	0.062-0.101	
Cruz *et al.*[27]	2020	333.15-453.15	60.30-400.70	NaCl+$CaCl_2$	NaCl	1.200	10
					$CaCl_2$	0.200	
dos Santos *et al.*[28]	2021	303.15-423.15	15.54-201.80	NaCl+Na_2SO_4	NaCl	3.000-6.000	24
					Na_2SO_4	1.000	

2.2.2. Phase Behavior Modeling for CO_2-Water/Brine Mixture

The phase behavior modeling of the CO_2-water/aqueous solution mixtures has been extensively studied due to its importance and complexity. The developed models can be divided into three categories: fugacity-fugacity (φ-φ) models, activity-fugacity (γ-φ) models and empirical correlations. In this section, we will introduce these three different modeling approaches separately.

2.2.2.1. φ-φ Models

In the models based on the φ-φ approach, an equation of state (EOS) is selected to calculate the fugacity of different phases[19]. Table 2-2 shows the summary of the proposed thermodynamic models for the CO_2-water mixtures based on the φ-φ approach. Soreide and Whitson[29] presented a thermodynamic model by modifying the mixing rule and α-function of Peng-Robinson equation of state (PR EOS)[30]. The modified α-function of water can be expressed as[29]:

$$\alpha_w = 1 + 0.4530\left(1 - \frac{T}{T_c}\right) + 0.0034\left(\left(\frac{T}{T_c}\right)^{-3} - 1\right) \quad (1)$$

Bamberger *et al.*[31] proposed a model by coupling PR EOS[30] with the modified α-function developed by Melhem *et al.*[32] to predict the phase equilibria of the CO_2-water system at 323 K-353 K and 0-160 bar. The modified α-function can be shown as[32]:

$$\ln \alpha = m\left(1 - \frac{T}{T_c}\right) + n\left(1 - \sqrt{\frac{T}{T_c}}\right) \quad (2)$$

where m and n are temperature-dependent correlation parameters that can be obtained by regressing the experimental vapor pressure data of each component, T and T_c are temperature and critical temperature, respectively. Constant binary interaction parameter (BIP) and temperature-dependent BIPs are both used in Bamberger *et al.*'s study[31]. The modeling results show that the average absolute percentage deviations (AAD%) of both CO_2 in the aqueous phase and water in

the CO_2-rich phase can be significantly reduced by the temperature-dependent BIPs, which can be calculated by[31]:

$$k_{12} = -0.4259 + 0.001028T \quad (3)$$

where k_{12} is the BIP between CO_2 and water, and T is the temperature. Chapoy *et al.*[33] proposed a model by using the Valderrama modification of the Patel-Teja equation of state (VPT EOS)[34] and non-density-dependent mixing rules (NDD)[35], and the model is tested in the range of 273.15 K-373.15 K and 1 bar-1000 bar. Three sets of BIPs between CO_2 and water are used for the temperature ranges of 273.15 K-277.13 K, 277.13 K-304.20 K and for the temperatures larger than 304.2 K. The BIP between supercritical CO_2 and water is set to 0.19650 as suggested by Tohidi[36]. The α-function for water proposed by Tohidi is also adopted, which can be expressed as[36]:

$$\alpha_w = 2.4968 - 3.0661\frac{T}{T_c} + 2.7048\left(\frac{T}{T_c}\right)^2 + 1.2219\left(\frac{T}{T_c}\right)^3 \quad (4)$$

Valtz *et al.*[37] introduced the Wong–Sandler mixing rule[38] in PR EOS[30] to calculate the phase composition of CO_2-water mixtures at the temperature of 273.15 K-333.15 K and the pressure of 0-160 bar. Generalized Mathias–Copeman α-functions[39] are applied in Valtz *et al.*'s work[37], which can be written as:

$$T < T_c, \alpha = [1 + c_1(1 - \sqrt{\frac{T}{T_c}}) + c_2\left(1 - \sqrt{\frac{T}{T_c}}\right)^2 + c_3\left(1 - \sqrt{\frac{T}{T_c}}\right)^3] \quad (5)$$

$$T \geq T_c, \alpha = [1 + c_1(1 - \sqrt{\frac{T}{T_c}})]^2 \quad (6)$$

Note that in Equations (5-6), c_1, c_2 and c_3 can be calculated using Equations (7-9):

$$c_1 = 1.0113\omega^2 + 1.1538\omega + 0.4021 \quad (7)$$

$$c_2 = -7.7867\omega^2 + 2.2590\omega - 0.2011 \text{ (8)}$$

$$c_3 = 2.8127\omega^2 - 1.0040\omega + 0.3964 \text{ (9)}$$

where ω is the acentric factor. The BIPs used in Valtz *et al.*'s study[37] are tuned for each temperature based on experimental data. A similar approach was also adopted by Zhao and Lvov[40] using Penge-Robinson-Stryjek-Vera (PRSV) EOS[41] at 273.15 K-623 K and 0-2000 bar. The α-function used in Zhao and Lvov's[40] study is given by[41]:

$$\alpha = [1 + \kappa(1 - \sqrt{\frac{T}{T_c}})]^2 \text{ (11)}$$

where the value of κ can be calculated by[41]:

$$\kappa = \kappa_0 + \kappa_1(1 + \sqrt{\frac{T}{T_c}})(0.7 - \sqrt{\frac{T}{T_c}}) \text{ (12)}$$

In equation 12, κ_0 can be calculated by[41]:

$$\kappa_0 = 0.378893 + 1.4897153\omega - 0.17131848\omega^2 + 0.0196554\omega^3 \text{ (13)}$$

Austegard *et al.*[42] used Soave-Redlich-Kwong (SRK) EOS[43] with van der Waals mixing rule[44] to predict the CO_2 solubility in the aqueous phase and water solubility in the CO_2-rich phase. Their results show that SRK EOS[43] with van der Waals mixing rule[44] cannot accurately predict the mutual solubilities of the CO_2-water mixtures. They also coupled SRK EOS[43] with Huron-Vidal mixing rule[45], and the α-function proposed by Twu *et al.*[46]:

$$\alpha = (\frac{T}{T_c})^{C_3(C_2-1)} e^{(C_1(1-(\frac{T}{T_c})^{C_2C_3}))} \text{ (14)}$$

where C_1, C_2 and C_3 are component-dependent constants. Two sets of temperature-dependent BIPs are applied, and the calculation results agree well with the experimental data. Cubic-plus-

association (CPA) EOS[47] with the cubic part using SRK EOS[43] was adopted by Austegard *et al.*[42]. With constant BIPs, the CPA-SRK EOS[43, 47] can yield an AAD% of 9.0 for the solubility of CO_2 in water and 16.8 for water in the CO_2-rich phase[42].

Sun and Dubessy[48] applied statistical associating fluid theory (SAFT) EOS[49] with Lennard-Jones (LJ) intermolecular potential[50] and two sets of temperature-dependent BIPs to model the phase behavior of CO_2-water mixtures. They obtained satisfactory results. However, it has been pointed out that this model is too complex and requires improvised interaction parameters[19]. Li and Yang[51] developed a model to predict the mutual solubilities between CO_2 and water using PR EOS coupled with the modified alpha functions and temperature-dependent BIPs. The authors also considered the effect of the presence of hydrocarbons when they calculate the solubility of CO_2. The model proposed by Li and Yang[51] is shown to be more accurate than Soreide and Whitson's model[29]. Aasen *et al.*[19] tested a series of thermodynamic models that use different EOSs with various types of mixing rules and α-functions at 274 K-478 K and pressure up to 608 bar. Out of the many models tested by Aasen *et al.*[19], we only include the four most accurate ones in Table 2-2: the volume-translated (VT) PR EOS, VT SRK EOS, CPA-SRK EOS and perturbed-chain statistical associating fluid theory (PC-SAFT) EOS[52]. The study by Aasen *et al.*[19] shows that the VT PR EOS[30] with Huron-Vidal mixing rule[45] yields the best results among the tested models, and the complex EOSs do not necessarily yield better results for the CO_2-water mixtures than cubic EOSs[19].

Table 2-2 Thermodynamic models for the CO_2-water mixtures based on the φ-φ approach. AAD_1 refers to the absolute average deviation of the solubility of CO_2 in the aqueous phase, while AAD_2 refers to the absolute average deviation of the solubility of H_2O in the CO_2-rich phase.

	EOS	Mixing rule	α function	Temperature (K)	Pressure (bar)	BIP between CO_2 and H_2O	AAD_1 (%)	AAD_2 (%)
Soreide and Whitson[29]	PR	Soreide and Whitson	Soreide and Whitson	423.15	100.00-400.00	$k_{12} = -0.31092 + 0.23580\frac{T}{T_c} - 21.2566e^{-6.7222\frac{T}{T_c}}$ (15)	-	-
Bamberger *et al.*[31]	PR	Panagiotopoulos and Reid	Melhem *et al.*	323.00-353.00	0-160.00	k_{12}=-0.0814	14	5.5
						Temperature dependent	1.6	3.7
Chapoy *et al.*[33]	VPT	NDD mixing rules	Kalorazi	273.15-373.15	1.00-1000.00	273.15 K≤T≤277.13 K, k_{12}=0.19314 277.13 K< T≤304.2 K, k_{12}= 0.16860 If CO2 is supercritical, k_{12}=0.19650	3.0	7.9
Valtz *et al.*[37]	PR	Wong–Sandler	Mathias–Copeman	273.15-333.15	0-160.00	Fitted for each temperature	4.4	6.4
Austegard *et al.*[42]	SRK	Van der Waals	Classic	293.15-323.15	0-600.00	k_{12}=0.193	93.0	7.3
						$k_{12} = -0.527 + 1.67 \times 10^{-3} \times T - 1.05 \times 10^{-6} \times T^2$ (16)	3.5	392
Austegard *et al.*[42]	SRK	Huron-Vidal	Twu *et al.*	293.15-323.15	0-600.00	$\frac{g_{12}}{R} = -3741 + 1.55T$ (17) $\frac{g_{21}}{R} = 6563 - 5.12T$ (18)	4.0	7.5
						$\frac{g_{12}}{R} = -1237 - 15.506T + 0.02896T^2$ (19) $\frac{g_{21}}{R} = 5858 + 2.411T - 0.01713T^2$ (20)	2.6	7.3

Austegard *et al.*[42]	CPA-SRK	Classic	Classic	293.15-323.15	0-600.00	k_{12}=0.06	9.0	16.8
Sun and Dubessy[48]	SAFT-LJ	Van der Waals	-	210.00-1000.00	0-100.00	For 273-647 K $k_{1,ij} = 0.3 - (T - 273.15) \times 0.001$ (21) $k_{2,ij} = k_{3,ij} = 0.8461 + 8d - 5 \times (T - 273.15)$ (22) For 647-1073 K $k_{1,ij} = -0.074$ $k_{2,ij} = k_{3,ij} = 0.87602$	-	-
						For 273-647 K $k_{1,ij} = -0.24 + 0.0004(T - 273.15)$ (23) $k_{2,ij} = 0.8367 + 6d - 5(T - 273.15)$ (24) $k_{3,ij} = 0.82 + 0.18 \times \rho^*$ (25) For 647-1073 K $k_{1,ij} = -0.0904$ $k_{2,ij} = 0.85914$ $k_{3,ij} = 0.82 + 0.18 \times \rho^*$ (26)	-	-
Tsivintzelis *et al.*[53]	CPA-SRK	Classic	Classic	298.00-478.00	0-550.00	Temperature dependent	12.9	11.9
Li and Yang[51]	PR	Van der Waals	Li and Yang[51]	273.16-647.10	0-700.00	Temperature dependent	6.12	-
Zhao and Lvov[40]	PRSV	Wong–Sandler	Stryjek and Vera	273.15-623.00	0-2000.00	Fitted for each temperature	6.8	7.4
Aasen *et al.*[19]	PC-SAFT	Classic	-	274.00-478.00	0-608.00	$k_{12} = -0.399 + 1.988\frac{T}{T_0} - 2.404(\frac{T}{T_0})^2$ (27)	8.3	8.8
Aasen *et al.*[19]	CPA-SRK	Classic	Classic	274.00-478.00	0-608.00	k_{12}=0.08831	9.7	14.2

Aasen *et al.*[19]	VTSRK	Huron-Vidal	Twu *et al.*	274.00-478.00	0-608.00	$\frac{g_{12}}{RT_0} = 5.82 - 2.565\frac{T}{T_0}$ (28) $\frac{g_{21}}{RT_0} = -3.339 + 0.139\frac{T}{T_0}$ (29)	4.1	5.5
Aasen *et al.*[19]	VTPR	Huron-Vidal	Twu *et al.*	274.00-478.00	0-608.00	$\frac{g_{12}}{RT_0} = 5.831 - 2.559\frac{T}{T_0}$ (30) $\frac{g_{21}}{RT_0} = -3.311 + 0.0377\frac{T}{T_0}$ (31)	3.5	5.6

Table 2-3 shows the developed models for CO_2-brine systems based on the φ-φ approach. Soreide and Whitson[29] proposed a thermodynamic model for the CO_2-water-NaCl system by modifying the mixing rules and the α-function of PR EOS. They also developed a new correlation of BIPs for the aqueous phase (${k_{12}}^A$), which is not only temperature-dependent but also related to the concentration of salt in water. This correlation is further adjusted by Chabab *et al.*[54] by regressing the experimental data[55] from the literature. Bermejo *et al.*[56] applied Anderko–Pitzer EOS[57, 58] to model the CO_2-water-Na_2SO_4 system at 288 K-368 K and 0-140 bar, with the Na_2SO_4 concentration from 0.25 mol/kg to 2.7 mol/kg. Sun and Dubessy[59] used SAFT-LJ EOS[50] to model the CO_2-water-NaCl mixture at wide ranges of temperature and pressure with a new term that considers the energetic contribution of the long-range electrostatic force between salt ions; their model is reasonably successful in correlating the experimental data. Chabab *et al.*[54] conducted phase equilibria calculations using CPA EOS[47] with the cubic part calculated by an electrolyte version of PR EOS (ePR EOS)[54]. In Chabab *et al.*'s model, the effect of temperature is included in the BIP between CO_2 and water, while the effect of salt concentration is taken into account in the BIP between CO_2 and different ions[54]. However, the aforementioned models cannot be used for the CO_2-water-mixed salt systems. In order to overcome this limitation, Sun[10] proposed a model by coupling PR EOS with Huron-Vidal mixing rule[45] and temperature-salt concentration-dependent BIPs to model the phase equilibria of CO_2-brine mixtures. The model was tested using 4 different CO_2-water-single salt systems and 6 different CO_2-

water-mixed salt systems, and their results are promising. But one deficiency of their model is that it can only consider four salt types: NaCl, KCl, $CaCl_2$, and $MgCl_2$.

In general, the performance of different thermodynamic models in predicting the mutual solubilities of CO_2-water/brine mixtures based on the φ-φ approach is strongly related to the selection of BIPs, α-functions and mixing rules. Association EOSs can provide more accurate predictions of the mutual solubilities of CO_2-water/brine mixtures when there are only a few tunable parameters[19]. However, by introducing Wong–Sandler or Huron-Vidal mixing rules, CEOSs can also provide accurate predictions of the mutual solubilities of the CO_2-water/brine mixtures since there will be more parameters that can be fitted based on experimental data[19]. Based on the results, it can be concluded that the thermodynamic models based on the φ-φ approach can well reproduce the mutual solubilities of the CO_2-water mixtures. Nevertheless, thermodynamic models dedicated to predicting the solubilities of CO_2 in brine based on the φ-φ approach can only consider the effect of certain types of salts. A universal φ-φ-approach-based model is still required to precisely calculate the solubility of CO_2 in different types of brine.

Table 2-3 Thermodynamic models for the CO_2-brine mixtures based on the φ-φ approach.

	EOS	Mixing rule	α function	BIP	Temperature (K)	Pressure (bar)	Salt	Salt Concentration (mol/kg)
Soreide and Whitson[29]	PR	Soreide and Whitson	Soreide and Whitson	${k_{12}}^{A} = -0.31092(1 + 0.15587c^{0.7505}) + 0.23580(1 + 0.17837c^{0.979})\frac{T}{T_c} - 21.2566e^{(-6.7222\frac{T}{T_c}-c)}$ (32)	423.15	100.00-400.00	NaCl	1.100-4.300
Bermejo *et al.*[56]	Anderko–Pitzer	Classic	-	$\alpha_{ij} = 1.1549 \times 10^{-6}T^2 - 1.1943 \times 10^{-3}T^2 + 0.41452T - 46.686$ (33)	288.00-368.00	0-140.00	Na_2SO_4	0.250-2.700
Sun and Dubessy[59]	SAFT-LJ	Van der Waals	-	$k_{2,ion-CO_2} = 0.00017e^{\frac{T}{72.2827}} + 0.9321$ (34)	313.15-523.15	0-1600.00	NaCl	0.529-6.000
Chabab *et al.*[54]	PR	Soreide and Whitson	Soreide and Whitson	${k_{12}}^{A} = \frac{T}{T_{c\,CO2}}\left(0.43575155 - 0.05766906744\frac{T}{T_{c\,CO_2}} + 8.26464849 \times 10^{-3}\frac{T}{T_{c\,CO2}} \times c\right) + c^2\left(1.29539193 \times 10^{-3} - 1.6698848 \times 10^{-3}\frac{T}{T_{c\,CO2}}\right) - 0.47866096$ (35)	298.00-433.06	0-500.00	NaCl	1.000-5.000

Chabab *et al.*[54]	CPA-ePR	Van der Waals	Classic	$k_{CO_2-Na^+} = -0.563937723 \times c - 4.352740149$ $k_{CO_2-Cl^-} = 0.347571193 \times c + 4.762185508$ (36)	298.00-433.06	0-500.00	NaCl	1.000-6.000	
Sun[10]	PR	Huron-Vidal	Classic	$k = -0.324T^2 + 0.001c^2 - 0.009Tc^2 - 0.002$ (37)	323.00-423.00	0-400.00	NaCl	1.000-5.000	
				$k = -0.224T^2 - 0.008Tc^2 - 0.001$ (38)	323.00-413.00	0-200.00	KCl	2.000-4.000	
				$k = -0.341T^2 - 0.012Tc^2 - 0.002$ (39)	313.00-374.00	0-800.00	$CaCl_2$	1.000-4.000	
				$k = -0.237T^2 - 0.024Tc^2 - 0.001$ (40)	309.00-425.00	0-800.00	$MgCl_2$	1.300-5.000	
				$k = \sum_{i=1}^{N} \alpha_i{}^{a_i} \frac{c_i}{\sum_{j=1}^{N} c_j + 10^{-10}} k_i - 1.045$ (41)	318.00	0-160.00	NaCl+ KCl	NaCl	1.190
								KCl	1.490
					308.00	0-160.00	NaCl+ KCl+ $CaCl_2$	NaCl	1.900
								KCl	1.490
								$CaCl_2$	1.000
					318.00	0-160.00	NaCl+ KCl+ $CaCl_2$	NaCl	2.850
								KCl	2.240
								$CaCl_2$	1.500
					328.00	0-160.00	NaCl+ KCl+ $CaCl_2$	NaCl	1.900
								KCl	1.500
								$CaCl_2$	1.000
					423.00	100.00-600.00	NaCl+ KCl+ $CaCl_2$+ $MgCl_2$	NaCl	4.100
								KCl	0.040
								$CaCl_2$	0.200
								$MgCl_2$	0.100

					328.00	0-200.00	NaCl+ KCl+ $CaCl_2$	NaCl	2.800
								KCl	2.200
								$CaCl_2$	1.500

2.2.2.2.*γ-φ* Models

In the *γ-φ* models, the activity coefficient models are applied to model the aqueous phase, whereas the EOS models are used to characterize the vapor phase. Supporting Information, Table S3 summarizes the thermodynamic models for the CO_2-water/brine mixtures based on the *γ-φ* approach. Li and Nghiem[60] proposed a model to calculate the phase equilibria of CO_2-water mixtures and CO_2-water-NaCl mixtures using PR EOS[30] and Henry's law[61]. The scaled particle theory[62] was also applied to account for the effect of salts on phase equilibria. Duan and Sun[63] developed a model by coupling Pitzer activity coefficient formulation[64] and Duan *et al.*'s EOS[65] to calculate the solubility of CO_2 in both pure water and single-salt solutions. This model was then further modified by Duan *et al.*[66] using a non-iterative equation instead of an EOS to calculate the fugacity coefficient of CO_2. This approach is shown to be accurate and efficient. Zhao *et al.*[67] established an approach by combining Redlich-Kwong (RK) EOS[68] with Pitzer activity coefficient formulation[64] to calculate the mutual solubilities of the water-rich phase and CO_2-rich phase at a wide pressure range (0-2000 bar). This model was then extended by Zhao *et al.*[69] by considering the effect of different salts. Akinfiev and Diamond[70] developed a model for the CO_2-water-NaCl system using both Akinfiev–Diamond[71] and Hill EOSs[72] with Pitzer's formulation[64]. Springer *et al.*[73] coupled the modified mixed-solvent electrolyte thermodynamic framework with SRK EOS[43] to calculate the CO_2 solubility in pure water, NaCl, KCl and $CaCl_2$ aqueous solutions, and water solubility in the CO_2-rich phase. dos Santos *et al.*[28] established a model using PR EOS[30] and Pitzer activity coefficient formulation[64], and the performance of the

proposed model was tested using the experimental data on single-salt and mixed-salt solutions. Although Pfizer formulation is widely accepted in predicting CO_2 solubility in brine, it requires a large database of system-dependent tunable parameters[74]. In addition, the computational cost of the activity coefficients can be expensive when the Pitzer activity coefficient-based models are applied in field-scale simulations[75]. Models based on the γ-φ approach have been widely used and obtained reasonably good results. However, it should be noted that the γ-φ models cannot be used to predict the liquid phase densities and the shift from VL two-phase equilibria to LL two-phase equilibria[19, 73]. It is also worth noting that the γ-φ models are incapable of predicting CO_2 solubilities at critical and supercritical regions. When it comes to the near critical region, the calculations results will begin to deviate from the experimental data, and will not converge if temperature or pressure increases further[67]. This is most likely due to the fact that two different models are selected to model the CO_2-rich phase and the aqueous phase, and the strong non-ideality of water molecule near the critical point[67].

2.2.2.3. Empirical Correlations

Although abundant thermodynamic models have been proposed based on either the φ-φ approach or γ-φ approach, these models require iterative algorithms. In order to increase the computational efficiency, several empirical correlations are proposed based on the experimental data. Table 2-4 summarizes the correlations developed for calculating the mutual solubility of the CO_2-water/brine systems. Chang *et al.*[76] developed a correlation for predicting the solubilities of CO_2 in water and NaCl brine and obtained satisfactory results. However, this correlation was proposed based on

limited experimental data. Spycher *et al.*[15] presented a correlation to predict the mutual solubility of CO_2-water mixtures from 285.15 K-373.15 K and 0-600 bar. This model is then extended by Spycher and Pruess[77, 78] to consider the effect of chloride salts[77] and to improve the accuracy of the correlation at elevated temperatures (up to 573.15 K)[78]. Darwish and Hilal[79] proposed a correlation to calculate the solubilities of CO_2 in NaCl brine. Although this model shows good agreement with the experimental data, it requires accurate experimental data of the CO_2 solubility in pure water at different temperatures/pressures as input parameters to calculate the corresponding solubility in brine. Sun *et al.*[12] developed a correlation to calculate the mutual solubility of the CO_2-water/brine systems at 283.15 K-523.15 K and 0-2000 bar. The correlation can be also used for mixed-salt solutions, making it more advantageous and versatile than other empirical correlations. The prediction results can reproduce the mutual solubilities of the CO_2-water/brine systems, including those near the phase-transition zone. These favorable features make the model developed by Sun *et al.*[12] a preferable choice over other similar models if one wants to apply the empirical solubility models in field-scale multiphase-flow simulators.

Table 2-4 Correlations for calculating the mutual solubility of the CO_2-water/brine systems.

	Year	Temperature (K)	Pressure (bar)	Salt (s)	Salt Concentration (mol/kg)	
Chang *et al.*[76]	1996	313.15-373.15	0-758.42	Pure water		
		323.15-373.15	0-275.79	NaCl	1.901-6.012	
Spycher *et al.*[15]	2003	285.15-373.15	0-600.00	Pure water		
Spycher and Pruess[77]	2005	303.15-363.15	0-600.00	NaCl	0.500-6.000	
		349.15-374.15	0-600.00	$CaCl_2$	1.05-3.95	
Spycher and Pruess[78]	2010	285.15-573.15	1-600.00	NaCl	0-6.000	
Darwish and Hilal[79]	2010	323.15-523.15	0-2000.00	NaCl	1.000-4.000	
Sun *et al.*[12]	2021	283.15-523.15	0-2000.00	Pure water		
		278.15-573.15	1.90-600.00	NaCl	1.000-5.000	
		297.00-433.10	1.00-548.30	KCl	1.000-5.000	
		309.52-424.68	12.50-544.80	$MgCl_2$	0.750-4.290	
		308.00-424.65	15.20-712.30	$CaCl_2$	1.000-3.900	
		318.15-328.15	0-300.00	NaCl+KCl+$CaCl_2$	NaCl	0.589
					KCl	0.462
					$CaCl_2$	0.310
		318.15	0-300.00	NaCl+KCl+$CaCl_2$	NaCl	0.857
					KCl	0.672
					$CaCl_2$	0.451
		323.15	0-300.00	NaCl+KCl+$CaCl_2$+$MgCl_2$	NaCl	4.119
					KCl	0.040
					$CaCl_2$	0.212
					$MgCl_2$	0.117

2.3.Phase Behavior Measurements and Modeling for CO_2-Oil Mixtures

CO_2 flooding is a practical method that is able to not only enhance oil recovery (EOR) but also reduce the amount of greenhouse gas emissions by storing CO_2 in subsurface formations, which makes it one of the most widely used CCUS methods that combine the utilization and storage of CO_2[80]. Compared with aquifer storage sites, oil reservoirs have better seal quality due to the fact that oil reservoirs are normally bounded by cap rocks. Besides, since the pressure is low in depleted reservoirs, a significant amount of CO_2 can be stored. In addition, the solubility of CO_2 in oil is generally higher than that in water/brine. More importantly, the depleted oil reservoirs are well characterized, which makes the evaluation of the CO_2 storage capacity more straightforward than that in aquifers[81]. However, this process involves complex phase changes that may influence the effectiveness of CO_2 storage. In this section, we review the phase behavior mechanisms that appear when storing CO_2 in depleted oil reservoirs.

2.3.1. CO_2 Flooding and Minimum Miscibility Pressure (MMP)

Solvent flooding has been proved to be an effective EOR method, especially if the solvent and crude oil can reach miscibility at reservoir conditions[82]. There are different solvents that can be used as injectants in the solvent flooding process, including air, nitrogen, natural gas, CO_2, etc.[82]. CO_2 flooding is the most popular solvent flooding method due to its high oil recovery efficiency and the growing interest in CO_2 sequestration. MMP is a key parameter in the design of the CO_2 flooding process. Theoretically, if MMP could be reached, CO_2 will be completely miscible with oil and the oil recovery rate can reach 100% since there will be no residual phases[82]. In order to precisely calculate MMP, many theoretical and experimental studies have been conducted.

Different experimental methods have been proposed over the past few decades to determine MMP, including the rising bubble method, the vanishing interfacial tension method, and the slim-tube method[83, 84]. Among these experimental methods, the slim tube test is the most accepted in the petroleum industry[84]. Table 2-5 summarized the experimental studies that measure the MMPs between CO_2 and different oil samples in the range of 294.82 K- 388.71 K. These experimental studies indicate that, in general, MMP increases with an increase in temperature, the molecular weight of the C_{7+} fraction in a crude oil, and the molar ratio of the light components to medium components in a crude oil.

Table 2-5 MMP measurements between CO_2 and crude oil.

	Year	Temperature range (K)	Number of data points
Holm and O'Brien[85]	1971	330.37	1
Rathmell *et al.*[86]	1971	312.55- 358.75	3
Jacobson[87]	1972	359.82	1
Dicharry et al.[88]	1973	305.35-330.35	3
Holm and Josendal[89]	1974	294.82-360.93	9
Metcalfe and Yarborough[90]	1974	315.95	1
Yellig and Metcalfe[91]	1980	308.15-362.04	14
Spence and Watkins[92]	1980	313.20-316.00	2
Graue and Zara[93]	1981	307.55-344.26	3
Gardner *et al.*[94]	1981	316.00	1
Orr and Taber[95]	1981	305.40	1
Holm and Josendal[96]	1982	330.35	1
Metcalfe[97]	1982	391.45	1
Henry and Metcalfe[98]	1983	344.25	1
Thakur *et al.*[99]	1984	322.05	1
Alston *et al.*[100]	1985	340.95-383.15	5
Sebastian *et al.*[101]	1985	314.20	1
Husodo *et al.*[102]	1985	373.20	1
Eakin and Mitch[103]	1988	355.37-388.71	4
Chaback *et al.*[104]	1989	327.59- 377.59	4
Haynes and Alston[105]	1990	346.48	1
Khan et al.[106]	1992	313.71-316.48	2
Zuo *et al.*[107]	1993	359.20	1
Shelton and Yarborough[108]	1997	307.55	1
Xue *et al.*[109]	1997	332.15	1
Dong *et al.*[110]	2001	332.15	1
Jaubert *et al.*[111]	2002	377.55	1

Sun *et al.*[112]	2006	339.15-379.15	2
Al-Ajmi *et al.*[113]	2009	363.71-365.37	2
Li *et al.*[114]	2012	372.15-381.55	4

Although various experimental methods are capable of measuring the MMPs between CO_2 and oil at different temperatures, they are still expensive and time-consuming[114]. Therefore, many efforts have been paid to develop accurate models for MMP predictions. The MMP prediction models are mainly based on three methods: the slim tube compositional simulation method, method of characteristics (MOC) and multiple-mixing-cell method (MMC)[83]. The slim tube compositional simulation method simulates the slim tube experiment in a fine one-dimensional compositional simulation model, and the MMP can be determined by identifying the inflection point on the recovery factor curve as a function of pressure[84, 115]. Although the slim tube compositional simulation method is able to effectively and accurately determine the MMPs, this method can be computationally demanding[83]. The MOC method is developed based on the analytical solution of the *n*-1 key tie lines (*n* is the number of components in the mixture), and the MMP is considered to be reached when the length of any of the key tie lines is zero[116-119]. However, this method could converge to a wrong key tie line and thus lead to inaccurate results[83].

Compared with the slim tube compositional simulation method and the MOC method, the MMC method has a broader application scope due to its simplicity and accuracy. There are mainly two MMC approaches that are widely accepted. The first approach is a simplified version of the slim tube compositional simulation method, in which the flow dynamics in the slim tube simulation are neglected[115]. This method was first proposed by Metcalfe *et al.*[115] and later modified by Jaubert *et al.*[120]. Figure 2-3 shows the simulation workflow proposed by Jaubert *et al*.[120]. It can be seen from Figure 2-3

that the cells are connected with each other and filled with oil. A certain amount of gas is injected into the first cell. After that, a two-phase VL equilibrium calculation is conducted at given temperature and pressure conditions to calculate the excess volume of gas, which will be moved to the second cell[83]. After the first batch of injection, this process is repeated until the given volume of gas is injected. The calculation will be performed at different pressures, and the MMP is considered to be reached when the oil recovery rate is larger than 97%. Recently, Xu and Li[84] improved Jaubert *et al.*'s method[120] by introducing a new mechanism, in which a cell is divided into two equally large sub-cells to improve the computational efficiency. Xu and Li[84] also proposed a new pressure search algorithm to accurately predict MMP when the MMP between oil and injection gas is lower than the saturation pressure.

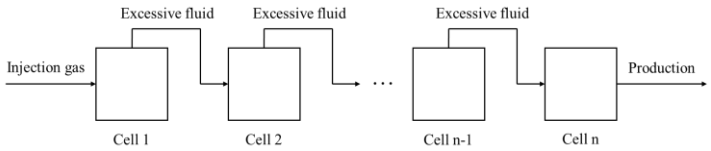

Fig. 2-3 Simulation workflow of the MMC method proposed by Jaubert *et al.*[120]. This chart is adapted from Jaubert *et al.*[120].

Ahmadi and Johns[121] proposed another MMC approach to predict the MMPs, which is independent of the relative permeability and the volume of cells and injection gas[83, 121]. In their method, the first contact happens between two cells, which are filled with oil and injection gas, respectively. Negative two-phase VL flash[122, 123] is applied during the first contact, and two more cells were subsequently obtained. Note that since the gas phase moves faster than the liquid phase, the equilibrium gas phase should always be put ahead of the liquid phase[83, 121]. After that, neighboring cells are contacted with each other until *n*-1 tie lines are obtained. This process is repeated at different pressures, and the MMP will be reached when the minimum tie-line length becomes zero. Recently, Li and Li[83] modified the MMC method by incorporating the asphaltene-precipitation

effect. Figure 2-4 shows a schematic of the modified MMC method considering the asphaltene-precipitation effect. Such modified MMC code could be used to evaluate the MMP between CO_2 and asphaltene-containing crude oils.

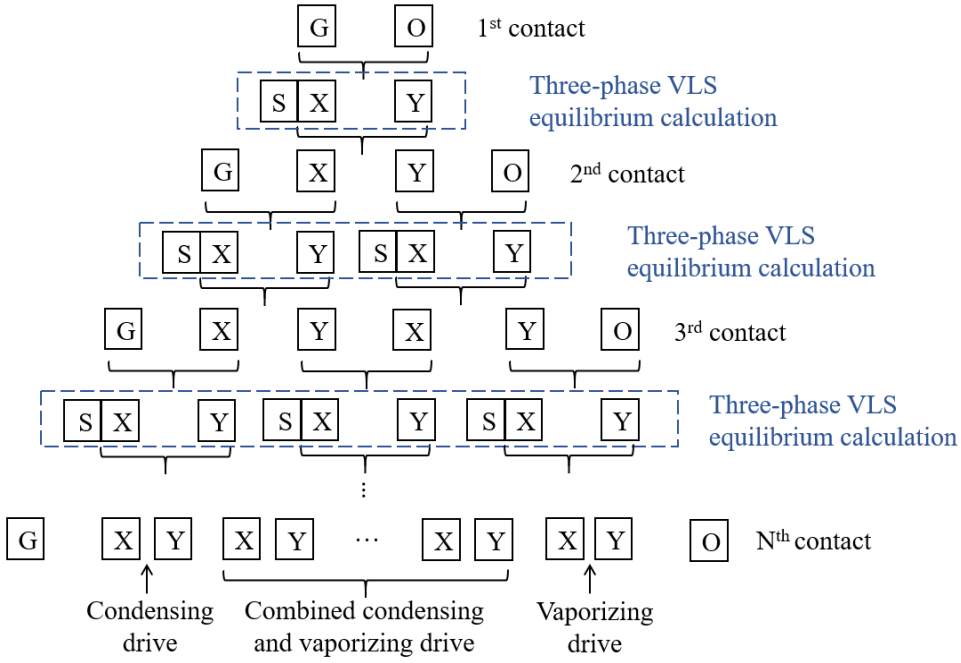

Fig. 2-4 Schematic of the modified MMC method[121] considering the asphaltene-precipitation effect[83]. G: injection gas; O: oil; X: equilibrium liquid phase; Y: equilibrium vapor phase; S: solid asphaltene phase. Reproduced with permission from ref. 83. Copyright (2019) American Chemical Society.

In order to further simplify the calculation of MMPs between CO_2 and oil, different MMP correlations are proposed based on the reservoir conditions and oil properties. Table 2-6 shows ten MMP correlations that are widely used to predict the MMPs between CO_2 and oil. It can be seen from Table 2-6 that the correlations proposed by Lee[124], Yelling and Metcalfe[91], and Orr and Jensen[125] are solely based on the reservoir temperature, while other correlations are normally also based on the molecular weight of the C_{5+}/C_{7+} component and oil compositions. It should be noted that although empirical correlations can provide a fast prediction of the CO_2-oil MMPs, the correlations are fitted based on limited experimental data. Therefore, they cannot replace the experimental and simulation methods, which could provide relatively accurate predictions of MMPs for specific scenarios. Lastly, interested readers can refer

to a recent review paper written by Dindoruk *et al.*[126] to obtain more detailed descriptions of the various aspects related to the measurement and modeling of MMP.

Table 2-6 Correlations for calculating MMPs of CO_2-oil systems. T_R: reservoir temperature; MW: molecular weight; $\boldsymbol{x_{INT}}$: mole fraction of intermediate components including CO_2, H_2S, and C_2-C_4; $\boldsymbol{x_{INT'}}$: mole fraction of intermediate components including CO_2, H_2S, and C_2-C_6; $\boldsymbol{x_{VOL}}$: mole fraction of volatile components including N_2 and CH_4; a_1-a_{10}, $\boldsymbol{A_{0n} - A_{3n}}$: empirical coefficients; $\boldsymbol{x_n}$: the nth independent variable (such as T_R).

Reference	Year	Correlation	
Cronquist[127]	1977	$MMP = 0.11027(1.8T_R + 32)^{0.744206+0.0011038MW_{C5+}+0.0015279C_1}$	
Lee[124]	1979	$MMP = 7.3924 \times 10^{2.772-[1519/(492+1.8T_R)]}$	
Yellig and Metcalfe[91]	1980	$MMP = 12.6472 + 0.01553(1.8T_R + 32) + 1.24192 \times 10^{-4}(1.8T_R + 32)^2 - \frac{716.9427}{(1.8T_R + 32)}$	
Orr and Jensen[125]	1984	$MMP = 0.101386 \times e^{[10.91-\frac{2015}{255.372+0.5556(1.8T_R+32)}]}$	
Glaso[128]	1985	$x_{INT} > 18\%$	$MMP = 5.5848 - 2.347 \times 0.01MW_{C7+} + 1.1721 \times 10^{-11}{MW_{C7+}}^{3.73}e^{786.8MW_{C7+}{}^{-1.058}}(1.8T_R + 32)$
		$x_{INT} < 18\%$	$MMP = 5.5848 - 2.347 \times 0.01MW_{C7+} + 1.1721 \times 10^{-11}{MW_{C7+}}^{3.73}e^{786.8MW_{C7+}{}^{-1.058}}(1.8T_R + 32) - 8.3564 \times 0.1x_{INT}$
Alston[100]	1985	$P_b \geq 3.45\ bar$	$MMP = 6.0536 \times 10^{-6}(1.8T_R + 32)^{1.06}(MW_{C5+})^{1.78}(\frac{x_{VOL}}{x_{INT'}})^{0.136}$
		$P_b < 3.45\ bar$	$MMP = 6.0536 \times 10^{-6}(1.8T_R + 32)^{1.06}(MW_{C5+})^{1.78}$
Emera and Sarma[129]	2004	$P_b \geq 3.45\ bar$	$MMP = 5.0093 \times 10^{-5}(1.8T_R + 32)^{1.164}(MW_{C5+})^{1.2785}(\frac{x_{VOL}}{x_{INT'}})^{0.1073}$
		$P_b < 3.45\ bar$	$MMP = 5.0093 \times 10^{-5}(1.8T_R + 32)^{1.164}(MW_{C5+})^{1.2785}$

Yuan *et al.*[130]	2005	$MMP = a_1 + a_2 MW_{C7+} - a_3 x_{INT} + \left(a_4 + a_5 MW_{C7+} + a_6 \frac{x_{INT}}{{MW_{C7+}}^2}\right)(1.8T_R + 32) + \left(a_7 + a_8 MW_{C7+} - a_9 {MW_{C7+}}^2 - a_{10} x_{INT}\right)(1.8T_R + 32)^2$
Shokir[131]	2007	$MMP = -0.068616z^3 + 0.31733z^2 + 4.9804z + 13.432$ $z = \sum_{n=1}^{8} z_n$ $z_n = A_{3n}x_n^3 + A_{2n}x_n^2 + A_{1n}x_n + A_{0n}$
Li *et al.*[114]	2012	$MMP = 7.30991 \times 10^{-5}[\ln(1.8T_R + 32)]^{5.33647}[\ln(MW_{C7+})]^{2.08836}(1 + \frac{x_{VOL}}{x_{INT}})^{0.201658}$

2.3.2. Phase Behavior Measurements and Modeling for CO_2-Oil Mixtures at Low-Temperature Reservoirs or Heavy Oil Reservoirs

The CO_2-crude oil mixtures can be commonly encountered when we try to store CO_2 in the depleted oil reservoirs. In the past, a lot of experimental efforts have been devoted to quantify the two-phase equilibria and minimum miscibility pressure of CO_2-oil mixtures. In general, the phase behavior involving only two phases is well understood. In the last several decades, it has been observed by several experimental studies that $VL_{CO2}L_{HC}$ three-phase equilibria can appear in low-temperature oil reservoirs or heavy oil reservoirs. Such low-temperature reservoirs can be found in West Texas and New Mexico in US, Alberta and Saskatchewan in Canada[86, 132]. Figure 2-5 shows some digital images of the CO_2 (83.2 mol%)-C_3H_8 (11.8 mol%)-heavy oil (5 mol%) mixture captured by Li *et al.*[133] at 298.55 K and different pressures. Their experiments tried to quantify the phase behavior mechanisms associated with the co-injection of CO_2 and C_3H_8 for heavy oil recovery in Canada. It can be observed from Figure 2-5 that the phase behavior of CO_2-crude oil mixtures at low temperatures is complex since such

mixtures may exhibit either vapor-liquid (VL) equilibrium, $L_{CO2}L_{HC}$ equilibrium or $VL_{CO2}L_{HC}$ equilibrium.

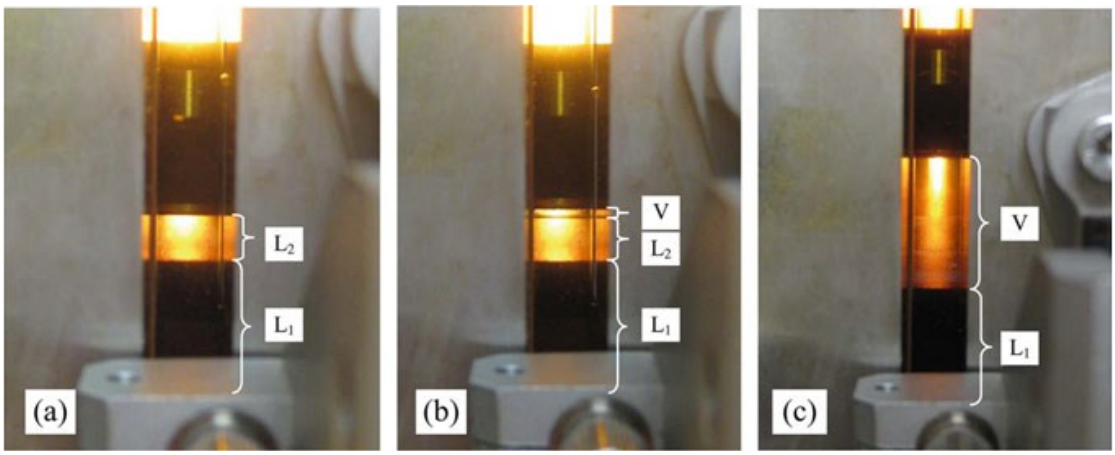

Fig. 2-5 Digital images of typical phase equilibria captured for the C_3H_8− CO_2−heavy oil system (mixture 3): (a) L_1L_2 phase equilibrium at 298.55 K and 6501 kPa, (b) L_1L_2V phase equilibrium at 298.55 K and 5538 kPa, and (c) L_1V phase equilibrium at 298.55 K and 5306 kPa. L_1: hydrocarbon-rich liquid phase; L_2: CO_2-rich liquid phase[133]. Reproduced with permission from ref. 133. Copyright (2013) American Chemical Society.

Experimental measurements of the CO_2-crude oil/hydrocarbon mixtures have been carried out for the last few decades. Table 2-7 shows an overview of the experimental studies of the CO_2-oil mixtures that measured the equilibrium phase compositions of different phases or the phase boundaries in the range of 293.15 K-322.04 K and 0 bar-558.60 bar. The appearance of two liquid phases is reported in these studies. Ideally, during CO_2 EOR and storage, we should inject CO_2 at pressures higher than the minimum miscibility pressure between CO_2 and crude oil. But if two immiscible liquid phases appear, we may not be able to achieve miscibility between CO_2 and crude oil. Hence, we have to carefully investigate how the appearance of three-phase equilibria affects the oil recovery efficiency as well as the CO_2 storage capacity via solubility trapping. Luckily, even in the case of three-phase equilibria, CO_2 can have a large solubility in the oleic phase and can extract a large amount of oleic components into the CO_2-rich phase.

Table 2-7 Phase behavior measurements of CO_2-oil/hydrocarbon mixtures.

	Year	Temperature (K)	Pressure (bar)	Phases Tested
Rathmell *et al.*[86]	1971	315.93	82.74-206.84	$VL_{CO2}L_{HC}$
Huang and Tracht[132]	1974	305.37	27.58-87.22	$VL_{CO2}L_{HC}$
Shelton and Yarborough[134]	1977	307.59	41.37-344.74	$VL_{CO2}L_{HC}$
Gardner *et al.*[94]	1981	313.71	93.08-137.90	$VL_{CO2}L_{HC}$
Orr *et al.*[135]	1981	294.26-305.37	0-206.84	$VL_{CO2}L_{HC}$
Orr and Jensen[125]	1984	305.37-322.04	0-344.74	$VL_{CO2}L_{HC}$
Li *et al.*[133]	2013	288.65-309.55	37.54-67.18	$VL_{CO2}L_{HC}$
Ghafri *et al.*[136]	2014	298.15-316.30	0.11-360.52	$VL_{CO2}L_{HC}$
Lucas *et al.*[137]	2016	293.15-313.15	55.30-250.10	$VL_{CO2}L_{HC}$
Simoncelli *et al.*[138]	2020	293.60-303.30	58.10-558.60	$VL_{CO2}L_{HC}$

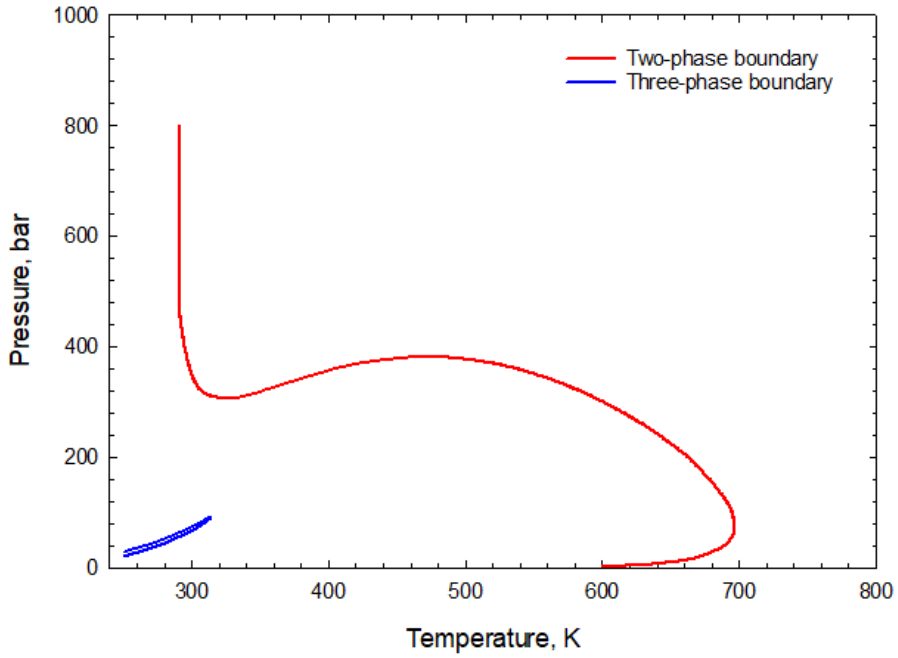

(a)

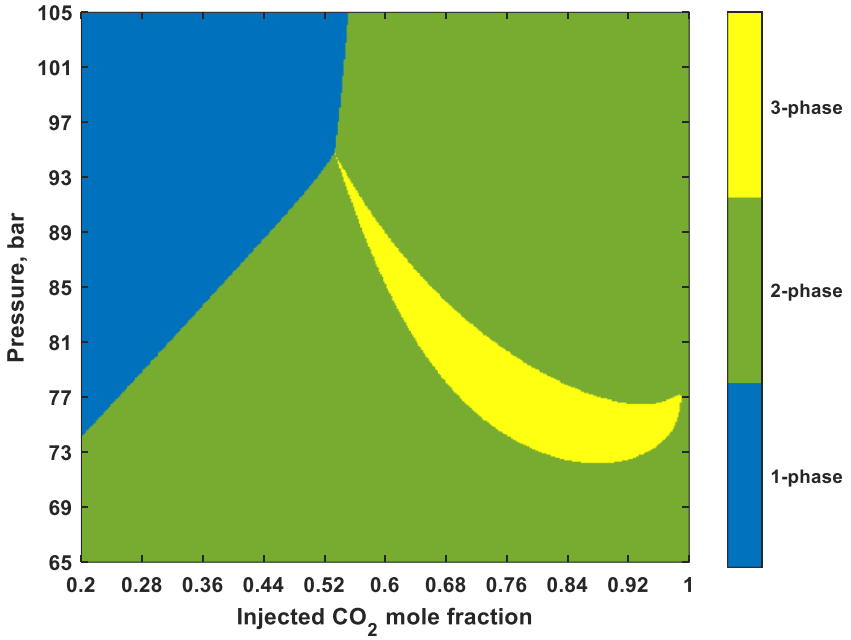

(b)

Fig. 2-6 *PT* and *Px* phase diagrams of oil sample G: (a) *PT* phase diagram with 70 mol% CO_2 injection; (b) *Px* phase diagram with CO_2 injection at 307.59 K[139]. Reproduced with permission from ref. 139. Copyright (2021) SPE.

Thermodynamic models of the CO_2-crude oil systems at low temperatures play an important role in designing the EOR and CCUS process. Figure 2-6 shows the *PT* and *Px* phase diagrams of oil sample G. The compositions of oil sample G are measured by Khan *et al.*[106]. It can be seen from Figure 2-6 that two liquid phases will appear at low temperatures during the process of CO_2 injection into the oil reservoir. Table 2-8 shows the three-phase $VL_{CO2}L_{HC}$ equilibrium calculation results of oil sample G at 75 bar and 307.59 K with 90 mol% CO_2 injection. It can be concluded from Table 2-8 that high CO_2 concentrations (92.6474411% and 60.7325336%) can be observed in both L_{CO2} and L_{HC} phases. This indicates that after the CO_2 flooding process, the residual oil left over in the reservoir has a large CO_2 storage potential.

Table 2-8 Three-phase $VL_{CO2}L_{HC}$ equilibrium calculation results of oil sample G at 75 bar and 307.59 K with 90 mol% CO_2 injection. The calculations are made using the thermodynamic model and three-phase flash algorithm presented in Lu *et al.*[162]

		Composition of the vapor phase, mol%	Composition of the lighter liquid phase, mol%	Composition of the heavier liquid phase, mol%
Phase composition	CO_2	94.6995909	92.6474411	60.7325336
	C_1	2.4110212	1.3860122	0.8468895
	C_{2-3}	1.9378638	2.3405775	3.0057743
	C_{4-6}	0.7812128	1.8633012	4.3151940
	C_{7-14}	0.1685048	1.6119065	15.0990183
	C_{15-25}	0.0018062	0.1499234	10.9727427
	C_{26+}	0.0000002	0.0008380	5.0278476
Phase fraction, mol%		10.41	41.18	48.40

Table 2-9 summarizes the thermodynamic models for the CO_2-oil/hydrocarbon mixtures. Fussell[140] developed a technique to conduct three-phase $VL_{CO2}L_{HC}$ equilibrium calculations by incorporating RK EOS[68] and minimum variable Newton-Raphson (MVNR) methods[140]. The results show that although the calculated $VL_{CO2}L_{HC}$ three-phase region is smaller than the measured one, the calculated phase boundaries have the same general trend as the measured phase boundaries. Similar research was also conducted by Mehra *et al.*[141] and Risnes and Dalen[142]. Nghiem and Li[143] proposed a more general method was using PR EOS[30]. The quasi-Newton successive-substitution (QNSS) method[144] is applied in their multiphase flash calculations, and the stability test is used to give initial guesses. The calculation results are compared with the measured ones, the performance of the proposed method is satisfactory.

Although the aforementioned methods are shown to be able to capture the phase boundaries of the CO_2-oil mixtures, convergence problems are frequently encountered in the phase equilibria calculations. In order to avoid this problem, Petitfrere and Nichita[145], Pan *et al.*[146] and Lu *et al.*[139] developed efficient and robust algorithms for three-phase $VL_{CO2}L_{HC}$ equilibrium calculations using the trust region method. Tens of millions of points are tested using these algorithms and not a single failure is encountered, which shows that these algorithms are robust and can be applied in compositional simulators for CO_2 injection in low-temperature reservoirs. A more specific review of these robust algorithms will be shown in Section 2.4.1.

Table 2-9 Thermodynamic models for the CO_2-oil/hydrocarbon mixtures.

	Year	EOS	Temperature (K)	Pressure (bar)
Fussell[140]	1979	RK	307.55	41.37-96.53
Mehra *et al.*[141]	1982	PR	294.26	0-193.05
Risnes and Dalen[142]	1984	PR+RK	294.26-307.59	40.00-100.00
Nghiem and Li[143]	1984	PR	283.15-322.04	34.47-241.32
Petitfrere and Nichita[145]	2014	PR	178.80-307.60	0-100.00
Pan *et al.*[146]	2019	PR	301.48-316.48	65.00-300.00
Lu *et al.*[139]	2021	PR	178.80-316.48	0.10-120

2.3.3. Phase Behavior Measurements and Modeling for CO_2-Asphaltic Oil Mixtures

During the process of CO_2 flooding and CO_2 storage in depleted oil reservoirs, the precipitation of asphaltene can appear frequently due to the composition change of reservoir fluids. Figure 2-7 shows the *Px* phase diagrams of an asphaltic oil with impure CO_2 (CO_2 94.45 mol%, N_2 2.68 mol%, C_1 2.87 mol%) injection generated by Li and Li[147]. The compositions of the asphaltic oil and the injection gas are measured by Srivastava *et al.*[148]. It can be seen from Figure 2-7 that the impure CO_2 injection can

significantly affect the phase behavior of reservoir fluids and induce asphaltene precipitation. Thus, the VLS three-phase equilibria must be considered to better design the CO_2 flooding and storage process.

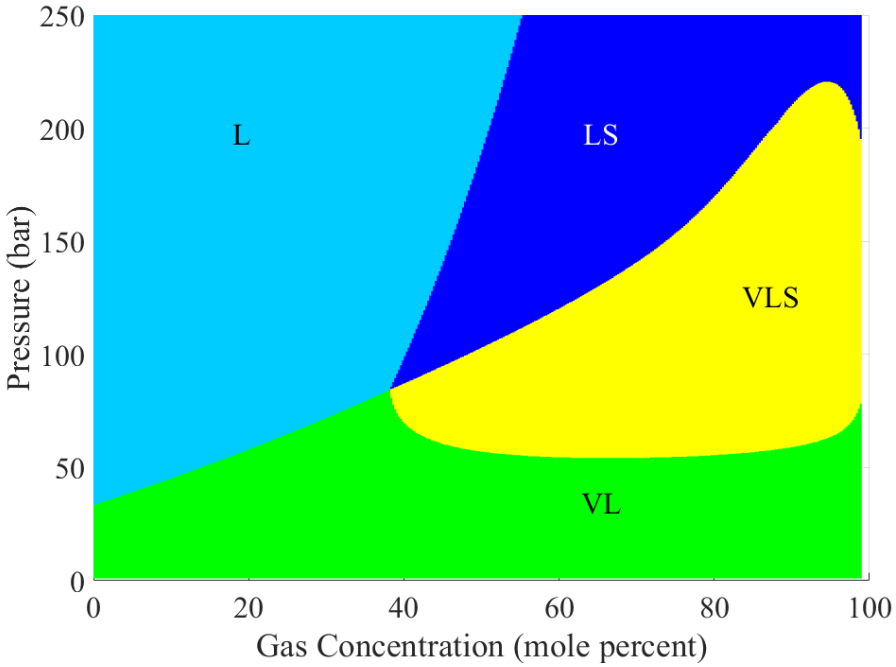

Fig. 2-7 *Px* phase diagrams of an asphaltic oil with impure CO_2[147]. Reproduced with permission from ref. 147. Copyright (2019) American Chemical Society.

2.3.3.1. Phase Behavior Measurements for CO_2-Asphaltic Oil Mixtures

The asphaltene precipitation measurements are normally conducted by using the gravimetric technique, acoustic resonance technique, light-scattering technique, filtration technique, electrical conductivity measurement technique, viscometric determination technique or through filtration experiments[149]. Table 2-10 summarizes the experimental studies about the effect of CO_2 injection on asphaltene precipitation from asphaltic crude oils in the range of 277.59 K-394.00 K, 118.31 bar-758.42 bar and 0.58 mol%-80.28 mol% CO_2. The experiments conducted by Srivastava *et al.*[148] focused on the asphaltene precipitation amount, while the experimental studies of Gonzalez *et al.*[150], Memon *et al.*[151] and Punnapala and Vargas[152] focused on the

asphaltene precipitation onsets. The experimental studies shown in Table 2-10 are of high quality and have been widely used to validate the various thermodynamic models dedicated to asphaltene precipitation prediction. It should be pointed out that the asphaltene-related phase behavior measurements on CO_2-oil mixtures are normally conducted at relatively low temperatures. More experiments should be carried out to investigate the effect of CO_2 injection on asphaltene precipitation at higher temperatures.

Table 2-10 Phase behavior measurements for CO_2-asphaltic oil mixtures.

	Year	Temperature (K)	Pressure (bar)	CO_2 Concentration (mol%)
Srivastava *et al.*[148]	1999	332.15-336.15	160.00	0.58-80.28
Gonzalez *et al.*[150]	2012	277.59-370.93	118.31-758.42	10.00
Memon *et al.*[151]	2012	363.15	247.00-440.00	6.03-15.08
Punnapala and Vargas[152]	2013	355.00-394.00	363.00-490.00	20.00-30.00

2.3.3.2.Phase Behavior Modeling for CO_2-Asphaltic Oil Mixtures

There are mainly two approaches to model asphaltene precipitation: consider the asphaltene phase as a solid phase or a high-dense liquid phase. The thermodynamic models for CO_2-asphaltic oil mixtures are summarized in Table 2-11. Punnapala and Vargas[152] developed a model using the liquid assumption for predicting asphaltene precipitation under CO_2 injection using PC-SAFT EOS[52] with a novel characterization method for asphaltene. The adjustable parameters will be further reduced compared with the method proposed by Panuganti *et al.*[153]. Arya *et al.*[154] compared the performance of SRK EOS[43], SRK EOS with Huron-Vidal mixing rule[45] and CPA EOS[47] in phase behavior modeling for CO_2-asphaltic oil mixtures by assuming asphaltene phase as a liquid phase. The results show that the Huron-Vidal mixing rule[45] has no

advantage in predicting asphaltene precipitation. Compared with SRK EOS[43], CPA EOS[47] gives a more reliable prediction of asphaltene precipitation onsets. Li and Li[147] built a robust algorithm that combines PR EOS[30] with the solid model proposed by Nghiem *et al.*[155] to calculate the vapor-liquid-asphaltene (VLS) three-phase equilibria under isothermal conditions. The algorithm is shown to be robust and efficient. The model is then improved by Chen *et al.*[156, 157] to account for the effect of temperature on asphaltene precipitation. The liquid assumption is also adopted by Abutaqiya *et al.*[158] to compare the performance of PC-SAFT EOS[52] with that of PR EOS[30] in calculating asphaltene precipitation onset pressure and concluded that results yielded by PR EOS[30] are as good as that of PC-SAFT EOS[52] if the oil samples are characterized properly.

Table 2-11 Thermodynamic models for the CO_2-asphaltic oil mixtures.

	Year	EOS	Temperature (K)	Pressure (bar)
Punnapala and Vargas[152]	2013	PC-SAFT	283.15-477.59	0-965.27
Arya *et al.*[154]	2017	SRK	250.00-500.00	0-1000.00
Arya *et al.*[154]	2017	CPA	250.00-500.00	0-1000.00
Li and Li[147]	2019	PR	332.15-373.15	0-400.00
Abutaqiya *et al.*[158]	2020	PC-SAFT	310.93-477.59	0-1034.21
Abutaqiya *et al.*[158]	2020	PR	310.93-477.59	0-1034.21
Chen *et al.*[156]	2021	PR	300.00-900.00	0-1000.00
Chen *et al.*[157]	2022	PR	300.00-1200.00	0-1300.00

2.4. Robust Multiphase Equilibrium Calculation Algorithms

2.4.1. $VL_{CO2}L_{HC}$ Three-Phase Equilibrium Calculation Algorithms

Three-phase $VL_{CO2}L_{HC}$ equilibria are very common in the process of CO_2 flooding and CO_2 storage in depleted oil reservoirs. As pointed out by Pan *et al.*[146] and Li[159], three concerns must be addressed in order to build a robust three-phase $VL_{CO2}L_{HC}$ equilibrium calculation algorithm. Firstly, good initial values of the equilibrium ratios

are necessary, especially the one related to the appearance of the second liquid phase. To solve this problem, a robust and efficient stability test must be developed[159]. Secondly, the two-phase equilibrium calculation results must be checked to prevent yielding the trivial two-phase equilibrium and thereby leading to a trivial three-phase equilibrium. This requires one to conduct two-phase flash calculations with different initial equilibrium ratios to yield the two-phase equilibrium with the minimum Gibbs free energy[147, 159]. Thirdly, a hybrid algorithm is required to ensure the robustness of the algorithm. This issue could be solved by using different equation-solving and optimization methods[159].

The first systematic multiphase flash approach was proposed by Michelsen[160]. To improve the robustness of the three-phase $VL_{CO2}L_{HC}$ equilibrium calculations, Li and Firoozabadi[161] developed a general initialization method for both stability tests and flash calculations. In traditional phase equilibrium calculations, Newton's method is normally applied with the initial value provided by the successive substitution method. Although fast convergence can be reached by using these two methods, the convergence problem can frequently appear in the near-critical regions or along with the stability test limit locus[139]. To overcome this limitation, Petitfrere and Nichita[145] proposed a trust-region method for both stability tests and flash calculations. They also suggested that the developed trust-region method should be applied when Newton's method failed[145]. Inspired by Petitfrere and Nichita's study[145], Pan *et al.*[146] proposed a trust-region-based pressure-temperature (*PT*) multiphase equilibrium calculation algorithm. Figure 2-8 shows the flow chart of this algorithm. It can be seen from Figure 2-8 that the two-phase flash is first conducted after the single-phase stability test. After that, the stability test will be conducted on both phases yielded by the previous flash calculations. If the result of the stability test is unstable, a three-phase flash will follow. Different

initialization methods will be tried if the flash calculation failed. In order to validate the robustness of the algorithm, nine different fluids were selected to generate the entire *Px* phase diagrams. Not a single failure was encountered during the calculation of tens of millions of points, which shows that the proposed algorithm is applicable in compositional simulators to model the phase behavior of CO_2-crude oil mixture in low-temperature reservoirs.

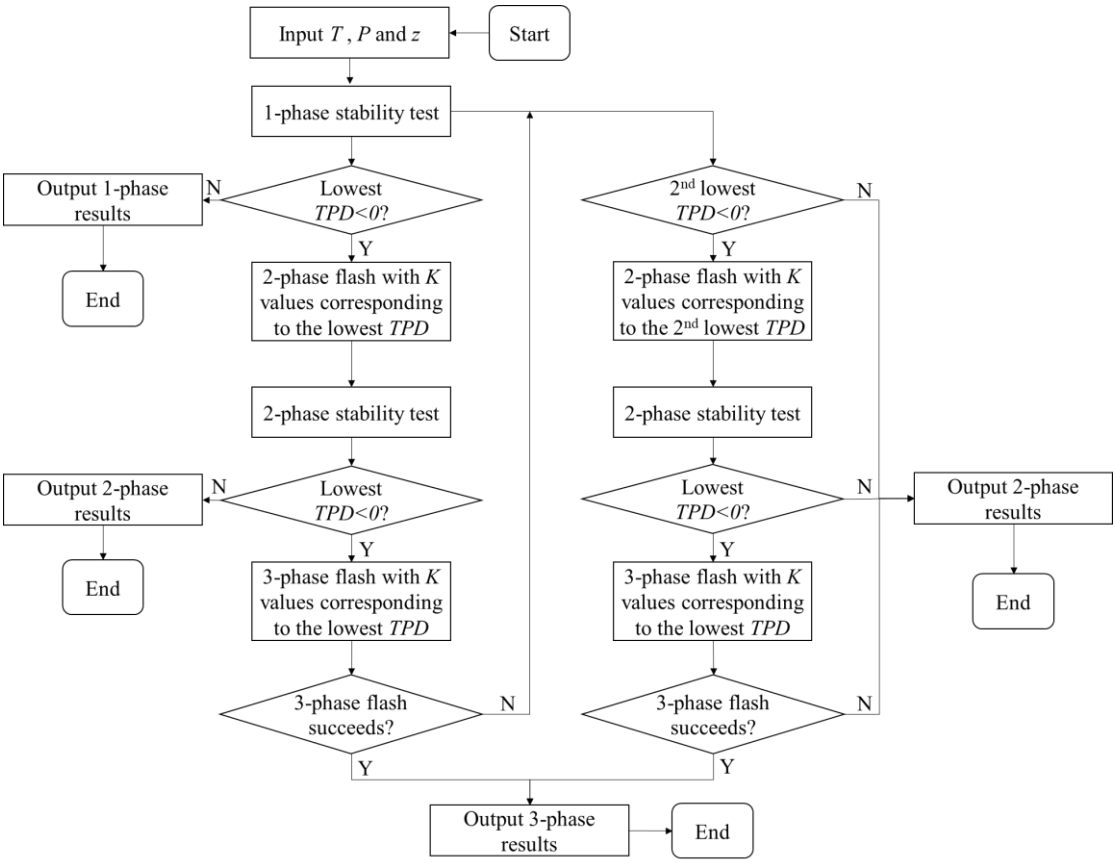

Fig. 2-8 Flowchart of the multiphase *PT* equilibrium calculation algorithm proposed by Pan *et al.*[146]. Reproduced with permission from ref. 139. Copyright (2021) SPE.

Although great strides have been made in *PT* multiphase equilibrium calculations, algorithms with volume-temperature (*VT*) specifications for the CO_2-crude oil mixture in low-temperature reservoirs are still missing. *VT* multiphase equilibrium calculation algorithms are proved to be also robust and efficient in compositional simulators[139]. Besides, such algorithms can be applied to help the design of storage tanks and the

separation process[139]. Based on the work done by Pan *et al.*[146], Lu *et al.*[139] proposed a robust *VT* multiphase equilibrium calculation algorithm to model the phase behavior CO_2-crude oil mixture in low-temperature reservoirs and the flow chart of such algorithm is shown in Figure 2-9. It can be seen from Figure 2-9 that a nested approach is applied to build such an algorithm. The trust-region-based *PT* algorithm developed by Pan *et al.*[146] is employed in the inner loop to calculate phase fractions and the compressibility factors of each phase, while Brent's method is called in the outer loop as an equation-solving algorithm to calculate the value of pressure at certain volume and temperature. This algorithm is then tested using several different reservoir fluids, and the results show that it is a robust VT three-phase equilibrium calculation algorithm.

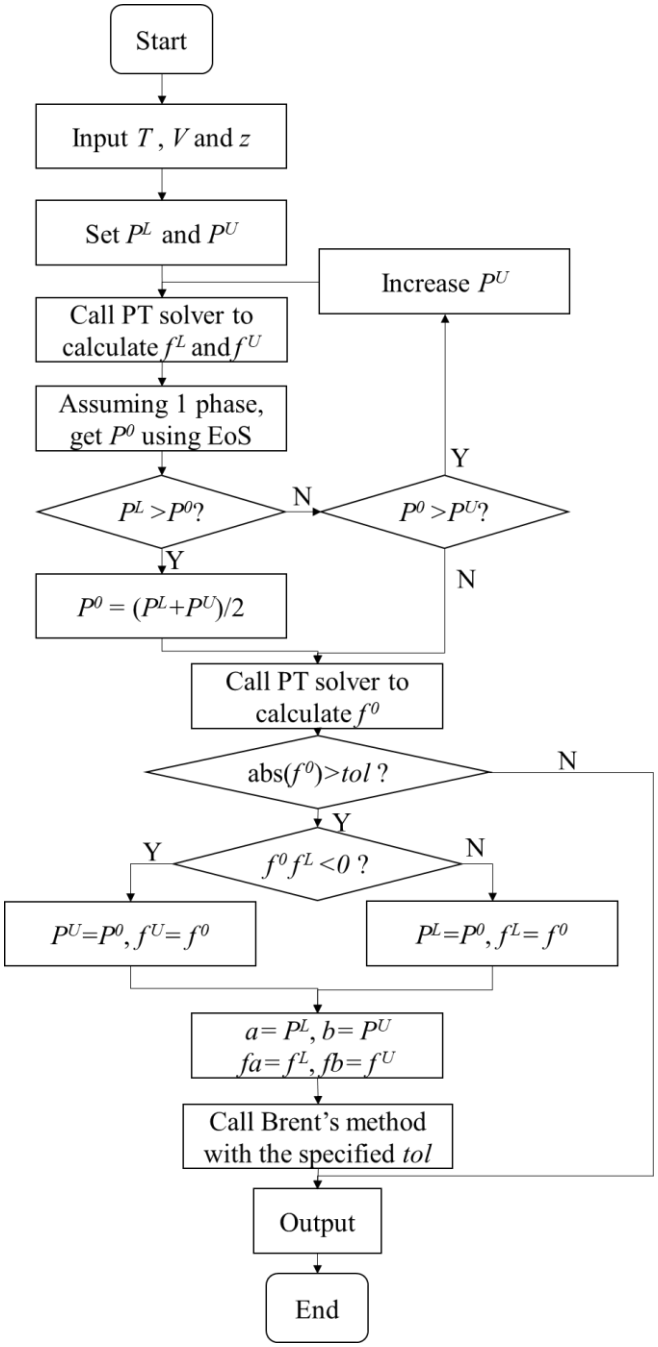

Fig. 2-9 Flowchart of the multiphase *VT* equilibrium calculation algorithm proposed by Lu *et al.*[139]. Reproduced with permission from ref. 139. Copyright (2021) SPE.

2.4.2. VLA Three-Phase Equilibrium Calculation Algorithms

The procedure of VLA three-phase equilibrium calculation is similar to that of the three-phase $VL_{CO2}L_{HC}$ equilibrium calculation. However, since the aqueous phase mainly

consists of water, the initialization method of the stability test needs to be modified, which can be shown as[161]:

$$K_i^{ST} = \left\{K_i^{Wilson}, 1/K_i^{Wilson}, \sqrt[3]{K_i^{Wilson}}, 1/\sqrt[3]{K_i^{Wilson}}, K_i^{H2O}\right\}, i = 1,2 \ldots, n_c \quad (42)$$

$$\text{where } K_i^{H2O} = \begin{cases} \frac{(1-10^{-15})}{z_i}, i = H_2O \\ \frac{(10^{-15})}{(n_c-1)z_i}, i \neq H_2O \end{cases} \quad (43)$$

Equation (43) is then modified by Connolly *et al.*[162] as:

$$K_i^{H2O} = \begin{cases} \frac{0.999}{z_i}, i = H_2O \\ \frac{0.001}{(n_c-1)z_i}, i \neq H_2O \end{cases} \quad (44)$$

To further simplify the VLA three-phase equilibrium calculation approach, the free-water assumption is proposed by Tang and Saha[163], in which the aqueous phase contains only water. However, this assumption cannot be applied if CO_2 exists in the system due to the fact that the solubility of CO_2 in the aqueous phase cannot be ignored. In this case, Pang and Li[164] developed an augmented VLA three-phase equilibrium calculation algorithm, in which the aqueous phase is considered only to contain water and CO_2. This approach is shown to be robust and more efficient than the full three-phase VLA equilibrium calculation algorithm.

2.4.3. VLS Three-Phase Equilibrium Calculation Algorithms

Compared with the three-phase $VL_{CO2}L_{HC}$ equilibrium calculation, much fewer efforts have been paid in developing robust three-phase VLS equilibrium calculation algorithms. Li and Li[147] developed an algorithm to perform robust VLS three-phase

equilibrium calculations. A new initialization method based on Li and Firoozabadi's work[161] for equilibrium ratios in stability tests is proposed:

$$K_i^{ST} = \left\{ K_i^{Wilson}, 1/K_i^{Wilson}, \sqrt[3]{K_i^{Wilson}}, 1/\sqrt[3]{K_i^{Wilson}}, K_i^{CO_2-NS}, K_i^{CO_2-S} \right\} \quad (45)$$

where K_i^{ST} represents the initial equilibrium ratio of component *i* used for stability tests.

K_i^{Wilson} represents the equilibrium ratio of component *i* calculated by Wilson equation and can be shown as[165]:

$$K_i^{Wilson} = \frac{P_{ci}}{P} exp\left[5.37(1+\omega_i)\left(1-\frac{T_{ci}}{T}\right)\right] \quad (46)$$

where P and P_{ci} represent pressure and the critical pressure of component *i*, respectively; T and T_{ci} represent temperature and the critical temperature of component *i*, respectively; and ω_i represents the acentric factor of component *i*. $K_i^{CO_2-NS}$ and $K_i^{CO_2-S}$ can be calculated by[147]:

$$K_i^{CO_2-NS} = \begin{cases} 0.8/z_i, i = 2 \\ [0.2/(c-1)]/z_i, i \neq 2 \end{cases} \quad (47)$$

$$K_i^{CO_2-S} = \begin{cases} 0.8/z_i, i = 2 \\ 10^{-8}/z_i, i = c \\ [(0.2-10^{-8})/(c-2)]/z_i, i \neq 2 \text{ and } c \end{cases} \quad (48)$$

where 2 and *c* represent components CO_2 and asphaltene, respectively. Empirical initialization methods are also proposed for flash calculations and one can refer to the original paper for details. Li and Li[147] also proposed two different VLS three-phase flash calculation algorithms and incorporated them into the VLS equilibrium calculation algorithm to enhance the robustness. This algorithm is validated by

generating *Px* phase diagrams with both pure and impure CO_2 injection and is shown to be able to converge at all test points.

2.4.4. Four-Phase Equilibrium Calculation Algorithms

Other than two-phase equilibria and three-phase equilibria, four-phase equilibria can also be relevant to the process of CO_2 storage in subsurface formations. For example, water could present when we try to store CO_2 in depleted low-temperature oil reservoirs, in which $VL_{CO2}L_{HC}A$ four-phase equilibria should be considered. $VL_{CO2}L_{HC}S$ four-phase equilibria could appear during the process of storing CO_2 in asphaltic oil reservoirs. Figure 2-10 shows the *Px* phase diagram of oil sample G with CO_2 injection. The water content in the oil sample G is set as 30 mol%. It can be seen from Figure 2-10 that the $VL_{CO2}L_{HC}A$ four-phase equilibria can also appear during the CO_2 flooding and CO_2 storage processes. Despite the fact that four-phase equilibria can be commonly encountered, much fewer studies are focusing on this research area. The most important reason is that four-phase equilibrium calculations can be much more complicated than those for the two-phase and three-phase equilibria. As pointed out by Li[159], there are four possible types of three-phase equilibria and six types of two-phase equilibria that may appear during the four-phase equilibrium calculations. Although thermodynamic models for four-phase $VL_{CO2}L_{HC}S$ equilibrium calculation are still missing, several four-phase $VL_{CO2}L_{HC}A$ equilibrium calculation algorithms have been proposed in recent years. Enick *et al.*[166] built a $VL_{CO2}L_{HC}A$ four-phase flash calculation algorithm by using a stabilized successive-substitution method. A four-phase $VL_{CO2}L_{HC}A$ equilibrium calculation algorithm was proposed by Mohebbinia *et al.*[167] using a reduced method. A complex initialization method was also developed by Mohebbinia *et al.*[167] to improve the robustness of this algorithm. Such an algorithm is proved to be much faster during the construction of the Jacobian matrix and more efficient when the fluid has a

large number of components. The reduced method was also used by Imai *et al.*[168] to conduct four-phase $VL_{CO2}L_{HC}A$ equilibrium calculations. By using the trust region method, the proposed algorithm is shown to be robust without using the initialization approach proposed by Mohebbinia *et al.*[167].

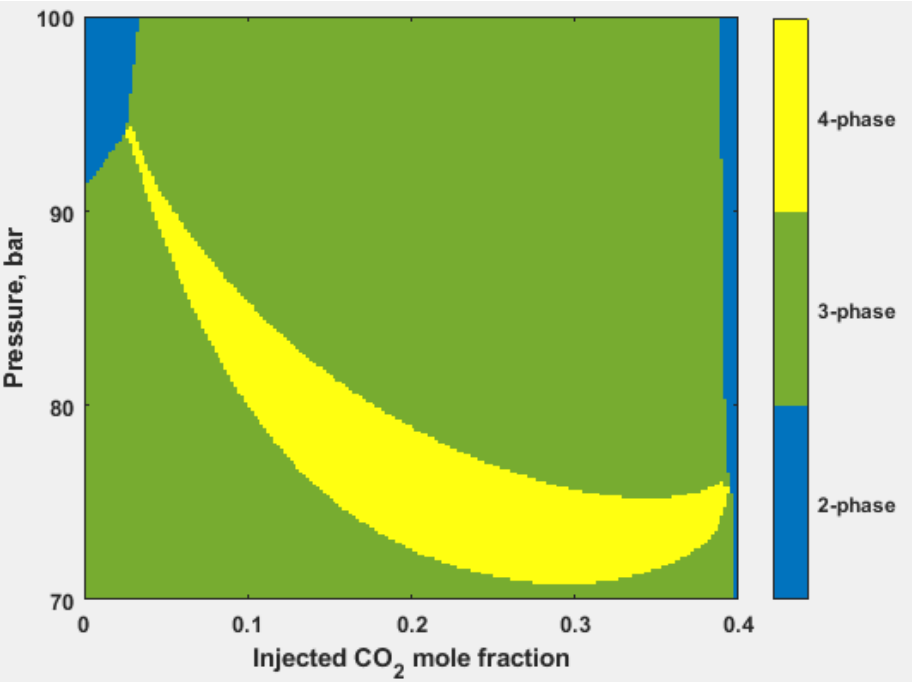

Fig. 2-10 *Px* phase diagram of oil sample G with CO_2 injection. The water content in the oil sample G is set as 30 mol%. The calculations are made using the thermodynamic model presented in Lu *et al.*[162]

2.5. Conclusions

We perform a review on the phase behavior mechanisms associated with CO_2 storage in subsurface formations. Both the experimental studies and the modeling studies are included in this review. Based on the review, the following conclusions can be drawn from the calculation results:

- Although sufficient experimental studies have been conducted to measure the solubilities of CO_2 in water, the composition of the CO_2-rich phase is still not

well characterized experimentally. Accurate measurements of the vapor phase composition are still required at different pressure/temperature conditions.

- More experimental data of CO_2 solubility in sulfate aqueous solutions at high pressure/temperature conditions and that in mixed-salt solutions are required to help develop, as well as validate, thermodynamic models dedicated to CO_2/brine mixtures.

- In general, the increase in salt concentrations yields a lower CO_2 solubility, implying that a saline aquifer with a lower salt concentration can potentially help to store more CO_2 via the solubility trapping mechanism.

- The performance of different thermodynamic models in predicting the mutual solubilities of CO_2-water/brine mixtures based on the φ-φ approach is strongly related to the selection of BIPs, α-functions and mixing rules, rather than EOSs[19].

- Thermodynamic models dedicated to predicting the solubilities of CO_2 in brine based on the φ-φ approach can only consider the effect of certain types of salts. A universal *φ*-*φ*-approach-based model remains to be developed to precisely calculate the solubility of CO_2 in different types of brine.

- The γ-φ models are incapable of predicting CO2 solubilities at critical and supercritical regions. When it comes to the near-critical region, the calculations results will begin to deviate from the experimental data, and will not converge if the temperature or pressure increases further[67].

- Compared with aquifer storage sites, oil reservoirs should normally have a better sealing quality since oil reservoirs are more often bounded by cap rocks. Besides, since the pressure is low in depleted reservoirs, a significant amount of

CO2 can be stored. Moreover, the solubility of CO_2 in oil is generally higher than that in water/brine. More importantly, the depleted oil reservoirs are well characterized, which makes the evaluation of the CO_2 storage capacity more straightforward than that in aquifers

- Three-phase $VL_{CO2}L_{HC}$ equilibria and four-phase $VL_{CO2}L_{HC}A$ equilibria can be encountered during CO_2 injection into low-temperature oil reservoirs. A high CO_2 concentration can be observed in both L_{CO2} and L_{HC} phases. This indicates that, after the CO_2 flooding process is completed, the residual oil left over in the reservoir can help store a large amount of CO_2 in the depleted reservoir.

- During the process of CO_2 flooding and CO_2 storage in asphaltic oil reservoirs, the precipitation of asphaltene can appear frequently due to the compositional change of reservoir fluids. As such, multiphase equilibria up to four phases can show up in the reservoir pore spaces. The precipitation of asphaltene can pose a significant effect on the flooding efficiency as well as the CO_2 storage efficiency.

- Although a few studies in the literature have developed thermodynamic models and algorithms dedicated to four-phase $VL_{CO2}L_{HC}A$ equilibrium calculations[169], less attention has been paid towards $VL_{CO2}L_{HC}S$ equilibria. Thus, more efforts should be made to build robust algorithms for four-phase $VL_{CO2}L_{HC}S$ equilibrium calculations. Besides, PVT experiments should be conducted to measure the four-phase equilibria that may exist and provide valuable experimental data to validate the corresponding four-phase equilibrium calculation models.

Supporting Information

The Supporting Information is available free of charge at https://pubs.acs.org/doi/10.1021/acs.iecr.2c00204.

Phase behavior measurements on CO_2-water mixtures (Table S1); phase behavior measurements on CO_2-water-single salt mixtures (Table S2); thermodynamic models for describing the phase behavior of CO_2-water/brine mixtures based on the γ-φ approach (Table S3)

Acknowledgments

The authors greatly acknowledge a Discovery Grant from the Natural Sciences and Engineering Research Council of Canada (NSERC) (Grant No.: NSERC RGPIN-2020-04571) to H. Li. Z. Chen greatly acknowledges the financial support provided by the China Scholarship Council (CSC) via a Ph.D. scholarship (No.: 201908180010). Y. Zhou greatly acknowledges the financial support provided by the China Scholarship Council (CSC) via a Ph.D. scholarship (No.: 202008180027).

References

1. Cao, C.; Liu, H.; Hou, Z.; Mehmood, F.; Liao, J.; Feng, W. A review of CO_2 storage in view of safety and cost-effectiveness. *Energies* **2020**, *13*, 600.

2. IEA., Energy technology perspectives, scenarios and strategies to 2050. 2010. Available online: www.iea.org/publications/freepublications/publication/etp2010.pdf

3. Ennis-King, J.; Paterson, L. Engineering aspects of geological sequestration of carbon dioxide. *SPE Asia Pacific Oil and Gas Conference and Exhibition*, **2002**; SPE: 2002.

4. Iglauer, S. Optimum storage depths for structural CO_2 trapping. *Int. J. Greenh. Gas Con.* **2018**, *77*, 82-87.

5. Ni, H.; Boon, M.; Garing, C.; Benson, S. M. Predicting CO_2 residual trapping ability based on experimental petrophysical properties for different sandstone types. *Int. J. Greenh. Gas Con.* **2019**, *86*, 158-176.

6. Bachu, S. CO_2 storage in geological media: Role, means, status and barriers to deployment. *Prog. Energy Combust. Sci.* **2008**, *34*, 254-273.

7. Sun, Q.; Ampomah, W.; Kutsienyo, E. J.; Appold, M.; Adu-Gyamfi, B.; Dai, Z.; Soltanian, M. R. Assessment of CO_2 trapping mechanisms in partially depleted oil-bearing sands. *Fuel* **2020**, *278*, 118356.

8. Zendehboudi, S.; Khan, A.; Carlisle, S.; Leonenko, Y. Ex situ dissolution of CO_2: a new engineering methodology based on mass-transfer perspective for enhancement of CO_2 sequestration. *Energy Fuels* **2011**, *25*, 3323-3333.

9. Ghomian, Y. Reservoir simulation studies for coupled carbon dioxide sequestration and enhanced oil recovery; The University of Texas at Austin, **2008**.

10. Sun, Z. Phase behavior modeling for carbon dioxide/brine mixtures. University of Alberta, **2021**.

11. Pérez-Salado Kamps, Á.; Meyer, E.; Rumpf, B.; Maurer, G. Solubility of CO_2 in aqueous solutions of KCl and in aqueous solutions of K_2CO_3. *J. Chem. Eng. Data* **2007**, *52*, 817-832.

12. Sun, X.; Wang, Z.; Li, H.; He, H.; Sun, B. A simple model for the prediction of mutual solubility in CO_2-brine system at geological conditions. *Desalination* **2021**, *504*, 114972.

13. Carroll, J. J.; Slupsky, J. D.; Mather, A. E. The solubility of carbon dioxide in water at low pressure. *J. Phys. Chem. Ref. Data* **1991**, *20*, 1201-1209.

14. Crovetto, R. Evaluation of solubility data of the system CO_2-H_2O from 273 K to the critical point of water. *J. Phys. Chem. Ref. Data* **1991**, *20*, 575-589.

15. Spycher, N.; Pruess, K.; Ennis-King, J. CO_2-H_2O mixtures in the geological sequestration of CO_2. I. Assessment and calculation of mutual solubilities from 12 to 100 ℃ and up to 600 bar. *Geochim. Cosmochim. Acta* **2003**, *67*, 3015-3031.

16. Mader, U. H_2O-CO_2 mixtures: A review of PVTx data and an assessment from a phase-equilibrium point of view. *Can. Mineral.* **1991**, *29*, 767-790.

17. Mather, A. E.; Franck, E. U. Phase equilibria in the system carbon dioxide-water at elevated pressures. *J. Phys. Chem.* **1992**, *96*, 6-8.

18. Blencoe, J. G.; Naney, M. T.; Anovitz, L. M. The CO_2-H_2O system: III. A new experimental method for determining liquid-vapor equilibria at high subcritical temperatures. *Am. Mineral.* **2001**, *86*, 1100-1111.

19. Aasen, A.; Hammer, M.; Skaugen, G.; Jakobsen, J. P.; Wilhelmsen, Ø. Thermodynamic models to accurately describe the PVTxy-behavior of water/carbon dioxide mixtures. *Fluid Phase Equilib.* **2017**, *442*, 125-139.

20. Drummond JR, S. E. Boiling and mixing of hydrothermal fluids: chemical effects on mineral precipitation. The Pennsylvania State University, **1981**.

21. Takenouchi, S.; Kennedy, G. C. The binary system H_2O-CO_2 at high temperatures and pressures. *Am. J. Sci.* **1964**, *262*, 1055-1074.

22. Deng, K.; Lin, Y.; Ning, H.; Liu, W.; Singh, A.; Zhang, G. Influences of temperature and pressure on CO_2 solubility in saline solutions in simulated oil and gas well environments. *Appl. Geochem.* **2018**, *99*, 22-30.

23. Yasunishi, A.; Tsuji, M.; Sada, E. Solubility of carbon dioxide in aqueous mixed-salt solutions. ACS Publications: **1979**.

24. Liu, Y.; Hou, M.; Yang, G.; Han, B. Solubility of CO_2 in aqueous solutions of NaCl, KCl, $CaCl_2$ and their mixed salts at different temperatures and pressures. *J. Supercrit. Fluids* **2011**, *56*, 125-129.

25. Tong, D.; Trusler, J. M.; Vega-Maza, D. Solubility of CO_2 in aqueous solutions of $CaCl_2$ or $MgCl_2$ and in a synthetic formation brine at temperatures up to 423 K and pressures up to 40 MPa. *J. Chem. Eng. Data* **2013**, *58*, 2116-2124.

26. Jacob, R.; Saylor, B. Z. CO_2 solubility in multi-component brines containing NaCl, KCl, $CaCl_2$ and $MgCl_2$ at 297 K and 1-14 MPa. *Chem. Geol.* **2016**, *424*, 86-95.

27. Lara Cruz, J.; Neyrolles, E.; Contamine, F. o.; Cézac, P. Experimental study of carbon dioxide solubility in sodium chloride and calcium chloride brines at 333.15 and 453.15 K for pressures up to 40 MPa. *J. Chem. Eng. Data* **2020**, *66*, 249-261.

28. dos Santos, P. F.; André, L.; Ducousso, M.; Lassin, A.; Contamine, F.; Lach, A.; Parmentier, M.; Cézac, P. An improved model for CO_2 solubility in aqueous Na^+-Cl^--SO_4^{2-} systems up to 473.15 K and 40 MPa. *Chem. Geol.* **2021**, *582*, 120443.

29. Søreide, I.; Whitson, C. H. Peng-Robinson predictions for hydrocarbons, CO_2, N_2, and H_2S with pure water and NaCl brine. *Fluid Phase Equilib.* **1992**, *77*, 217-240.

30. Peng, D. Y.; Robinson, D. B. A new two-constant equation of state. *Ind. Eng. Chem. Fundam.* **1976**, *15*, 59-64.

31. Bamberger, A.; Sieder, G.; Maurer, G. High-pressure (vapor + liquid) equilibrium in binary mixtures of (carbon dioxide + water or acetic acid) at temperatures from 313 to 353 K. *J. Supercrit. Fluids* **2000**, *17*, 97-110.

32. Melhem, G. A.; Saini, R.; Goodwin, B. M. A modified Peng-Robinson equation of state. *Fluid Phase Equilib.* **1989**, *47*, 189-237.

33. Chapoy, A.; Mohammadi, A.; Chareton, A.; Tohidi, B.; Richon, D. Measurement and modeling of gas solubility and literature review of the properties for the carbon dioxide-water system. *Ind. Eng. Chem. Res.* **2004**, *43*, 1794-1802.

34. Valderrama, J. O. A generalized Patel-Teja equation of state for polar and nonpolar fluids and their mixtures. *J. Chem. Eng. Jpn*. **1990**, *23*, 87-91.

35. Avlonitis, D.; Danesh, A.; Todd, A. Prediction of VL and VLL equilibria of mixtures containing petroleum reservoir fluids and methanol with a cubic EoS. *Fluid Phase Equilib.* **1994**, *94*, 181-216.

36. Kalorazi, B. T. Gas hydrate equilibria in the presence of electrolyte solutions. Heriot-Watt University, **1995**.

37. Valtz, A.; Chapoy, A.; Coquelet, C.; Paricaud, P.; Richon, D. Vapour-liquid equilibria in the carbon dioxide-water system, measurement and modelling from 278.2 to 318.2 K. *Fluid Phase Equilib.* **2004**, *226*, 333-344.

38. Wong, D. S. H.; Sandler, S. I. A theoretically correct mixing rule for cubic equations of state. *AIChE J.* **1992**, *38*, 671-680.

39. Mathias, P. M.; Copeman, T. W. Extension of the Peng-Robinson equation of state to complex mixtures: evaluation of the various forms of the local composition concept. *Fluid Phase Equilib.* **1983**, *13*, 91-108.

40. Zhao, H.; Lvov, S. N. Phase behavior of the CO_2-H_2O system at temperatures of 273-623 K and pressures of 0.1-200 MPa using Peng-Robinson-Stryjek-Vera equation of state with a modified Wong-Sandler mixing rule: an extension to the CO_2-CH_4-H_2O system. *Fluid Phase Equilib.* **2016**, *417*, 96-108.

41. Stryjek, R.; Vera, J. PRSV: An improved Peng-Robinson equation of state for pure compounds and mixtures. *Can. J. Chem. Eng.* **1986**, *64*, 323-333.

42. Austegard, A.; Solbraa, E.; De Koeijer, G.; Mølnvik, M. J. Thermodynamic models for calculating mutual solubilities in H_2O-CO_2-CH_4 mixtures. *Chem. Eng. Res. Des.* **2006**, *84*, 781-794.

43. Soave, G. Equilibrium constants from a modified Redlich-Kwong equation of state. *Chem. Eng. Sci.* **1972**, *27*, 1197-1203.

44. Waals, V. d. On the continuity of the gaseous and liquid states. Ph.D. Dissertation. Universiteit Leiden **1873**.

45. Huron, M.-J.; Vidal, J. New mixing rules in simple equations of state for representing vapour-liquid equilibria of strongly non-ideal mixtures. *Fluid Phase Equilib*. **1979**, *3*, 255-271.

46. Twu, C. H.; Bluck, D.; Cunningham, J. R.; Coon, J. E. A cubic equation of state with a new alpha function and a new mixing rule. *Fluid Phase Equilib.* **1991**, *69*, 33-50.

47. Kontogeorgis, G. M.; Voutsas, E. C.; Yakoumis, I. V.; Tassios, D. P. An equation of state for associating fluids. *Ind. Eng. Chem. Res.* **1996**, *35*, 4310-4318.

48. Sun, R.; Dubessy, J. Prediction of vapor–liquid equilibrium and PVTx properties of geological fluid system with SAFT-LJ EOS including multi-polar contribution. Part I: Application to H_2O-CO_2 system. *Geochim. Cosmochim. Acta* **2010**, *74*, 1982-1998.

49. Huang, S. H.; Radosz, M. Equation of state for small, large, polydisperse, and associating molecules. *Ind. Eng. Chem. Res.* **1990**, *29*, 2284-2294.

50. Kraska, T.; Gubbins, K. E. Phase equilibria calculations with a modified SAFT equation of state. 1. Pure alkanes, alkanols, and water. *Ind. Eng. Chem. Res.* **1996**, *35*, 4727-4737.

51. Li, X.; Yang, D. Determination of mutual solubility between CO_2 and water by using the Peng-Robinson equation of state with modified alpha function and binary interaction parameter. *Ind. Eng. Chem. Res.* **2013**, *52*, 13829-13838.

52. Gross, J.; Sadowski, G. Perturbed-chain SAFT: An equation of state based on a perturbation theory for chain molecules. *Ind. Eng. Chem. Res.* **2001**, *40*, 1244-1260.

53. Tsivintzelis, I.; Kontogeorgis, G. M.; Michelsen, M. L.; Stenby, E. H. Modeling phase equilibria for acid gas mixtures using the CPA equation of state. Part II: Binary mixtures with CO_2. *Fluid Phase Equilib.* **2011**, *306*, 38-56.

54. Chabab, S.; Théveneau, P.; Corvisier, J.; Coquelet, C.; Paricaud, P.; Houriez, C.; El Ahmar, E. Thermodynamic study of the CO_2-H_2O-NaCl system: Measurements of CO_2 solubility and modeling of phase equilibria using Soreide and Whitson, electrolyte CPA and SIT models. *Int. J. Greenh. Gas Con.* **2019**, *91*, 102825.

55. Hou, S. X.; Maitland, G. C.; Trusler, J. M. Phase equilibria of (CO_2 +H_2O+NaCl) and (CO_2 +H_2O+KCl): Measurements and modeling. *J. Supercrit. Fluids* **2013**, *78*, 78-88.

56. Bermejo, M.; Martín, A.; Florusse, L.; Peters, C.; Cocero, M. The influence of Na_2SO_4 on the CO_2 solubility in water at high pressure. *Fluid Phase Equilib.* **2005**, *238*, 220-228.

57. Anderko, A.; Pitzer, K. S. Equation-of-state representation of phase equilibria and volumetric properties of the system NaCl-H_2O above 573 K. *Geochim. Cosmochim. Acta* **1993**, *57*, 1657-1680.

58. Kosinski, J. J.; Anderko, A. Equation of state for high-temperature aqueous electrolyte and nonelectrolyte systems. *Fluid Phase Equilib.* **2001**, *183*, 75-86.

59. Sun, R.; Dubessy, J. Prediction of vapor-liquid equilibrium and PVTx properties of geological fluid system with SAFT-LJ EOS including multi-polar contribution. Part II: Application to H_2O-NaCl and CO_2-H_2O-NaCl System. *Geochim. Cosmochim. Acta* **2012**, *88*, 130-145.

60. Li, Y. K.; Nghiem, L. X. Phase equilibria of oil, gas and water/brine mixtures from a cubic equation of state and Henry's law. *Can. J. Chem. Eng.* **1986**, *64*, 486-496.

61. Henry, W. III. Experiments on the quantity of gases absorbed by water, at different temperatures, and under different pressures. *Philos. Trans. R. Soc. Lond.* **1803**, *93*, 29-274.

62. Lebowitz, J. L.; Helfand, E.; Praestgaard, E. Scaled particle theory of fluid mixtures. *J. Chem. Phys.* **1965**, *43*, 774-779.

63. Duan, Z.; Sun, R. An improved model calculating CO_2 solubility in pure water and aqueous NaCl solutions from 273 to 533 K and from 0 to 2000 bar. *Chem. Geol.* **2003**, *193*, 257-271.

64. Pitzer, K. S. Thermodynamics of electrolytes. I. Theoretical basis and general equations. *J. Phys. Chem.* **1973**, *77*, 268-277.

65. Duan, Z.; Møller, N.; Greenberg, J.; Weare, J. H. The prediction of methane solubility in natural waters to high ionic strength from 0 to 250 °C and from 0 to 1600 bar. *Geochim. Cosmochim. Acta* **1992**, *56*, 1451-1460.

66. Duan, Z.; Sun, R.; Zhu, C.; Chou, I. M. An improved model for the calculation of CO_2 solubility in aqueous solutions containing Na^+, K^+, Ca^{2+}, Mg^{2+}, Cl^-, and SO_4^{2-}. *Mar. Chem.* **2006**, *98*, 131-139.

67. Zhao, H.; Fedkin, M. V.; Dilmore, R. M.; Lvov, S. N. Carbon dioxide solubility in aqueous solutions of sodium chloride at geological conditions: Experimental results at 323.15, 373.15, and 423.15 K and 150 bar and modeling up to 573.15 K and 2000 bar. *Geochim. Cosmochim. Acta* **2015**, *149*, 165-189.

68. Redlich, O.; Kwong, J. N. On the thermodynamics of solutions. V. An equation of state. Fugacities of gaseous solutions. *Chem. Rev.* **1949**, *44*, 233-244.

69. Zhao, H.; Dilmore, R. M.; Lvov, S. N. Experimental studies and modeling of CO_2 solubility in high temperature aqueous $CaCl_2$, $MgCl_2$, Na_2SO_4, and KCl solutions. *AIChE J.* **2015**, *61*, 2286-2297.

70. Akinfiev, N. N.; Diamond, L. W. Thermodynamic model of aqueous CO_2-H_2O-NaCl solutions from -22 to 100 °C and from 0.1 to 100 MPa. *Fluid Phase Equilib.* **2010**, *295*, 104-124.

71. Akinfiev, N. N.; Diamond, L. W. Thermodynamic description of aqueous nonelectrolytes at infinite dilution over a wide range of state parameters. *Geochim. Cosmochim. Acta* **2003**, *67*, 613-629.

72. Hill, P. G. A unified fundamental equation for the thermodynamic properties of H_2O. *J. Phys. Chem. Ref. Data* **1990**, *19*, 1233-1274.

73. Springer, R. D.; Wang, Z.; Anderko, A.; Wang, P.; Felmy, A. R. A thermodynamic model for predicting mineral reactivity in supercritical carbon dioxide: I. Phase behavior of carbon dioxide-water-chloride salt systems across the H_2O-rich to the CO_2-rich regions. *Chem. Geol.* **2012**, *322*, 151-171.

74. Møller, N. The prediction of mineral solubilities in natural waters: A chemical equilibrium model for the Na-Ca-Cl-SO_4-H_2O system, to high temperature and concentration. *Geochim. Cosmochim. Acta* **1988**, *52*, 821-837.

75. Beygi, M. R.; Delshad, M.; Wheeler, M. F.; Pope, G. A. Aqueous phase relative permeability from a unified thermodynamics-petrophysics-geochemistry-electrolyte model. *SPE Western Regional Meeting*, **2016**; SPE: 2016.

76. Chang, Y. B.; Coats, B. K.; Nolen, J. S. In A compositional model for CO_2 floods including CO_2 solubility in water, *Permian Basin Oil and Gas Recovery Conference*, **1996**; SPE: 1996.

77. Spycher, N.; Pruess, K. CO_2-H_2O mixtures in the geological sequestration of CO_2. II. Partitioning in chloride brines at 12-100 °C and up to 600 bar. *Geochim. Cosmochim. Acta* **2005**, *69*, 3309-3320.

78. Spycher, N.; Pruess, K. A phase-partitioning model for CO_2-brine mixtures at elevated temperatures and pressures: application to CO_2-enhanced geothermal systems. *Transp. Porous Media* **2010**, *82*, 173-196.

79. Darwish, N.; Hilal, N. A simple model for the prediction of CO_2 solubility in H_2O-NaCl system at geological sequestration conditions. *Desalination* **2010**, *260*, 114-118.

80. Eshraghi, S. E.; Rasaei, M. R.; Zendehboudi, S. J. Optimization of miscible CO_2 EOR and storage using heuristic methods combined with capacitance/resistance and Gentil fractional flow models. *J. Nat. Gas Sci. Eng.* **2016**, *32*, 304-318.

81. Liao, C.; Liao, X.; Zhao, X.; Ding, H.; Liu, X.; Liu, Y.; Chen, J.; Lu, N. J. Comparison of different methods for determining key parameters affecting CO_2 storage capacity in oil reservoirs. *Int. J. Greenh. Gas Control.* **2014**, *28*, 25-34.

82. Lake, L. W.; Johns, R.; Rossen, B.; Pope, G. A. Fundamentals of enhanced oil recovery; Society of Petroleum Engineers Richardson, TX, **2014**, pp: 319-380.

83. Li, R.; Li, H. A modified multiple-mixing-cell algorithm for minimum miscibility pressure prediction with the consideration of the asphaltene-precipitation effect. *Ind. Eng. Chem. Res.* **2019**, *58*, 15332-15343.

84. Xu, L.; Li, H. A modified multiple-mixing-cell method with sub-cells for MMP determinations. *Energies* **2021**, *14*, 7846.

85. Holm, L.; O'Brien, L. Carbon dioxide test at the Mead-Strawn Field. *J. Pet. Technol.* **1971**, *23*, 431-442.

86. Rathmell, J.; Stalkup, F.; Hassinger, R. A. laboratory investigation of miscible displacement by carbon dioxide. *Fall Meeting of the Society of Petroleum Engineers of AIME*, **1971**; SPE: 1971.

87. Jacobson, H. Acid gases and their contribution to miscibility. *J. Can. Pet. Technol.* **1972**, *11*, 56-59.

88. Dicharry, R. M.; Perryman, T.; Ronquille, J. Evaluation and design of a CO_2 miscible flood project-SACROC unit, Kelly-Snyder field. *J. Pet. Technol.* **1973**, *25*, 1309-1318.

89. Holm, L.; Josendal, V. Mechanisms of oil displacement by carbon dioxide. *J. Pet. Technol.* **1974**, *26*, 1427-1438.

90. Metcalfe, R.; Yarborough, L. Discussion of mechanisms of oil displacement by carbon dioxide. *J. Pet. Technol.* **1974**, *26*, 1436-1437.

91. Yellig, W.; Metcalfe, R. Determination and prediction of CO_2 minimum miscibility pressures (includes associated paper 8876). *J. Pet. Technol.* **1980**, 32, 160-168.

92. Spence, A. P.; Watkins, R. W. The effect of microscopic core heterogeneity on miscible flood residual oil saturation. *SPE Annual Technical Conference and Exhibition*, **1980**; SPE: 1980.

93. Graue, D. J.; Zana, E. Study of a possible CO_2 flood in Rangely Field. *J. Pet. Technol.* **1981**, *33*, 1312-1318.

94. Gardner, J.; Orr, F.; Patel, P. The effect of phase behavior on CO_2-flood displacement efficiency. *J. Pet. Technol.* **1981**, *33*, 2067-2081.

95. Orr Jr, F.; Taber, J. J. Displacement of oil by carbon dioxide. Final report; New Mexico Inst. of Mining and Technology, Socorro (USA), **1981**.

96. Holm, L. W.; Josendal, V. A. Effect of oil composition on miscible-type displacement by carbon dioxide. *SPE J.* **1982**, *22*, 87-98.

97. Metcalfe, R. S. Effects of impurities on minimum miscibility pressures and minimum enrichment levels for CO_2 and rich-gas displacements. *SPE J.* **1982**, *22*, 219-225.

98. Henry, R. L.; Metcalfe, R. S. Multiple-phase generation during carbon dioxide flooding. *SPE J.* **1983**, *23*, 595-601.

99. Thakur, G.; Lin, C.; Patel, Y. CO_2 minitest, little knife field, ND: a case history. *SPE enhanced oil recovery symposium*, **1984**; SPE: 1984.

100. Alston, R.; Kokolis, G.; James, C. CO_2 minimum miscibility pressure: a correlation for impure CO_2 streams and live oil systems. *SPE J.* **1985**, *25*, 268-274.

101. Sebastian, H.; Wenger, R.; Renner, T. Correlation of minimum miscibility pressure for impure CO_2 streams. *J. Pet. Technol.* **1985**, *37*, 2076-2082.

102. Husodo, W.; Sudibjo, R.; Walsh, B. W. Laboratory experiment on CO_2 injection. *14th Annual Convention Proceedings*, **1985**, 141-156; AAPG: 1985.

103. Eakin, B.; Mitch, F. Measurement and correlation of miscibility pressures of reservoir oils. *SPE Annual Technical Conference and Exhibition*, **1988**; SPE: 1988.

104. Chaback, J.; Harmon, R.; Grigg, R. Discussion of vapor-density measurement for estimating minimum miscibility pressure. *SPE Res. Eng.* **1989**, *4*, 253-254.

105. Haynes, S.; Alston, R. Study of the mechanisms of carbon dioxide flooding and applications to more efficient EOR projects. *SPE/DOE Enhanced Oil Recovery Symposium*, **1990**; SPE: 1990.

106. Khan, S.; Pope, G.; Sepehrnoori, K. Fluid characterization of three-phase CO_2/oil mixtures. *SPE/DOE Enhanced Oil Recovery Symposium*, **1992**; SPE: 1992.

107. Zuo, Y. X.; Chu, J. Z.; Ke, S. L.; Guo, T. M., A study on the minimum miscibility pressure for miscible flooding systems. *J. Pet. Sci. Eng.* **1993**, *8*, 315-328.

108. Shelton, J. L.; Yarborough, L. Multiple phase behavior in porous media during CO_2 or rich-gas flooding. *J. Pet. Technol.* **1977**, *29*, 1171-1178.

109. Xue, G.; Datta-Gupta, A.; Valko, P.; Blasingame, T. Optimal transformations for multiple regression: application to permeability estimation from well logs. *SPE Form. Evaluation* **1997**, *12*, 85-94.

110. Dong, M.; Huang, S.; Dyer, S. B.; Mourits, F. M. A comparison of CO_2 minimum miscibility pressure determinations for Weyburn crude oil. *J. Pet. Sci. Eng.* **2001**, *31*, 13-22.

111. Jaubert, J. N.; Avaullee, L.; Souvay, J. F. A crude oil data bank containing more than 5000 PVT and gas injection data. *J. Pet. Sci. Eng.* **2002**, *34*, 65-107.

112. Sun, Y. H.; Lv, G. Z.; Wang, Y. F.; Dong, A. Q. A method of state equation for determining minimum miscible pressure of CO_2. *Pet. Geol. Recovery Efficiency.* **2006**, *13*, 82−84 (in Chinese)

113 Al-Ajmi, M. F.; Alomair, O. A.; Elsharkawy, A. M. Planning miscibility tests and gas injection projects for four major Kuwaiti reservoirs. *Kuwait international petroleum conference and exhibition*, **2009**; SPE: 2009.

114. Li, H.; Qin, J.; Yang, D. An improved CO_2-oil minimum miscibility pressure correlation for live and dead crude oils. *Ind. Eng. Chem. Res.* **2012**, *51*, 3516-3523.

115. Metcalfe, R.; Fussell, D.; Shelton, J. A multicell equilibrium separation model for the study of multiple contact miscibility in rich-gas drives. *SPE J.* **1973**, *13*, 147-155.

116. Jessen, K.; Michelsen, M. L.; Stenby, E. H. Global approach for calculation of minimum miscibility pressure. *Fluid Phase Equilib.* **1998**, *153*, 251-263.

117. Johns, R. T.; Dindoruk, B.; Orr, F. Analytical theory of combined condensing/vaporizing gas drives. *SPE Adv. Technol. Ser.* **1993**, *1*, 7-16.

118. Johns, R. T.; Orr, F. M. Miscible gas displacement of multicomponent oils. *SPE J.* **1996**, *1*, 39-50.

119. Wang, Y.; Orr Jr, F. M. Analytical calculation of minimum miscibility pressure. *Fluid Phase Equilib.* **1997**, *139*, 101-124.

120. Jaubert, J.-N.; Wolff, L.; Neau, E.; Avaullee, L. A very simple multiple mixing cell calculation to compute the minimum miscibility pressure whatever the displacement mechanism. *Ind. Eng. Chem. Res.* **1998**, *37*, 4854-4859.

121. Ahmadi, K.; Johns, R. T. Multiple-mixing-cell method for MMP calculations. *SPE J.* **2011**, *16*, 733-742.

122. Leibovici, C. F.; Nichita, D. V. A new look at multiphase Rachford-Rice equations for negative flashes. *Fluid Phase Equilib.* **2008**, *267*, 127-132.

123. Whitson, C. H.; Michelsen, M. L. The negative flash. *Fluid Phase Equilib.* **1989**, *53*, 51-71.

124. Lee, I. Effectiveness of carbon dioxide displacement under miscible and immiscible conditions. *Technical Report*, **1979**, Report Number: PRI-7910; CE-02239.

125. Orr, F.; Jensen, C. Interpretation of pressure-composition phase diagrams for CO_2/crude-oil systems. *SPE J.* **1984**, *24*, 485-497.

126. Dindoruk, B.; Johns, R.; Orr, F. M. Measurement and modeling of minimum miscibility pressure: A state-of-the-art review. *SPE Reserv. Evaluation Eng*. **2021**, *24*, 367-389.

127. Cronquist, C. Carbon dioxide dynamic miscibility with light reservoir oils. *Proc. Fourth Annual US DOE Symposium*, Tulsa, **1978**; Vol. 1, pp: 28-30.

128. Glaso, O. Generalized minimum miscibility pressure correlation (includes associated papers 15845 and 16287). *SPE J.* **1985**, *25*, 927-934.

129. Emera, M. K.; Sarma, H. K. Use of genetic algorithm to estimate CO_2–oil minimum miscibility pressure-a key parameter in design of CO_2 miscible flood. *J. Pet. Sci. Eng.* **2005**, *46*, 37-52.

130. Yuan, H.; Johns, R. T. Simplified method for calculation of minimum miscibility pressure or enrichment. *SPE J.* **2005**, *10*, 416-425.

131. Shokir, E. M. E. M. CO_2–oil minimum miscibility pressure model for impure and pure CO_2 streams. *J. Pet. Sci. Eng.* **2007**, *58*, 173-185.

132. Huang, E. T.; Tracht, J. H. The displacement of residual oil by carbon dioxide, *SPE Improved Oil Recovery Symposium*, **1974**; SPE: 1974.

133. Li, H.; Yang, D.; Li, X. Determination of three-phase boundaries of solvent (s)-CO_2-heavy oil systems under reservoir conditions. *Energy Fuels* **2013**, *27*, 145-153.

134. Shelton, J.; Yarborough, L. Multiple phase behavior in porous media during the displacement of residual oil by carbon dioxide or rich-gas flooding. *J. Pet. Technol.* **1977**, *29*, 1171-1178.

135. Orr, F.; Yu, A.; Lien, C. Phase behavior of CO_2 and crude oil in low-temperature reservoirs. *SPE J.* **1981**, *21*, 480-492.

136. Al Ghafri, S. Z.; Maitland, G. C.; Trusler, J. M. Experimental and modeling study of the phase behavior of synthetic crude oil + CO_2. *Fluid Phase Equilib.* **2014**, *365*, 20-40.

137. Lucas, M. A.; Borges, G. R.; da Rocha, I. C.; Santos, A. F.; Franceschi, E.; Dariva, C. Use of real crude oil fractions to describe the high pressure phase behavior of crude oil in carbon dioxide. *J. Supercrit. Fluids* **2016**, *118*, 140-147.

138. Simoncelli, A. P.; Goméz, W.; Charin, R. M.; Fleming, F. P.; Ndiaye, P. M.; Tavares, F. W. Phase behavior of systems with high CO_2 content: Experiments and thermodynamic modeling. *Fluid Phase Equilib.* **2020**, *515*, 112574.

139. Lu, C.; Jin, Z.; Li, H.; Xu, L. Simple and robust algorithm for multiphase equilibrium computations at temperature and volume specifications. *SPE J.* **2021**, *26*, 1-20.

140. Fussell, L. T. A technique for calculating multiphase equilibria (includes associated papers 8734 and 8746). *SPE J.* **1979**, *19*, 203-210.

141. Mehra, R. K.; Heidemann, R. A.; Aziz, K. Computation of multiphase equilibrium for compositional simulation. *SPE J.* **1982**, *22*, 61-68.

142. Risnes, R.; Dalen, V. Equilibrium calculations for coexisting liquid phases. *SPE J.* **1984**, *24*, 87-96.

143. Nghiem, L. X.; Li, Y. K. Computation of multiphase equilibrium phenomena with an equation of state. *Fluid Phase Equilib.* **1984**, *17*, 77-95.

144. Nghiem, L.; Heidemann, R. In General acceleration procedure for multiphase flash calculation with application to oil-gas-water systems, *Proceedings of the 2nd European Symposium on Enhanced Oil Recovery*, **1982**; pp 303-316.

145. Petitfrere, M.; Nichita, D. V. Robust and efficient trust-region based stability analysis and multiphase flash calculations. *Fluid Phase Equilib.* **2014**, *362*, 51-68.

146. Pan, H.; Connolly, M.; Tchelepi, H. Multiphase equilibrium calculation framework for compositional simulation of CO_2 injection in low-temperature reservoirs. *Ind. Eng. Chem. Res.* **2019**, *58*, 2052-2070.

147. Li, R.; Li, H. Robust three-phase vapor-liquid-asphaltene equilibrium calculation algorithm for isothermal CO_2 flooding applications. *Ind. Eng. Chem. Res.* **2019**, *58*, 15666-15680.

148. Srivastava, R.; Huang, S.; Dong, M. Asphaltene deposition during CO_2 flooding. *SPE Prod. Facil.* **1999**, *14*, 235-245.

149. Pedersen, K. S.; Christensen, P. L.; Shaikh, J. A.; Christensen, P. L. Phase behavior of petroleum reservoir fluids. CRC press: **2006**.

150. Gonzalez, D. L.; Mahmoodaghdam, E.; Lim, F.; Joshi, N. Effects of gas additions to deepwater Gulf of Mexico reservoir oil: Experimental investigation of asphaltene precipitation and deposition, *SPE Annual Technical Conference and Exhibition*, **2012**; SPE: 2012.

151. Memon, A.; Qassim, B.; Al Ajmi, M.; Kumar Tharanivasan, A.; Gao, J.; Ratulowski, J.; Al-Otaibi, B.; Khan, R. A. Miscible gas injection and asphaltene flow assurance fluid characterization: A laboratory case study for a black oil reservoir, *SPE EOR Conference at Oil and Gas West Asia*, **2012**; SPE: 2012.

152. Punnapala, S.; Vargas, F. M. Revisiting the PC-SAFT characterization procedure for an improved asphaltene precipitation prediction. *Fuel* **2013**, *108*, 417-429.

153. Panuganti, S. R.; Vargas, F. M.; Gonzalez, D. L.; Kurup, A. S.; Chapman, W. G. PC-SAFT characterization of crude oils and modeling of asphaltene phase behavior. *Fuel* **2012**, *93*, 658-669.

154. Arya, A.; Liang, X.; von Solms, N.; Kontogeorgis, G. M. Prediction of gas injection effect on asphaltene precipitation onset using the cubic and cubic-plus-association equations of state. *Energy Fuels* **2017**, *31*, 3313-3328.

155. Nghiem, L.; Hassam, M.; Nutakki, R.; George, A. Efficient modelling of asphaltene precipitation, *SPE Annual Technical Conference and Exhibition*, **1993**; SPE: 1993.

156. Chen, Z.; Li, R.; Li, H. An improved vapor-liquid-asphaltene three-phase equilibrium computation algorithm. *Fluid Phase Equilib.* **2021**, *537*, 113004.

157. Chen, Z.; Li, R.; Li, H. A new vapor-liquid-asphaltene three-phase equilibrium computation algorithm based on the free-asphaltene assumption. *Fluid Phase Equilib.* **2022**, 113392.

158. Abutaqiya, M. I.; Sisco, C. J.; Khemka, Y.; Safa, M. A.; Ghloum, E. F.; Rashed, A. M.; Gharbi, R.; Santhanagopalan, S.; Al-Qahtani, M.; Al-Kandari, E. Accurate modeling of asphaltene onset pressure in crude oils under gas injection using Peng-Robinson equation of state. *Energy Fuels* **2020**, *34*, 4055-4070.

159. Li, H. Multiphase equilibria of complex reservoir fluids: An equation of state modeling approach. Springer Nature: **2021**, pp: 163-202.

160. Michelsen, M. L. The isothermal flash problem. Part II. Phase-split calculation. *Fluid Phase Equilib.* **1982**, *9*, 21-40.

161. Li, Z.; Firoozabadi, A. General strategy for stability testing and phase-split calculation in two and three phases. *SPE J.* **2012**, *17*, 1096-1107.

162. Connolly, M.; Pan, H.; Tchelepi, H. Three-phase equilibrium computations for hydrocarbon-water mixtures using a reduced variables method. *Ind. Eng. Chem. Res.* **2019**, *58*, 14954-14974.

163. Tang, Y.; Saha, S. An efficient method to calculate three-phase free-water flash for water-hydrocarbon systems. *Ind. Eng. Chem. Res.* **2003**, *42*, 189-197.

164. Pang, W.; Li, H. A. An augmented free-water three-phase Rachford-Rice algorithm for CO_2/hydrocarbons/water mixtures. *Fluid Phase Equilib.* **2017**, *450*, 86-98.

165. Wilson, G. A modified Redlich–Kwong EOS, application to general physical data calculations, *AIChE 65th National Meeting*, **1968**.

166. Enick, R. M., Klara, S. M. CO_2 solubility in water and brine under reservoir conditions. *Chem. Eng. Commun.* **1990**, *90*, 23-33.

167. Mohebbinia, S.; Sepehrnoori, K.; Johns, R. T. Four-phase equilibrium calculations of carbon dioxide/hydrocarbon/water systems with a reduced method. *SPE J.* **2013**, *18*, 943-951.

168. Imai, M.; Pan, H.; Connolly, M.; Tchelepi, H.; Kurihara, M. Reduced variables method for four-phase equilibrium calculations of hydrocarbon-water-CO_2 mixtures at a low temperature. *Fluid Phase Equilib.* **2019**, *497*, 151-163.

169. Li, S.; Xu, L.; Li, H. Four-phase flash calculation algorithm based on the free-water assumption. *Ind. Eng. Chem. Res.* **2022***, 61*, 3742-3753.

CHAPTER 3 AN IMPROVED VAPOR-LIQUID-ASPHALTENE THREE-PHASE EQUILIBRIUM COMPUTATION ALGORITHM

A version of this chapter has been published in *Fluid Phase Equilibria*.

Abstract

Asphaltene precipitation is one of the major flow-assurance problems in petroleum engineering. Asphaltene precipitation in the reservoirs can lead to formation damage, while asphaltene precipitation in the production tubing can reduce the production rate and even plug the production tubing. It may occur to the naturally produced oil experiencing pressure/temperature changes or during gas injection processes (e.g., CO_2 flooding) for enhanced oil recovery. It is a prerequisite to accurately predicting under what conditions asphaltene precipitation will occur and how much precipitates if it occurs in order to better predict and control flow assurance problems due to asphaltene precipitation. In this work, a robust three-phase vapor-liquid-asphaltene precipitation algorithm is developed. To make the algorithm more robust and effective, the new algorithm is built based upon two previously proven works: the asphaltene precipitation model proposed by Kohse *et al.* (1993) which considers the effects of pressure, temperature and gas injection on asphaltene precipitation, and the initialization method and algorithm developed by Li and Li (2019) which does not consider the effect of temperature on asphaltene precipitation. The algorithm is validated using the asphaltene precipitation data measured by Jamaluddin *et al.* (2000 and 2002) and Gonzalez *et al.* (2004). As for the first two oil samples (Jamaluddin *et al.*, 2000 and 2002), both the onset conditions and the amounts of asphaltene precipitation are computed with the consideration of varied pressure-temperature conditions and the injection of different gases. The pressure-temperature (*PT*) phase diagrams and the pressure-composition (*Px*) phase diagrams are drawn to illustrate the calculation results. Our algorithm is shown to be converged at every test point involved in the three-phase equilibrium calculations for constructing the *PT* and *Px* phase diagrams. After being calibrated using the measured asphaltene onset data for the second and third oil samples, the three-phase

VLS equilibrium calculation algorithm is shown to be capable of making reliable predictions of the *PT* phase diagrams with gas injection and the precipitated asphaltene amounts versus injectant concentration.

3.1. Introduction

Asphaltenes are defined as n-pentane or n-heptane insoluble fractions and generally thought as the heaviest and most polar components in crude oil[1]. The precipitation of asphaltene may lead to formation damage and tubing plugging, and thus has become one of the major concerns during the production and transportation of asphaltenic crude oil[2]. The pressure-temperature conditions and gas injections have great influences on the asphaltene precipitation. Asphaltene molecules may become destabilized during the pressure/temperature changes or due to the introduced gas compounds, which can cause the asphaltene components to precipitate out from oil[3]. Therefore, it is of great importance to have a good understanding of the vapor-liquid-asphaltene three-phase equilibria at different pressure and temperature conditions, and to build a thermodynamic model to evaluate the risk of asphaltene precipitation from reservoir fluids.

Over the past thirty years, many modeling efforts have been made to develop thermodynamic models to predict asphaltene precipitation. The models can be roughly divided into two categories: the ones based on colloidal theory and the ones based on solubility theory. As for the colloidal-theory-based models, the asphaltene particles exist as suspended solid particles with resins adsorbed on their surface due to the polar-polar interactions[4]. This theory also assumes that the process of asphaltene precipitation is irreversible[4]. Leontaritis and Mansoori proposed that the asphaltene phase stability actually depends on the chemical potential of asphaltene components in both oil and asphaltene phases[5]. There were also other improvements made in this area since then[6-8]. However, a large number of parameters need to be fitted in the colloidal-based asphaltene precipitation models[9]. Besides, the experimental results show that it is the dispersion force, rather than the polar force, dominates the phase behavior of

asphaltenes[10-13], which refutes the idea of using the colloidal theory for asphaltene precipitation predictions. The solubility theory approach is established based on the regular solution theory or equation of state (EOS), which assumes that asphaltene components are dissolved in crude oil. Models based on the regular solution theory[14-18] have been used to predict the asphaltene phase behavior by several researchers[19-29]. However, the regular-solution-based models are not applicable for vapor-liquid phase equilibrium calculations, which can lead to inaccurate results in vapor-liquid-asphaltene three-phase equilibrium predictions[30]. To avoid this problem, EOS-based models are applied to account for the effect of compressibility factor as a function of temperature, pressure and compositions, enabling it to be a good choice to model the phase behavior of asphaltene-inclusive reservoir fluids. Statistical associating fluid theory (SAFT)[31] is one of the most commonly used EOS models in predicting asphaltene precipitation. In 2003, Ting *et al.*[32] modeled asphaltene precipitation using SAFT EOS[31] by assuming van der Waals interactions dominate the phase behavior of asphaltene in oil. The calculation results agree well with the experimental data. Inspired by that, perturbed-chain SAFT (PC-SAFT)[33] was also adopted to model asphaltene phase behavior by many researchers and has shown good prediction capacity[30, 34-37]. However, the biggest concern of using SAFT EOS in compositional simulations is its higher computational cost. To avoid this problem, Mohebbinia *et al.*[38] proposed a speedup procedure for phase behavior calculations considering asphaltene precipitation based on Yan *et al.*'s work[39], and the computational time was reduced 20% to 40%. Nevertheless, the computational cost required for conducting phase equilibrium calculations using PC-SAFT[33] is still much higher than that using cubic EOS[38].

The single-component solid model based on cubic EOS is also widely used because of its simplicity and good agreement with experimental results[40-47]. In 1993, Nghiem *et*

al.[44] developed a thermodynamic model to predict the precipitation of asphaltene from crude oil under isothermal conditions. In this model, the precipitated asphaltene is considered as a solid phase that only contains asphaltene. They also divided the heaviest component into two parts: non-precipitating component and precipitating component. These two components have the same critical properties and acentric factors but different binary interaction parameters (BIPs) with the other light components. However, this model fails to include the effect of temperature and can only be used at the reference temperature. In order to consider the effect of temperature, Kohse *et al.*[42] developed a pure solid model that considers both the effect of temperature and pressure on asphaltene precipitation. Two unknown parameters can be tuned by using two experimentally determined asphaltene onset precipitation pressures. A good match can be seen from the calculation results and the experimental data at different temperature and pressure conditions. However, the model has not been validated at relatively high temperature, where asphaltene phase may separate as a high dense liquid phase with other oil components rather than solid particles.

Although significant efforts have been made towards the development of asphaltene precipitation models, the existing models mainly focus on the accuracy of predicting the precipitation onset of asphaltene. It is still a challenging task to generate complete three-phase vapor-liquid-solid (VLS) pressure-temperature (*PT*) and pressure-composition (*Px*) diagrams due to the convergence problems that can frequently appear in the VLS equilibrium calculations. One of the reasons causing the convergence problem is that the stability test fails to give the negative stationary points on the TPD surface[48]. Thus, different sets of initialization methods are required for stability tests. Different initialization methods may also be required for different fluids. On the other hand, the convergence problem can also be caused by more than one two-phase

equilibria appear due to multiple initial equilibrium ratios[48] in flash calculations. Due to these problems, it is challenging to develop a robust algorithm that can correctly predict the onset of asphaltene precipitation and the precipitation amount under varied conditions.

In this work, we develop a robust three-phase VLS equilibrium calculation algorithm that coupled Peng-Robinson EOS (PR-EOS)[49] with the Kohse *et al.* model[42]. The modified initialization methods proposed by Li and Li[48] are applied to both stability test and flash calculations in order to avoid the previously mentioned initialization problems. In order to enhance the robustness of the newly developed algorithm, two different VLS equilibrium calculation algorithms developed by Li and Li[48] are also applied in the algorithm. Compared with the algorithm proposed by Li and Li, this three-phase VLS equilibrium calculation algorithm can properly account for the effect of temperature. Temperature in the wellbore can vary significantly with the change of depth during the oil and gas production process. According to previous studies and our simulation results, temperature change can pose a significant influence on asphaltene precipitation. The calculation results are first validated by comparing the calculation results with the experimental data measured for three oil samples. The performance of the improved algorithm is then tested by generating the complete *Px* and *PT* phase diagrams for the first reservoir fluid with and without gas injection. The three-dimensional pressure-temperature-weight percent of asphaltene precipitation (3-D *P*-*T*-*WA*) diagrams are also generated to study the effects of temperature, pressure and injection gas on the amount of asphaltene precipitation.

3.2. Mathematical Formulations

3.2.1. Thermodynamic Model of Asphaltene Precipitation

The model developed by Kohse *et al.*[42] is applied in our newly developed algorithm to calculate the fugacity of asphaltene, which is shown as[42]:

$$lnf_a = lnf_a^* + \frac{v_a}{R}\left(\frac{P-P_{tp}}{T} - \frac{P^*-P_{tp}}{T^*}\right) - \frac{\Delta H_{tp}}{R}\left(\frac{1}{T} - \frac{1}{T^*}\right) - \frac{\Delta C_p}{R}\left[\ln\left(\frac{T}{T^*}\right) - T_{tp}\left(\frac{1}{T} - \frac{1}{T^*}\right)\right] \quad (1)$$

where f_a and f_a^* represent the fugacities of asphaltene in the asphaltene phase at P and P^*, respectively; P and P^* represent the actual pressure and the reference pressure, respectively; v_a represents the asphaltene molar volume; ΔH_{tp} and ΔC_p represent the heat fusion difference and the heat capacity difference, respectively; R represents the universal gas constant; T represents temperature; the subscript a represents the asphaltene phase; T_{tp} and P_{tp} represent the triple point temperature and triple point pressure, respectively. The triple point pressure of asphaltene is very low and can be set to zero[42]. The triple point temperature is close to the melting temperature of asphaltene at atmospheric pressure, and can be calculated as[50]:

$$T_{tp} = 374.5 + 0.02617M_a - 20172/M_a \quad (2)$$

where M_a is the molecular weight of the asphaltene component.

The experimental onset pressures at two or three temperatures are necessary to calculate the unknown parameters in Equation (1). If only two data points are used, the heat capacity difference can be set to zero[42]. If three data points are used, the heat fusion and the heat capacity difference can both be calculated. The fugacities of the asphaltene component in the liquid phase and in the solid phase are calculated by PR-EOS[49]. As such, the thermodynamic model can be used to predict asphaltene precipitation at varied pressure and temperature conditions.

3.2.2. Phase Stability Test

The appearance of the asphaltene phase can be checked by the following equations[42],

$$\begin{cases} f_{ax} < f_{as}, \text{ asphaltene phase does not appear} \\ f_{ax} \geq f_{as}, \text{ asphaltene phase appears} \end{cases} \quad (3)$$

where f_{ax} and f_{as} represent the fugacities of asphaltene component in the non-asphaltene phase calculated by PR EOS and that in the asphaltene phase calculated by Equation (1), respectively, and the subscripts *a*, *x*, and *s* represent asphaltene component, non-asphaltene phase, and solid phase, respectively. The conventional phase stability test is used to detect the appearance of vapor and liquid phase at specified pressure and temperature. Michelsen[51] proposed a well-known algorithm to conduct the phase stability test. The tangent plane distance (TPD) function of redu__ced molar Gibbs free energy is applied in such algorithm. The TPD function is given by[51]:

$$TPD = \sum_{i=1}^{c} y_i[ln\varphi_i(y) + lny_i - ln\varphi_i(z) - lnz_i] \quad (4)$$

where y and z represent the trial phase composition and the feed composition, respectively, φ_i is the fugacity coefficient of component *i*, and *c* is the number of components. A given mixture is considered to be stable if all TPD values are greater than or equal to zero. In order to improve the computational efficiency, Michelsen suggested detecting the values of TPD function at all stationary points instead of calculating all the TPD values[51]. At the stationary point of TPD, the following equation holds[51]:

$$ln\varphi_i(y) + lny_i - ln\varphi_i(z) - lnz_i = k, i=1, 2, \ldots, c \quad (5)$$

where *k* is a constant corresponding to the stationary point. If we apply $Y_i = y_i e^{-k}$ to Equation (5), Equation (5) will become[51]:

$$ln\varphi_i(Y) + lnY_i - ln\varphi_i(z) - lnz_i = 0,\ i=1, 2, \ldots, c\ (6)$$

As such, Equation (6) is transformed to[51]:

$$TPDM = 1 + \sum_{i=1}^{c} Y_i[ln\varphi_i(Y) + lnY_i - ln\varphi_i(z) - lnz_i - 1]\ (7)$$

3.2.3. Flash Calculations

3.2.3.1. Two-Phase Vapor-Liquid (VL) Flash Calculation

The two-phase flash calculation algorithm developed by Michelsen[52] is adopted for our two-phase VL flash calculations. The convergence of two-phase VL flash calculations will be reached when the material balance constraint and the equal-fugacity constraint are satisfied[52]. The Rachford-Rice (RR) equation used to calculate the phase fractions is given by[53]:

$$RR_y = \sum_{i=1}^{c}(y_i - x_i) = \sum_{i=1}^{c} \frac{z_i(K_{iy}-1)}{1+\beta_y(K_{iy}-1)} = 0\ (8)$$

where x_i and y_i represent the mole fractions of component i in phase x and phase y, respectively, z_i represents the feed mole fraction, and β_y is the phase mole fraction of phase y. K_{iy} is the equilibrium ratio of component i in phase y:

$$K_{iy} = \frac{y_i}{x_i} = \frac{\varphi_{ix}}{\varphi_{iy}}\ (9)$$

Eventually, the phase compositions can be calculated as[53]:

$$x_i = \frac{z_i}{1+\beta_y(K_{iy}-1)}\ (10)$$

$$y_i = z_i K_{iy}\ (11)$$

3.2.3.2. Two-Phase Vapor/Liquid-Solid (V/L-S) Flash Calculation

In the two-phase V/L-S flash calculation, the equal-fugacity constraint can be simplified as follows based on the pure solid assumption:

$$f_{ax} = f_{as} \quad (12)$$

where f_{ax} and f_{as} represent the fugacity of asphaltene in the non-asphaltene phase and the asphaltene phase, respectively. f_{as} can be calculated based on Equation (1), while f_{ax} can be calculated based on PR EOS with a given composition of the non-asphaltene phase. The subscripts a, x, and s represent the asphaltene component, the non-asphaltene phase, and the asphaltene phase, respectively. By applying the material balance constraint, the composition of the non-asphaltene phase can be calculated by the following equation[48],

$$x_i = \begin{cases} z_i/(1-\beta_s), i = 1, \ldots, a-1 \\ (z_i - \beta_s)/(1-\beta_s), i = a \end{cases} \quad (13)$$

where β_s represents the mole fraction of the asphaltene phase; x_i and z_i represent the mole fractions of component i in the non-asphaltene phase and the feed, respectively. By updating β_s, the equal-fugacity constraint can be satisfied.

3.2.3.3. Three-Phase Vapor-Liquid-Solid (VLS) Flash Calculation

For the three-phase vapor-liquid-solid flash calculations, the equal fugacity constraints can be expressed by[44]:

$$f_{ix} = f_{iy}, i = 1, \ldots, a \quad (14)$$

$$f_{ax} = f_{ay} = f_{as} \quad (15)$$

As an alternative to the equation solving approach, the three-phase vapor-liquid-solid flash calculations can be also formulated as a minimization problem. Inspired by

Michelsen[54] and Leibovci and Nichita[55], Okuno *et al.*[56] developed a robust algorithm for RR-based multiphase flash. By simplifying the objective function and reducing the constraints developed by Okuno *et al.*[56], Li and Li[57] derived the objective function of the minimization problem (together with the constraints) for three-phase vapor-liquid-aqueous (VLA) flash calculations based on the free-water assumption. The objective function and the constraints developed by Li and Li[57] are applied in the three-phase vapor-liquid-solid flash calculation Algorithm #1. The objective function and the constraints for the three-phase VLS flash calculations are given by[57]:

$$minf(\beta_y) = \sum_{i=1}^{c-1} -z_i \ln\left[\left(K_{iy} - K_{ay}^*\right)\beta_y + K_{az}^*\right] \quad (16)$$

subject to[57]

$$\left(K_{ay}^* - K_{iy}\right)\beta_y \leq min\left\{K_{az}^* - z_i, K_{az}^* - K_{iy}z_i\right\}, i \neq a \quad (17)$$

where[57]

$$\begin{cases} K_{ay}^* = \frac{1-y_a}{1-x_a} \\ K_{az}^* = \frac{1-z_a}{1-x_a} \end{cases} (18)$$

where x_a, y_a, and z_a represent the mole fractions of asphaltene component in the liquid phase, the vapor phase, and the feed, respectively. In this case, there is only one unknown β_y in the objective function. Equation 17 forms a reliable feasible region of β_y[57]. The mole fraction of the solid phase (β_s) can be calculated using Equation 19[48], which is similar to the one proposed by Lapene *et al.*[58]:

$$\beta_s = \frac{z_c + (x_a - y_a)\beta_y - x_a}{1 - x_a} \quad (19)$$

The mole fraction of the liquid phase (β_x) can thus be calculated using the following equation[48]:

$$\beta_x = 1 - \beta_y - \beta_s (20)$$

Subsequently, the composition of the liquid phase (x_i) can be calculated as per[48]:

$$x_i = \begin{cases} \frac{z_i}{K_{iy} - K^*_{ay}\beta_y + K^*_{az}}, i \neq a \\ \frac{1}{K_{is}}, i = a \end{cases} \quad (21)$$

where[48]

$$K_{is} = \frac{s_i}{x_i} = \frac{\emptyset_{ix}}{\emptyset_{is}}, i = 1, \ldots, a \ (22)$$

where s_i represents the mole fraction of component i in the asphaltene phase. Based on the assumption that the solid phase only contains asphaltene, the value of s_i can be obtained by,

$$s_i = \begin{cases} 1, i = a \\ 0, i \neq a \end{cases} (23)$$

The composition of the vapor phase can be calculated by[48]:

$$y_i = K_{iy} x_i \ (24)$$

where ϕ_{is} represents the fugacity coefficient of component i in the solid phase.

Li and Li[48] also proposed another three-phase VLS flash calculation algorithm to enhance the robustness of the algorithm. In the inner loop of this algorithm, the two-phase VL flash calculations are conducted to satisfy Equation (14), while the outer loop is used to update β_s to give a new feed used in the inner loop[48]. Equation (15) in the equal-fugacity constraint should be satisfied in the outer loop. The feed used in the inner loop can be updated by[48],

$$z_{i2} = \begin{cases} z_i/(1 - \beta_s), i = 1, \ldots, a - 1 \\ (z_i - \beta_s)/(1 - \beta_s), i = a \end{cases} (25)$$

where z_{i2} represents the mole fraction of component i in the feed used in the inner loop. Although this algorithm is more reliable when three-phase equilibrium appears, it is time-consuming due to the repetitive execution of the two-phase VL flash calculations. The procedure of the three-phase VLS equilibrium calculation algorithm closely follows the one proposed by Li and Li[48]. In order to enhance the robustness and efficiency of the algorithm, there are three different approaches applied to conduct the three-phase vapor-liquid-asphaltene flash calculations. In general, the algorithm is only slower at the region near the phase boundary between the LS two-phase region and the VLS three-phase region.

3.3. Results and Discussion

In this section, three example calculations are firstly conducted, and the calculation results are compared with the experimental data to validate our model. Then, the algorithm is used to generate *PT* and *Px* phase diagrams for oil sample 1 and oil sample 2 mixed with different gases. We also compute the variation of the weight fraction of asphaltene precipitation as a function of pressure/temperature and gas-injection amount.

3.3.1. Oil Sample Characterization

3.3.1.1. Oil Sample 1

Tables 3-1 and 3-2 show the composition and the SARA content of oil sample 1, respectively, as measured by Jamaluddin *et al.*[59] . Oil sample 1 is a stock tank oil from the Middle East region. The API gravity of this oil sample is 39° API and the weight fraction of asphaltene components in oil sample 1 is 1.3%[59]. The molecular weight of the oil sample is 82.49 g/mol[59]. The molecular weight and density of the C_{7+} fraction are 228.07 g/mol and 0.865 g/cm[59]. The C_{7+} components are split using the exponential distribution function proposed by Pedersen *et al.*[60]:

$$z_i = z_{C_n} e^{A(1-n)} \quad (26)$$

where n is the carbon number of the plus fraction, i is the carbon number of the split fraction, z_{C_n} and A are constants given by[60]:

$$z_{C_n} = \frac{14}{M_{C_{n+}}} - 14(n-1) - h \quad (27)$$

$$A = 1 - z_{C_n} \quad (28)$$

where $M_{C_{n+}}$ is the molecular weight of the plus fraction, and h is a constant which is set as -2. These components are then lumped using the method proposed by Whitson[61]:

$$N_H = 1 + 3.3\log(i_{max} - n) \quad (29)$$

where N_H is the number of lumped pseudo components, i_{max} is the maximum carbon number of the reservoir fluid, and n is the carbon number of the plus fraction.

The critical temperature, critical pressure and acentric factors of the lumped pseudocomponents are calculated using the Lee-Kesler correlations[62, 63]. The critical temperature can be calculated using the following equations[62]:

$$T_c = 341.7 + 811\gamma + (0.4224 + 0.1174\gamma)T_b + (0.4669 - 3.2623\gamma) \times 10^5 T_b^{-1} \quad (30)$$

where γ is the specific gravity and T_b is the boiling temperature calculated by[64]:

$$T_b = 1928.3 - (1.695 \times 10^5 M_i^{-0.03522} \gamma_i^{3.266}) \times e^{[-(4.922\times10^{-3})M_i - 4.7658\gamma_i + (3.462\times10^{-3})M_i\gamma_i]} \quad (31)$$

where M is the molecular weight. The critical pressure can be calculated as[62]:

$$lnP_c = 8.3634 - \frac{0.0566}{\gamma} - \left[\left(0.24244 + \frac{2.2898}{\gamma} + \frac{0.11857}{\gamma^2}\right) \times 10^{-3}\right] T_b +$$

$$\left[\left(1.4685 + \frac{3.648}{\gamma} + \frac{0.47227}{\gamma^2}\right) \times 10^{-7}\right] T_b^2 - [(0.42019 + \frac{1.6977}{\gamma^2}) \times 10^{-10}] \times T_b^3 \quad (32)$$

The following correlations can be used for estimating acentric factors:

If T_b/T_c<0.8[63],

$$\omega = \frac{-ln\frac{P_c}{14.7} + A_1 + A_2 T_{br}^{-1} + A_3 ln T_{br} + A_4 T_{br}^6}{A_5 + A_6 T_{br}^{-1} + A_7 ln T_{br} + A_8 T_{br}^6} \quad (33)$$

where A_1= -5.92714, A_2= 6.09648, A_3=1.28862, A_4= - 0.169347, A_5= 15.2518, A_6= -15.6875, A_7= - 13.4721, A_8= 0.43577.

If $T_b/T_c \geqslant$0.8[62],

$$\omega = -7.904 + 0.1352K_w - 0.007465K_w^2 + 8.359T_{br} + (1.408 - 0.01063K_w)T_{br}^{-1} \quad (34)$$

where K_w is the Watson factor that can be calculated by the following equation[61]:

$$K_w = 4.5579 {M_{C_{n+}}}^{0.15178} {\gamma_{C_{n+}}}^{-0.84573} \quad (35)$$

The Riazi-Daubert correlation[65] is used to calculate the critical volumes:

$$v_c = (7.0434 \times 10^{-7}) T_b^{2.3829} \gamma^{-1.683} \quad (36)$$

The heaviest component in oil sample 1 is split into non-asphaltene component (NA) and asphaltene component (A). These components have the same acentric factors and critical properties but different binary interaction parameters (BIP) with other components. The mole fraction of the asphaltene component can be calculated as[44]:

$$z_{Cn+A} = \frac{w_{Cn+A} \times MW_{oil}}{MW_{Cn+A}} \quad (37)$$

where z_{Cn+A} represents the mole fraction of the asphaltene component, w_{Cn+A} represents the experimentally decided weight fraction of the asphaltene content, MW_{oil} and MW_{Cn+A} represent the molecular weights of the oil sample and the asphaltene component, respectively. The final characterization scheme of oil sample 1 is shown in Table 3-3. Note that the critical properties of the first ten components are taken from literature[66].

Table 3-1 Composition of oil sample 1[59].

Component	Composition (mol%)
N_2	0.48
CO_2	0.92
C_1	43.43
C_2	11.02
C_3	6.55
i-C_4	0.79
n-C_4	3.70
i-C_5	1.28
n-C_5	2.25
C_6	2.70
C_{7+}	26.88

Table 3-2 SARA content of oil sample 1[59].

Saturates	68.3
Aromatics	11.6
Resins	18.8
Asphaltene	1.3

Table 3-3 Characterization results of oil sample 1.

Component	Composition (mol%)	T_c (K)	P_c (bar)	V_c (m^3/kmol)	ω	MW (g/mol)
N_2	0.0048	126.2	34.4	0.090	0.04	28.01
CO_2	0.0092	304.7	74.8	0.094	0.23	44.01
C_1	0.4343	190.6	46.7	0.099	0.01	16.04
C_2	0.1102	305.4	49.5	0.148	0.10	30.07
C_3	0.0655	369.8	43.0	0.203	0.15	44.10
i-C_4	0.0079	408.1	37.0	0.263	0.18	58.12

n-C_4	0.0370	419.5	38.0	0.255	0.20	58.12
i-C_5	0.0128	460.4	34.3	0.306	0.23	72.15
n-C_5	0.0225	465.9	34.0	0.304	0.24	72.15
C_6	0.0270	507.4	29.7	0.370	0.30	86.18
C_7-C_8	0.0491	564.5	30.7	0.414	0.33	102.65
C_9-C_{10}	0.0401	617.2	26.2	0.515	0.42	130.65
C_{11}-C_{13}	0.0469	671.9	22.3	0.636	0.53	165.06
C_{14}-C_{17}	0.0440	733.7	18.7	0.787	0.65	213.24
C_{18}-C_{23}	0.0403	801.4	15.7	0.966	0.80	280.91
C_{24}-C_{39}	0.0388	894.3	13.0	1.211	0.96	410.25
C_{40+NA}	0.0081	1050.2	17.5	1.111	0.85	690.07
C_{40+A}	0.0016	1050.2	17.5	1.111	0.85	690.07

3.3.1.2. Oil Sample 2

Table 3-4 summarized the composition of oil sample 2 measured by Jamaluddin *et al.* in 2000[67]. Table 3-5 shows the SARA content of oil sample 2[67]. Oil sample 2 is a live oil sample from Sahil reservoir in the United Arab Emirates. It has a 40.4° API gravity and its weight fraction of asphaltene components is 1.3%[67]. The molecular weight of the oil sample is measured to be 126.6 g/mol[67]. The C_8+ component of oil sample 2 has a molecular weight of 222 g/mol and a density of 0.855 g/cm^3 [67]. The same lumping method as used for oil sample 1 is applied to oil sample 2. Table 3-6 shows the characterization results of oil sample 2. The acentric factors and the critical properties of the first ten components are taken from the literature[66].

Table 3-4 Composition of oil sample 2[67].

Component	Composition (mol%)	Component	Composition (mol%)
N_2	0.32	C_{14}	2.25
CO_2	2.29	C_{15}	2.14
H_2S	0.01	C_{16}	1.79
C_1	17.67	C_{17}	1.47
C_2	5.25	C_{18}	1.32
C_3	6.14	C_{19}	1.26
i-C_4	1.91	C_{20}	1.15

n-C_4	4.72	C_{21}	0.99
i-C_5	2.51	C_{22}	0.89
n-C_5	3.33	C_{23}	0.78
C_6	5.00	C_{24}	0.70
C_7	5.12	C_{25}	0.62
C_8	5.53	C_{26}	0.58
C_9	4.84	C_{27}	0.53
C_{10}	4.48	C_{28}	0.49
C_{11}	3.78	C_{29}	0.46
C_{12}	3.09	C_{30}+	3.83
C_{13}	2.78		

Table 3-5 SARA content of oil sample 2[67].

Saturates	66.7
Aromatics	27.0
Resins	5.0
Asphaltene	1.3

Table 3-6 Characterization results of oil sample 2.

Component	Composition (mol%)	T_c (K)	P_c (bar)	V_c (m^3/kmol)	ω	MW (g/mol)
N_2	0.32	126.20	34.4	0.0901	0.04	28.01
CO_2	2.29	304.70	74.8	0.094	0.23	44.01
H_2S	0.01	373.60	90.6	0.0976	0.1	34.08
C_1	17.67	190.60	46.7	0.0993	0.01	16.04
C_2	5.25	305.43	49.5	0.1479	0.10	30.07
C_3	6.14	369.80	43.0	0.2029	0.15	44.10
i-C_4	0.91	408.10	37.0	0.2627	0.18	58.12
n-C_4	4.72	419.50	38.0	0.2547	0.20	58.12
i-C_5	2.51	460.40	34.3	0.3058	0.23	72.15
n-C_5	3.33	465.90	34.0	0.3040	0.24	72.15
C_6	5.00	507.40	29.7	0.3700	0.30	86.18
C_7	5.12	540.00	27.4	0.4280	0.35	96.00
C_8-C_9	10.37	586.49	26.7	0.4822	0.39	116.53
C_{10}-C_{11}	8.26	633.51	23.1	0.5831	0.48	144.41
C_{12}-C_{14}	8.12	682.90	19.9	0.7025	0.58	178.55
C_{15}-C_{19}	7.98	746.26	16.6	0.8714	0.72	232.09
C_{20}-C_{29}	7.19	832.16	13.3	1.1157	0.91	329.13

$C_{30+\ NA}$	3.51	999.32	16.9	1.0892	0.86	546.57
$C_{30+\ A}$	0.30	999.32	16.9	1.0892	0.86	546.57

3.3.1.3. Oil sample 3

Table 3-7 summarizes the composition of oil sample 3 measured by Buenrostro‐Gonzalez *et al.*[68]. Table 3-8 shows the SARA content of oil sample 3[68]. Oil sample 3 is a live oil sample from Mexico. Its molecular weight is measured to be 238.1 g/mol[68]. The C_7+ component of oil sample 3 has a molecular weight of 334.66 g/mol and a density of 0.8822 g/cm^3 [68]. Again, the same lumping method as used for oil sample 1 is applied to oil sample 3. The characterization results of oil sample 3 are shown in Table 3-9.

Table 3-7 Composition of oil sample 3[68].

Component	Composition (mol%)
N_2	0.91
CO_2	1.57
H_2S	5.39
C_1	24.02
C_2	10.09
C_3	9.58
i-C_4	1.83
n-C_4	4.83
i-C_5	2.27
n-C_5	2.74
C_6	4.77
C_{7+}	32.00

Table 3-8 SARA content of oil sample 3[68].

Saturates	54.67
Aromatics	28.89
Resins	12.66
Asphaltene	3.80

Table 3-9 Characterization results of oil sample 3.

Component	Composition (mol%)	T_c (K)	P_c (bar)	V_c (m^3/kmol)	ω	MW (g/mol)
N_2	0.91	126.2	34.4	0.0901	0.04	28.01
CO_2	1.57	304.7	74.8	0.0940	0.23	44.01
H_2S	5.39	373.6	90.6	0.0976	0.10	34.08
C_1	24.02	190.6	46.7	0.0993	0.01	16.04
C_2	10.09	305.4	49.5	0.1479	0.10	30.07
C_3	9.58	369.8	43.0	0.2029	0.15	44.10
i-C_4	1.83	408.1	37.0	0.2627	0.18	58.12
n-C_4	4.83	419.5	38.0	0.2547	0.20	58.12
i-C_5	2.27	460.4	34.3	0.3058	0.23	72.15
n-C_5	2.74	465.9	34.0	0.3040	0.24	72.15
C_6	4.77	507.4	29.7	0.3700	0.30	86.18
C_7-C_9	5.03	570.9	26.0	0.4813	0.38	109.47
C_{10}-C_{12}	4.24	639.1	20.9	0.6347	0.51	151.47
C_{13}-C_{15}	3.57	695.0	17.5	0.7808	0.64	193.47
C_{16}-C_{19}	3.91	748.5	14.9	0.9344	0.77	242.00
C_{20}-C_{24}	3.78	804.1	12.8	1.1029	0.90	304.41
$C_{25+\ NA}$	9.93	990.3	13.8	1.2605	1.00	586.66
$C_{25+\ A}$	1.54	990.3	13.8	1.2605	1.00	586.66

3.3.2. Validation of the Three-Phase VLS Equilibrium Calculation Algorithm

The BIPs between asphaltene components and other components should be tuned to match the experimental data. The model proposed by Chueh and Prausnitz[69] is adopted by Kohse *et al.*[42] to calculate BIPs,

$$k_{ij} = 1 - \left[\frac{2v_{ci}^{1/6}v_{cj}^{1/6}}{v_{ci}^{1/3}+v_{cj}^{1/3}}\right]^{\theta} \quad (38)$$

where k_{ij} is the BIP between component i and component j; v_{ci} and v_{cj} are the critical volumes of component i and component j, respectively; θ is the exponent; the subscripts i and j represent component i and component j, respectively. The value of θ can be tuned based on the experimental data. The BIPs between hydrocarbon components (HCs) can also be tuned using equation (27) to match the experimental data. Table 3-10, Table 3-11 and Table 3-12 summarize the BIPs used for oil sample 1, oil sample 2 and oil

sample 3, respectively. In Table 3-10, 3-11 and 3-12, the BIPs between N_2, H_2S and other components are taken from literature[66].

Table 3-10 BIPs used for oil sample 1[66].

	N_2	CO_2	C_{40}+ A
N_2	0	-0.017	0.257772
CO_2	-0.017	0	0.250531
C_1	0.031	0.086	0.241220
C_2	0.052	0.070	0.176314
C_3	0.085	0.070	0.129444
i-C_4	0.103	0.070	0.095218
n-C_4	0.080	0.070	0.099097
i-C_5	0.092	0.070	0.077099
n-C_5	0.100	0.070	0.077773
C_6	0.100	0.070	0.056722
C_7-C_8	0.100	0.070	0.045978
C_9-C_{10}	0.100	0.070	0.028187
C_{11}-C_{13}	0.100	0.070	0.014992
C_{14}-C_{17}	0.100	0.070	0.005727
C_{18}-C_{23}	0.100	0.070	0.000943
C_{24}-C_{39}	0.100	0.070	0.000366
C_{40+NA}	0.100	0.070	0.000000
C_{40+A}	0.258	0.251	0.000000

Table 3-11 BIPs used for oil sample 2[66].

	N_2	H_2S	CO_2	C_{30}+ A
N_2	0	0.177	-0.017	0.209355
CO_2	-0.017	0.097	0	0.203233
H_2S	0.177	0	0.097	0.197844
C_1	0.031	0.080	0.070	0.195381
C_2	0.052	0.083	0.070	0.141227
C_3	0.085	0.088	0.070	0.102742
i-C_4	0.103	0.047	0.070	0.074968
n-C_4	0.080	0.060	0.070	0.078101
i-C_5	0.092	0.060	0.070	0.060383
n-C_5	0.100	0.060	0.070	0.060924
C_6	0.100	0.060	0.070	0.044087
C_7	0.100	0.060	0.070	0.033227
C_8-C_9	0.100	0.060	0.070	0.025413
C_{10}-C_{11}	0.100	0.060	0.070	0.015036
C_{12}-C_{14}	0.100	0.060	0.070	0.007441

C_{15}-C_{19}	0.100	0.060	0.070	0.001932
C_{20}-C_{29}	0.100	0.060	0.070	0.000023
$C_{30}+_{NA}$	0.100	0.060	0.086	0.000000
$C_{30}+_{A}$	0.209	0.198	0.203	0.000000

Table 3-12 BIPs used for oil sample 3[66].

	N_2	H_2S	CO_2	C_{25}+ A
N_2	0	0.177	-0.017	0.312612
CO_2	-0.017	0.097	0	0.304595
H_2S	0.177	0	0.097	0.297503
C_1	0.031	0.080	0.070	0.294252
C_2	0.052	0.083	0.070	0.221063
C_3	0.085	0.088	0.070	0.166860
i-C_4	0.103	0.047	0.070	0.126375
n-C_4	0.080	0.060	0.070	0.131010
i-C_5	0.092	0.060	0.070	0.104545
n-C_5	0.100	0.060	0.070	0.105363
C_6	0.100	0.060	0.070	0.079553
C_7-C_9	0.100	0.060	0.070	0.049975
C_{10}-C_{12}	0.100	0.060	0.070	0.025761
C_{13}-C_{15}	0.100	0.060	0.070	0.012651
C_{16}-C_{19}	0.100	0.060	0.070	0.004965
C_{20}-C_{24}	0.100	0.060	0.070	0.000990
$C_{25+\ NA}$	0.100	0.060	0.070	0.000000
$C_{25+\ A}$	0.313	0.298	0.305	0.000000

Another adjustable parameter in Kohse's model is the molar volume of asphaltene (v_a)[42]. As suggested by Kohse *et al.*[42], v_a can be adjusted to have a slightly higher value than that calculated by PR-EOS[49] to match the experimental data. The values of the adjustable parameters used in our algorithm for oil sample 1, oil sample 2 and oil sample 3 are shown in Table 3-13. Although they seem to be very different for the three oil samples, the BIP values are quite similar. The different values of θ and BIPs of different oil samples are mainly caused by different splitting and lumping results.

Table 3-13 Adjusted parameters used for oil samples 1-3.

	Oil sample 1	Oil sample 2	Oil sample 3
θ between hydrocarbons (θ_1)	0.1	1.5	0.5
θ between other components and asphaltene (θ_2)	3.5	2.8	2.2
v_a (cm^3/mol)	450.0	411.4	489.7

Figure 3-1 shows the comparison between the calculated *PT* phase envelope and the measured one by Jamaluddin *et al.*[59, 67] and Buenrostro - Gonzalez *et al.*[68]. The green lines represent the asphaltene onset boundaries, while the red line represents the saturation pressure line. It can be seen from Figure 3-1 that calculated saturation pressure and the upper/lower asphaltene onset boundaries match well with the experimental data, verifying the efficacy of our algorithm in modeling asphaltene precipitation phenomena at different pressure/temperature conditions.

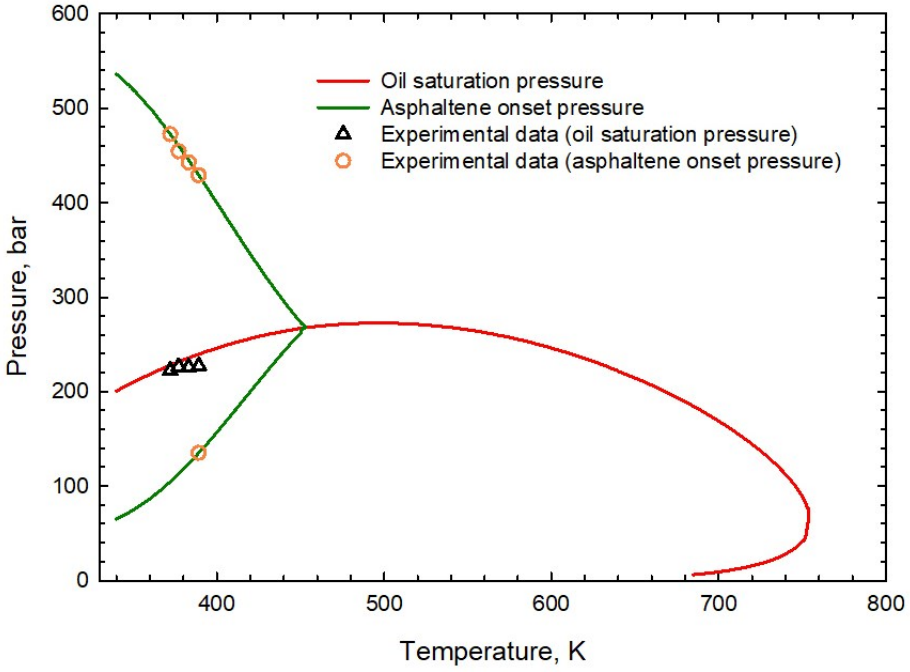

(a)

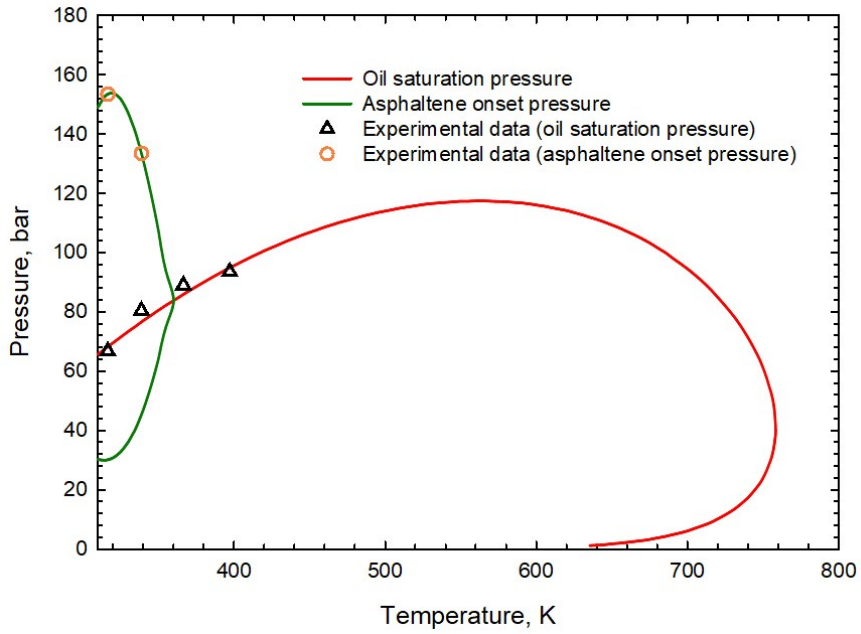

(b)

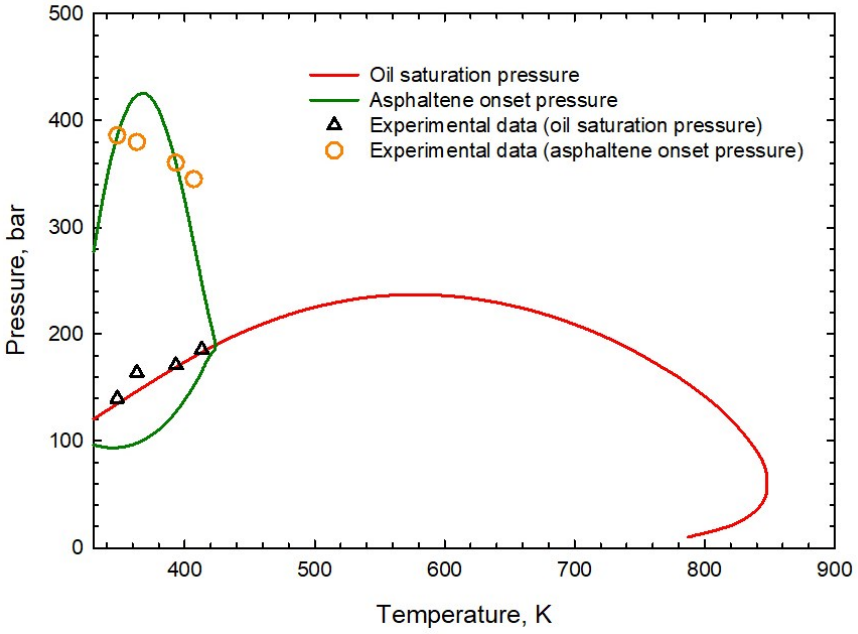

(c)

Fig. 3-1 Comparison between the calculated *PT* phase diagram using the newly developed algorithm and the experimental data[59, 67, 68]: (a) Oil sample 1; (b) Oil sample 2; (c) Oil sample 3.

The tuned parameters for oil sample 2 are subsequently used to calculate the *PT* phase diagram with 45% gas injection. The injection gas composition is shown in Table 3-14. Figure 3-2 shows the comparison between the calculated results and the experimental

data. As shown in Figure 3-2, the calculated results match reasonably well with the experimental data, which indicates that our algorithm can accurately model asphaltene precipitation with gas injection.

Table 3-14 Composition of the injection gas[67].

Component	Composition (mol%)
N_2	0.59
CO_2	5.03
H_2S	0.03
C_1	65.76
C_2	11.32
C_3	8.58
i-C_4	2.16
n-C_4	3.62
i-C_5	1.24
n-C_5	1.14
C_6	0.51
C_7	0.03

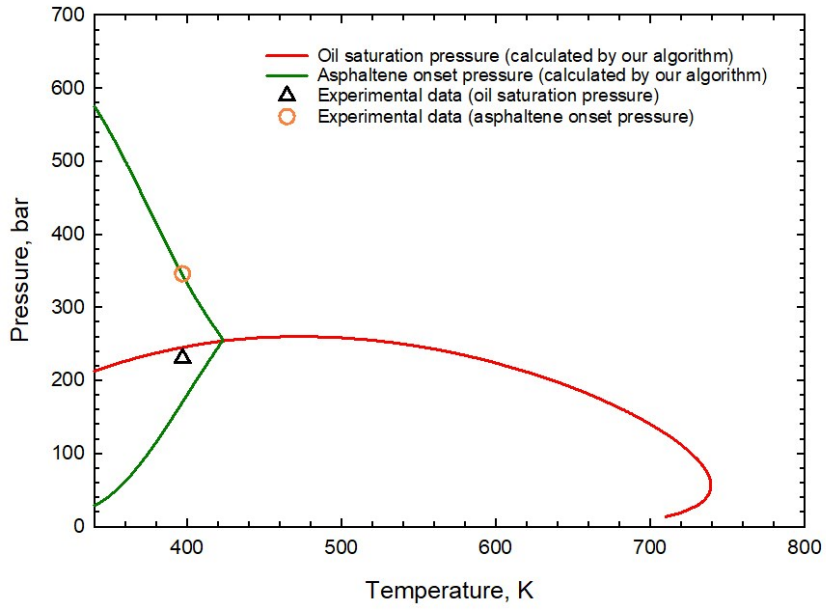

Fig. 3-2 Comparison between the calculated *PT* phase diagram with 45 mol% gas injection using the newly developed algorithm and the experimental data[67].

The tuned parameters for oil sample 3 are also used to predict the asphaltene precipitation amounts induced by n-C_5 addition. Since the precipitation experiment is

conducted at ambient conditions (25°C, 1.01 bar) using the produced dead oil, we first conduct gas-oil two-phase flash calculation on the live oil sample and the oleic phase composition is selected to conduct the precipitation amount calculation. The measured weight fraction of precipitated asphaltene and the converted results are shown in Table 3-15[68].

Table 3-15 Precipitated-asphaltene weights from oil sample 3 by adding n-C_5[68].

R_{n-C_5} (cm^3 of n-C_5 per gram of oil)	$mol\%_{C5}$	wt_{asp}/wt_{oil} (ratio of weight of precipitated asphaltene over weight of oil sample)	$wt\%_{asp}$
0.52	51.9	0	0
1	67.4	0.0107	0.6581
2	80.6	0.0171	0.7593
3	86.1	0.0231	0.8026
4	89.2	0.0252	0.7192
7	93.5	0.0290	0.5388
10	95.4	0.0354	0.4876
30	98.4	0.0369	0.1865
50	99.0	0.0381	0.1180

The comparison between the calculation results and the experimental data are shown in Figure 3-3. It can be seen from Figure 3-3 that the calculated asphaltene precipitation amounts agree reasonably well with the experimental data, which indicates that the algorithm can also predict the data that are not used in the tuning process.

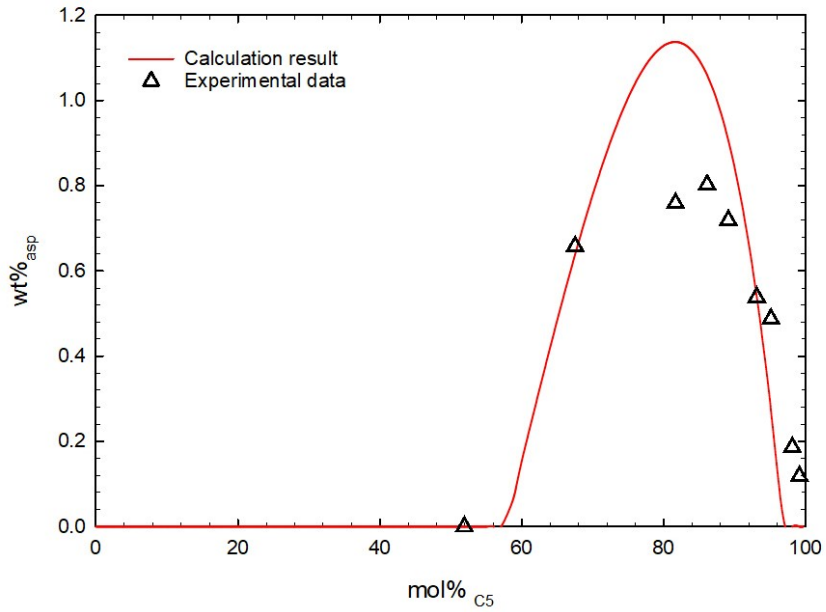

Fig. 3-3 Comparison between the calculated asphaltene precipitation amounts using the newly developed algorithm and the experimental data[68].

Figure 3-4 shows the comparison between the calculated wt_{asp}/wt_{oil} and the measured ones. It should be noted that like all the EOS-based asphaltene precipitation models, our algorithm also does not accurately predict the asphaltene precipitation amount at very high pentane concentration (>90 *mol%* in this case) due to the incorrectly predicted 100% asphaltene solubility at very high dilution.

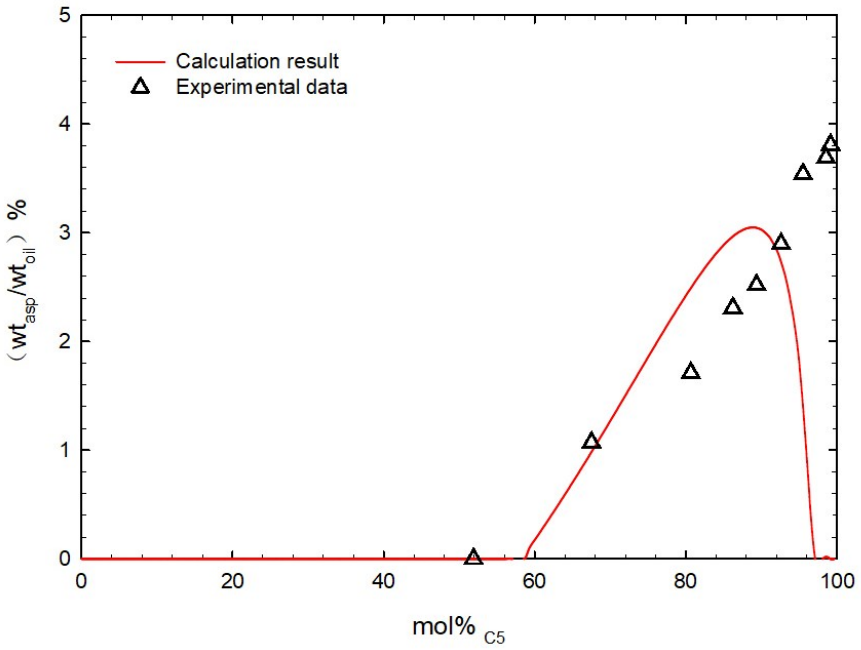

Fig. 3-4 Comparison between the calculated wt_{asp}/wt_{oil} using the newly developed algorithm and the experimental data[68].

3.3.3. Effect of Different Tuned Parameters on *PT* Phase Diagrams

In this part, we take oil sample 1 as an example to show the effect of different tuned parameters on *PT* phase diagrams. Figure 3-5 shows the effect of using different values of v_a on the onset of asphaltene precipitation for oil sample 1. Three onset boundaries for oil sample 1 calculated by our algorithm are shown in Figure 3-5. The molar volumes used to generate Figure 3-5 are 403.5 cm^3/mol, 450 cm^3/mol and 500 cm^3/mol. It can be seen from Figure 3-5 that there is no significant shift on the upper onset of asphaltene precipitation with an increasing molar volume of asphaltene. However, the lower onset of asphaltene precipitation will shift much to the lower side with an increasing molar volume. Therefore, the experimental data of the lower onsets of asphaltene precipitation can be well matched by adjusting the molar volume of the asphaltene component.

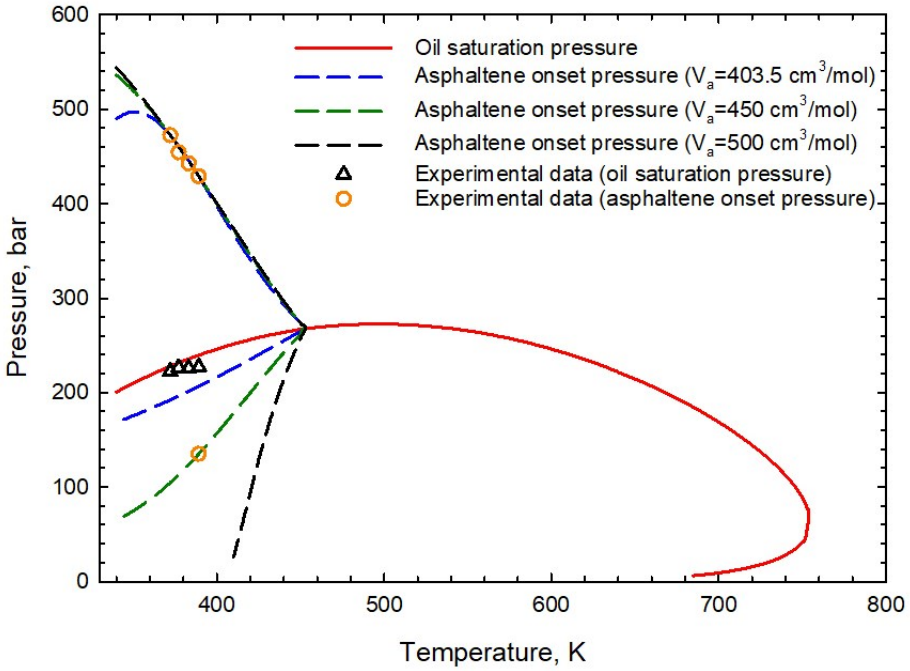

Fig. 3-5 Effect of asphaltene molar volume on the calculated onset boundaries of asphaltene precipitation for oil sample 1.

Figure 3-6 shows the effect of different exponential parameter θ_1 on *PT* phase diagrams of oil sample 1. The *PT* phase diagrams are calculated by our algorithm with the tuned parameters shown in Table 3-13 except θ_1. The values of θ_1 used to generate Figure 3-6 are 0.1, 0.5 and 1, respectively. It can be seen that the value of θ_1 does not have significant effect on the upper onset of asphaltene precipitation, but the bubble point pressure will increase with the increasing value of θ_1. It can be also concluded from Figure 3-6 that the area of asphaltene precipitation in the *PT* phase diagram will be shrunk by the increase of θ_1.

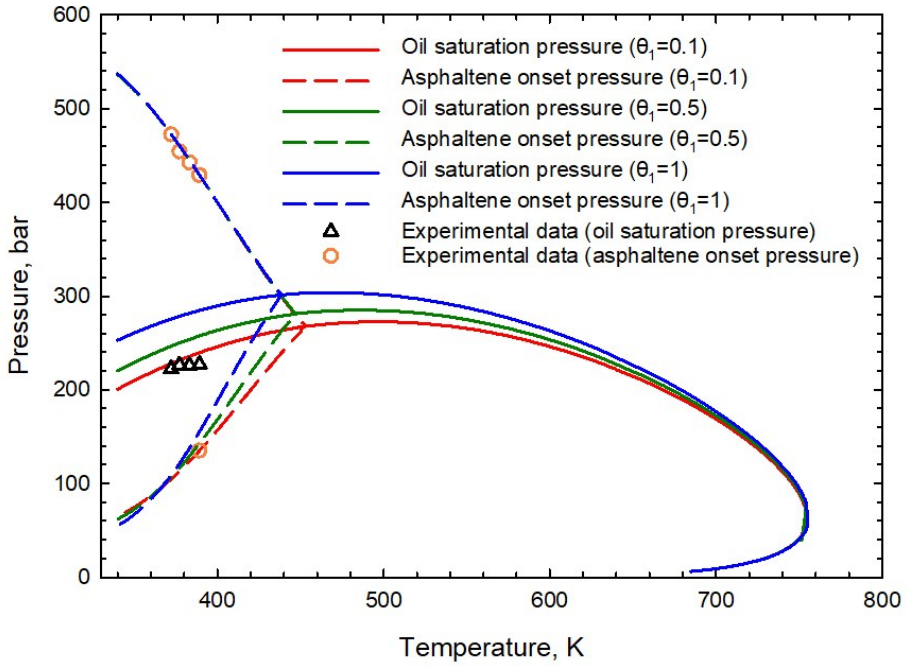

Fig. 3-6 Effect of θ_1 on the calculated *PT* phase diagrams of oil sample 1.

Figure 3-7 shows the effect of different exponential parameter θ_2 on *PT* phase diagrams of oil sample 1. The *PT* phase diagrams are calculated by our algorithm with the tuned parameters shown in Table 3-13 except θ_2. The values of θ_2 used to generate Figure 3-7 are 2.5, 3.5 and 5, respectively. As shown in Figure 3-7, the lower onset of asphaltene precipitation will be lowered by the reduced value of θ_2, and will be lifted by the increasing value of θ_2.

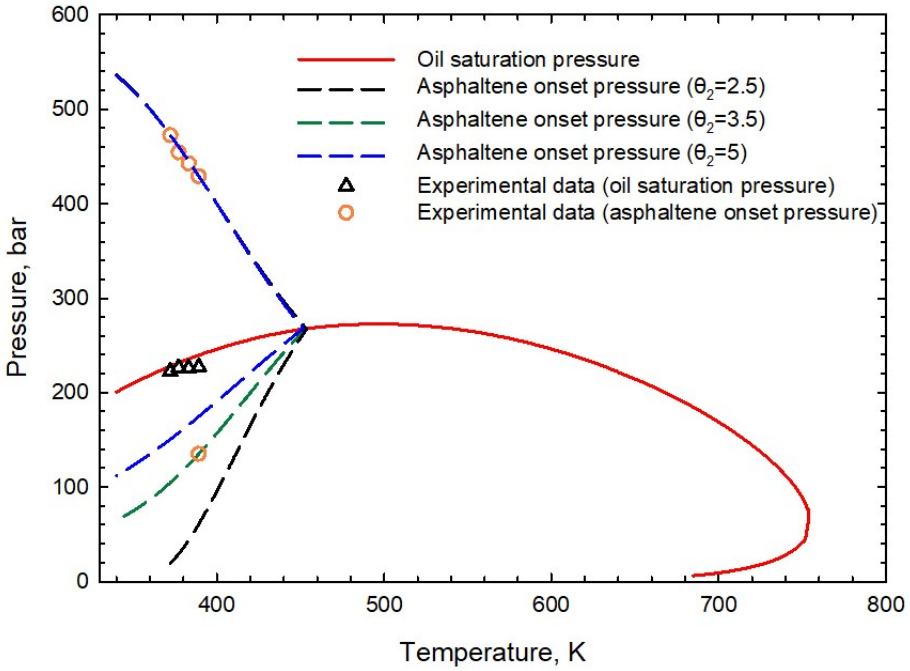

Fig. 3-7 Effect of θ_2 on the calculated *PT* phase diagrams of oil sample 1.

3.3.4. Comparison Between the Results Calculated by the Three-Phase VLS Equilibrium Calculation Algorithm and PVTsim

In this part, the *PT* phase diagrams of oil sample 1 and oil sample 2 calculated by our algorithm are compared with those calculated by PVTsim using PR-EOS. In PVTsim, the C_{50+} component is considered to be the pseudo component which contains asphaltene and will be split into asphaltene component and non-asphaltene component. The weight fraction of aromatic components in C_{50+} in the oil sample is set as the asphaltene weight fraction. The critical temperature and critical pressure of the asphaltene component, asphaltene content in oil sample and the BIPs are tuned to match the experimental data. Figure 3-8 shows the comparison between the saturation pressure and the upper/lower asphaltene onset boundaries calculated by our algorithm and that calculated by PVTsim with tuned parameters[66]. We can see from Figure 3-8 that the results calculated by our algorithm agree better with experimental data than that

calculated by PVTsim. It can be also concluded that our algorithm can generate more complete phase diagrams than PVTsim.

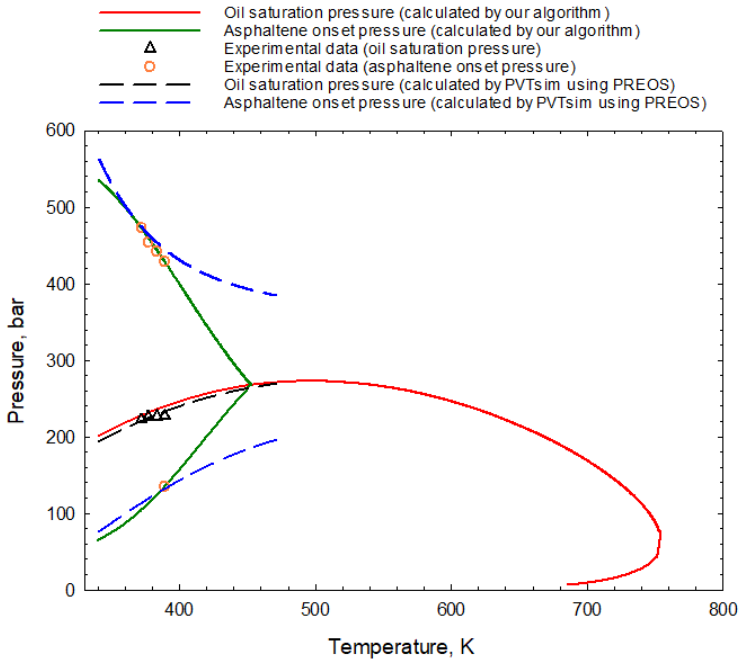

(a)

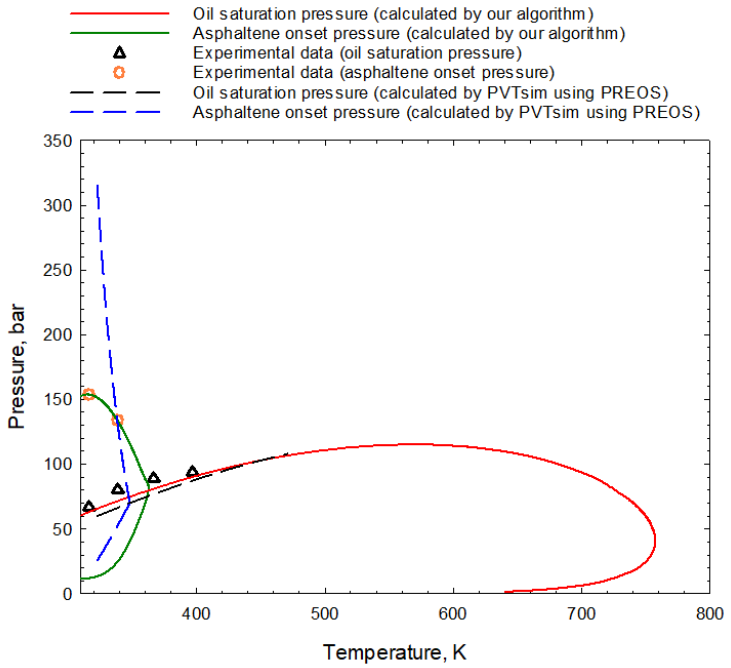

(b)

Fig. 3-8 Comparison between the *PT* phase diagrams calculated by our algorithm and that calculated by PVTsim[66].

3.3.5. Complete Phase Diagrams

To test the performance of our three-phase VLS equilibrium calculation algorithm, the complete *PT*, *Px* phase diagrams and the three-dimensional pressure-temperature-weight percent of asphaltene precipitation (3-D *P-T-WA*) diagrams of oil sample 1 are generated. Figure 3-9 shows the complete *PT* phase diagram of oil sample 1. In Figure 3-9, the temperature is varied between 300 K and 900 K with a step size of 1 K, while the pressure varies from 1 bar to 1000 bar with a step size of 1 bar. Our algorithm is run at 601000 times to generate Figure 3-9. As shown in Figure 3-9, the new algorithm converges at every test point and each phase-envelope boundary appears to be smooth and continuous.

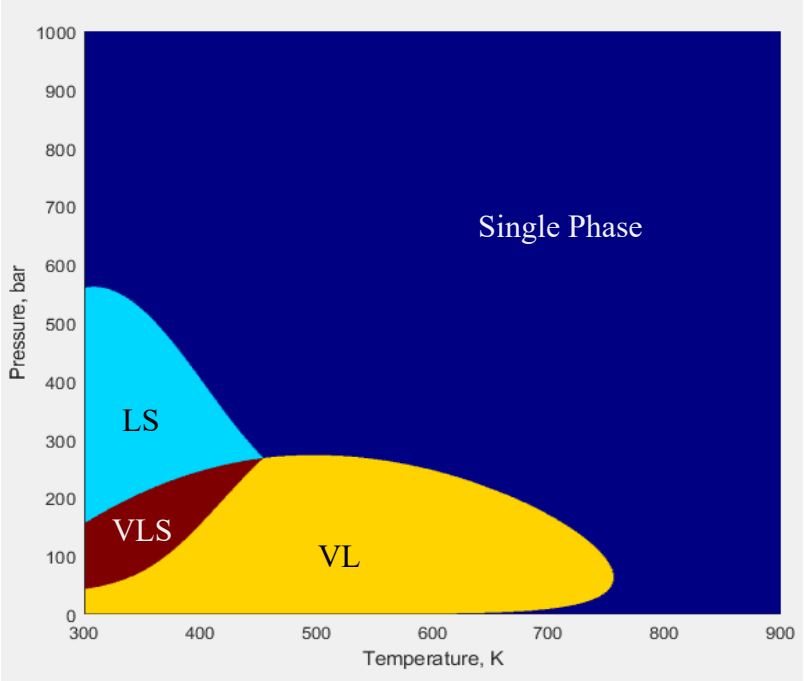

Fig. 3-9 *PT* phase diagrams calculated by our algorithm for oil sample 1.

Figure 3-10 shows the *Px* phase diagrams of oil sample 1 calculated by our algorithm at 300K with CH_4 injection. The algorithm is run a total of 198000 times to generate Figure 3-10. Our algorithm converges in every run. As shown in Figures 3-10, CH_4 injection leads to a large area of asphaltene precipitation in the *Px* phase diagram.

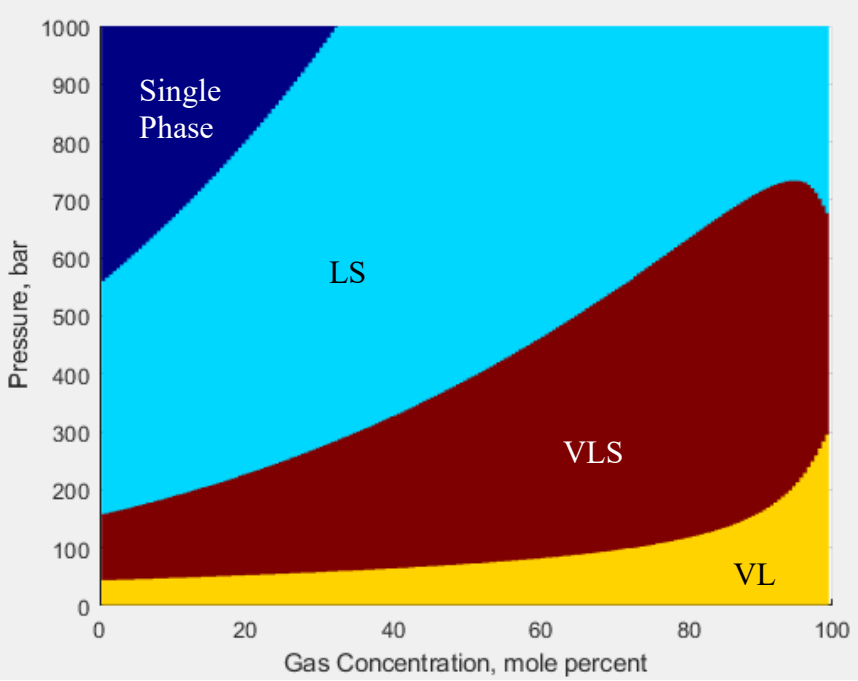

Fig. 3-10 *Px* phase diagrams calculated by our algorithm for oil sample 1 with CH_4 injection.

The 3-D P-T-WA diagrams are generated using the new algorithm to study the effect of pressure and temperature on the amount of asphaltene precipitation. Figure 3-11 shows the 3-D P-T-WA diagrams generated for oil sample 1. The three-phase VLS equilibrium calculation algorithm is run 601000 times to generate Figure 3-11. It can be seen from Figure 3-11 that, as pressure increases at a given temperature, the amount of asphaltene precipitation first increases, reaches the maximum value, and then decreases. As temperature increases at a given pressure, the amount of asphaltene precipitation shows a decreasing trend.

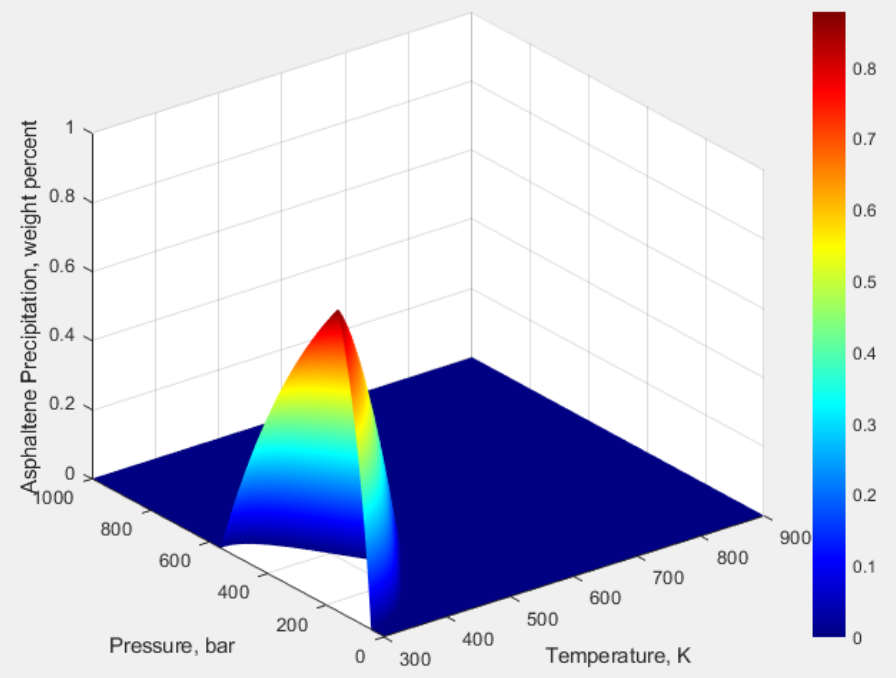

(a)

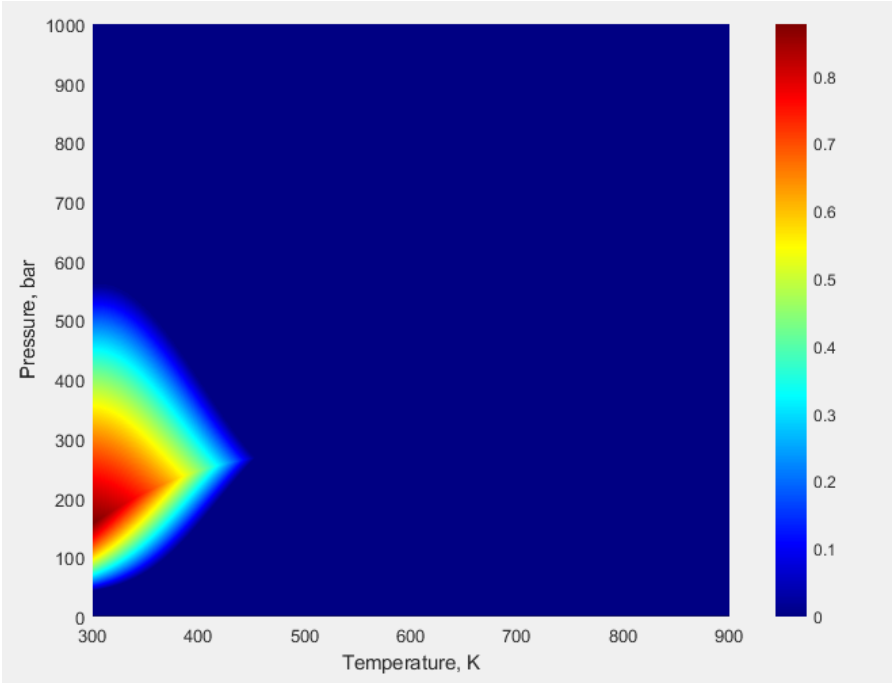

(b)

Fig. 3-11 3-D P-T-WA diagram of oil sample 1: (a) 3-D plot; (b) contour plot.

3.4. Conclusions

A three-phase VLS equilibrium calculation algorithm is developed in this study. This work aims to improve the robustness of the three-phase VLS equilibria calculation and better predict the asphaltene precipitation phenomenon during oil production process. The performance of this algorithm is tested by three oil samples and the following conclusions can be drawn from the results of this study:

- A good agreement can be seen between the results calculated with the new algorithm and the experimental data, which indicates that our algorithm can reliably model asphaltene precipitation phenomena at different pressure/temperature conditions.
- In the case study conducted for oil sample 2 and oil sample 3, it is shown that after being calibrated using the measured asphaltene onset data, the three-phase VLS equilibrium calculation algorithm can be used to make reliable predictions of the phase boundary and asphaltene precipitation amount with different injectants.
- The molar volume of asphaltene component can significantly affect the lower boundary of asphaltene precipitation in the *PT* phase diagram: the larger the molar volume, the lower the boundary is.
- The value of the exponential parameters θ_1 and θ_2 can also alter the phase boundaries in the phase diagram. The bubble point pressure will be increased with the increasing value of θ_1. The lower onset of asphaltene precipitation will be lowered by the reduced value of θ_2, and will be lifted by the increasing value of θ_2.
- Pressure and temperature have significant effect on asphaltene precipitation. When the temperature is fixed, the amount of asphaltene precipitation first

increases, reaches the maximum value, and then decreases with an increasing pressure. The amount of asphaltene precipitation decreases with an increasing temperature at certain pressure.

- The maximum weight fraction of asphaltene precipitation decreases with an increasing temperature. The region where asphaltene precipitation appears shrinks with an increasing temperature.
- The newly developed algorithm can converge to the correct results at all the tested conditions for the three oil samples examined in this study. It is able to generate complete *PT* and *Px* diagrams. With additional testing and further validation, it has the potential of being used to provide robust asphaltene-precipitation computations at various pressure, temperature and gas injection conditions for different oil samples.

Acknowledgments

The authors greatly acknowledge a Discovery Grant from the Natural Sciences and Engineering Research Council of Canada (NSERC) (Grant No.: NSERC RGPIN-2020-04571) to H. Li. Z. Chen also greatly acknowledges the financial support provided by the China Scholarship Council (CSC) via a PhD scholarship (No.: 201908180010).

References

1. Mullins, O. C.; Sheu, E. Y.; Hammami, A.; Marshall, A. G., Asphaltenes, heavy oils, and petroleomics. Springer Science & Business Media: 2007.

2.Behbahani, T. J.; Ghotbi, C.; Taghikhani, V.; Shahrabadi, A., Experimental investigation and thermodynamic modeling of asphaltene precipitation. *Sci. Iran.* 2011, 18, (6), 1384.

3.Angle, C. W.; Long, Y.; Hamza, H.; Lue, L., Precipitation of asphaltenes from solvent-diluted heavy oil and thermodynamic properties of solvent-diluted heavy oil solutions. *Fuel* 2006, 85, (4), 492.

4.Nellensteyn, F., The colloidal structure of bitumens. *Pet. Sci.* 1938, 4, 401.

5.Leontaritis, K. J.; Mansoori, G. A., Asphaltene flocculation during oil production and processing: A thermodynamic colloidal model, presented at *SPE International Symposium on Oilfield Chemistry*, San Antonio, TX, Feb. 4-6, 1987; SPE 1987; Paper No. SPE-16258-MS.

6.Pan, H.; Firoozabadi, A., A thermodynamic micellization model for asphaltene precipitation: Part I: Micellar size and growth. *SPE Prod. Faci.* 1998, 13, (2), 118.

7.Victorov, A. I.; Firoozabadi, A., Thermodynamic micellizatin model of asphaltene precipitation from petroleum fluids. *AIChE J.* 1996, 42, (6), 1753.

8.Wu, J.; Prausnitz, J. M.; Firoozabadi, A., Molecular‐thermodynamic framework for asphaltene‐oil equilibria. *AIChE J.* 1998, 44, (5), 1188.

9.Punnapala, S.; Vargas, F. M., Revisiting the PC-SAFT characterization procedure for an improved asphaltene precipitation prediction. *Fuel* 2013, 108, (1), 417.

10.Boek, E. S.; Yakovlev, D. S.; Headen, T. F., Quantitative molecular representation of asphaltenes and molecular dynamics simulation of their aggregation. *Energy Fuels* 2009, 23, (3), 1209.

11.Buckley, J.; Hirasaki, G.; Liu, Y.; Von Drasek, S.; Wang, J.; Gill, B., Asphaltene precipitation and solvent properties of crude oils. *Petro. Sci. Technol.* 1998, 16, (3-4), 251.

12.Czarnecki, J., Stabilization of water in crude oil emulsions. Part 2. *Energy Fuels* 2009, 23, (3), 1253.

13.Goual, L., Impedance spectroscopy of petroleum fluids at low frequency. *Energy Fuels* 2009, 23, (4), 2090.

14.Flory, P. J., Thermodynamics of high polymer solutions. *J. Chem. Phys.* 1942, 10, (1), 51.

15.Hildebrand, J. H., Solubility. III. Relative values of internal pressures and their practical application. *J. Am. Chem. Soc.* 1919, 41, (7), 1067.

16.Huggins, M. L., Solutions of long chain compounds. *J. Chem. Phys.* 1941, 9, (5), 440.

17.Scatchard, G., Equilibria in non-electrolyte solutions in relation to the vapor pressures and densities of the components. *Chem. Rev.* 1931, 8, (2), 321.

18.Scott, R. L.; Magat, M., The Thermodynamics of high‐polymer solutions: I. The free energy of mixing of solvents and polymers of heterogeneous distribution. *J. Chem. Phys.* 1945, 13, (5), 172.

19.Alboudwarej, H.; Akbarzadeh, K.; Beck, J.; Svrcek, W. Y.; Yarranton, H. W., Regular solution model for asphaltene precipitation from bitumens and solvents. *AIChE J.* 2003, 49, (11), 2948.

20.Andersen, S. I.; Speight, J. G., Thermodynamic models for asphaltene solubility and precipitation. *J. Petro. Sci. Eng.* 1999, 22, (1-3), 53.

21.Cimino, R.; Correra, S.; Sacomani, P.; Carniani, C. Thermodynamic modelling for prediction of asphaltene deposition in live oils, presented at *SPE International*

Symposium on Oilfield Chemistry, San Antonio, TX, Feb. 14-17, 1995; SPE 1995; Paper No. SPE-28993-MS.

22.Correra, S.; Merino-Garcia, D., Simplifying the thermodynamic modeling of asphaltenes in upstream operations. *Energy Fuels* 2007, 21, (3), 1243.

23.De Boer, R.; Leerlooyer, K.; Eigner, M.; Van Bergen, A., Screening of crude oils for asphalt precipitation: theory, practice, and the selection of inhibitors. *SPE Prod. Faci.* 1995, 10, (01), 55.

24.Gonzalez, D. L.; Vargas, F. M.; Mahmoodaghdam, E.; Lim, F.; Joshi, N., Asphaltene stability prediction based on dead oil properties: Experimental evaluation. *Energy Fuels* 2012, 26, (10), 6218.

25.Kawanaka, S.; Park, S. J.; Mansoori, G. A., Organic deposition from reservoir fluids: A thermodynamic predictive technique. *SPE Res. Eng.* 1991, 6, (2), 185.

26.Kraiwattanawong, K.; Fogler, H. S.; Gharfeh, S. G.; Singh, P.; Thomason, W. H.; Chavadej, S., Thermodynamic solubility models to predict asphaltene instability in live crude oils. *Energy Fuels* 2007, 21, (3), 1248.

27.Wang, J.; Buckley, J., A two-component solubility model of the onset of asphaltene flocculation in crude oils. *Energy Fuels* 2001, 15, (5), 1004.

28.Wang, J.; Buckley, J.; Burke, N.; Creek, J., A practical method for anticipating asphaltene problems (includes associated papers 104235 and 105396). *SPE Prod. Faci.* 2004, 19, (03), 152.

29.Yarranton, H. W.; Masliyah, J. H., Molar mass distribution and solubility modeling of asphaltenes. *AIChE J.* 1996, 42, (12), 3533.

30.Vargas, F. M.; Gonzalez, D. L.; Hirasaki, G. J.; Chapman, W. G., Modeling asphaltene phase behavior in crude oil systems using the perturbed chain form of the statistical associating fluid theory (PC-SAFT) equation of state. *Energy Fuels* 2009, 23, (3), 1140.

31.Chapman, W. G.; Gubbins, K. E.; Jackson, G.; Radosz, M., New reference equation of state for associating liquids. *Ind. Eng. Chem. Res.* 1990, 29, (8), 1709.

32.Ting, D. P.; Hirasaki, G. J.; Chapman, W. G., Modeling of asphaltene phase behavior with the SAFT equation of state. *Petrol. Sci. Tech.* 2003, 21, (3-4), 647.

33.Gross, J.; Sadowski, G., Perturbed-chain SAFT: An equation of state based on a perturbation theory for chain molecules. *Ind. Eng. Chem. Res.* 2001, 40, (4), 1244.

34.Gonzalez, D. L.; Hirasaki, G. J.; Creek, J.; Chapman, W. G., Modeling of asphaltene precipitation due to changes in composition using the perturbed chain statistical associating fluid theory equation of state. *Energy Fuels* 2007, 21, (3), 1231.

35.Gonzalez, D. L.; Ting, P. D.; Hirasaki, G. J.; Chapman, W. G., Prediction of asphaltene instability under gas injection with the PC-SAFT equation of state. *Energy Fuels* 2005, 19, (4), 1230.

36.Gonzalez, D. L.; Vargas, F. M.; Hirasaki, G. J.; Chapman, W. G., Modeling study of CO_2-induced asphaltene precipitation. *Energy Fuels* 2008, 22, (2), 757.

37.Panuganti, S. R.; Vargas, F. M.; Gonzalez, D. L.; Kurup, A. S.; Chapman, W. G., PC-SAFT characterization of crude oils and modeling of asphaltene phase behavior. *Fuel* 2012, 93, 658.

38.Mohebbinia, S.; Sepehrnoori, K.; Johns, R. T.; Korrani, A. K. N., Simulation of asphaltene precipitation during gas injection using PC-SAFT EOS. *J. Petrol. Sci. Eng.* 2017, 158, 693.

39.Yan, W.; Michelsen, M. L.; Stenby, E. H. On application of non-cubic EoS to compositional reservoir simulation, presented at *SPE EUROPEC/EAGE Annual Conference and Exhibition*, Vienna, Austria. May 23-26, 2011; SPE 2011; Paper No. SPE-142955-MS.

40.Darabi, H.; Shirdel, M.; Kalaei, M. H.; Sepehrnoori, K. Aspects of modeling asphaltene deposition in a compositional coupled wellbore/reservoir simulator, presented at *SPE Improved Oil Recovery Symposium*, Oklahoma, USA, Apr. 12-16, 2014; SPE 2014; Paper No. SPE-169121-MS.

41.Fazelipour, W. In Predicting asphaltene precipitation in oilfields via the technology of compositional reservoir simulation, presented at *SPE International Symposium on Oilfield Chemistry*, Texas, USA, Apr. 11-13, 2011; SPE 2011; Paper No. SPE-141148.

42.Kohse, B. F.; Nghiem, L. X.; Maeda, H.; Ohno, K. Modelling phase behaviour including the effect of pressure and temperature on asphaltene precipitation, presented at *SPE Asia Pacific Oil and Gas Conference and Exhibition*, Brisbane, Australia, Oct. 16-18, 2000; SPE 2000; Paper No. SPE-64465-MS.

43.Kord, S.; Ayatollahi, S., Asphaltene precipitation in live crude oil during natural depletion: experimental investigation and modeling. *Fluid Phase Equilibr.* 2012, 336, 63.

44.Nghiem, L.; Hassam, M.; Nutakki, R.; George, A., Efficient modelling of asphaltene precipitation, presented at *SPE Annual Technical Conference and Exhibition*, Houston, TX, Oct. 3-6,1993; SPE 1993; Paper No. SPE-26642-MS.

45.Nguele, R.; Ghulami, M. R.; Sasaki, K.; Said-Al Salim, H.; Widiatmojo, A.; Sugai, Y.; Nakano, M., Asphaltene aggregation in crude oils during supercritical gas injection. *Energy Fuels* 2016, 30, (2), 1266.

46.Qin, X.; Wang, P.; Sepehrnoori, K.; Pope, G. A., Modeling asphaltene precipitation in reservoir simulation. *Ind. Eng. Chem. Res.* 2000, 39, (8), 2644.

47.Zanganeh, P.; Dashti, H.; Ayatollahi, S., Visual investigation and modeling of asphaltene precipitation and deposition during CO2 miscible injection into oil reservoirs. *Fuel* 2015, 160, 132.

48.Li, R.; Li, H., Robust three-phase vapor–liquid–asphaltene equilibrium calculation algorithm for isothermal CO_2 flooding applications. *Ind. Eng. Chem. Res.* 2019, 58, (34), 15666.

49.Peng, D.Y.; Robinson, D. B., A new two-constant equation of state. *Ind. Eng. Chem. Fundam.* 1976, 15, (1), 59.

50.Won, K., Thermodynamics for solid solution-liquid-vapor equilibria: wax phase formation from heavy hydrocarbon mixtures. *Fluid Phase Equilibr.* 1986, 30, 265.

51.Michelsen, M. L., The isothermal flash problem. Part I. Stability. *Fluid Phase Equilibr.* 1982, 9, (1), 1.

52.Michelsen, M. L., The isothermal flash problem. Part II. Phase-split calculation. *Fluid Phase Equilibr.* 1982, 9, (1), 21.

53.Rachford Jr, H.; Rice, J., Procedure for use of electronic digital computers in calculating flash vaporization hydrocarbon equilibrium. *J. Pet. Technol.* 1952, 4, (10), 19.

54.Michelsen, M., Calculation of multiphase equilibrium. *Comput. Chem. Eng.* 1994, 18, (7), 545.

55.Leibovici, C. F.; Nichita, D. V., A new look at multiphase Rachford–Rice equations for negative flashes. *Fluid Phase Equilibr.* 2008, 267, (2), 127.

56.Okuno, R.; Johns, R.; Sepehrnoori, K., A new algorithm for Rachford-Rice for multiphase compositional simulation. *SPE J.* 2010, 15, (02), 313.

57.Li, R.; Li, H. A., New two-phase and three-phase Rachford-Rice algorithms based on free‐water assumption. *Can. J. Chem. Eng.* 2018, 96, (1), 390.

58.Lapene, A.; Nichita, D. V.; Debenest, G.; Quintard, M., Three-phase free-water flash calculations using a new Modified Rachford–Rice equation. *Fluid Phase Equilibr.* 2010, 297, (1), 121.

59.Jamaluddin, A.; Creek, J.; Kabir, C.; McFadden, J.; D'cruz, D.; Manakalathil, J.; Joshi, N.; Ross, B., Laboratory techniques to measure thermodynamic asphaltene instability. *J. Can. Pet. Tech.* 2002, 41, (07) 44.

60.Pedersen, K. S.; Fredenslund, A.; Thomassen, P., Properties of oils and natural gases. Gulf Publishing Company: 1989; Vol. 5.

61.Whitson, C. H., Characterizing hydrocarbon plus fractions. *SPE J.* 1983, 23, (04), 683.

62.Kesler, M. G.; BI, L., Improve prediction of enthalpy of fractions. *Hydrocarb. Process.* 1976, 55, (1), 153.

63.Lee, B. I.; Kesler, M. G., A generalized thermodynamic correlation based on three‐parameter corresponding states. *AIChE J.* 1975, 21, (3), 510.

64.Soreide, I., Improved phase behavior predictions of petroleum reservoir fluids from a cubic equation of state. *Dr. Techn. Thesis* 1989.

65.Riazi, M.; MR, R.; TE, D., Simplify property predictions. *Hydrocarb. Process.* 1980, 59, (1), 115.

66.PVT sim 20.0, Calsep A/S: Copenhagen, Denmark. 2011.

67.Jamaluddin, A.; Nighswander, J.; Kohse, B. F.; El Mahdi, A.; Binbrek, M.; Hogg, P. Experimental and theoretical assessment of the asphaltene precipitation characteristics of the Sahil field under a proposed miscible gas injection scheme, presented at *Abu Dhabi International Petroleum Exhibition and Conference*, Abu Dhabi, United Arab Emirates, Oct. 13-15, 2000; SPE 2000; Paper No. SPE-87292-MS.

68.Buenrostro‐Gonzalez, E.; Lira‐Galeana, C.; Gil‐Villegas, A.; Wu, J., Asphaltene precipitation in crude oils: Theory and experiments. *AIChE J.* 2004, 50, (10), 2552.

69.Chueh, P.; Prausnitz, J., Vapor‐liquid equilibria at high pressures: Calculation of partial molar volumes in nonpolar liquid mixtures. *AIChE J.* 1967, 13, (6), 1099.

CHAPTER 4 A NEW VAPOR-LIQUID-ASPHALTENE THREE-PHASE EQUILIBRIUM COMPUTATION ALGORITHM BASED ON THE FREE-ASPHALTENE ASSUMPTIONS

A version of this chapter has been published in *Fluid Phase Equilibria*.

Abstract

Asphaltene precipitation is one of the major flow-assurance problems in petroleum engineering and can occur at different stages of oil production due to pressure/temperature changes or compositional changes. It can cause formation damage in the reservoir and choking of oil tubing in the wellbore, thus leading to the reduction of production rates. Accurately predicting under what conditions asphaltene precipitation is a prerequisite to the effective mitigation of the flow assurance problems related to asphaltene precipitation. In this work, a new three-phase vapor-liquid-asphaltene precipitation algorithm is developed based on Li and Li's work (Li and Li, 2019) using the free-asphaltene assumption, in which the asphaltene phase is considered as a liquid phase that only contains asphaltene component (Nascimento *et al.*, 2018). The algorithm is validated by comparing the calculation results with the asphaltene precipitation data of five different oil samples. The tuned parameters for oil sample 3 and oil sample 4 are then used to predict asphaltene precipitation with different gas injections. The calculation results agree well with the experimental data. It indicates that the three-phase VLA equilibrium calculation algorithm can make reliable predictions of the *PT* and *Px* phase diagrams with different gas injections as well as the asphaltene precipitation amount. The calculation results yielded by the free-asphaltene assumption are also compared with the results yielded by the solid assumption and the liquid assumption. The algorithm developed using the free-asphaltene assumption is shown to be able to perform slightly better than the algorithm developed using the solid assumption, and perform as well as the algorithm developed using the liquid assumption.

4.1. Introduction

Asphaltenes are the heaviest and most polar components in crude oil, which are insoluble in n-pentane or n-heptane but soluble in aromatic solvents [1-3]. The precipitation of asphaltene can happen in all stages of oil production and transportation due to the pressure, temperature or compositional changes. It leads to issues including formation damage and choking of production tubing [4, 5]. Therefore, it is highly important to build a thermodynamic model to improve the prediction of asphaltene precipitation and help design engineering means to mitigate the associated flow assurance problems.

Many asphaltene-inclusive phase behavior models have been proposed over the last thirty years, which are based either on colloidal theory or solubility theory. Asphaltene precipitation models based on the colloidal theory assume asphaltene as solid particles stabilized by resins adsorbed on the surface [6]. Although the modeling results based on the colloidal theory agree reasonably well with the experimental data [7-10], the assumption of polar-polar interactions between asphaltenes and resins may not be appropriate [11-14]. Besides, asphaltenes are nanocolloidal in oil [15-18]. Different from colloidal theory, the solution theory assumes asphaltenes are dissolved in crude oil and the asphaltene precipitation phenomenon can be described using either liquid-liquid or solid-liquid equilibria [19]. Asphaltene precipitation models using the solution theory are generally based on the regular solution theory or an equation of state (EOS) [5]. Different regular solution theories [20-24] are applied by several researchers to predict the onset conditions of asphaltene precipitation [25-35], but the modeling results based on regular solution theories can be inaccurate when vapor phase appears [36]. In order to overcome this limitation, Zuo *et al.* [17] proposed a simplified version of Flory-Huggins-Zuo equation of state by coupling an EOS with a modified Flory-Huggins

regular-solution theory [17]. However, their research focuses on the predictions of asphaltene concentration gradients (i.e. asphaltene concentration at different depth) [15] and tar mat formations rather than asphaltene onset pressures and asphaltene precipitation amounts. On the other hand, EOS-based models account for the influences of temperature, pressure and compositions on the phase equilibria, which makes them good candidates for performing vapor-liquid-asphaltene three-phase equilibrium calculations. Asphaltene precipitation models based on cubic-plus-association (CPA) EOS have been extensively studied over the last decade [37-43] and the results are promising. However, these models require more tuning parameters for every associating component [44]. Statistical associating fluid theory (SAFT) [45] and perturbed-chain SAFT (PC-SAFT) [46] are advanced EOS models that are also widely used in predicting asphaltene precipitation [3, 5, 36, 47-56] and these models exhibit a good modeling performance. However, even with a speed-up procedure [57, 58], the models based on SAFT EOS and PC-SAFT bear a higher computational cost than the cubic EOSs (CEOSs) [57].

CEOS-based asphaltene precipitation models are frequently used in compositional simulators due to their simplicity and reasonable agreement with experimental data. The simplest asphaltene precipitation model based on CEOS is the solid model proposed by Nghiem *et al.* [59]. In the solid model, the precipitated asphaltene is considered as a pure solid phase that only contains the asphaltene component [59]. This model is then improved by Kohse *et al.* [60] to account for the effect of temperature. The pure solid model is adopted by many researchers [61-66] to conduct the three-phase vapor-liquid-solid (VLS) equilibrium calculations. In fact, the asphaltene phase might not be an entirely pure phase; the asphaltene fraction in the asphaltene phase may vary much at different pressure/temperature conditions and behave like a high-dense liquid

phase. In addition, at least two experimentally measured asphaltene onsets are required to tune the parameters used in the calculation process [60]. To overcome these limitations, Pedersen and Christensen proposed an improved approach by assuming asphaltene precipitation as a conventional liquid-high dense liquid split [6]. It has been proved that, if properly tuned, this approach can have the same accuracy as the advanced EOS models (such as SAFT and PC-SAFT EOSs) [44]. However, it should be also noticed that the models based on cubic EOSs cannot predict asphaltene gradients without the incorporation of the nanocolloidal structure of asphaltenes [18].

In this study, an improved three-phase vapor-liquid-asphaltene precipitation algorithm is developed based on Li and Li's work [67] using the free-asphaltene assumption (i.e. the asphaltene phase is considered as a dense liquid phase represented by a single asphaltene component). In this case, the appearance of the asphaltene phase can be simply detected by comparing the fugacity of the asphaltene component in the asphaltene and the non-asphaltene phases. Besides, no additional thermodynamic model needs to be introduced to describe the asphaltene phase [16, 68]. However, it should be noticed that this assumption has a limitation. In reality, the asphaltene phase may precipitate with other oil components rather than only containing asphaltene. Similar free-asphaltene assumption was also applied by Nascimento *et al.* [69] to use CPA EOS for asphaltene-related phase behavior modeling. Nascimento *et al.* [69] showed a simplified method to calculate the upper onset pressures, but they did not predict the lower onset pressures. Besides, in Nascimento *et al.*'s study [69], the bubble point is calculated by the traditional vapor-liquid equilibrium calculation algorithm, which is not proper as the bubble point is actually a three-phase bubble point and the asphaltene precipitation amount will reach the maximum value at the bubble point pressure. It should be noted that the approach by Nascimento *et al.* [69] could be further

enhanced with the asphaltene-related flash approach by Pedersen *et al.* [6] to perform liquid-asphaltene two-phase flash calculations or vapor-liquid-asphaltene three-phase flash calculations. In this study, the original algorithm developed by Li and Li [67] is enhanced with additional measures to improve the robustness of the algorithm. Several case studies are conducted to validate the reliability of the new modeling approach for the prediction of asphaltene precipitation onsets and asphaltene precipitation amounts with and without gas injections.

4.2. Mathematical Formulations

4.2.1. Free-Asphaltene Assumption and Fugacity of the Asphaltene Phase

In this study, a VLA three-phase equilibrium calculation algorithm is proposed based on the so-called free-asphaltene assumption, in which the asphaltene phase is considered as a pure liquid phase that only contains asphaltene. As a result of this assumption, both the stability test and flash calculations can be greatly simplified. PR-EOS [70] is applied to conduct the flash calculations, which is given by Equations (1-3) in terms of *Z* factor:

$$Z^3 - (1 - B)Z^2 + (A - 3B^2 - 2B)Z - (AB - B^2 - B^3) = 0 \quad (1)$$

$$A = \frac{aP}{(RT)^2} \quad (2)$$

$$B = \frac{bP}{RT} \quad (3)$$

where P is pressure, T is temperature, R is the ideal gas constant. In Equations (2-3), a and b are two EOS constants that can be calculated by [70]:

$$a = 0.45724 \frac{R^2 T_c^2}{P_c} \alpha(T_r, \omega) \quad (4)$$

$$b = 0.0778\frac{RT_c}{P_c} \text{ (5)}$$

where P_c is critical pressure, T_c is critical temperature, α is the alpha function, T_r is the reduced temperature (T_r=T/T_c), and ω is acentric factor. The α-function is given by [70]:

$$\alpha = [1 + m(1 - \sqrt{T_r})]^2 \text{ (6)}$$

If $\omega \leq 0.49$, m is given by [70]:

$$m = 0.37464 + 1.54226\omega - 0.26992\omega^2 \text{ (7)}$$

If $\omega > 0.49$, m can be expressed by [70]:

$$m = 0.3796 + 1.485\omega - 0.1644\omega^2 + 0.1667\omega^3 \text{ (8)}$$

In the free-asphaltene assumption, the asphaltene phase is assumed to contain only asphaltene. Based on this assumption, we can calculate the fugacity of the asphaltene phase as per [70]:

$$ln\frac{f_a}{P} = Z - 1 - \ln(Z - B) - \frac{A}{2\sqrt{2}}\ln\left[\frac{Z+(1+\sqrt{2})B}{Z+(1-\sqrt{2})B}\right] \text{ (9)}$$

where f_a represents the fugacity of asphaltene in the asphaltene phase. As seen from Equation (9), the fugacity of the asphaltene phase can be readily evaluated using PR-EOS at given temperature and pressure. This is the major difference between the algorithms based on the pure solid assumption [67, 71] and the algorithm proposed in this work. In the solid-assumption approach, an empirical correlation is normally used to calculate the fugacity of the asphaltene phase. This may give rise to a thermodynamic inconsistency issue: the vapor and liquid phases are described using PR-EOS, while the asphaltene phase is described using the empirical fugacity model. As shown by Li and

Li [67], due to this thermodynamic inconsistency issue, we may encounter the appearance of some unusual phase equilibria when we attempt to draw the pressure-composition (*Px*) phase diagrams by using the VLS algorithm developed with the solid-assumption approach. But we do not encounter this problem when performing phase equilibrium calculations using the VLA algorithm developed using the free-asphaltene-assumption approach. Besides, in the solid assumption, the heat fusion difference and the heat capacity difference have to be regressed based on two or three experimentally measured asphaltene precipitation onsets, and the asphaltene molar volume and BIPs need to be tuned to match the measured saturation pressure and the asphaltene precipitation amount. While, in our approach, only the critical properties of the asphaltene component and BIPs need to be tuned based on at least one measured upper onset pressure and one measured saturation pressure. This forms the main difference in the tuning process between our approach and the solid-assumption approach.

4.2.2. Phase Stability Test

One obvious advantage of the free-asphaltene assumption is that it can significantly reduce the complexity of the stability test involved in the multiphase equilibrium calculations. Based on the free-asphaltene assumption, the appearance of the asphaltene phase can be detected by checking the inequality shown in the following equation [67],

$$\begin{cases} f_{ax} < f_{aa}, \text{ asphaltene phase does not appear} \\ f_{ax} \geq f_{aa}, \text{ asphaltene phase appears} \end{cases} \quad (10)$$

where f_{ax} and f_{aa} represent the fugacities of asphaltene component in the non-asphaltene phase and the asphaltene phase, respectively. In this study, the fugacities of the asphaltene component in the asphaltene phase and the asphaltene phase are calculated by PR EOS [70], leading to a consistent thermodynamic description of the asphaltene component across all the phases. The conventional phase stability test algorithm

proposed by Michelsen [72] is applied in this study to check the appearance of a vapor phase or a liquid phase. The tangent plane distance (*TPD*) function used in the stability analysis is given by [72]:

$$TPD = \sum_{i=1}^{n} y_i[ln\varphi_i(y) + lny_i - ln\varphi_i(z) - lnz_i] \quad (11)$$

where y and z represent the trial phase composition and the feed composition, respectively, φ_i is the fugacity coefficient of component i, and n is the number of components. Note that the last component (i.e., when $i=n$) is the asphaltene component. If the values of *TPD* at any compositions of the trial phase are larger than or equal to zero, the mixture will be considered stable. Otherwise, it is not stable.

4.2.3. Flash Calculations

4.2.3.1. Two-Phase Flash Calculations

Two possible two-phase equilibria can be yielded by three-phase equilibrium calculations: two-phase vapor-liquid (VL) equilibria and two-phase vapor/liquid-asphaltene (V/L-A) equilibria. The convergence of two-phase flash calculations depends on two conditions being met: the material balance constraint and the equal-fugacity constraint.

For the two-phase VL flash calculations, the algorithm proposed by Michelsen [73] is adopted in this study. The equal-fugacity constraint can be shown as:

$$f_{ix} = f_{iy}, i = 1, \dots, n \quad (12)$$

where f_{ix} and f_{iy} represent the fugacities of component i in the liquid phase and vapor phase, respectively. The Rachford-Rice (RR) equation [74] is developed based on material balance and can be used to calculate the phase fractions:

$$RR_y = \sum_{i=1}^{n}(y_i - x_i) = \sum_{i=1}^{n} \frac{z_i(K_{iy}-1)}{1+\beta_y(K_{iy}-1)} = 0 \quad (13)$$

where x_i and y_i represent the mole fractions of component *i* in phase *x* and phase *y*, respectively, z_i represents the mole fraction of component *i* in the feed, and β_y is the phase mole fraction of phase *y*. K_{iy} is the equilibrium ratio of component *i* in phase *y* and can be calculated by:

$$K_{iy} = \frac{y_i}{x_i} = \frac{\varphi_{ix}}{\varphi_{iy}} \quad (14)$$

Based on the free-asphaltene assumption, the equal-fugacity constraint of the two-phase V/L-A flash calculation can be simplified as follows since only the asphaltene component appears in the asphaltene phase [67]:

$$f_{ax} = f_{aa} \quad (15)$$

where f_{ax} and f_{aa} represent the fugacity of asphaltene in the non-asphaltene phase and the asphaltene phase, respectively. The value of f_{aa} and f_{ax} can be calculated based on PR EOS [70] at given composition, pressure and temperature. The composition of the non-asphaltene phase can be calculated based on the material balance constraint [67]:

$$x_i = \begin{cases} z_i/(1-\beta_a), i = 1, \ldots, n-1 \\ (z_i - \beta_a)/(1-\beta_a), i = n \end{cases} \quad (16)$$

where β_a represents the mole fraction of the asphaltene phase, x_i and z_i represent the mole fractions of component *i* in the non-asphaltene phase and the feed, respectively. By updating β_a, the equal-fugacity constraint can be satisfied.

4.2.3.2. Three-Phase VLA Flash Calculation

The equal fugacity constraints for the three-phase vapor-liquid-asphaltene flash calculations can be simplified as the following equations based on the free-asphaltene assumption [67]:

$$f_{ix} = f_{iy}, i = 1, \ldots, n \text{ (17)}$$

$$f_{ax} = f_{ay} = f_{aa} \text{ (18)}$$

Based on previous researchers' work and the free-water assumption [75-77], Li and Li [78] simplified the objective function and constraints of the minimization problem for three-phase vapor-liquid-aqueous flash calculations [79]. The objective function and the constraints given by Li and Li [78] can be also applied in this study. The objective function and the constraints for the three-phase VLS flash calculations are given by [78]:

$$min\, f(\beta_y) = \sum_{i=1}^{n-1} -z_i \ln\left[\left(K_{iy} - K_{ay}^*\right)\beta_y + K_{az}^*\right] \text{ (19)}$$

subjected to [78]

$$\left(K_{ay}^* - K_{iy}\right)\beta_y \le min\left\{K_{az}^* - z_i, K_{az}^* - K_{iy}z_i\right\}, i = 1, \ldots, n-1 \text{ (20)}$$

where [78]

$$\begin{cases} K_{ay}^* = \frac{1-y_a}{1-x_a} \\ K_{az}^* = \frac{1-z_a}{1-x_a} \end{cases} \text{ (21)}$$

where x_a, y_a, and z_a represent the mole fractions of asphaltene component in the liquid phase, the vapor phase, and the feed, respectively. In this case, there is only one unknown β_y in the objective function. Equation (20) forms a reliable feasible region of

β_y. The mole fraction of the asphaltene phase (β_a) can be calculated using Equation (22), which is similar to the one proposed by Lapene *et al.* [80]:

$$\beta_a = \frac{z_a + (x_a - y_a)\beta_y - x_a}{1 - x_a} \quad (22)$$

The mole fraction of the liquid phase (β_x) can thus be calculated using the following equation [78]:

$$\beta_x = 1 - \beta_y - \beta_a \quad (23)$$

Subsequently, the composition of the liquid phase (x_i) can be calculated as per [78]:

$$x_i = \begin{cases} \frac{z_i}{K_{iy} - K_{ay}^* \beta_y + K_{az}^*}, i = 1, \dots, n-1 \\ \frac{1}{K_{ia}}, i = n \end{cases} \quad (24)$$

where [78]

$$K_{ia} = \frac{a_i}{x_i} = \frac{\phi_{ix}}{\phi_{ia}}, i = 1, \dots, n \quad (25)$$

where a_i represents the mole fraction of component *i* in the asphaltene phase and ϕ_{ia} represents the fugacity coefficient of component *i* in the asphaltene phase. Based on the assumption that the asphaltene phase only contains asphaltene, the values of a_i are either 0 (i.e., non-asphaltene components) or 1 (i.e., asphaltene component). The composition of the vapor phase can be calculated using Equation (14).

4.3. Three-Phase VLA Equilibrium Calculation Algorithm

The proposed three-phase VLA equilibrium calculation algorithm is modified based on the three-phase VLS equilibrium calculation algorithm proposed by Li and Li [67] and the flow chart is shown in Figure 4-1. The major modification lies in that when the result of stability test is stable and the appearance of asphaltene phase is detected, both

VL two-phase flash and V/L-A two-phase flash are conducted. If multiple two-phase equilibria are yielded, the one with the lowest Gibbs free energy is chosen. The V/L-A flash calculation algorithm and the three-phase VLA flash calculation algorithm closely follow the algorithms proposed by Li and Li [67]. The detailed procedure of performing the three-phase VLA equilibrium calculation is shown as follows:

(1) The initialization method proposed by Li and Li [67] based on Li and Firoozabadi's work [81] is applied in this algorithm. The compositions of the trail phases at all the stationary points that have negative *TPD* values are output as x_0_i. x_01_i, x_02_i, *etc*.

(2) If the feed composition is stable, continue; if not, go to step (7);

(3) Check the appearance of asphaltene phase using Equation (10). If asphaltene phase appears, continue; if not, output one-phase equilibrium.

(4) Conduct two-phase V/L-A flash calculations and calculate the Gibbs free energy of the two-phase system G_a.

(5) Conduct two-phase VL flash calculations with multiple initial equilibrium ratios that are calculated by the following equations [67],

$$\boldsymbol{K_{iy} = z_i/x\_0_i},\ \boldsymbol{K_{iy} = z_i/x\_01_i},\ \boldsymbol{K_{iy} = z_i/}x\_02_i,\ \boldsymbol{etc.\ i = 1,\ldots,n} \quad (26)$$

If multiple two-phase equilibria are yielded, select the one with the lowest Gibbs free energy and output it as *G*.

(6) If $G_a<G$, output two-phase V/L-A equilibrium; otherwise, output two-phase VL equilibrium.

(7) Check the appearance of asphaltene phase using Equation (10). If asphaltene phase appears, go to step (10); if not, continue.

(8) Conduct two-phase VL flash calculation with the initial equilibrium ratios given by Equation (26) and output vapor-phase compositions ($x_i^{2\text{-}VL}$ and $y_i^{2\text{-}VL}$) and mole

fractions of liquid phase and vapor phase ($\beta_x^{2\text{-}VL}$ and $\beta_y^{2\text{-}VL}$).

(9) Check the appearance of asphaltene phase using Equation (10). If asphaltene phase appears, conduct three-phase VLA flash calculation using Algorithm #1 proposed by Li and Li [67] and output three-phase VLA equilibrium; if not, output two-phase VL equilibrium. The initial equilibrium ratios proposed by Li and Li [67] are used in the three-phase VLA flash calculation:

$$\boldsymbol{K_{iy} = y_i^{2-VL}/x_i, i = 1, \ldots, n} \quad (27)$$

where

$$\boldsymbol{x_i = \begin{cases} x_i^{2-VL}/(1 - 0.99 \times x_a^{2-VL}), i \neq n \\ 0.01 \times x_i^{2-VL}/(1 - 0.99 \times x_a^{2-VL}), i = n \end{cases}} \quad (28)$$

(10) Use Algorithm #1 proposed by Li and Li [67] to conduct three-phase VLA flash calculation. The Wilson equation [82] is used to initialize the equilibrium ratios:

$$\boldsymbol{K_i^{Wilson} = \frac{P_{ci}}{P} exp\left[5.37(1 + \omega_i)\left(1 - \frac{T_{ci}}{T}\right)\right]} \quad (29)$$

Output liquid-phase, vapor-phase, and asphaltene-phase compositions ($x_i^{3\text{-}1}$, $y_i^{3\text{-}1}$, and $a_i^{3\text{-}1}$) and mole fractions of liquid, vapor, and asphaltene phases ($\beta_x^{3\text{-}1}$, $\beta_y^{3\text{-}1}$, and $\beta_a^{3\text{-}1}$). If the results calculated by Algorithm #1 [67] are physical, output three-phase VLA equilibrium; otherwise, continue.

(11) If $\beta_a^{3\text{-}1}<0$, conduct two-phase VL flash with the initial equilibrium ratios calculated by:

$$\boldsymbol{K_{iy} = y_i^{3-1}/x_i^{3-1}, i = 1, \ldots, n} \quad (30)$$

Otherwise, use Equation (26) to conduct two-phase VL flash. If multiple two-phase equilibria are yielded, select the one with the lowest Gibbs free energy and output liquid-phase and vapor-phase compositions ($x_i^{2\text{-}VL}$ and $y_i^{2\text{-}VL}$) and mole fractions of liquid phase and vapor phase ($\beta_x^{2\text{-}VL}$ and $\beta_y^{2\text{-}VL}$).

(12) Perform stability test. Inequality in Equation (10) is again checked on the two

phases yielded by the two-phase VL flash calculation. If either of these two phases is unstable, conduct three-phase VLA flash calculation using Algorithm #1 [67]. The equilibrium ratios given in Equation (27) are used to initialize the three-phase VLA flash. Output liquid-phase, vapor-phase, and asphaltene-phase compositions ($x_i^{3\text{-}2}$, $y_i^{3\text{-}2}$, and $a_i^{3\text{-}2}$) and mole fractions of liquid, vapor, and asphaltene phases ($\beta_x^{3\text{-}2}$, $\beta_y^{3\text{-}2}$, and $\beta_a^{3\text{-}2}$), and go to Step 13. If both phases are stable, output two-phase VL equilibrium.

(13) If physical results can be obtained from the three-phase VLA flash calculation, output three-phase VLA equilibrium. Otherwise, conduct two-phase V/L-A flash calculation and output non-asphaltene-phase and asphaltene-phase compositions ($x_i^{2\text{-}V/L\text{-}A}$ and $a_i^{2\text{-}V/L\text{-}A}$) and mole fractions of non-asphaltene phase and asphaltene phase ($\beta_x^{2\text{-}V/L\text{-}A}$ and $\beta_a^{2\text{-}V/L\text{-}A}$).

Check the stability of the non-asphaltene phase yielded by the two-phase V/L-A flash calculation. If the result of the stability test is stable, output two-phase V/L-A equilibrium; otherwise, conduct three-phase VLA flash calculation using Algorithm #2 [67] and output three-phase VLA equilibrium.

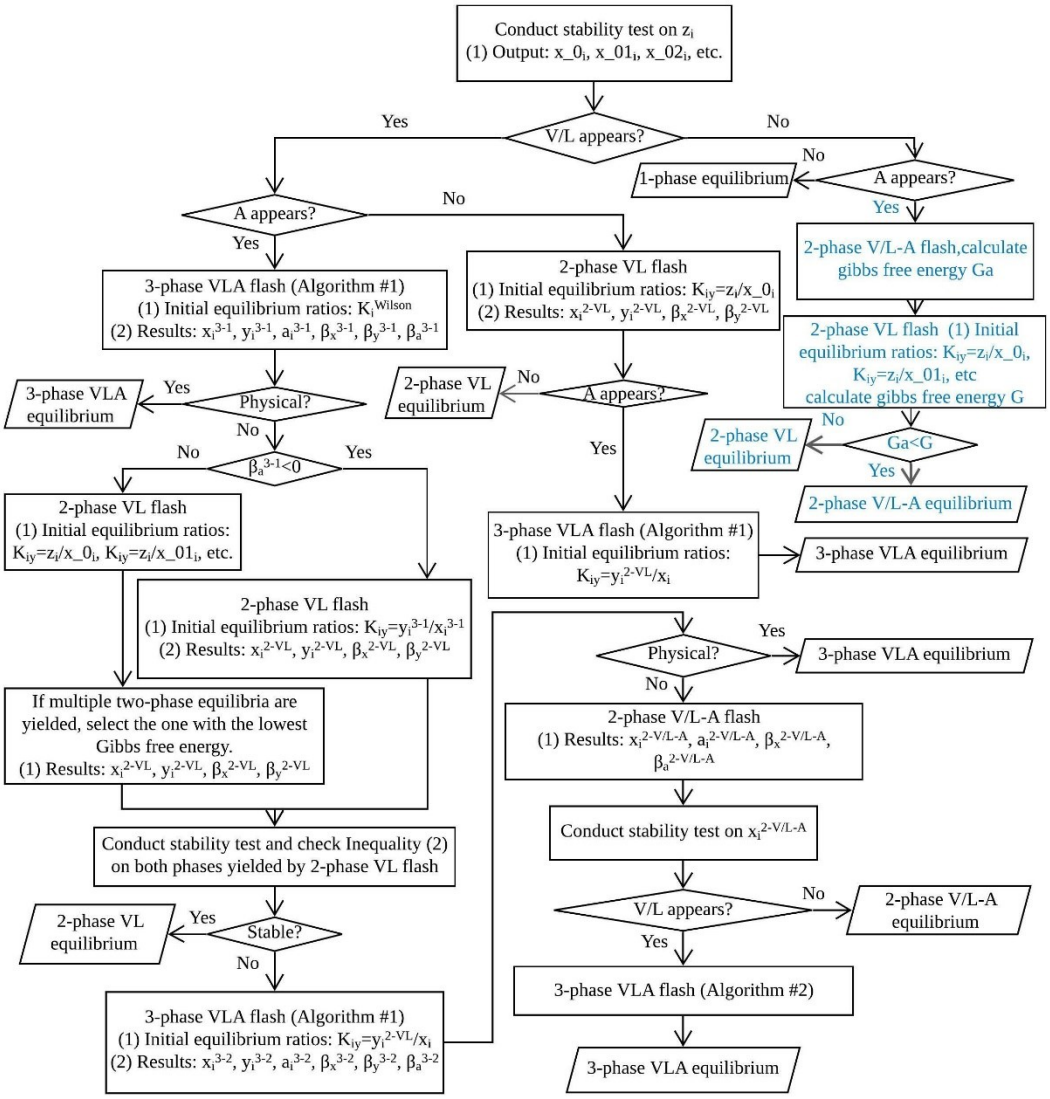

Fig. 4-1 Flowchart of the three-phase VLA equilibrium calculation algorithm. This is modified based on the one proposed by Li and Li's [67]. The modifications are highlighted with blue texts.

4.4. Results and Discussion

In this section, example calculations are conducted based on five different reservoir fluids collected from the literature. Here we assume that a thermodynamic equilibrium is valid for all these five oil samples. However, it should be noted that an equilibrium state may not be attainable for some crude oils under reservoir conditions [83]. The calculation results are compared with the experimental data to check the robustness of

the modified algorithm. We also compare the calculation results yielded by different assumptions to verify the feasibility of the free-asphaltene assumption and examine which assumption gives better asphaltene-precipitation predictions.

4.4.1. Oil Sample Characterizations

4.4.1.1. Oil Sample 1

Oil sample 1 is a stock tank oil from the Middle East region studied by Jamaluddin *et al.* [84]. The composition of oil sample 1 is shown in Table 4-1. The API gravity of this oil sample is 39° API [84]. The molecular weight of the oil sample is 82.49 g/mol [84]. The molecular weight and density of the C_{7+} fraction are 228.07 g/mol and 0.865 g/cm^3, respectively [84]. The oil characterization is done using the approach developed by Pedersen *et al.* [6]. In this approach, each pseudoconponent heavier than C_{49} is split into asphaltene and non-asphaltene components. If there are more than one non-asphaltene components, the non-asphaltene components are lumped together using the lumping method proposed by Pedersen *et al.* [6]. The critical temperature, critical pressure and acentric factor of the non-asphaltene component can be calculated by Equations (31-33) [6].

$$T_{ci} = z_{i\,NA} T_{ci\,NA} + z_{i\,A} T_{ci\,A} \quad (31)$$

$$\frac{1}{P_{ci}} = \frac{(z_{i\,NA})^2}{P_{ci\,NA}} + \frac{(z_{i\,A})^2}{P_{ci\,A}} + \frac{2 \times z_{i\,NA} \times z_{i\,A}}{\sqrt{P_{ci\,NA} * P_{ci\,A}}} \quad (32)$$

$$\omega_i = z_{i\,NA} \omega_{i\,NA} + z_{i\,A} \omega_{i\,A} \quad (33)$$

where T_{ci}, P_{ci} and ω_i represent the critical temperature, critical pressure and acentric factor of pseudocomponent i, respectively. The subscripts A and NA represent the asphaltene component and the non-asphaltene component, respectively. $z_{i\,NA}$ and $z_{i\,A}$ are the fractions of the non-asphaltene component and the asphaltene component,

respectively. The critical temperature, critical pressure and acentric factor of the asphaltene component are by default set as 1398.5 K, 14.95 bar and 1.274, respectively [6]. The critical properties of the asphaltene component can be tuned to match the experimental data. For oil sample 1, the critical temperature and critical pressure of the asphaltene component are tuned to be 1423.076 K and 16.7 bar, respectively. The final characterization scheme of oil sample 1 is shown in Table 4-2. Note that the critical properties of the first nine components are taken from the literature [85].

The binary interaction parameters (BIPs) can also be tuned to better match the experimental data. The model proposed by Chueh and Prausnitz [86] is adopted in this study to calculate BIPs,

$$k_{ij} = 1 - \left[\frac{2v_{ci}^{1/6}v_{cj}^{1/6}}{v_{ci}^{1/3}+v_{cj}^{1/3}}\right]^{\theta} \quad (34)$$

where k_{ij} is the BIP between component i and component j, v_{ci} and v_{cj} are the critical volumes of component i and component j, respectively, θ is the exponent, and the subscripts i and j represent component i and component j, respectively. In this study, we set the exponent θ as 0.005 when calculating the BIPs between hydrocarbon components. The exponent θ between the asphaltene component and other components is tuned to be 0.005 for oil sample 1. The BIPs used for oil sample 1 are shown in Table 4-3. In Table 4-3, the BIPs between N_2 and the non-asphaltene components are taken from the literature [85].

Table 4-1 Composition of oil sample 1 [84].

Component	Composition (mol%)
N_2	0.48
CO_2	0.92
C_1	43.43
C_2	11.02
C_3	6.55

i-C_4	0.79
n-C_4	3.70
i-C_5	1.28
n-C_5	2.25
C_6	2.70
C_{7+}	26.88

Table 4-2 Characterization results of oil sample 1.

Component	Composition (mol%)	T_c (K)	P_c (bar)	V_c (m^3/kmol)	ω	MW (g/mol)
N_2	0.481	126.200	33.94	89.80	0.040	28.014
CO_2	0.922	304.200	73.76	94.00	0.225	44.01
C_1	43.501	190.600	46.00	99.00	0.008	16.043
C_2	11.038	305.400	48.84	148.00	0.098	30.070
C_3	6.561	369.800	42.46	203.00	0.152	44.097
i-C_4	0.791	408.100	36.48	263.00	0.176	58.124
n-C_4	3.706	425.200	38.00	255.00	0.193	58.124
i-C_5	1.282	460.400	33.84	306.00	0.227	72.151
n-C_5	2.254	469.600	33.74	304.00	0.251	72.151
C_6	2.704	507.400	29.69	370.00	0.296	86.178
C_7	2.488	538.119	29.9	446.59	0.338	96.000
C_8	2.257	558.729	27.59	476.11	0.374	107.000
C_9	2.047	582.505	25.16	522.24	0.421	121.000
C_{10}-C_{12}	5.070	622.122	22.00	616.07	0.505	146.458
C_{13}-C_{14}	2.643	669.274	19.15	754.01	0.615	182.135
C_{15}-C_{17}	3.113	715.409	17.21	919.98	0.731	220.660
C_{18}-C_{20}	2.324	760.422	15.85	1102.36	0.846	262.221
C_{21}-C_{23}	1.734	802.703	14.91	1294.39	0.952	303.790
C_{24}-C_{27}	1.648	847.816	14.15	1518.93	1.058	350.513
C_{28}-C_{33}	1.530	910.362	13.39	1860.17	1.181	419.041
C_{34}-C_{42}	1.124	996.391	12.68	2376.67	1.275	519.014
C_{43}-C_{80}	0.692	1135.398	11.45	3547.56	1.020	721.267
C_{43}-C_{80} A	0.089	1423.076	16.70	3547.56	1.274	721.267

Table 4-3 BIPs used for oil sample 1 [85].

	N_2	CO_2	C_{43}-C_{80} A
N_2	0.00000	-0.01700	0.08000
CO_2	-0.01700	0.00000	0.10000
C_1	0.03110	0.12000	0.00084
C_2	0.05150	0.12000	0.00067
C_3	0.08520	0.12000	0.00055

i-C_4	0.10330	0.12000	0.00046
n-C_4	0.08000	0.12000	0.00047
i-C_5	0.09220	0.12000	0.00041
n-C_5	0.10000	0.12000	0.00041
C_6	0.08000	0.12000	0.00035
C_7	0.08000	0.10000	0.00029
C_8	0.08000	0.10000	0.00027
C_9	0.08000	0.10000	0.00025
C_{10}-C_{12}	0.08000	0.10000	0.00021
C_{13}-C_{14}	0.08000	0.10000	0.00016
C_{15}-C_{17}	0.08000	0.10000	0.00013
C_{18}-C_{20}	0.08000	0.10000	0.00009
C_{21}-C_{23}	0.08000	0.10000	0.00007
C_{24}-C_{27}	0.08000	0.10000	0.00005
C_{28}-C_{33}	0.08000	0.10000	0.00003
C_{34}-C_{42}	0.08000	0.10000	0.00001
C_{43}-C_{80}	0.08000	0.10000	0
C_{43}-C_{80} A	0.08000	0.10000	0

4.4.1.2. Oil Sample 2

Oil sample 2 is a live oil sample from Mexico studied by Buenrostro‐Gonzalez *et al.* [87]. Table 4-4 summarizes the composition of oil sample 2. The C_7+ component of oil sample 2 has a molecular weight of 334.66 g/mol and a density of 0.8822 g/cm^3 [87]. Oil sample 2 is also characterized using the method proposed by Petersen *et al.* [6] and the characterization results are shown in Table 4-5. The critical temperature, critical pressure and the exponent θ between asphaltene and other components in Equation (34) are tuned to be 1679.781 K, 13.2 bar and 0.030 for oil sample 2. The BIPs used for oil sample 2 are shown in Table 4-6. In Table 4-6, the BIPs between N_2, H_2S and other components except for the asphaltene component are taken from the literature [85].

Table 4-4 Composition of oil sample 2 [87].

Component	Composition (mol%)
N_2	0.91
CO_2	1.57
H_2S	5.39

C_1	24.02
C_2	10.09
C_3	9.58
i-C_4	1.83
n-C_4	4.83
i-C_5	2.27
n-C_5	2.74
C_6	4.77
C_{7+}	32.00

Table 4-5 Characterization results of oil sample 2.

Component	Composition (mol%)	T_c (K)	P_c (bar)	V_c (m^3/kmol)	ω	MW (g/mol)
N_2	0.937	126.200	33.94	89.80	0.040	28.014
CO_2	1.617	304.200	73.76	94.00	0.225	44.010
H_2S	5.551	373.200	89.37	98.50	0.100	34.080
C_1	24.740	190.600	46.00	99.00	0.008	16.043
C_2	10.392	305.400	48.84	148.00	0.098	30.070
C_3	9.867	369.800	42.46	203.00	0.152	44.097
iC_4	1.885	408.100	36.48	263.00	0.176	58.124
nC_4	4.975	425.200	38.00	255.00	0.193	58.124
iC_5	2.338	460.400	33.84	306.00	0.227	72.151
nC_5	2.822	469.600	33.74	304.00	0.251	72.151
C_6	4.913	507.400	29.69	370.00	0.296	86.178
C_7	1.312	538.851	30.10	433.59	0.338	96.000
C_8	1.257	559.155	27.69	468.83	0.374	107.000
C_9	1.204	582.660	25.20	519.71	0.421	121.000
C_{10}-C_{16}	7.128	662.330	19.62	751.15	0.603	173.920
C_{17}-C_{22}	4.619	766.814	15.47	1151.31	0.866	268.651
C_{23}-C_{28}	3.572	846.502	13.90	1530.00	1.059	350.742
C_{29}-C_{33}	2.350	915.931	13.02	1900.57	1.195	428.801
C_{34}-C_{40}	2.548	986.513	12.41	2310.52	1.273	511.604
C_{41}-C_{47}	1.888	1065.615	11.93	2800.55	1.268	609.604
C_{48}-C_{80}	3.610	1196.515	11.11	4070.84	0.717	837.328
C_{48}-C_{80} A	0.475	1679.781	13.20	4070.84	1.274	837.328

Table 4-6 BIPs used for oil sample 2 [85].

	N_2	CO_2	H_2S	C_{43}-C_{80} A
N_2	0.00000	-0.01700	0.17700	0.00568
CO_2	-0.01700	0.00000	0.09700	0.00555
H_2S	0.17700	0.09700	0.00000	0.00542

C_1	0.03100	0.07000	0.08000	0.00541
C_2	0.05200	0.07000	0.08300	0.00435
C_3	0.08500	0.07000	0.08800	0.00359
iC_4	0.10300	0.07000	0.04700	0.00302
nC_4	0.08000	0.07000	0.06000	0.00309
iC_5	0.09200	0.07000	0.06000	0.00270
nC_5	0.10000	0.07000	0.06000	0.00272
C_6	0.08000	0.07000	0.06000	0.00233
C_7	0.08000	0.07000	0.06000	0.00204
C_8	0.08000	0.07000	0.06000	0.00190
C_9	0.08000	0.07000	0.06000	0.00173
C_{10}-C_{16}	0.08000	0.07000	0.06000	0.00117
C_{17}-C_{22}	0.08000	0.07000	0.06000	0.00066
C_{23}-C_{28}	0.08000	0.07000	0.06000	0.00040
C_{29}-C_{33}	0.08000	0.07000	0.06000	0.00024
C_{34}-C_{40}	0.08000	0.07000	0.06000	0.00013
C_{41}-C_{47}	0.08000	0.07000	0.06000	0.00006
C_{48}-C_{80}	0.08000	0.07000	0.06000	0
C_{48}-C_{80} A	0.00568	0.00555	0.00542	0

4.4.1.3. Oil Sample 3

Oil sample 3 is a black oil sample reported by Jamaluddin *et al.* [88]. Table 4-7 shows the composition of oil sample 3. Oil sample 3 has the API gravity of 32° API [88]. The molecular weight of the oil sample is 102.04 g/mol [88]. The molecular weight and density of the C_{12+} fraction are 337.94 g/mol and 0.906 g/cm^3, respectively [88]. Again, we characterize this oil sample using the approach proposed by Petersen *et al*. [6]. Table 4-8 shows the characterization results of oil sample 3. For oil sample 3, the critical temperature, critical pressure and the exponent θ between asphaltene and other components are tuned to be 1325.721 K, 17.24 bar and 0.08. The BIPs used for oil sample 3 are shown in Table 4-9. Note that the BIPs between N_2, H_2S and other components except for the asphaltene component are taken from the literature [85]. The BIP between N_2 and asphaltene component is tuned to be 0.38000.

Table 4-7 Composition of oil sample 3 [88].

Component	Composition (mol%)
N_2	0.49
CO_2	11.37
H_2S	3.22
C_1	27.36
C_2	9.41
C_3	6.70
i-C_4	0.81
n-C_4	3.17
i-C_5	1.22
n-C_5	1.98
C_6	2.49
C_7	2.87
C_8	3.14
C_9	2.74
C_{10}	2.32
C_{11}	1.90
C_{12+}	18.82

Table 4-8 Characterization results of oil sample 3.

Component	Composition (mol%)	T_c (K)	P_c (bar)	V_c (m^3/kmol)	ω	MW (g/mol)
N_2	0.498	126.200	33.94	89.80	0.040	28.014
CO_2	11.567	304.200	73.76	94.00	0.225	44.010
H_2S	3.276	373.200	89.37	98.50	0.100	34.080
C_1	27.833	190.600	46.00	99.00	0.008	16.043
C_2	9.573	305.400	48.84	148.00	0.098	30.070
C_3	6.816	369.800	42.46	203.00	0.152	44.097
iC_4	0.824	408.100	36.48	263.00	0.176	58.124
nC_4	3.225	425.200	38.00	255.00	0.193	58.124
iC_5	1.241	460.400	33.84	306.00	0.227	72.151
nC_5	2.014	469.600	33.74	304.00	0.251	72.151
C_6	2.533	507.400	29.69	370.00	0.296	86.178
C_7	2.92	536.488	29.45	475.55	0.337	96.000
C_8	3.194	558.043	27.42	487.84	0.374	107.000
C_9	2.787	582.078	25.06	529.18	0.421	121.000
C_{10}-C_{13}	6.324	625.359	21.64	638.09	0.515	148.824
C_{14}-C_{17}	3.388	706.030	17.45	896.21	0.709	212.553
C_{18}-C_{21}	2.654	767.205	15.59	1140.15	0.865	268.996
C_{22}-C_{26}	2.524	828.113	14.39	1424.06	1.014	329.955
C_{27}-C_{31}	1.860	892.979	13.51	1764.39	1.152	400.293

C_{32}-C_{37}	1.598	959.483	12.90	2148.52	1.250	476.513
C_{38}-C_{45}	1.396	1039.375	12.39	2649.51	1.282	572.530
C_{45}-C_{80}	1.630	1206.013	10.95	3934.64	0.802	791.017
C_{45}-C_{80} A	0.325	1325.721	17.24	3934.64	1.274	791.017

Table 4-9 BIPs used for oil sample 3 [85].

	N_2	CO_2	H_2S	C_{43}-C_{80} A
N_2	0.00000	-0.01700	0.17700	0.38000
CO_2	-0.01700	0.00000	0.09700	0.01448
H_2S	0.17700	0.09700	0.00000	0.01414
C_1	0.03100	0.07000	0.08000	0.01411
C_2	0.05200	0.07000	0.08300	0.01134
C_3	0.08500	0.07000	0.08800	0.00935
iC_4	0.10300	0.07000	0.04700	0.00784
nC_4	0.08000	0.07000	0.06000	0.00801
iC_5	0.09200	0.07000	0.06000	0.00701
nC_5	0.10000	0.07000	0.06000	0.00705
C_6	0.08000	0.07000	0.06000	0.00604
C_7	0.08000	0.07000	0.06000	0.00485
C_8	0.08000	0.07000	0.06000	0.00474
C_9	0.08000	0.07000	0.06000	0.00438
C_{10}-C_{13}	0.08000	0.07000	0.06000	0.00362
C_{14}-C_{17}	0.08000	0.07000	0.06000	0.00241
C_{18}-C_{21}	0.08000	0.07000	0.06000	0.00169
C_{22}-C_{26}	0.08000	0.07000	0.06000	0.00114
C_{27}-C_{31}	0.08000	0.07000	0.06000	0.00071
C_{32}-C_{37}	0.08000	0.07000	0.06000	0.00041
C_{38}-C_{45}	0.08000	0.07000	0.06000	0.00017
C_{45}-C_{80}	0.08000	0.07000	0.06000	0
C_{45}-C_{80} A	0.38000	0.01448	0.01414	0

4.4.1.4. Oil Sample 4

Oil sample 4 is a single-phase bottomhole sample measured by Memon *et al.* [89]. The composition of oil sample 4 is shown in Table 4-10. The API gravity of oil sample 4 is 32.4° API [89]. The molecular weight of the oil sample is 102.6 g/mol[89]. The molecular weight and density of the C_{20+} fraction of oil sample 4 are 444.98 g/mol and 0.929 g/cm^3, respectively [89]. Oil sample 4 is also characterized using the approach

proposed by Petersen *et al*. [6] and the characterization results are shown in Table 4-11. For oil sample 4, the critical temperature, critical pressure and the exponent θ are tuned to be 1115.526 K, 20.92 bar and 0.065. The BIPs used for oil sample 4 are shown in Table 4-12. Note that the BIPs between N_2 and other components except for the asphaltene component are taken from the literature [85]. The BIP between CO_2 and asphaltene is tuned to be 0.35000.

Table 4-10 Composition of oil sample 4 [89].

Component	Composition (mol%)
N_2	0.39
CO_2	0.84
C_1	36.63
C_2	8.63
C_3	6.66
i-C_4	1.21
n-C_4	3.69
i-C_5	1.55
n-C_5	2.25
C_6	3.36
C_7	3.34
C_8	3.44
C_9	3.04
C_{10}	2.77
C_{11}	2.23
C_{12}	1.82
C_{13}	1.66
C_{14}	1.45
C_{15}	1.31
C_{16}	1.07
C_{17}	0.98
C_{18}	0.87
C_{19}	0.83
C_{20+}	9.98

Table 4-11 Characterization results of oil sample 4.

Component	Composition (mol%)	T_c (K)	P_c (bar)	V_c (m^3/kmol)	ω	MW (g/mol)
N_2	0.394	126.200	33.94	89.80	0.040	28.014

CO_2	0.848	304.200	73.76	94.00	0.225	44.010
C_1	36.965	190.600	46.00	99.00	0.008	16.043
C_2	8.709	305.400	48.84	148.00	0.098	30.070
C_3	6.721	369.800	42.46	203.00	0.152	44.097
iC_4	1.221	408.100	36.48	263.00	0.176	58.124
nC_4	3.724	425.200	38.00	255.00	0.193	58.124
iC_5	1.564	460.400	33.84	306.00	0.227	72.151
nC_5	2.271	469.600	33.74	304.00	0.251	72.151
C_6	3.391	507.400	29.69	370.00	0.296	86.178
C_7	3.371	536.488	29.45	475.55	0.337	96.000
C_8	3.471	558.043	27.42	487.84	0.374	107.000
C_9	3.068	582.078	25.06	529.18	0.421	121.000
C_{10}-C_{12}	6.882	620.063	21.64	621.31	0.515	145.456
C_{13}-C_{15}	4.460	678.459	17.45	784.83	0.709	189.109
C_{16}-C_{18}	2.947	731.573	15.59	989.38	0.865	235.675
C_{19}-C_{23}	2.742	785.293	14.39	1220.84	1.014	286.092
C_{24}-C_{29}	2.163	860.587	13.51	1591.04	1.152	364.168
C_{30}-C_{36}	1.754	941.196	12.90	2040.68	1.250	454.862
C_{37}-C_{44}	1.318	1028.079	12.39	2575.49	1.282	558.884
C_{45}-C_{80}	1.708	1244.563	10.71	3811.83	0.810	784.844
C_{45}-C_{80} A	0.307	1115.526	20.92	3811.83	1.274	784.844

Table 4-12 BIPs used for oil sample 4 [85].

	N_2	CO_2	C_{43}-C_{80} A
N_2	0.00000	-0.01700	0.08000
CO_2	-0.01700	0.00000	0.35000
C_1	0.03100	0.12000	0.01129
C_2	0.05200	0.12000	0.00905
C_3	0.08500	0.12000	0.00745
iC_4	0.10300	0.12000	0.00623
nC_4	0.08000	0.12000	0.00637
iC_5	0.09200	0.12000	0.00557
nC_5	0.10000	0.12000	0.00559
C_6	0.08000	0.12000	0.00478
C_7	0.08000	0.10000	0.00383
C_8	0.08000	0.10000	0.00374
C_9	0.08000	0.10000	0.00345
C_{10}-C_{12}	0.08000	0.10000	0.00292
C_{13}-C_{15}	0.08000	0.10000	0.00223
C_{16}-C_{18}	0.08000	0.10000	0.00163
C_{19}-C_{23}	0.08000	0.10000	0.00116
C_{24}-C_{29}	0.08000	0.10000	0.00069
C_{30}-C_{36}	0.08000	0.10000	0.00035

C_{37}-C_{44}	0.08000	0.10000	0.00014
C_{45}-C_{80}	0.08000	0.10000	0
C_{45}-C_{80} A	0.08000	0.35000	0

4.4.1.5. Oil Sample 5

Oil sample 5 is a live oil sample measured by Srivastava *et al.* [90] and the composition is shown in Table 4-13. The API gravity and density of oil sample 4 are 29° API and 0.8335 g/cm^3, respectively [90]. The molecular weight of the C_{5+} fraction of oil sample 5 is 205 g/mol [91]. Oil sample 5 is characterized by the method proposed by Petersen *et al.* [6] and the characterization results are shown in Table 4-14. The critical temperature, critical pressure and the exponent θ between asphaltene and other components in Equation (34) are tuned to be 1398.5 K, 16.55 bar and 0.003 for oil sample 2. The BIPs used for oil sample 5 are shown in Table 4-15. In Table 4-15, the BIPs between N_2, H_2S and other components except for the asphaltene component are taken from the literature [85]. The BIP between CO_2 and asphaltene is tuned to be 0.061.

Table 4-13 Composition of oil sample 5 [90].

Component	Composition (mol%)
N_2	0.96
CO_2	0.58
H_2S	0.30
C_1	4.49
C_2	2.99
C_3	4.75
i-C_4	0.81
n-C_4	1.92
i-C_5	1.27
n-C_5	2.19
C_{6+}	79.74

Table 4-14 Characterization results of oil sample 4.

Component	Composition	T_c (K)	P_c (bar)	V_c	ω	MW

	(mol%)			(m^3/kmol)		(g/mol)
N_2	1.027	126.200	33.94	89.80	0.040	28.014
CO_2	0.620	304.200	73.76	94.00	0.225	44.010
H_2S	0.321	373.200	89.37	98.50	0.100	34.080
C_1	4.803	190.600	46.00	99.00	0.008	16.043
C_2	3.198	305.400	48.84	148.00	0.098	30.070
C_3	5.081	369.800	42.46	203.00	0.152	44.097
iC_4	0.866	408.100	36.48	263.00	0.176	58.124
nC_4	2.054	425.200	38.00	255.00	0.193	58.124
iC_5	1.358	460.400	33.84	306.00	0.227	72.151
nC_5	2.342	469.600	33.74	304.00	0.251	72.151
C_6	8.717	507.400	29.69	370.00	0.296	86.178
C_7	5.380	546.682	32.2	294.56	0.339	96.000
C_8	4.965	567.327	29.69	329.13	0.375	107.000
C_9	4.582	591.133	27.07	381.99	0.422	121.000
C_{10}-C_{13}	15.06	640.540	22.98	519.79	0.529	152.880
C_{14}-C_{16}	8.514	706.376	19.20	755.72	0.687	205.145
C_{17}-C_{19}	6.693	755.924	17.37	971.55	0.813	249.638
C_{20}-C_{23}	6.752	804.037	16.15	1208.91	0.935	295.816
C_{24}-C_{27}	4.899	857.005	15.15	1499.00	1.060	350.820
C_{28}-C_{32}	4.279	914.347	14.38	1843.96	1.175	413.760
C_{33}-C_{38}	3.313	980.021	13.75	2271.84	1.263	489.738
C_{39}-C_{48}	2.956	1068.09	13.17	2893.42	1.272	595.835
C_{49}-C_{80}	0.700	1075.003	10.49	4268.55	0.433	812.373
C_{49}-C_{80} A	1.518	1398.500	16.55	4268.55	1.274	812.373

Table 4-15 BIPs used for oil sample 5 [85].

	N_2	CO_2	H_2S	C_{43}-C_{80} A
N_2	0	-0.01700	0.17700	0.08000
CO_2	-0.01700	0	0.09700	0.06100
H_2S	0.17670	0.09740	0	0.06000
C_1	0.03110	0.06000	0.08000	0.00056
C_2	0.05150	0.06000	0.08300	0.00045
C_3	0.08520	0.06000	0.08800	0.00037
iC_4	0.10330	0.06000	0.04700	0.00031
nC_4	0.08000	0.06000	0.06000	0.00032
iC_5	0.09220	0.06000	0.06000	0.00028
nC_5	0.10000	0.06000	0.06000	0.00028
C_6	0.08000	0.06000	0.06000	0.00024
C_7	0.08000	0.06000	0.06000	0.00029
C_8	0.08000	0.06000	0.06000	0.00027
C_9	0.08000	0.06000	0.06000	0.00024
C_{10}-C_{13}	0.08000	0.06000	0.06000	0.00018

C_{14}-C_{16}	0.08000	0.06000	0.06000	0.00012
C_{17}-C_{19}	0.08000	0.06000	0.06000	0.00009
C_{20}-C_{23}	0.08000	0.06000	0.06000	0.00007
C_{24}-C_{27}	0.08000	0.06000	0.06000	0.00005
C_{28}-C_{32}	0.08000	0.06000	0.06000	0.00003
C_{33}-C_{38}	0.08000	0.06000	0.06000	0.00002
C_{39}-C_{48}	0.08000	0.06000	0.06000	0.00001
C_{49}-C_{80}	0.08000	0.06000	0.06000	0
C_{49}-C_{80} A	0.08000	0.06100	0.06000	0

4.4.2. Validation of the Three-Phase VLA Equilibrium Calculation Algorithm

Figure 4-2 shows the comparison between the calculated *PT* phase envelopes and the measured ones from the literature [84, 87-89]. The red lines represent the asphaltene onset boundaries, while the green line represents the saturation pressure line. As seen from Figure 4-2, a good agreement exists between the calculated results and the experimental data, which indicates that our algorithm can be used to reliably reproduce the experimental data. Two types of topologies can be observed from the *PT* phase diagrams shown in Figure 4-2. Oil samples 1 and 2 exhibit the first type. In the first type (See Figures 4-2a and 4-2b), the upper onset pressure curve does not intersect with the saturation pressure curve, while the lower onset pressure curve does intersect with the saturation pressure curve. Oil samples 3 and 4 exhibit the second type. In the second type (See Figures 4-2c and 4-2d), the upper onset pressure curve and the lower onset pressure curve intersect with the saturation pressure curve at the same point.

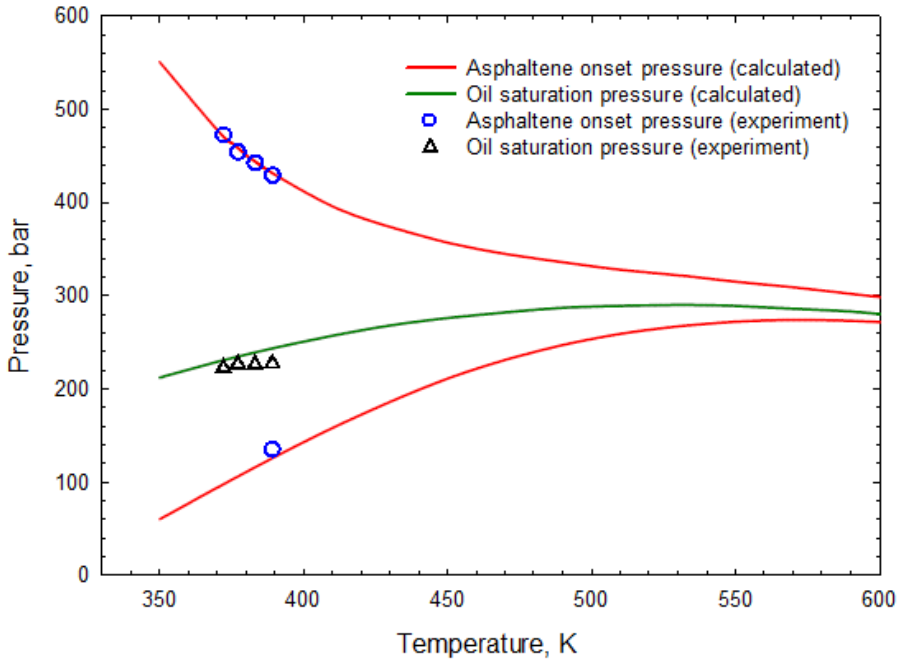
Asphaltene onset pressure (calculated)
Oil saturation pressure (calculated)
Asphaltene onset pressure (experiment)
Oil saturation pressure (experiment)
Pressure, bar
Temperature, K
0
100
200
300
400
500
600
350
400
450
500
550
600

(a)

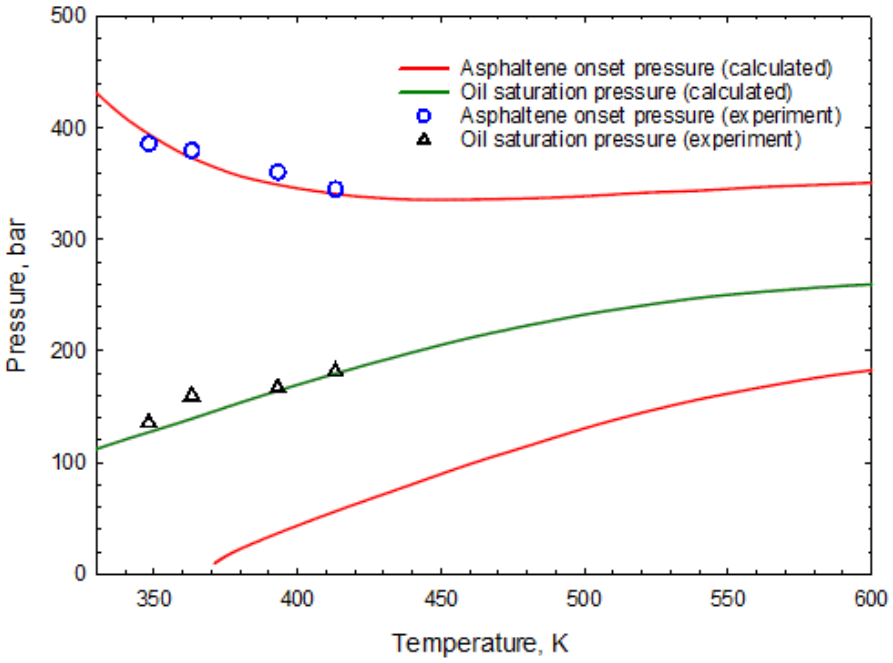
Asphaltene onset pressure (calculated)
Oil saturation pressure (calculated)
Asphaltene onset pressure (experiment)
Oil saturation pressure (experiment)
Pressure, bar
Temperature, K
0
100
200
300
400
500
350
400
450
500
550
600

(b)

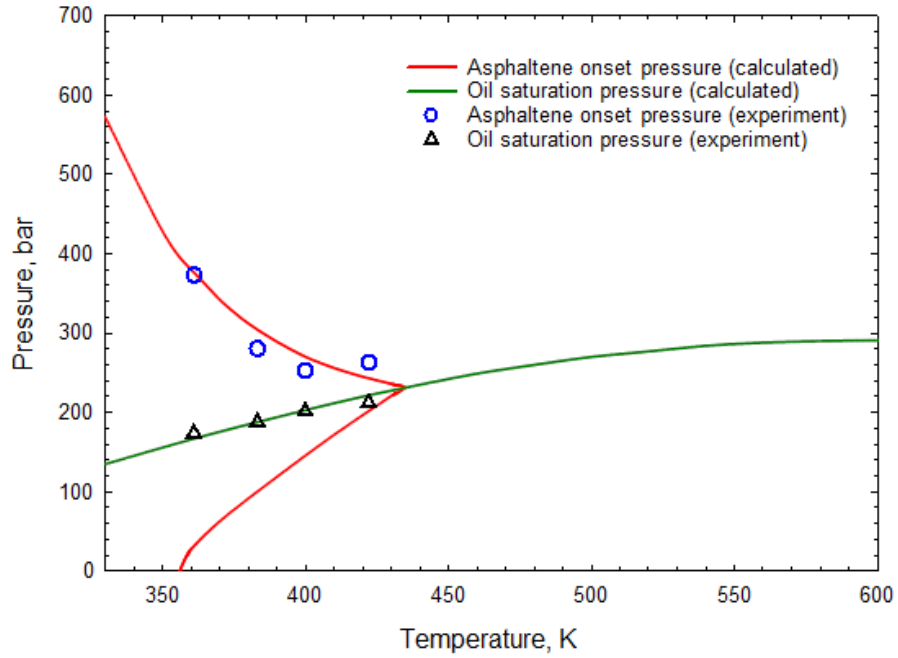

(c)

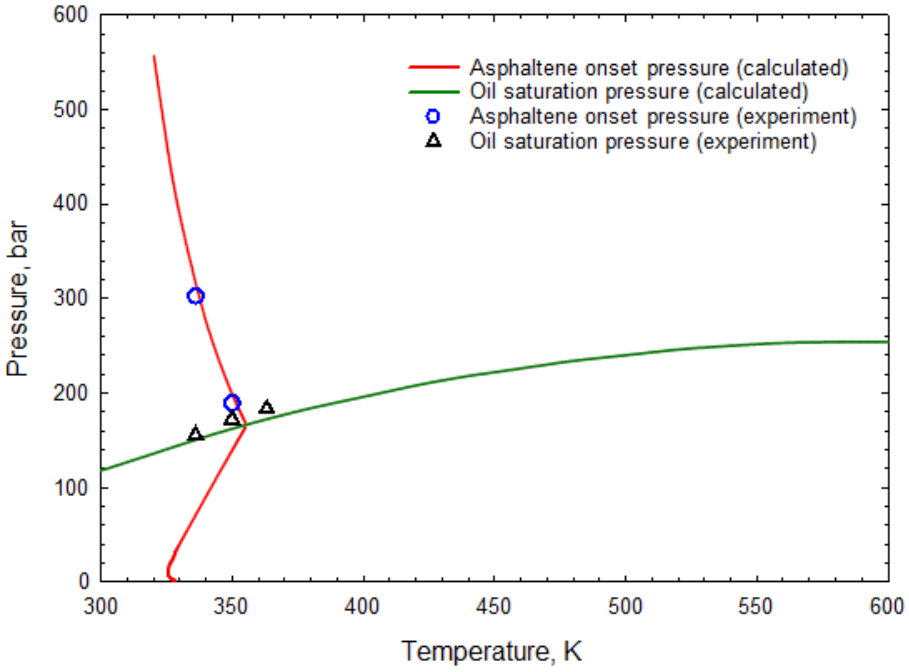

(d)

Fig. 4-2 Comparison between the calculated *PT* phase envelopes using the newly developed algorithm and the experimental data [84, 87-89]: (a) Oil sample 1; (b) Oil sample 2; (c) Oil sample 3; (d) Oil sample 4.

Immiscible gas injection is an effective enhanced oil recovery (EOR) method to maintain the reservoir pressure [88]. In order to test the performance of our algorithm in carrying out phase behavior calculations during immiscible gas injections, the tuned parameters for oil sample 3 are subsequently used to predict the *PT* phase diagram of oil sample 3 subjected to N_2 injection. Figure 4-3 shows the comparison between the calculated *PT* phase envelope and the measured one by Jamaluddin *et al*. [88]. Figure 4-3 (a), Figure 4-3 (b) and Figure 4-3 (c) show the *PT* phase diagrams with 5%, 10% and 20% N_2 injection, respectively. It can be seen from Figure 4-3 that the calculation results match reasonably well with the experimental data, verifying the efficacy of our algorithm in modeling asphaltene precipitation during gas injections. It can be also concluded that the immiscible gas injection will lead to expanded asphaltene-precipitation regions, causing a more serious asphaltene precipitation problem thereof.

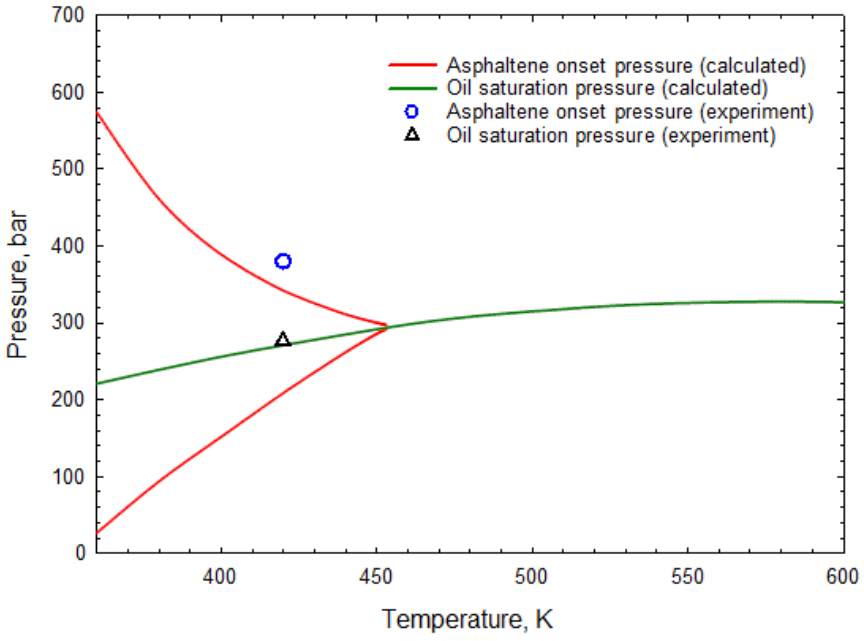

(a)

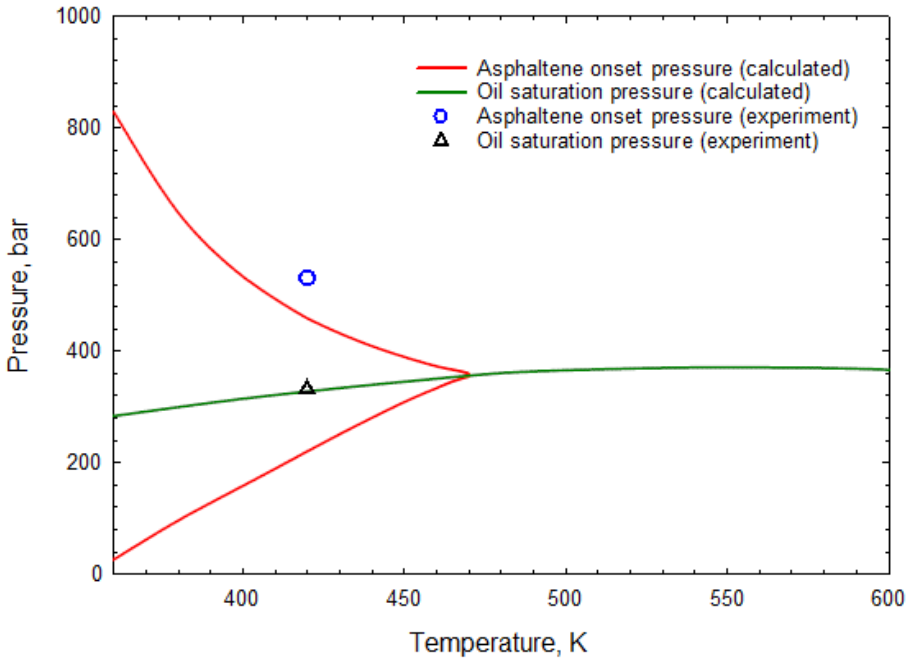

(b)

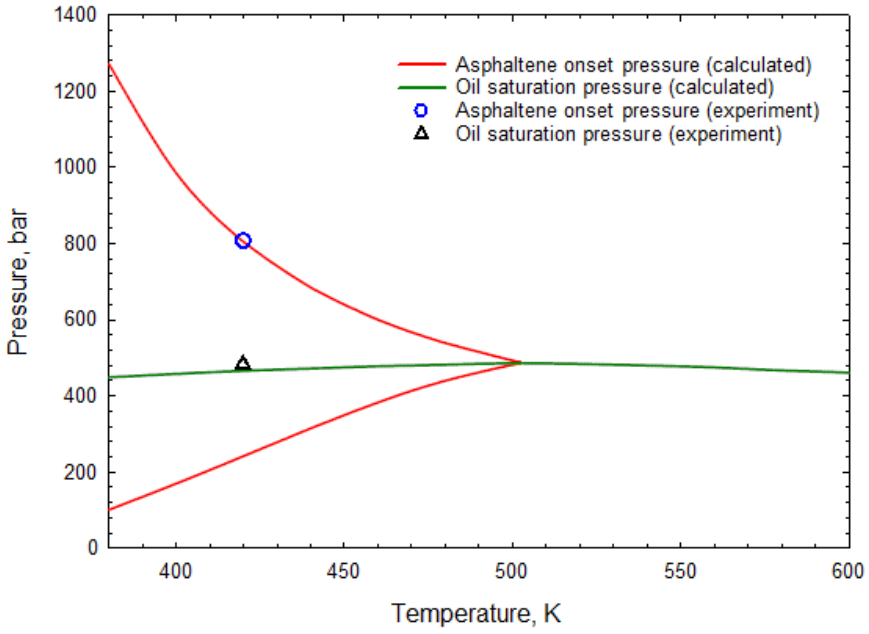

(c)

Fig. 4-3 Comparison between the calculated *PT* phase diagrams of oil sample 3 and the experimental data with: (a) 5% N_2 injection; (b) 10% N_2 injection; (c) 20% N_2 injection.

Miscible gas flooding with CO_2 is more popular than immiscible gas flooding due to the lower minimum miscibility pressure (MMP) between CO_2 and oil [92-94]. The miscible displacement leads to a higher oil recovery efficiency than the immiscible displacement at the same pressure and temperature [95]. But, CO_2 injection could cause a severe asphaltene precipitation problem in some reservoirs [90, 96]. Here, we also use the tuned parameters for oil sample 4 to generate the *Px* phase diagram and the *P-x-WA* (weight fraction of precipitated asphaltene) with CO_2 injection at the reservoir temperature of 363.15 K. The composition of the impure CO_2 stream is shown in Table 4-9. Figure 4-4 shows the comparison between the calculated *Px* phase diagram of oil sample 4 and the experimental data. The green line, red line and blue line represent the upper asphaltene onset boundary, the saturation pressure line and the lower asphaltene onset boundary, respectively. It can be seen from Figure 4-4 that the calculated *Px* diagram agrees well with the experimental data, which indicates that our algorithm can be used to accurately model asphaltene precipitation under gas injection conditions. Herein, it is worthwhile mentioning that we do not encounter any difficulty in converging to the correct phase equilibria, which could be otherwise encountered by Li and Li [58]. This can be attributed to the fact that the same thermodynamic model (PR-EOS) has been used to describe the fugacity of the equilibrium phases. Figure 4-4 also shows that the upper asphaltene onset pressure is increased substantially during the gas injection process, which is because the solubility of asphaltene component will decrease with an increase in the amount of injected gas [6].

Figure 4-5 shows the *P-x-WA* diagram of oil sample 4. We can see from Figure 4-5 that the largest precipitation amount always appears at the oil saturation pressure. This can be attributed to the fact that oil has the highest amount of dissolved gas at the saturation pressure and thus has the lowest amount of dissolved asphaltene [6]. As the pressure

decreases, the amount of dissolved gas decreases, which makes asphaltene more soluble in the oil. When pressure increases from the oil saturation pressure, although the amount of dissolved gas stays the same, the solubility of asphaltene tends to slightly increase with pressure. As a result, the precipitated asphaltene will redissolve in oil at sufficiently high pressures [6].

Table 4-16 Composition of the injection gas [89].

Component	Composition (mol%)
CO_2	60.32
C_1	10.73
C_2	7.55
C_3	9.09
i-C_4	0.00
n-C_4	6.47
i-C_5	0.03
n-C_5	5.82

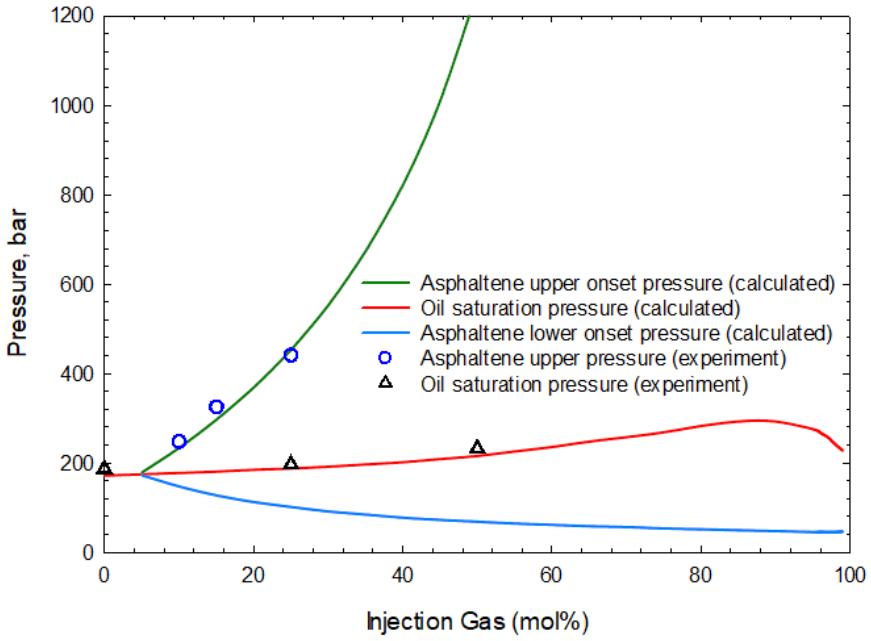

Fig. 4-4 Comparison between the calculated Px phase diagram of oil sample 4 and the experimental data at the reservoir temperature of 363.15 K.

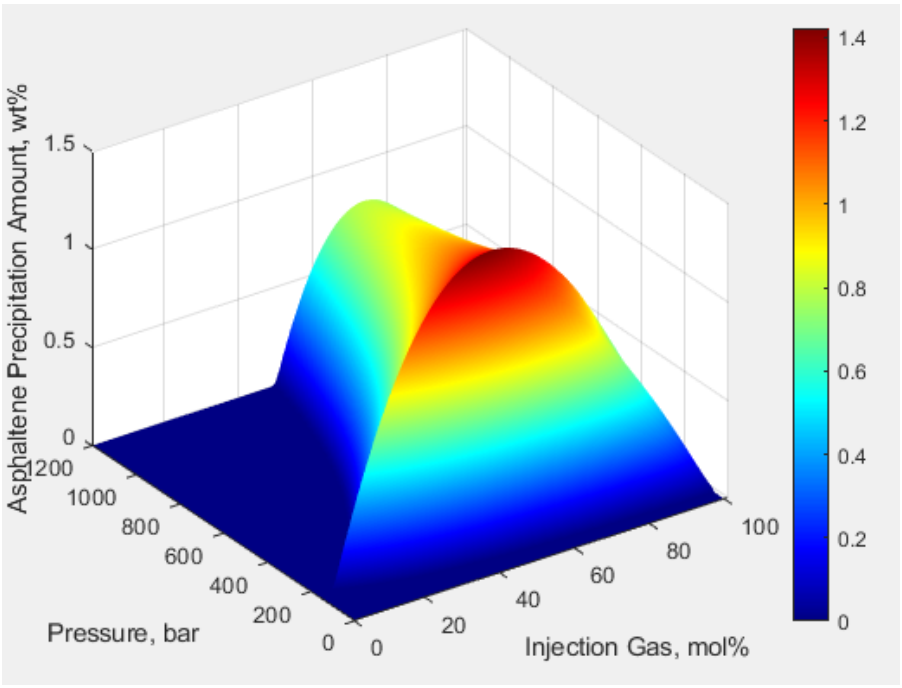

(a)

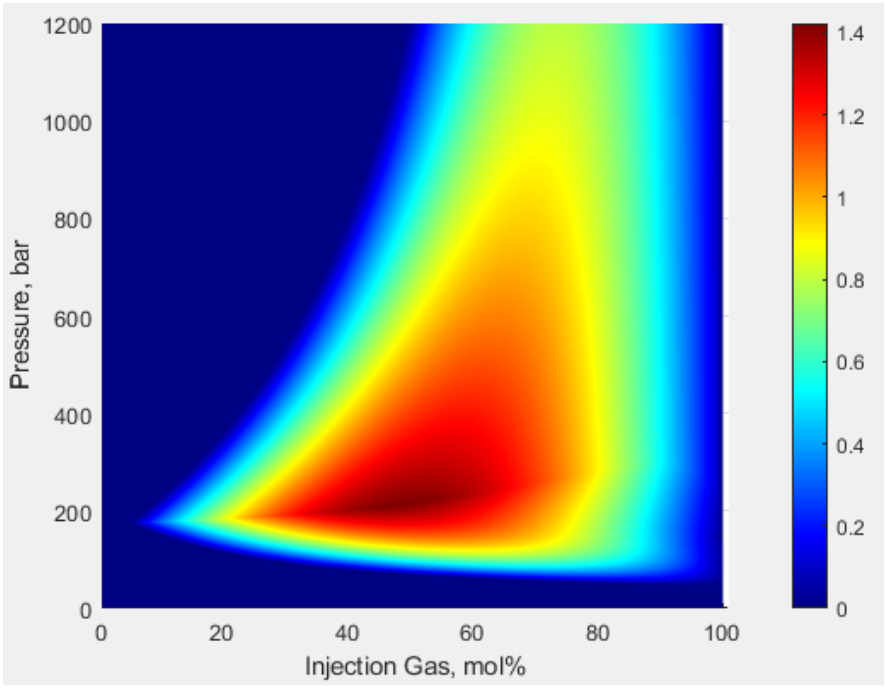

(b)

Fig. 4-5 3-D P-x-WA diagram of oil sample 4: (a) 3-D plot; (b) contour plot.

Figure 4-6 shows the comparison between the calculated asphaltene precipitation amounts of oil sample 5 during CO_2 injection and the experimental data at the reservoir temperature of 323.15 K and 160 bar. The green line shows the predicted asphaltene

precipitation amount and the red triangles represent the measured ones. It can be observed from Figure 4-6 that the calculated results agree reasonably well with experimental data, which shows that our algorithm can be used to predict the amount of asphaltene precipitation [90].

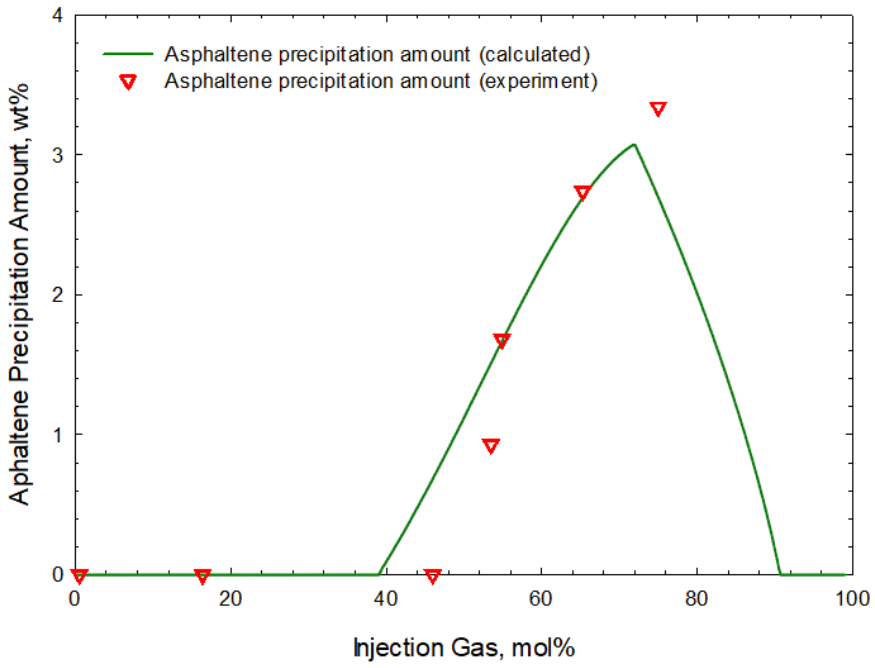

Fig. 4-6 Comparison between the calculated asphaltene precipitation amount of oil sample 5 and the experimental data at 323.15 K and 160 bar.

4.4.3. Comparison Between Pure-Solid Assumption and Free-Asphaltene Assumption

In this section, we take oil samples 1, 2 and 5 as examples to show the comparison between the results yielded by the pure-solid assumption and the free-asphaltene assumption. Figure 4-7 compares the calculated *PT* phase diagrams of oil samples 1 and 2 yielded by different assumptions against the experimental data. In Figure 4-7, the solid lines represent the phase boundaries yielded by the free-asphaltene assumption, while the dashed lines represent the phase boundaries yielded by the solid assumption. It can be concluded from Figure 4-7 that the free asphaltene assumption yields slightly better results than the solid assumption. However, additional experimental data at the

high-temperature region are needed to further prove which assumption gives better asphaltene precipitation predictions under high-temperature conditions.

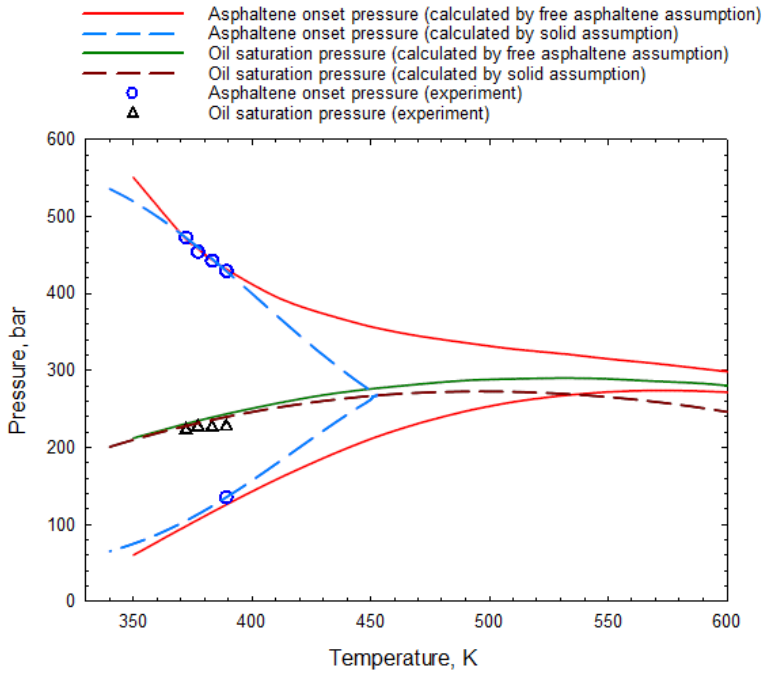

(a)

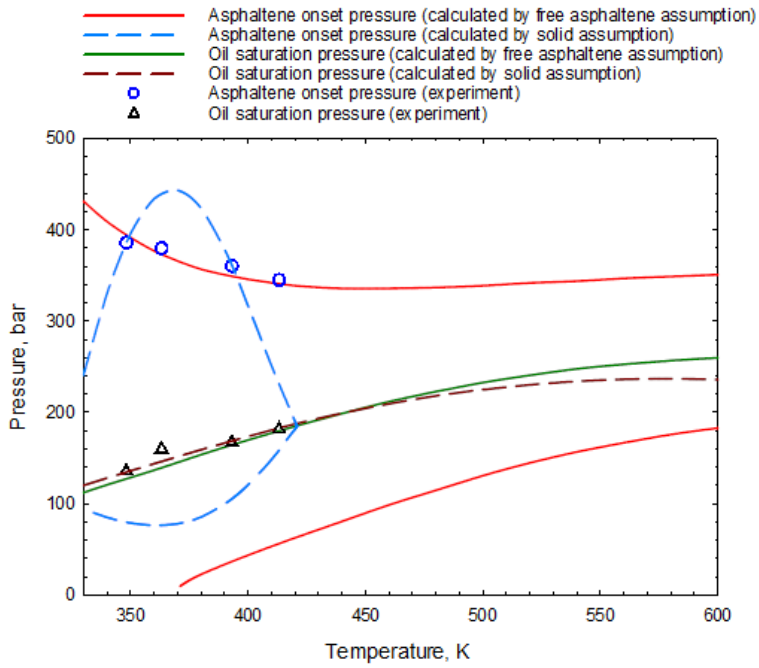

(b)

Fig. 4-7 Comparison between the calculated *PT* phase diagrams yielded by different assumptions and the experimental data: (a) Oil sample 1; (b) Oil sample 2.

Figure 4-8 shows the comparison between the calculated asphaltene precipitation amounts yielded by different assumptions and the experimental data. In Figure 4-8, the solid lines represent the asphaltene precipitation amounts yielded by the free-asphaltene assumption, while the dashed lines represent the asphaltene precipitation amounts yielded by the solid assumption. It can be seen from Figure 4-8 that the results calculated based on the free asphaltene assumption and the solid assumption are similar. Also note that both methods fail to match the maximum amount of the precipitated asphaltene, which could be attributed to the assumption that the asphaltene phase only contains asphaltene.

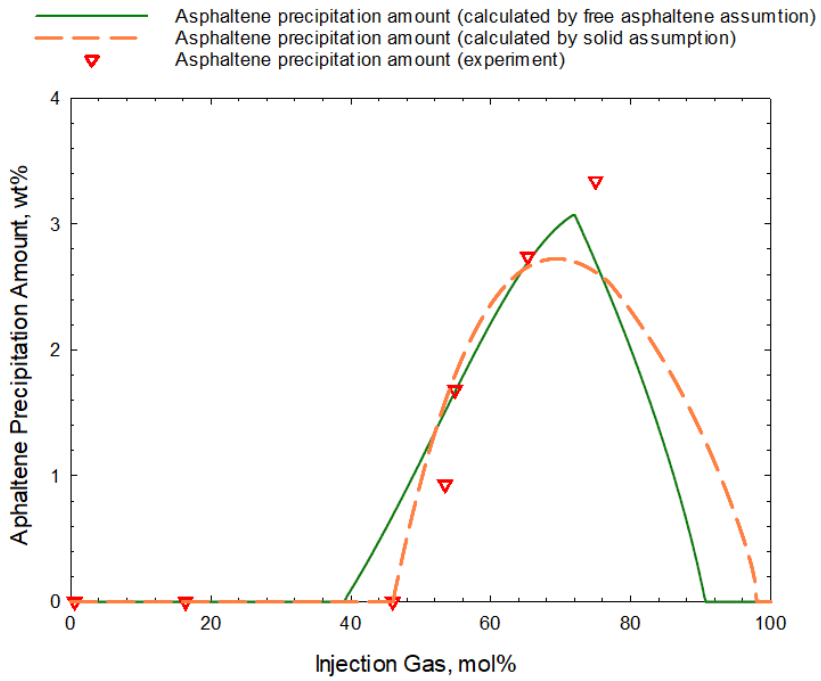

Fig. 4-8 Comparison between the calculated asphaltene precipitation amount yielded by different assumptions and the experimental data.

4.4.4. Comparison Between Liquid Assumption and Free Asphaltene Assumption

Figure 4-9 compares the *PT* phase diagrams of oil samples 1 and 2 calculated by our algorithm based on the free-asphaltene assumption against that calculated by PVTsim [85] based on the liquid assumption. In Figure 4-9, the solid lines and the dashed lines

represent the phase boundaries yielded by the free-asphaltene assumption and the liquid assumption, respectively. It can be observed from Figure 4-9 that the calculated results yielded by the free-asphaltene assumption are very close to the results based on the liquid assumption calculated by PVTsim [85], which verifies the effectiveness of the free-asphaltene assumption.

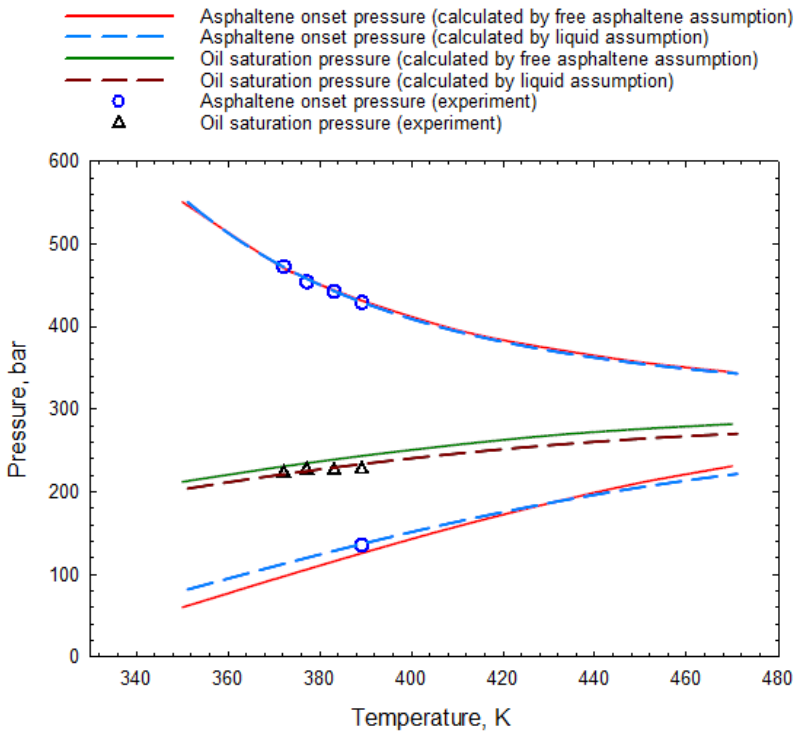

(a)

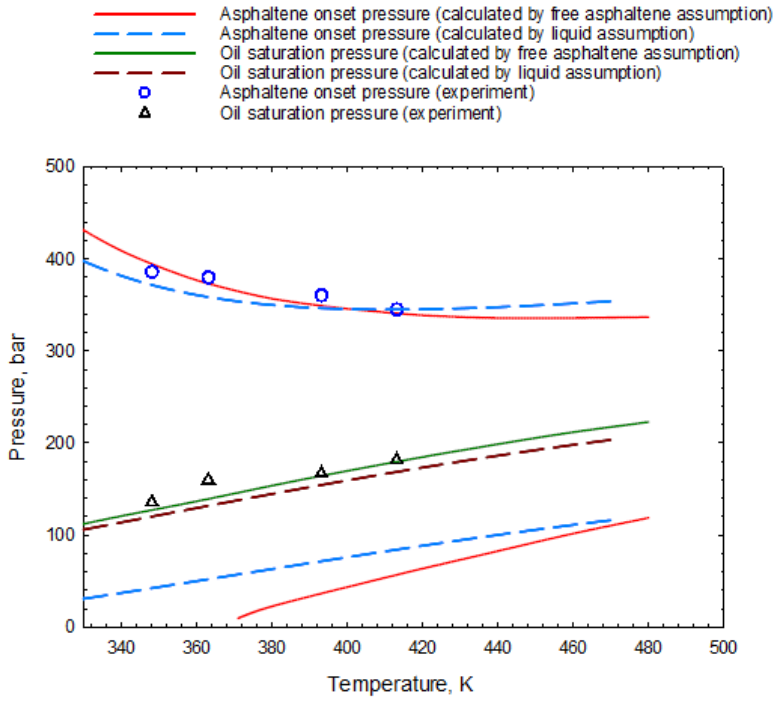

(b)

Fig. 4-9 Comparison between the *PT* phase diagrams calculated by our algorithm yielded by the free asphaltene assumption and that calculated by PVTsim yielded by the liquid assumption: (a) Oil sample 1; (b) Oil sample 2.

4.5. Conclusions

A modified three-phase VLA equilibrium calculation algorithm is developed in this study based on the newly proposed free-asphaltene assumption. We test the performance of this algorithm by applying it to four oil samples. The following conclusions can be drawn from the calculation results:

- A good agreement can be seen between the results calculated by our algorithm based on the free-asphaltene assumption and the experimental data, leading to the conclusion that the modified algorithm together with the new assumption can have a good description of asphaltene precipitation phenomena at varied pressure/temperature conditions.
- The three-phase VLA equilibrium calculation algorithm can be used to predict the phase boundaries with different injectants after being calibrated by the

experimentally determined asphaltene onset data.

- The calculation results based on the free-asphaltene assumption agree slightly better with the experimental data than the calculation results yielded by the solid assumption. However, further validation at the high-temperature region is still required to prove which assumption can provide more accurate asphaltene-precipitation predictions.
- The phase envelopes yielded by the algorithm with the free-asphaltene assumption are very close to the results yielded by the algorithm with the liquid assumption, which proves the feasibility and effectiveness of the free-asphaltene assumption.

Acknowledgments

The authors greatly acknowledge a Discovery Grant from the Natural Sciences and Engineering Research Council of Canada (NSERC) (Grant No.: NSERC RGPIN-2020-04571) to H. Li. Z. Chen greatly acknowledges the financial support provided by the China Scholarship Council (CSC) via a Ph.D. scholarship (No.: 201908180010).

References

[1] A. Hirschberg, L.N. deJong, B. Schipper, J. Meijer, Influence of temperature and pressure on asphaltene flocculation, *SPE J.*, 24 (3) (1984) 283.

[2] J. Speight, Petroleum Asphaltenes-Part 1: Asphaltenes, resins and the structure of petroleum, *Oil Gas Sci. Technol.*, 59 (5) (2004) 467.

[3] F.M. Vargas, M. Garcia-Bermudes, M. Boggara, S. Punnapala, M. Abutaqiya, N. Mathew, S. Prasad, A. Khaleel, M. Al Rashed, H. Al Asafen, On the development of an enhanced method to predict asphaltene precipitation, presented at *Offshore*

Technology Conference, Houston, TX, May 5-8, 2014; SPE 2014; Paper No. OTC-25294-MS.

[4] J.L. Creek, Freedom of action in the state of asphaltenes: Escape from conventional wisdom, *Energy Fuels*, 19 (4) (2005) 1212.

[5] S. Punnapala, F.M. Vargas, Revisiting the PC-SAFT characterization procedure for an improved asphaltene precipitation prediction, *Fuel*, 108 (1) (2013) 417.

[6] K.S. Pedersen, P.L. Christensen, J.A. Shaikh, P.L. Christensen, Phase behavior of petroleum reservoir fluids, CRC press, 2006.

[7] K.J. Leontaritis, G.A. Mansoori, Asphaltene flocculation during oil production and processing: A thermodynamic colloidal model, presented at *SPE International Symposium on Oilfield Chemistry*, San Antonio, TX, Feb. 4-6, 1987; SPE 1987; Paper No. SPE-16258-MS.

[8] H. Pan, A. Firoozabadi, A thermodynamic micellization model for asphaltene precipitation: Part I: Micellar size and growth, *SPE Prod. Faci.*, 13 (2) (1998) 118.

[9] A.I. Victorov, A. Firoozabadi, Thermodynamic micellizatin model of asphaltene precipitation from petroleum fluids, *AIChE J.*, 42 (6) (1996) 1753.

[10] J. Wu, J.M. Prausnitz, A. Firoozabadi, Molecular-thermodynamic framework for asphaltene-oil equilibria, *AIChE J.*, 44 (5) (1998) 1188.

[11] E.S. Boek, D.S. Yakovlev, T.F. Headen, Quantitative molecular representation of asphaltenes and molecular dynamics simulation of their aggregation, *Energy Fuels*, 23 (3) (2009) 1209.

[12] J. Buckley, G. Hirasaki, Y. Liu, S. Von Drasek, J. Wang, B. Gill, Asphaltene precipitation and solvent properties of crude oils, *Petro. Sci. Technol.*, 16 (3-4) (1998) 251.

[13] J. Czarnecki, P. Tchoukov, T. Dabros, Possible role of asphaltenes in the stabilization of water-in-crude oil emulsions, *Energy Fuels*, 26 (3) (2012) 5782.

[14] L. Goual, Impedance spectroscopy of petroleum fluids at low frequency, *Energy Fuels*, 23 (4) (2009) 2090.

[15] D.E. Freed, O.C. Mullins, J.Y. Zuo, Theoretical treatment of asphaltene gradients in the presence of GOR gradients, *Energy Fuels*, 24 (7) (2010) 3942.

[16] J.Y. Zuo, H. Elshahawi, O.C. Mullins, C. Dong, D. Zhang, N. Jia, H. Zhao, Asphaltene gradients and tar mat formation in reservoirs under active gas charging, *Fluid Phase Equilibr.*, 315 (1) (2012) 91.

[17] J.Y. Zuo, O.C. Mullins, D. Freed, H. Elshahawi, C. Dong, D.J. Seifert, Advances in the Flory–Huggins–Zuo equation of state for asphaltene gradients and formation evaluation, *Energy Fuels*, 27 (4) (2013) 1722.

[18] O.C. Mullins, The modified Yen model, *Energy Fuels*, 24 (4) (2010) 2179.

[19] P. D. Ting, G.J. Hirasaki, W.G. Chapman, Modeling of asphaltene phase behavior with the SAFT equation of state, *Petrol. Sci. Tech.*, 21 (3-4) (2003) 647.

[20] P.J. Flory, Thermodynamics of high polymer solutions, *J. Chem. Phys.*, 9 (8) (1941) 660.

[21] J.H. Hildebrand, Solubility. III. Relative values of internal pressures and their practical application, *J. Am. Chem. Soc.*, 41 (7) (1919) 1067.

[22] M.L. Huggins, Solutions of long chain compounds, *J. Chem. Phys.*, 9 (5) (1941) 440.

[23] G. Scatchard, Equilibria in non-electrolyte solutions in relation to the vapor pressures and densities of the components, *Chem. Rev.*, 8 (2) (1931) 321.

[24] R.L. Scott, M. Magat, The thermodynamics of high-polymer solutions: I. The free energy of mixing of solvents and polymers of heterogeneous distribution, *J. Chem. Phys.*, 13 (5) (1945) 172.

[25] H. Alboudwarej, K. Akbarzadeh, J. Beck, W.Y. Svrcek, H.W. Yarranton, Regular solution model for asphaltene precipitation from bitumens and solvents, *AIChE J.*, 49 (11) (2003) 2948.

[26] S.I. Andersen, J.G. Speight, Thermodynamic models for asphaltene solubility and precipitation, *J. Petro. Sci. Eng.*, 22 (1-3) (1999) 53.

[27] R. Cimino, S. Correra, P. Sacomani, C. Carniani, Thermodynamic modelling for prediction of asphaltene deposition in live oils, presented at *SPE International Symposium on Oilfield Chemistry*, San Antonio, TX, Feb. 14-17, 1995; SPE 1995; Paper No. SPE-28993-MS.

[28] S. Correra, D. Merino-Garcia, Simplifying the thermodynamic modeling of asphaltenes in upstream operations, *Energy Fuels*, 21 (3) (2007) 1243.

[29] R. De Boer, K. Leerlooyer, M. Eigner, A. Van Bergen, Screening of crude oils for asphalt precipitation: theory, practice, and the selection of inhibitors, *SPE Prod. Faci.*, 10 (1) (1995) 55.

[30] D.L. Gonzalez, F.M. Vargas, E. Mahmoodaghdam, F. Lim, N. Joshi, Asphaltene stability prediction based on dead oil properties: Experimental evaluation, *Energy Fuels*, 26 (10) (2012) 6218.

[31] S. Kawanaka, S.J. Park, G.A. Mansoori, Organic deposition from reservoir fluids: a thermodynamic predictive technique, *SPE Res. Eng.*, 6 (2) (1991) 185.

[32] K. Kraiwattanawong, H.S. Fogler, S.G. Gharfeh, P. Singh, W.H. Thomason, S. Chavadej, Thermodynamic solubility models to predict asphaltene instability in live crude oils, *Energy Fuels*, 21 (3) (2007) 1248.

[33] J. Wang, J. Buckley, A two-component solubility model of the onset of asphaltene flocculation in crude oils, *Energy Fuels*, 15 (5) (2001) 1004.

[34] J. Wang, J. Buckley, N. Burke, J. Creek, A practical method for anticipating asphaltene problems (includes associated papers 104235 and 105396), *SPE Prod. Faci.*, 19 (3) (2004) 152.

[35] H.W. Yarranton, J.H. Masliyah, Molar mass distribution and solubility modeling of asphaltenes, *AIChE J.*, 42 (12) (1996) 3533.

[36] F.M. Vargas, D.L. Gonzalez, G.J. Hirasaki, W.G. Chapman, Modeling asphaltene phase behavior in crude oil systems using the perturbed chain form of the statistical associating fluid theory (PC-SAFT) equation of state, *Energy Fuels*, 23 (3) (2009) 1140.

[37] A. Arya, X. Liang, N. Von Solms, G.M. Kontogeorgis, Modeling of asphaltene onset precipitation conditions with cubic plus association (CPA) and perturbed chain statistical associating fluid theory (PC-SAFT) equations of state, *Energy Fuels*, 30 (8) (2016) 6835.

[38] A. Arya, X. Liang, N. von Solms, G.M. Kontogeorgis, Modeling of asphaltene precipitation from crude oil with the cubic plus association equation of state, *Energy Fuels*, 31 (2) (2017) 2063.

[39] A. Arya, X. Liang, N. von Solms, G.M. Kontogeorgis, Prediction of gas injection effect on asphaltene precipitation onset using the cubic and cubic-plus-association equations of state, *Energy Fuels*, 31 (3) (2017) 3313.

[40] A. Arya, N. von Solms, G.M. Kontogeorgis, Determination of asphaltene onset conditions using the cubic plus association equation of state, *Fluid Phase Equilibr.*, 400 (1) (2015) 8.

[41] A. Arya, N. von Solms, G.M. Kontogeorgis, Investigation of the gas injection effect on asphaltene onset precipitation using the cubic-plus-association equation of state, *Energy Fuels*, 30 (5) (2016) 3560.

[42] H. Nasrabadi, J. Moortgat, A. Firoozabadi, New three-phase multicomponent compositional model for asphaltene precipitation during CO2 injection using CPA-EOS, *Energy Fuels*, 30 (4) (2016) 3306.

[43] H. Nasrabadi, J. Moortgat, A. Firoozabadi, A new three-phase multicomponent compositional model for asphaltene precipitation using CPA-EOS, presented at the *SPE Reservoir Simulation Symposium*, The Woodlands, TX, Feb. 18, 2013; SPE 2013; Paper No. SPE-163587-MS.

[44] M.I. Abutaqiya, C.J. Sisco, Y. Khemka, M.A. Safa, E.F. Ghloum, A.M. Rashed, R. Gharbi, S. Santhanagopalan, M. Al-Qahtani, E. Al-Kandari, Accurate modeling of asphaltene onset pressure in crude oils under gas injection using Peng–Robinson equation of state, *Energy Fuels*, 34 (4) (2020) 4055.

[45] W.G. Chapman, K.E. Gubbins, G. Jackson, M. Radosz, New reference equation of state for associating liquids, *Ind. Eng. Chem. Res.*, 29 (8) (1990) 1709.

[46] J. Gross, G. Sadowski, Perturbed-chain SAFT: An equation of state based on a perturbation theory for chain molecules, *Ind. Eng. Chem. Res.*, 40 (4) (2001) 1244.

[47] S.R. Panuganti, F.M. Vargas, D.L. Gonzalez, A.S. Kurup, W.G. Chapman, PC-SAFT characterization of crude oils and modeling of asphaltene phase behavior, *Fuel*, 93 (1) (2012) 658.

[48] M.I. Abutaqiya, C.J. Sisco, F.M. Vargas, A linear extrapolation of normalized cohesive energy (LENCE) for fast and accurate prediction of the asphaltene onset pressure, *Fluid Phase Equilibr.*, 483 (1) (2019) 52.

[49] M.I. Abutaqiya, C.J. Sisco, J. Wang, F.M. Vargas, Systematic investigation of asphaltene deposition in the wellbore and near-wellbore region of a deepwater oil reservoir under gas injection. Part 1: thermodynamic modeling of the phase behavior of polydisperse asphaltenes, *Energy Fuels*, 33 (5) (2019) 3632.

[50] D.L. Gonzalez, G.J. Hirasaki, J. Creek, W.G. Chapman, Modeling of asphaltene precipitation due to changes in composition using the perturbed chain statistical associating fluid theory equation of state, *Energy Fuels*, 21 (3) (2007) 1231.

[51] D.L. Gonzalez, F.M. Vargas, G.J. Hirasaki, W.G. Chapman, Modeling study of CO2-induced asphaltene precipitation, *Energy Fuels*, 22 (2) (2008) 757.

[52] D.L. Gonzalez Rodriguez, Modeling of asphaltene precipitation and deposition tendency using the PC-SAFT equation of state, Rice University, 2008.

[53] S.R. Panuganti, M. Tavakkoli, F.M. Vargas, D.L. Gonzalez, W.G. Chapman, SAFT model for upstream asphaltene applications, *Fluid Phase Equilibr.*, 359 (1) (2013) 2.

[54] S.R. Panuganti, F.M. Vargas, W.G. Chapman, Modeling reservoir connectivity and tar mat using gravity-induced asphaltene compositional grading, *Energy Fuels*, 26 (5) (2012) 2548.

[55] N. Rajan Babu, P.H. Lin, M.I. Abutaqiya, C.J. Sisco, J. Wang, F.M. Vargas, Systematic investigation of asphaltene deposition in the wellbore and near-wellbore region of a deepwater oil reservoir under gas injection. Part 2: computational fluid dynamics modeling of asphaltene deposition, *Energy Fuels*, 33 (5) (2018) 3645.

[56] M. Tavakkoli, A. Chen, F.M. Vargas, Rethinking the modeling approach for asphaltene precipitation using the PC-SAFT Equation of State, *Fluid Phase Equilibr.*, 416 (1) (2016) 120.

[57] S. Mohebbinia, K. Sepehrnoori, R.T. Johns, A.K.N. Korrani, Simulation of asphaltene precipitation during gas injection using PC-SAFT EOS, *J. Pet. Sci. Eng.*, 158 (1) (2017) 693.

[58] W. Yan, L.M. Michael, H.S. Erling, On application of non-cubic EoS to compositional reservoir simulation, presented at *SPE EUROPEC/EAGE Annual Conference and Exhibition*, Vienna, Austria. May 23-26, 2011; SPE 2011; Paper No. SPE-142955-MS.

[59] L. Nghiem, M. Hassam, R. Nutakki, A. George, Efficient modelling of asphaltene precipitation, presented at *SPE Annual Technical Conference and Exhibition*, Houston, TX, Oct. 3-6,1993; SPE 1993; Paper No. SPE-26642-MS.

[60] Kohse, B. F.; Nghiem, L. X.; Maeda, H.; Ohno, K. Modelling phase behaviour including the effect of pressure and temperature on asphaltene precipitation, presented at *SPE Asia Pacific Oil and Gas Conference and Exhibition*, Brisbane, Australia, Oct. 16-18, 2000; SPE 2000; Paper No. SPE-64465-MS.

[61] H. Darabi, M. Shirdel, M.H. Kalaei, K. Sepehrnoori, Aspects of modeling asphaltene deposition in a compositional coupled wellbore/reservoir simulator, presented at *SPE Improved Oil Recovery Symposium*, Oklahoma, USA, Apr. 12-16, 2014; SPE 2014; Paper No. SPE-169121-MS.

[62] W. Fazelipour, In Predicting asphaltene precipitation in oilfields via the technology of compositional reservoir simulation, presented at *SPE International Symposium on Oilfield Chemistry*, Texas, USA, Apr. 11-13, 2011; SPE 2011; Paper No. SPE-141148-MS.

[63] S. Kord, S. Ayatollahi, Asphaltene precipitation in live crude oil during natural depletion: Experimental investigation and modeling, *Fluid Phase Equilibr.*, 336 (1) (2012) 63.

[64] R. Nguele, M.R. Ghulami, K. Sasaki, H. Said-Al Salim, A. Widiatmojo, Y. Sugai, M. Nakano, Asphaltene aggregation in crude oils during supercritical gas injection, *Energy Fuels*, 30 (2) (2016) 1266.

[65] X. Qin, P. Wang, K. Sepehrnoori, G.A. Pope, Modeling asphaltene precipitation in reservoir simulation, *Ind. Eng. Chem. Res.*, 39 (8) (2000) 2644.

[66] P. Zanganeh, H. Dashti, S. Ayatollahi, Visual investigation and modeling of asphaltene precipitation and deposition during CO2 miscible injection into oil reservoirs, *Fuel*, 160 (1) (2015) 132.

[67] R. Li, H. Li, Robust three-phase vapor–liquid–asphaltene equilibrium calculation algorithm for isothermal CO_2 flooding applications, *Ind. Eng. Chem. Res.*, 58 (34) (2019) 15666.

[68] D.J. Seifert, A. Qureshi, M. Zeybek, A.E. Pomerantz, J.Y. Zuo, O.C. Mullins, Heavy oil and tar mat characterization within a single oil column utilizing novel asphaltene science, presented at the *SPE Kuwait International Petroleum Conference and Exhibition*, Kuwait City, Kuwait, Dec. 10, 2012; SPE 2012; Paper Number: SPE-163291-MS.

[69] F.P. Nascimento, M.M. Souza, G.M. Costa, S.A. Vieira de Melo, Modeling of the asphaltene onset pressure from few experimental data: A comparative evaluation of the Hirschberg method and the cubic-plus-association equation of state, *Energy Fuels*, 33 (5) (2018) 3733.

[70] D.Y. Peng, D.B. Robinson, A new two-constant equation of state, *Ind. Eng. Chem. Fundam.*, 15 (1) (1976) 59.

[71] Z. Chen, R. Li, H. Li, An improved vapor-liquid-asphaltene three-phase equilibrium computation algorithm, *Fluid Phase Equilibr.*, 537 (1) (2021) 113004.

[72] M.L. Michelsen, The isothermal flash problem. Part I. Stability, *Fluid Phase Equilibr.*, 9 (1) (1982) 1.

[73] M.L. Michelsen, The isothermal flash problem. Part II. Phase-split calculation, *Fluid Phase Equilibr.*, 9 (1) (1982) 21.

[74] H.H. Rachford, J. Rice, Procedure for use of electronic digital computers in calculating flash vaporization hydrocarbon equilibrium, *J. Pet. Technol.*, 4 (10) (1952) 19.

[75] R. Okuno, R.T. Johns, K. Sepehrnoori, A new algorithm for Rachford-Rice for multiphase compositional simulation, *SPE J.*, 15 (2) (2010) 313.

[76] M. Michelsen, Calculation of multiphase equilibrium, *Comput. Chem. Eng.*, 18 (7) (1994) 545.

[77] C.F. Leibovici, D.V. Nichita, A new look at multiphase Rachford–Rice equations for negative flashes, *Fluid Phase Equilibr.*, 267 (2) (2008) 127.

[78] R. Li, H.A. Li, New two-phase and three-phase Rachford-Rice algorithms based on free-water assumption, *Can. J. Chem. Eng.*, 96 (1) (2018) 390.

[79] Y. Tang, S. Saha, An efficient method to calculate three-phase free-water flash for water-hydrocarbon systems, *Ind. Eng. Chem. Fundam.*, 42 (1) (2003) 189.

[80] A. Lapene, D.V. Nichita, G. Debenest, M. Quintard, Three-phase free-water flash calculations using a new Modified Rachford–Rice equation, *Fluid Phase Equilibr.*, 297 (1) (2010) 121.

[81] Z. Li, A. Firoozabadi, General strategy for stability testing and phase-split calculation in two and three phases, *SPE J.*, 17 (4) (2012) 1096.

[82] G. Wilson, A modified Redlich–Kwong EOS, Application to general physical data calculations, presented at *the Annual AICHE National Meeting*, Cleveland, Ohio, USA, May 1968; Paper No. 15c.

[83] L. Zhang, P. Chen, S. Pan, F. Liu, V. Pauchard, A.E. Pomerantz, S. Banerjee, N. Yao, O.C. Mullins, Structure–dynamic function relations of asphaltenes, *Energy Fuels*, 35 (17) (2021) 13610.

[84] A. Jamaluddin, J. Creek, C. Kabir, J. McFadden, D. D'cruz, J. Manakalathil, N. Joshi, B. Ross, Laboratory techniques to measure thermodynamic asphaltene instability, *J. Can. Pet. Tech.*, 41 (7) (2002) 44.

[85] PVT sim 20.0, Calsep A/S: Copenhagen, Denmark. 2011.

[86] P. Chueh, J. Prausnitz, Vapor-liquid equilibria at high pressures: Calculation of partial molar volumes in nonpolar liquid mixtures, *AIChE J.*, 13 (6) (1967) 1099.

[87] E. Buenrostro-Gonzalez, C. Lira-Galeana, A. Gil-Villegas, J. Wu, Asphaltene precipitation in crude oils: Theory and experiments, *AIChE J.*, 50 (10) (2004) 2552.

[88] A. Jamaluddin, N. Joshi, F. Iwere, O. Gurpinar, An investigation of asphaltene instability under nitrogen injection, presented at *SPE International Petroleum Conference and Exhibition in Mexico*, Villahermosa, Mexico, Feb. 10-12, 2002; SPE 2002; Paper No. SPE-74393-MS.

[89] A. Memon, B. Qassim, M. Al-Ajmi, A. Kumar Tharanivasan, J. Gao, J. Ratulowski, B. Al-Otaibi, R.A. Khan, Miscible gas injection and asphaltene flow assurance fluid characterization: a laboratory case study for a black oil reservoir, presented at *SPE EOR Conference at Oil and Gas West Asia*, Muscat, Oman, Apr. 16-18, 2012; SPE 2012; Paper No. SPE-150938-MS.

[90] R. Srivastava, S. Huang, M. Dong, Asphaltene deposition during CO_2 flooding, *SPE Prod. & Fac.*, 14 (4) (1999) 235.

[91] M. Dong, S. Huang, S.B. Dyer, F.M. Mourits, A comparison of CO_2 minimum miscibility pressure determinations for Weyburn crude oil, *J. Pet. Sci. Eng.*, 31 (1) (2001) 13.

[92] Q.M. Malik, M. Islam, CO2 Injection in the Weyburn field of Canada: optimization of enhanced oil recovery and greenhouse gas storage with horizontal wells, presented at *SPE/DOE Improved Oil Recovery Symposium*, Tulsa, Oklahoma, USA, Apr. 3-5, 2000; SPE 2000; Paper No. SPE-59327-MS.

[93] F.I. Stalkup, Displacement behavior of the condensing/vaporizing gas drive process, presented at *SPE Annual Technical Conference and Exhibition*, Dallas, Texas, USA, Sep. 27-30, 1987; SPE 1987; Paper No. SPE-16715-MS.

[94] W.L. Holm, Evolution of the carbon dioxide flooding processes, *J. Pet. Technol.*, 39 (11) (1987) 1337.

[95] J.J. Taber, A study of technical feasibility for the utilization of CO2 for enhanced oil recovery, P. Reimer (ed.), IEA Greenhouse Gas R&D Programme, Cheltenham, England (1994) Appendix B, 134.

[96] R. Srivastava, S. Huang, M. Dong, Laboratory investigation of Weyburn CO2 miscible flooding, *J. Can. Pet. Tech.*, 39 (2) (2000) 235.

CHAPTER 5 A ROBUST AND EFFICIENT ALGORITHM FOR VAPOR-LIQUID-EQUILIBRIUM/LIQUID-LIQUID-EQUILIBRIUM (VLE/LLE) PHASE BOUNDARY TRACKING

A version of this chapter has been published in *Chemical Engineering Science*.

Abstract

Three-phase equilibria, including three-phase vapor-liquid-asphaltene equilibria and three-phase vapor-liquid-liquid equilibria, can appear in gas injection-based enhanced oil recovery (EOR) processes. The appearance of either an asphaltene phase or a second liquid phase can significantly affect the relative permeability curves and thus influence the oil recovery efficiency. Therefore, it is of critical importance to accurately describe the phase behavior of reservoir fluids that exhibit such three-phase equilibria in EOR applications and to reliably predict the different types of phase diagrams exhibited by these reservoir fluids. In this study, a novel phase-boundary tracking method is proposed to precisely capture the vapor-liquid/liquid-asphaltene and vapor-liquid/liquid-liquid two-phase boundaries in pressure-temperature and pressure-composition phase diagrams. The two-phase boundaries determined by the proposed phase-boundary tracking method intersect the three-phase boundary at the apex of the three-phase region, which indicates the continuation of the three-phase region. The calculated phase boundaries are validated against those documented in the literature, and the results indicate very good agreement between the two.

Keywords: Vapor-liquid equilibria, Liquid-liquid equilibria, Phase diagram, Phase boundary, Equation of state, Algorithm development

5.1 Introduction

In addition to traditional vapor-liquid (VL) two-phase equilibria, three-phase equilibria also frequently appear during gas injection-based enhanced oil recovery (EOR) applications. For instance, vapor-liquid-asphaltene (VLA) three-phase equilibria are encountered during the production of asphaltenic reservoirs; this occurs as asphaltene can drop out due to gas injections or changes in the temperature/pressure conditions (Angle *et al.*, 2006; Chen *et al.*, 2022b). The appearance of the asphaltene phase can cause formation damage, potentially reducing oil recovery efficiency (Creek, 2005; Punnapala and Vargas, 2013). Another type of three-phase equilibrium is the vapor-liquid-liquid (VL_1L_2) three-phase equilibrium, which normally occurs during CO_2 flooding in low-temperature reservoirs (Pan *et al.*, 2015; Pasqualette *et al.*, 2020). In three-phase VL_1L_2 equilibria, the L_1 phase represents the heavier liquid phase, whereas the L_2 phase is the lighter liquid phase, which contains a significant amount of gaseous solvents (Li *et al.*, 2013). The presence of a second liquid phase can have a significant impact on the oil recovery efficiency because it induces changes in the relative permeability curves (Badamchi-Zadeh *et al.*, 2009a; Badamchi-Zadeh *et al.*, 2009b; Li *et al.*, 2013; Simon *et al.*, 1978). It is therefore important to develop robust and efficient algorithms to correctly describe the three-phase equilibria exhibited by a variety of reservoir fluids and to predict the corresponding pressure-temperature (*PT*) and pressure-composition (*Px*) phase diagrams.

Figures 5-1(a) and (b) schematically show the possible types of phase equilibria that could be encountered in three-phase VLA and VL_1L_2 equilibrium calculations, respectively. It can be seen from Figure 5-1 that there are five possible phase equilibria when the third phase appears. Robust phase equilibrium calculation algorithms have been developed for three-phase VLA and VL_1L_2 equilibrium calculations. For example,

Pan *et al.* (2019) proposed a trust-region-based three-phase VL_1L_2 equilibrium calculation algorithm based on the work of Petitfrere and Nichita (2014), which was shown to be robust and efficient for a number of CO_2-crude oil mixtures. Several robust three-phase VLA equilibrium calculation algorithms have recently been proposed (Chen *et al.*, 2021, 2022a; Li and Li, 2019). However, it should be noted that in these algorithms, the asphaltene phase is considered a pure phase (i.e., the asphaltene phase only contains the asphaltene component), which may lead to inaccurate results when the pure-asphaltene-phase assumption does not hold (Chen *et al.*, 2021). Because the asphaltene phase can be considered a heavier liquid phase that contains both asphaltene and other hydrocarbon components, the trust-region-based three-phase VL_1L_2 equilibrium calculation algorithm can be naturally extended to conduct three-phase VLA equilibrium calculations.

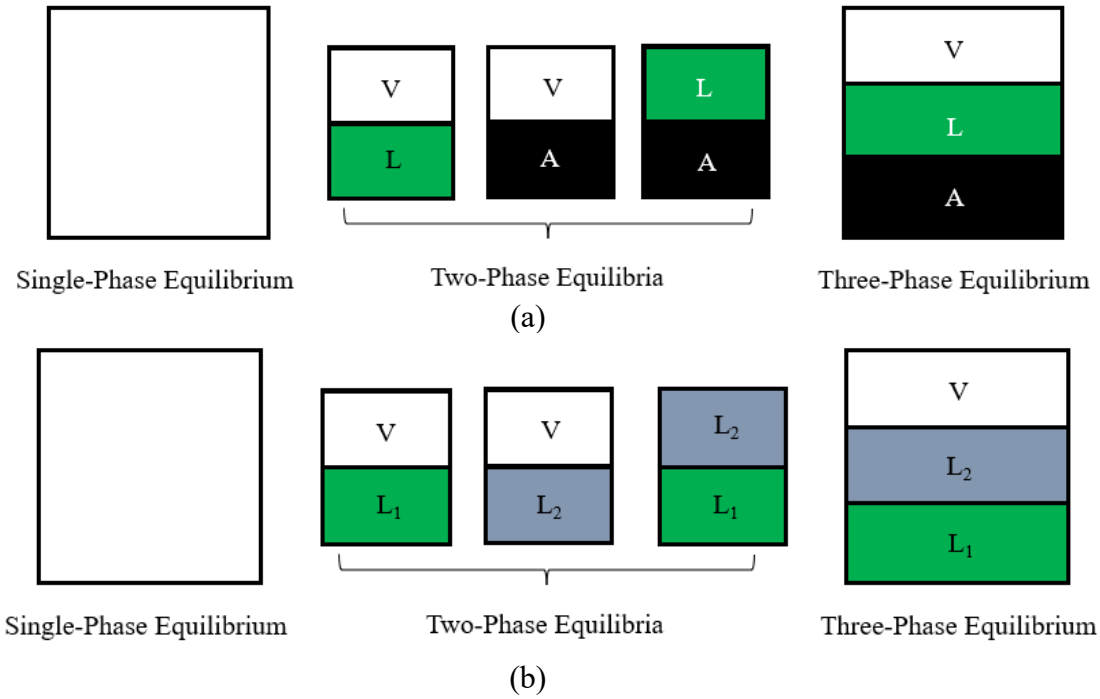

Fig. 5-1 Schematics of possible phase equilibria of some reservoir fluids exhibiting three-phase equilibria: (a) three-phase VLA equilibrium and (b) three-phase VL_1L_2 equilibrium [adapted from Li (2022)].

It is challenging to properly identify the three types of two-phase equilibria that can possibly appear in three-phase equilibrium calculations: two-phase VL (or VL_1) equilibrium, two-phase VA (or VL_2) equilibrium, and two-phase LA (or L_1L_2) equilibrium. Distinguishing which two-phase equilibrium is present under the given conditions is crucial because it could affect the calculations of some important properties in modeling multiphase flow in situ, such as relative permeability and capillary pressure (Bennett and Schmidt, 2017). Various phase-identification methods have been proposed to determine the correct phase types. These methods are based on either the calculated pseudo-critical points, the molar volumes, or the isothermal/isobaric compressibility factors that are output from multiphase equilibrium calculations. Note that these phase-identification methods have not been successfully applied to asphaltic oil systems to capture the VL/LA phase boundaries. In addition, determining the VL/LL and VL/LA phase boundaries still relies on conducting point-to-point phase equilibrium calculations, which is cumbersome and time-consuming. To the best of our knowledge, no algorithm has been developed to accurately and efficiently track the VL/LL and VL/LA phase boundaries that appear in *PT* and *Px* phase diagrams.

In both the three-phase VLA and VL_1L_2 equilibrium calculations, the composition of the asphaltene phase or the low-density liquid phase is dominated either by the asphaltene component or a gaseous solvent component, respectively. Therefore, the mole fraction of the asphaltene component is selected to track the VL/LA phase boundaries, whereas the mole fraction of the gaseous component is chosen to track the VL/LL phase boundaries. The three-phase VL_1L_2 equilibrium calculation algorithm based on the trust-region method proposed by Pan *et al.* (2019) is first extended to conduct three-phase VLA equilibrium calculations, and the calculation results are

validated by comparing them to experimental data from the literature. The validation results demonstrate that the trust-region-based VLA three-phase equilibrium calculation algorithm is accurate and robust. Subsequently, a novel phase boundary tracking method is proposed, in which the second derivative of the mole fraction of the most dominant component in either the asphaltene phase or the low-density liquid phase with respect to temperature or pressure is used to identify the VL/LL and VL/LA phase boundaries. A robust numerical solution algorithm, that is, Brent's method (Brent, 1971), is then implemented to ensure the accuracy and efficiency of the phase boundary tracking algorithm.

5.2 A Brief Review of Phase Identification Methods

Several phase identification methods have been proposed over the past few decades. The simplest method is the critical point method (Gosset *et al.*, 1986), in which a phase is considered a vapor phase if the temperature is higher than the phase critical temperature ($T > T_c$) or if the phase volume exceeds the phase critical volume ($V > V_c$). The critical properties of the different phases can be calculated using the method proposed by Asselineau *et al.* (1979). The temperature criterion using the critical temperature calculated by Li's mixing rule (Li, 1971) is then adopted by the compositional reservoir simulator ECLIPSE (Schlumberger, 2015).

The isothermal compressibility method is also a widely accepted phase labeling method. The isothermal compressibility can be calculated using the following equation (Bennett and Schmidt, 2017):

$$k = -\left(\frac{\partial \log V}{\partial P}\right)_T = -\frac{1}{V}\left(\frac{\partial V}{\partial P}\right)_T \quad (1)$$

where k is the isothermal compressibility, V is the molar volume of the phase, and P and T are the pressure and temperature, respectively. Since the isothermal compressibility of the vapor phase is much larger than that of the liquid phase, Poling *et al.* (1981) proposed a new phase-identification method, in which a phase is labeled as a liquid phase if $kP < 0.005$, and a vapor phase if $0.9 < kP < 3$. Instead of using the values of kP, Pasad and Venkatarathnam (1999) found that the value of $\frac{\partial k}{\partial T}$ can be used to determine whether the phase is a liquid phase or a vapor phase. If $\frac{\partial k}{\partial T} > 0$, the fluid is liquid; if $\frac{\partial k}{\partial T} < 0$, the fluid is vapor. Similarly, Bennett and Schmidt (2017) proposed using the thermal expansion coefficient (α) as an indicator for phase identification; α can be calculated as follows (Bennett and Schmidt, 2017):

$$\alpha = -\left(\frac{\partial \log V}{\partial T}\right)_P = -\frac{1}{V}\left(\frac{\partial V}{\partial T}\right)_P \quad (2)$$

If the value of $\frac{\partial k}{\partial T} > 0$, the fluid is liquid; if $\frac{\partial k}{\partial T} < 0$, the fluid is vapor. There are also phase identification methods based on the mole fractions of the key components. Perschke (1988) used the heaviest hydrocarbon component to determine the oleic phase when three-phase equilibria appear and the density of the remaining phases to identify the vapor phase and the second liquid phase. When there are only two equilibrium phases, the L_1 phase is assumed to exist, and the other phase is determined by the mass density (Perschke, 1988). If the mass density of the second phase is lower than the specified threshold value, the phase is labeled as the vapor phase; otherwise, it is labeled as an L_2 phase (Perschke, 1988). This method has been widely implemented in compositional flow simulators, such as UTCOMP (Chang, 1990; Neshat *et al.*, 2020). However, the fixed mass density threshold does not perform well for phase labeling in the two-phase region (Mohanty *et al.*, 1995; Xu and Okuno, 2015). This method was then modified

by Xu and Okuno (2015), and the phase with the higher methane concentration was identified as the vapor phase.

When constructing the *PT* and *Px* phase diagrams, we pay less attention to the VL/LA and VL/LL boundaries. To determine the VL/LA and VL/LL phase boundaries using traditional phase identification methods, point-to-point phase equilibrium calculations are conducted over a certain temperature/pressure range with a certain step size. Different phase labeling methods are then applied based on the results of the phase equilibrium calculations, and the VL/LA and VL/LL phase boundaries are delineated based on the phase identification results. The use of such an exhaustive procedure implies that the accuracy in determining the VL/LA and VL/LL phase boundaries is highly dependent on the step size used. To increase the calculation accuracy, a rather small step size must be used, which, however, would significantly increase the computational cost. Therefore, a robust and efficient phase boundary tracking method is urgently needed to accurately identify the VL/LA and VL/LL phase boundaries when constructing *PT* and *Px* phase diagrams involving VLA or VL_1L_2 phase equilibria.

5.3 VL/LA and VL/LL Phase Boundary Tracking Algorithm

5.3.1 VL/LA and VL/LL Phase Boundary Tracking Algorithm for Generating *PT* Phase Diagrams

In this study, we propose a novel VL/LA and VL/LL phase boundary tracking method. The phase boundary can be captured using information pertinent to the mole fraction of the gaseous component or the asphaltene component. In *PT* phase diagrams, the VL/LA phase boundary is considered to be reached if the following equation is satisfied:

$$\frac{\partial^2 x_d^{V/A}}{\partial T^2} = 0 \quad (3)$$

where $x_d^{V/A}$ represents the mole fraction of the asphaltene component in the vapor phase or in the asphaltene phase.

Similarly, the VL/LL phase boundary is obtained by solving the following equation:

$$\frac{\partial^2 x_d^{V/L_2}}{\partial T^2} = 0 \quad (4)$$

where x_d^{V/L_2} represents the mole fraction of the gaseous component in the vapor phase or in the lighter liquid phase. The central finite difference method is used to approximate the second derivative shown in Equations (3-4).

Brent's method (Brent, 1971) is applied to solve either Equation (3) or Equation (4) in this study. Compared with traditional methods, Brent's method (Brent, 1971) is fast and can guarantee convergence when searching for the zero of a function. In addition, the results obtained using Brent's method are highly accurate. The detailed procedure of Brent's method is presented in Brent (1971) and Lu *et al.* (2021).

Figure 5-2 shows the flow chart of the VL/LA and VL/LL phase boundary tracking method for constructing *PT* phase diagrams. The details of the stepwise procedure are as follows:

1. Input initial pressure (P_{init}), fluid properties (T_c, P_c, and ω), binary interaction parameters (BIPs), and feed composition. While tracking the VL/LA phase boundaries, the maximum pressure at which a VLA three-phase region exists (P_{apex}) is first sought. The initial pressure is then determined using the following equation:

$$\boldsymbol{P_{init}} = \frac{\boldsymbol{P_{apex}}}{\mathbf{2}} \quad (5)$$

When we track the VL/LL phase boundaries in the *PT* phase diagrams, we record the corresponding temperature, T_{apex}, after obtaining the value of P_{apex}. The pressure

at the single-phase/two-phase boundary at T_{apex} is then recorded as P_{12}. The initial pressure is then calculated as follows:

$$\boldsymbol{P_{init}} = \frac{\boldsymbol{P_{apex}+P_{12}}}{\boldsymbol{2}} \quad (6)$$

2. Determine the temperature range [T_{min}, T_{max}] that brackets the VL/LA or VL/LL phase boundaries. In this study, T_{max} is set as the temperature of the single-phase/two-phase boundary at a given pressure, whereas $T_{min} = T_{apex} - 200$ K.

3. Under a given pressure, two stability tests are conducted on the given mixture at T_{min} and T_{max}. If the results show two-phase equilibria, proceed to Step 4. If not, go to Step 2 and reset the temperature range by setting $T_{min} = T_{min} + 10$ K.

4. Under the given pressure, calculate the values of $\frac{\partial^2 x_d^{V/L_2}}{\partial T^2}$ or $\frac{\partial^2 x_d^{V/A}}{\partial T^2}$ at T_{min} and T_{max}. The following equation must be satisfied to guarantee that a solution exists so that Brent's method can be applied:

$$\left[\frac{\partial^2 x_d^{V/L_2(A)}}{\partial T^2}\right]_{T=T_{min}} \times \left[\frac{\partial^2 x_d^{V/L_2(A)}}{\partial T^2}\right]_{T=T_{max}} < \mathbf{0} \quad (7)$$

   If Equation (7) is not satisfied, reset the temperature range by setting $T_{min} = T_{min} - 10$ K.

5. Call Brent's method (Brent, 1971) to solve Equations (3) or (4) and record the temperature corresponding to the VL/LA or VL/LL phase boundary at the given pressure.

6. Update the value of pressure by using $P = P + 0.01$ bar and go to Step 2 until the VL/LA or the VL/LL phase boundary intersects other phase boundaries. Then, update the value of pressure by $P = P - 0.01$ bar and repeat the calculations until either the VL/LA or the VL/LL phase boundary intersects other phase boundaries or the pressure is less than 1 bar.

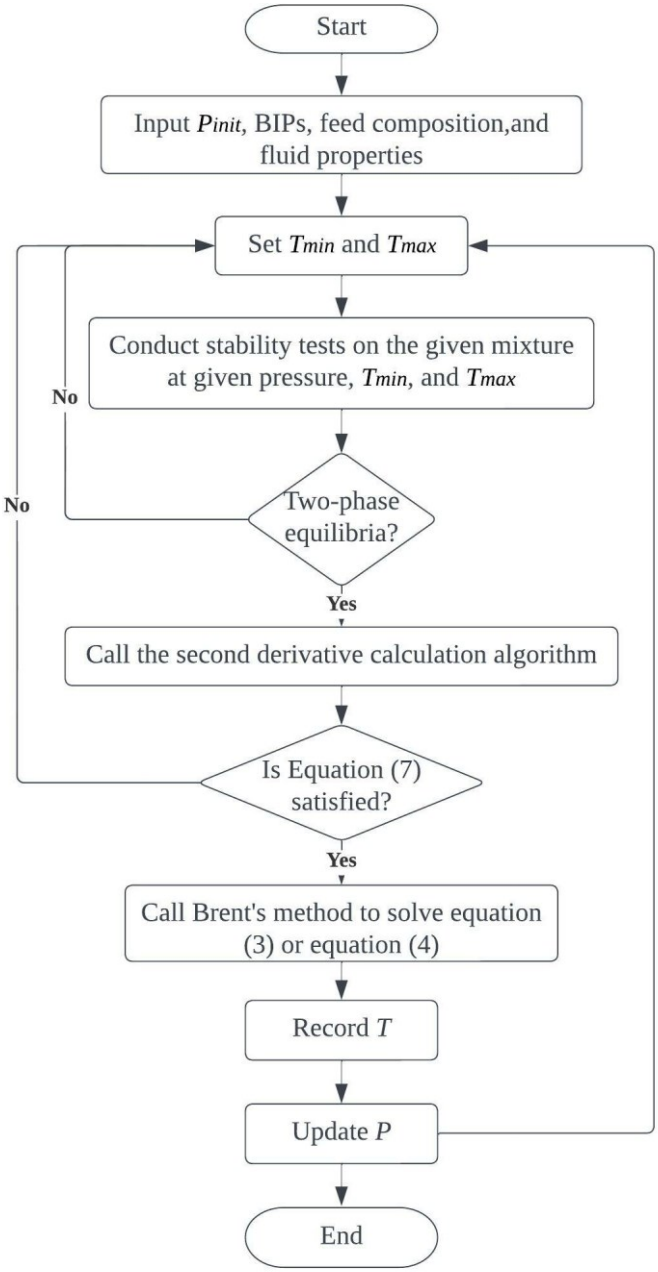

Fig. 5-2 Flow chart of the VL/LA and VL/LL phase boundary tracking method for constructing *PT* phase diagrams.

5.3.2 VL/LL Phase Boundary Tracking Algorithm for Generating *Px* Phase Diagrams

In *Px* phase diagrams, since the temperature is held constant, the VL/LL phase boundary is identified using the following equation:

$$\frac{\partial^2 x_d^{V/L_2}}{\partial P^2} = 0 \text{ (8)}$$

Note that the central finite difference method is applied to approximate the second derivative shown in Equation (8).

A flow chart of the VL/LL phase boundary tracking algorithm used to generate the *Px* phase diagrams is shown in Figure 5-3. The detailed procedure is summarized as follows:

1. Input the temperature (T), initial mole fraction of the injection gas (x_{init}), fluid properties (T_c, P_c, ω), BIPs, and feed composition. The initialization procedure will vary in different scenarios. Figure 5-4 shows three different types of *Px* phase diagrams that may appear. In Scenario 1, where the VL_1L_2 three-phase boundary intersects the single-phase/two-phase boundary [see Figure 5-4 (a)] and the maximum mole fraction of the injection gas at which a VL_1L_2 three-phase region exists (x_{max}) is smaller than or equal to 99.99 mol%, x_{init} can be calculated using the following equation:

$$\boldsymbol{x_{init}} = \frac{\boldsymbol{x_{max}+1}}{\boldsymbol{2}} \text{ (9)}$$

   For Scenario 2, where the VL_1L_2 three-phase boundary does not intersect the single-phase/two-phase boundary and x_{max} > 99.99 mol% [Figure 5-4 (b)], we first record the minimum mole fraction of the injection gas at which a VL_1L_2 three-phase region exists (x_{min}), as well as the corresponding pressure (P_3) at such a mole fraction. We then draw a horizontal line with a pressure level of P_3. The intersection of this horizontal line with the single-phase/two-phase boundary is denoted as (x_{12}, P_3). We then determine x_{init} using the following equation:

$$\boldsymbol{x_{init}} = \frac{\boldsymbol{x_{min}+x_{12}}}{\boldsymbol{2}} \text{ (10)}$$

For Scenario 3, where the VL_1L_2 three-phase boundary does not intersect the single-phase/two-phase boundary and x_{apex} < 99.99 mol% [see Figure 5-4 (c)], we first track the VL/LL two-phase boundary on the left of the VL_1L_2 three-phase boundary using the initialization method applicable to Scenario 2 and then track the VL/LL two-phase boundary on the right of the VL_1L_2 three-phase boundary using the initialization method applicable to Scenario 1.

2. Determine the pressure range [P_{min}, P_{max}] that brackets the VL/LL phase boundaries at a given mole fraction of the injection gas. In this study, P_{min} is set as the saturation pressure of the mixture when there is 0 mol% injection gas. It should be noted that the selection of P_{max} is empirical. In general, for Scenario 1, the maximum pressure could be set at any pressure higher than P_3. For Scenario 2, P_{max} could be set as the pressure of the single-phase/two-phase boundary at the given mole fraction of the injection gas. For Scenario 3, when tracking the VL/LL two-phase boundary on the left of the VL_1L_2 three-phase region, we set up the pressure range [P_{min}, P_{max}] as per the setup method applicable to Scenario 2, and when tracking the VL/LL two-phase boundary on the right of the VL_1L_2 three-phase region, we set up the pressure range [P_{min}, P_{max}] as per the setup method applicable to Scenario 1.

3. Under a given temperature and mole fraction of the injection gas, two stability tests are conducted on the given mixture at P_{min} and P_{max}. If the results of the stability tests correspond to two-phase equilibria, continue; otherwise, go to Step 2 and reset the pressure range [P_{min}, P_{max}] by setting P_{max} as P_{max} −5 bar.

4. Under a given temperature and mole fraction of the injection gas, calculate the values of $\frac{\partial^2 x_d^{V/L_2}}{\partial P^2}$ at P_{min} and P_{max}. Then, check whether the following criterion is satisfied:

$$\left[\frac{\partial^2 x_d^{V/L_2}}{\partial P^2}\right]_{P=P_{min}} \times \left[\frac{\partial^2 x_d^{V/L_2}}{\partial P^2}\right]_{P=P_{max}} < \mathbf{0} \quad (11)$$

If Equation (11) is not satisfied, return to Step 2 and adjust the pressure range [P_{min}, P_{max}] by setting P_{max} as P_{max} + 5 bar; otherwise, continue.

5. Call Brent's method (Brent, 1971) to solve Equation (8) and record the pressure of the phase boundary at the given temperature and mole fraction of the injection gas.

6. Update the value of x as $x = x - 0.001$, go to Step 2, and repeat the calculations until the VL/LL phase boundary intersects the other phase boundaries. Then, update the value of x as $x = x + 0.001$, go to Step 2, and repeat the calculations until the VL/LL phase boundary intersects the other phase boundaries or when the value of x is greater than 99.9%.

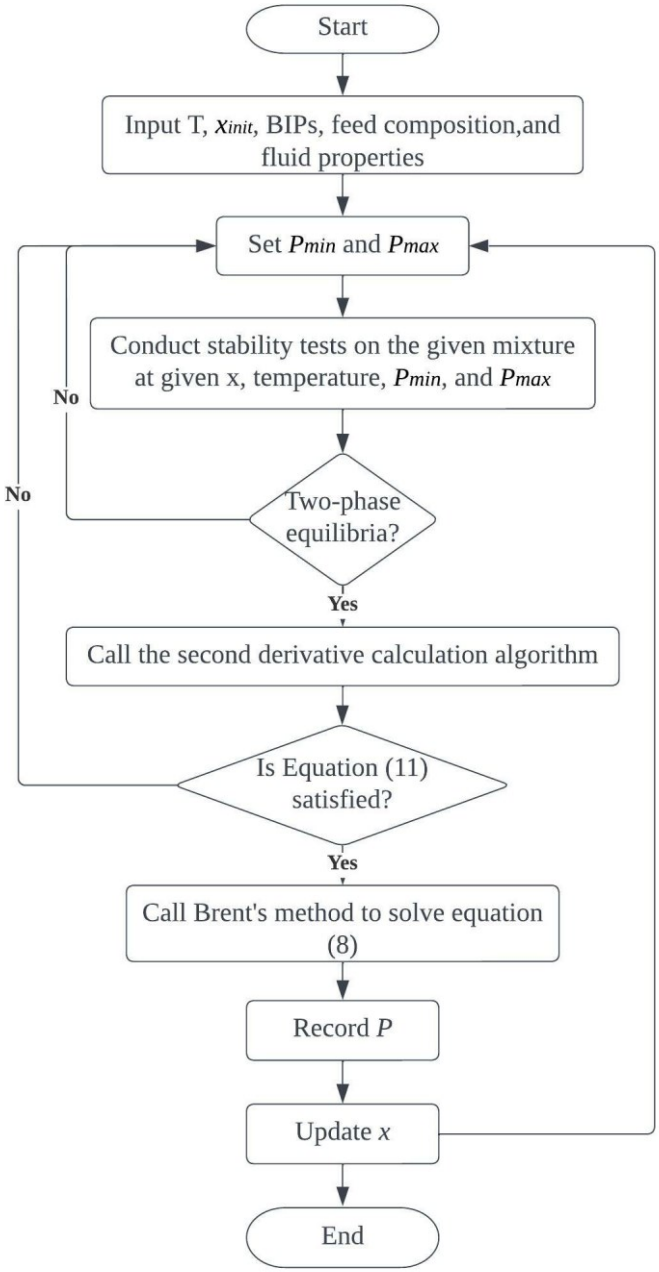

Fig. 5-3 Flow chart of the VL/LA and VL/LL phase boundary tracking method for constructing *Px* phase diagrams.

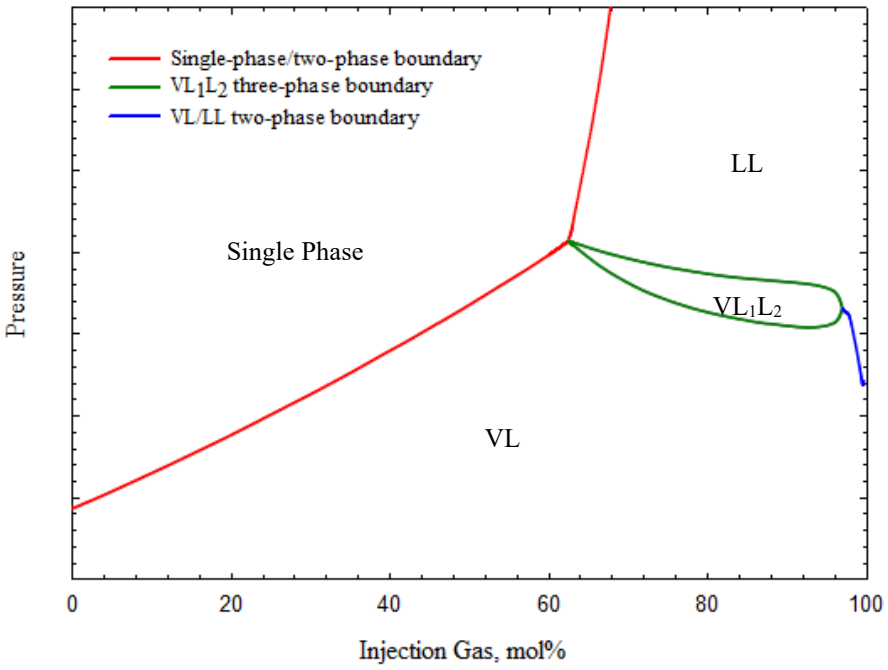
Single-phase/two-phase boundary
VL1L2 three-phase boundary
VL/LL two-phase boundary
LL
Single Phase
VL1L2
VL
Pressure
0
20
40
60
80
100
Injection Gas, mol%

(a)

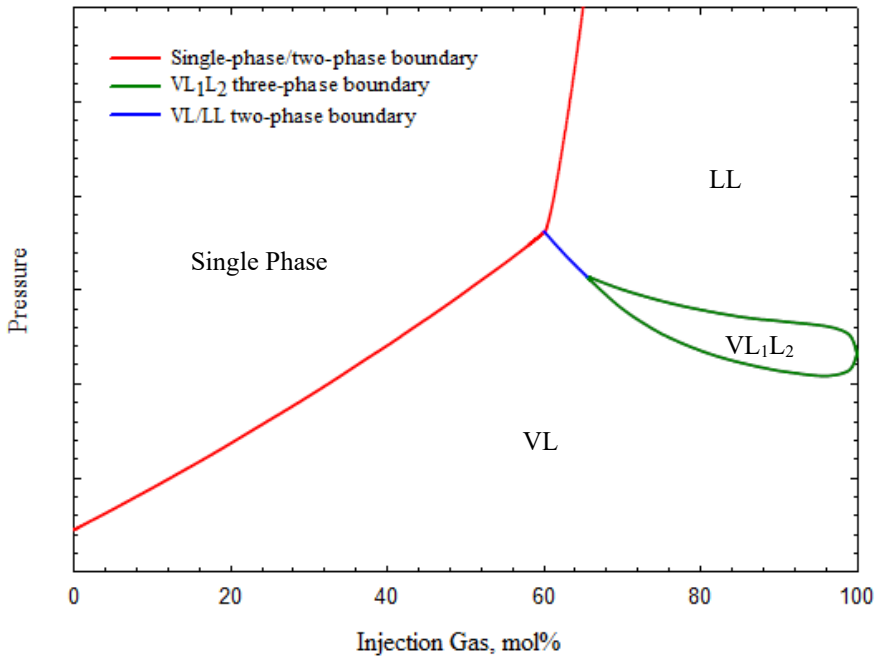
Single-phase/two-phase boundary
VL1L2 three-phase boundary
VL/LL two-phase boundary
LL
Single Phase
VL1L2
VL
Pressure
0
20
40
60
80
100
Injection Gas, mol%

(b)

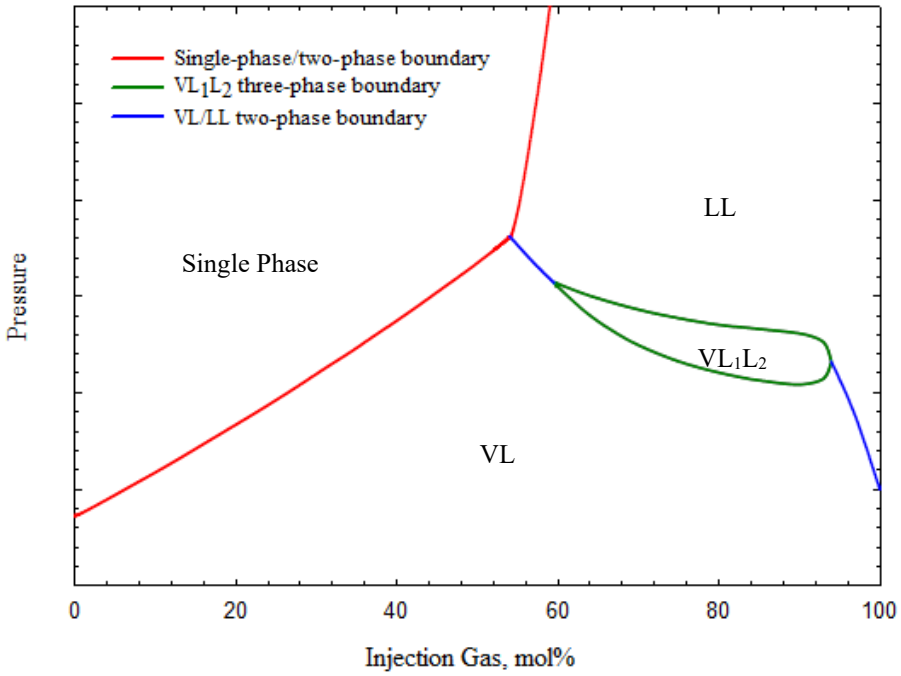

(c)

Fig. 5-4 Schematics of different types of *Px* phase diagrams that may appear during the gas injection process: (a) Scenario 1; (b) Scenario 2; and (c) Scenario 3.

5.4 Results and Discussion

In this section, *PT* and *Px* phase diagrams are generated for two reservoir fluids that are prone to asphaltene precipitation and three reservoir fluids that are prone to form a second liquid phase. To test the performance of the newly proposed method, the phase diagrams generated by the newly proposed method are compared with either the available experimental data or the calculated results reported in previous studies. The Peng-Robinson equation of state (PR EOS) (Peng and Robinson, 1976) is applied to conduct the phase equilibrium calculations.

5.4.1 Generation of Phase Diagrams with Asphaltene Precipitation

Oil samples 1 and 2, both of which exhibited asphaltene precipitation during the PVT experiments, are first characterized using the method proposed by Pedersen *et al.* (2006). Although the present characterization method is the same as that used by Chen *et al.*

(2022a), the characterization results are different since we do not use the free-asphaltene assumption as used in Chen *et al.* (2022a).

Figure 5-5 shows the *PT* phase diagrams generated for oil samples 1 and 2. Note that the VL/LA phase boundaries are generated by the newly proposed phase boundary tracking algorithm, whereas the other phase boundaries (such as the three-phase VLA boundary) are generated based on point-to-point calculations made using the trust-region-based three-phase equilibrium calculation algorithm (Lu *et al.*, 2021; Pan *et al.*, 2019). As shown in Figure 5-5, the calculated phase boundaries agree well with the experimental data, indicating that the trust-region-based multiphase equilibrium calculation algorithm proposed by Pan *et al.* (2019) can be extended to reliably conduct three-phase VLA equilibrium calculations. More importantly, Figure 5-5 shows that the predicted VL/LA two-phase boundaries are smooth and continuous. Besides, the VL/LA phase boundaries intersect the three-phase region at the apex, and the VL/LA two-phase boundaries can be considered as extensions of the VLA three-phase region, which indicates the continuation of the three-phase region (Bennett and Schmidt, 2017). Therefore, it can be concluded that the proposed VL/LA phase-boundary-tracking algorithm performs well in predicting the VL/LA phase boundaries.

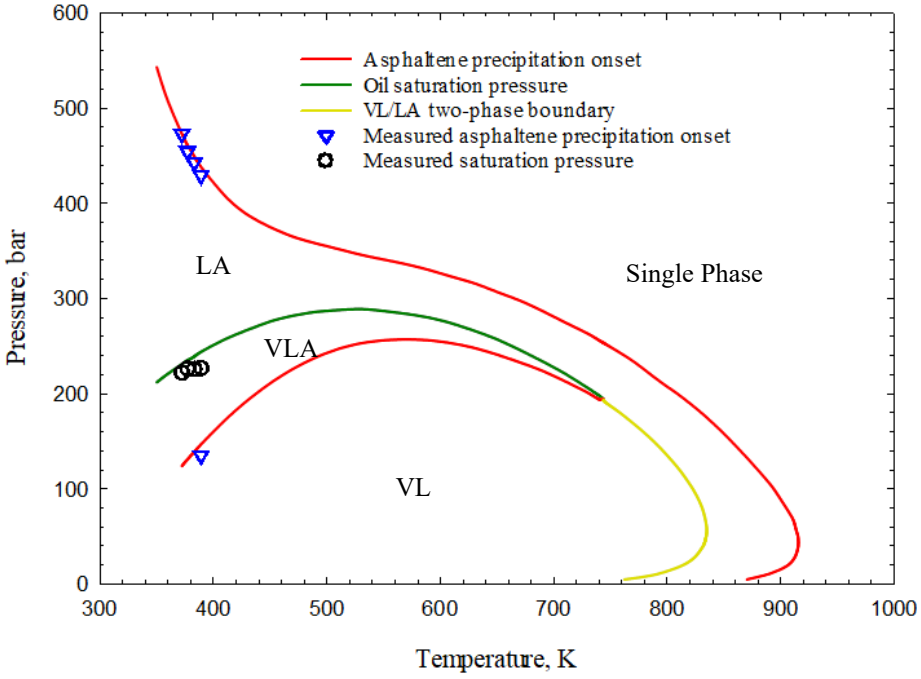

(a)

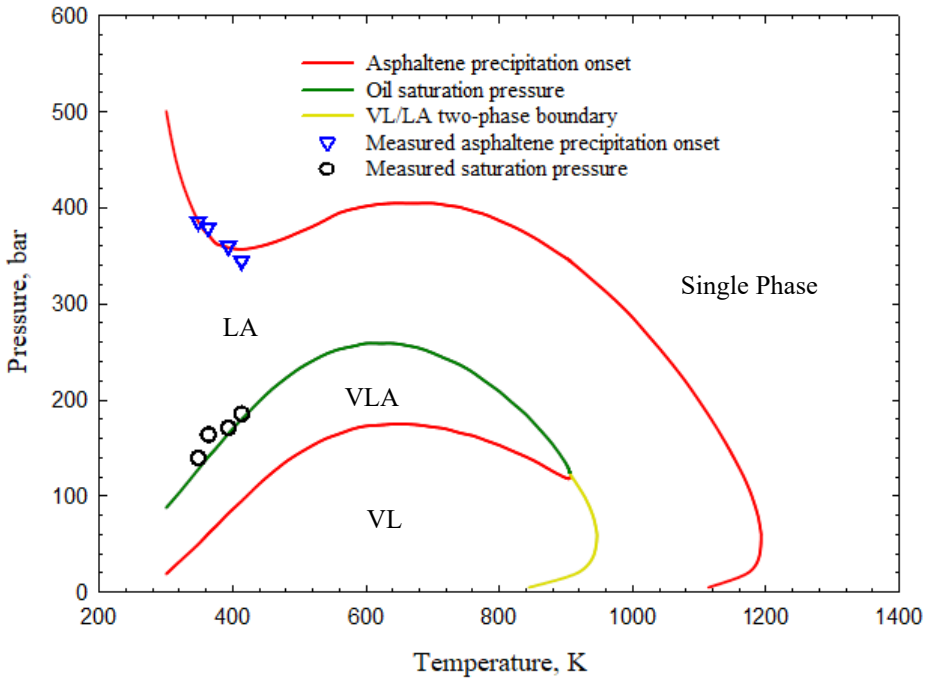

(b)

Fig. 5-5 *PT* phase diagrams with asphaltene precipitation: (a) oil sample 1; (b) oil sample 2.

Here, we use two example calculations to show the detailed process of how to determine the VL/LA phase boundary. Figures 5-6 (a) and (b) show the variations in $\frac{\partial^2 x_d^{V/A}}{\partial T^2}$ versus temperature at 100 bar for oil samples 1 and 2, respectively. As shown in Figure 5-6,

the solution of Equation (3) is between 820 K and 830 K for oil sample 1 and between 920 K and 930 K for oil sample 2. By applying Brent's method (Brent, 1971), we readily determine the VL/LA phase boundaries at 100 bar to be 822.5197 K for oil sample 1 and 927.5712 K for oil sample 2.

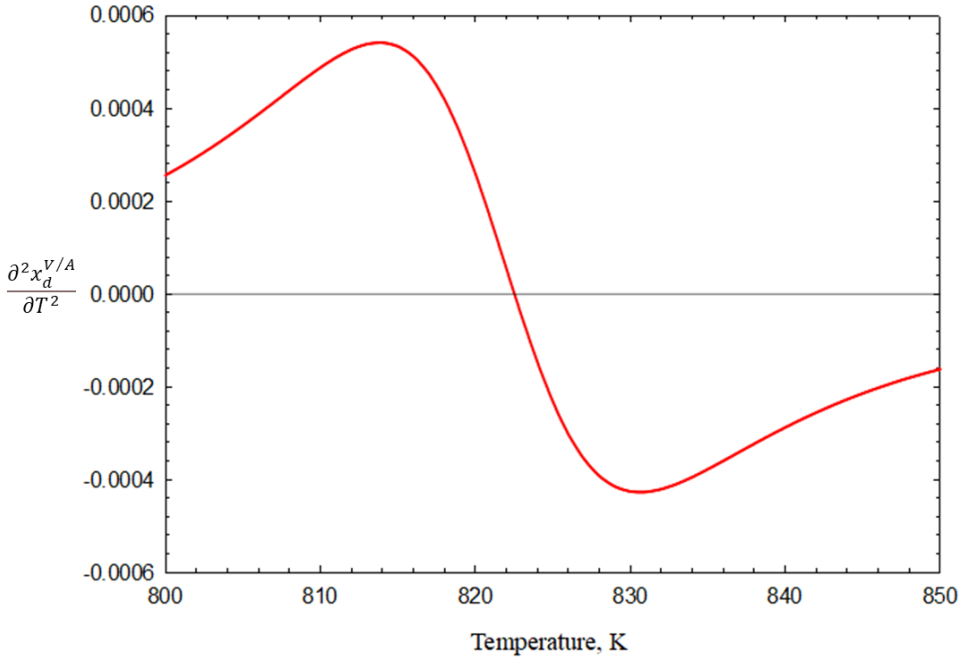

(a)

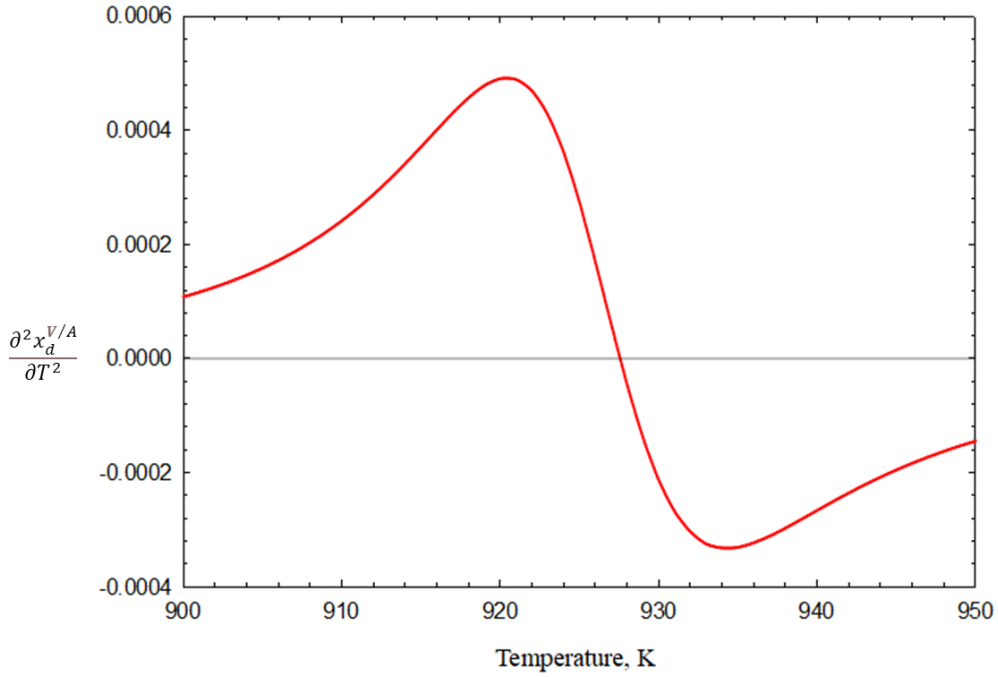

(b)

Fig. 5-6 Variation of $\frac{\partial^2 x_d^{V/A}}{\partial T^2}$ versus temperature at 100 bar for: (a) oil sample 1; (b) oil sample 2.

5.4.2 Generation of Phase Diagrams with the Appearance of the Second Liquid Phase

VL_1L_2 equilibrium calculations are conducted for the three oil samples. Tables 5-1, 5-2 and 5-3 show the compositions and fluid properties of the three oil samples [i.e., oil G, North Ward Estes (NWE) oil, and Bob Slaughter Block (BSB) oil] (Khan *et al.*, 1992; Okuno *et al.*, 2011). The BIPs between the CO_2 and hydrocarbon components are also shown in Tables 5-1, 5-2 and 5-3. These three oil samples were obtained from three different low-temperature oil reservoirs in West Texas and were experimentally confirmed to form VL_1L_2 three-phase regions during gas injection processes. Note that the BIPs between the hydrocarbon components are set to zero in the three-phase VL_1L_2 equilibrium calculations.

Table 5-1 Composition and fluid properties of Oil G (Khan *et al.*, 1992).

Component	Composition	T_c (K)	P_c (bar)	ω	MW	BIP with

	(mol%)				(g/mol)	CO_2
CO_2	1.690	304.200	73.76	0.225	44.010	0
C_1	17.520	174.444	46.00	0.008	16.043	0.085
C_{2-3}	22.440	347.263	44.69	0.133	37.909	0.085
C_{4-6}	16.730	459.740	34.18	0.236	68.672	0.085
C_{7-14}	24.220	595.135	21.87	0.598	135.093	0.104
C_{15-25}	12.160	729.981	16.04	0.912	261.103	0.104
C_{26+}	5.240	910.183	15.21	1.244	479.698	0.104

Table 5-2 Composition and fluid properties of NWE Oil (Khan *et al.*, 1992).

Component	Composition (mol%)	T_c (K)	P_c (bar)	ω	MW (g/mol)	BIP with CO_2
CO_2	0.770	304.200	73.77	0.225	44.010	0
C_1	20.250	190.600	46.00	0.008	16.040	0.120
PC_1	11.800	343.640	45.05	0.130	38.400	0.120
PC_2	14.840	466.410	33.51	0.244	72.820	0.120
PC_3	28.630	603.070	24.24	0.600	135.820	0.090
PC_4	14.900	733.790	18.03	0.903	257.750	0.090
PC_5	8.810	923.200	17.26	1.229	479.950	0.090

Table 5-3 Composition and fluid properties of BSB Oil (Khan *et al.*, 1992). This oil is characterized as a quaternary fluid by Okuno *et al.* (2011).

Component	Composition (mol%)	T_c (K)	P_c (bar)	ω	MW (g/mol)	BIP with CO_2
CO_2	3.370	304.200	73.77	0.225	44.01	0
C_1	8.610	160.000	46.00	0.008	16.04	0.055
PC_1	64.780	529.030	27.32	0.481	98.45	0.081
PC_2	23.240	795.330	17.31	1.042	354.2	0.105

Figure 5-7 shows the *PT* phase diagram of Oil G with 70 mol% CO_2 injection, and Figures 5-8 and 5-9 show the *Px* phase diagrams of BSB Oil and NWE Oil, respectively, with impure CO_2 injection. As shown in Figures 5-7, 5-8 and 5-9, the VL/LL two-phase boundary intersects the VL_1L_2 three-phase region at the apex of the VL_1L_2 three-phase boundary, which indicates the continuation of the three-phase region (Bennett and Schmidt, 2017). The calculated phase diagrams are also compared with those of

previous studies to validate the accuracy of our calculations. We can see from Figures 5-7, 5-8 and 5-9 that the calculated phase boundaries agree well with those reported in previous studies (Bennett and Schmidt, 2017; Li and Firoozabadi, 2012; Lu *et al.*, 2021). Note that in Figure 5-9, the calculated VL/LL two-phase boundary using the newly proposed phase boundary identification method is compared with that calculated by the thermal expansion coefficient method proposed by Bennet and Schmidt (2017), and the calculation results are almost identical. Thus, we can conclude that the newly proposed phase boundary identification method can be used to reliably predict the VL/LL two-phase boundary.

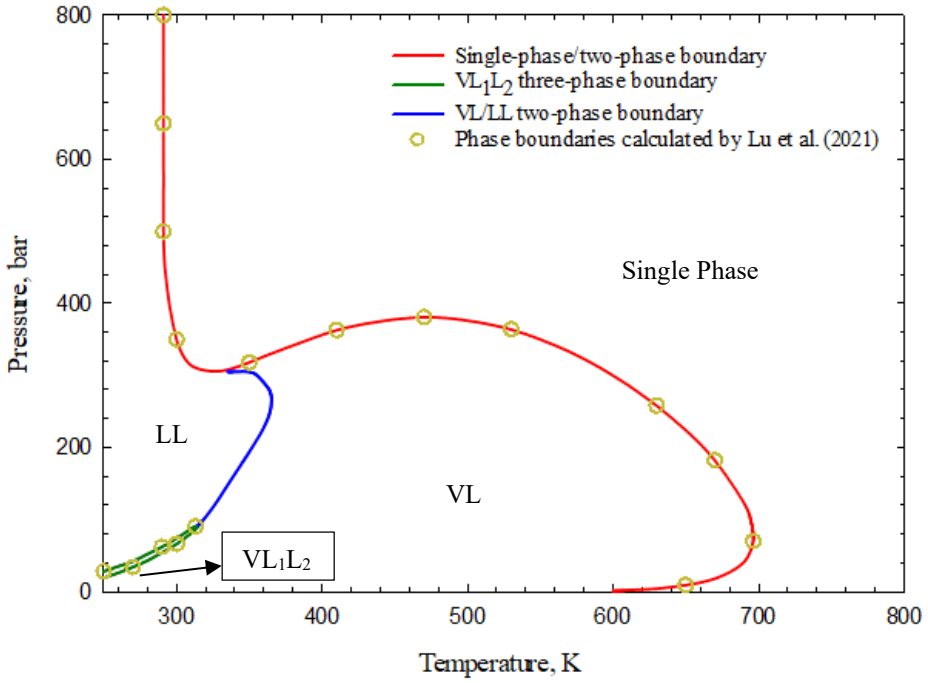

Fig. 5-7 *PT* phase diagram of Oil G with 70 mol% CO_2 injection.

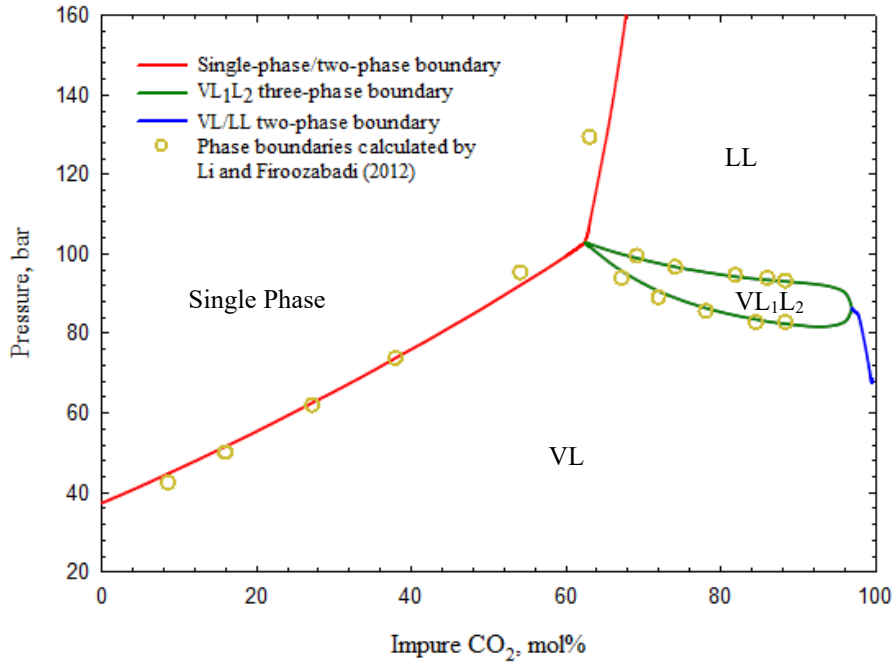

Fig. 5-8 *Px* phase diagram of BSB Oil with impure CO_2 injection. The impure CO_2 stream contains 95 mol% CO_2 and 5 mol% C_1.

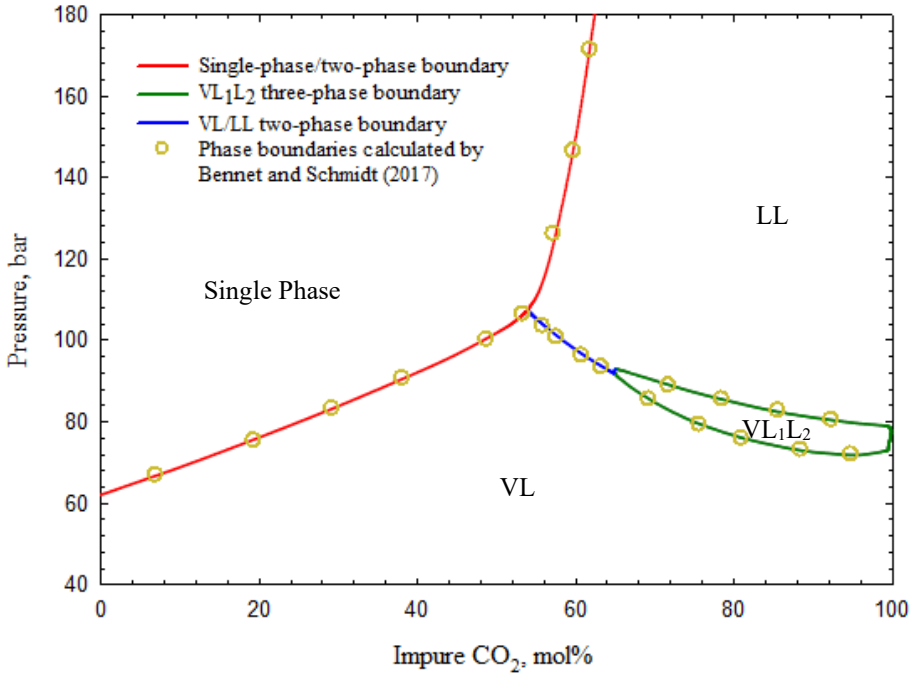

Fig. 5-9 *Px* phase diagram of NWE Oil with impure CO_2 injection. The impure CO_2 stream contains 95 mol% CO_2 and 5 mol% C_1.

Oil G with 70 mol% CO_2 injection is used as an example to illustrate the application of the proposed methodology to locate the VL/LL phase boundary in the *PT* phase diagrams. The change of $\frac{\partial^2 x_d^{V/L_2}}{\partial T^2}$ versus the temperature at 200 bar for Oil G with 70

mol% CO_2 injection is shown in Figure 5-10. As shown in the figure, the solution of Equation (4) at 200 bar is between 350 K and 360 K for Oil G with 70 mol% CO_2 injection. By applying Brent's method (Brent, 1971), we determine the pressure at the VL/LL phase boundary to be 351.8622 K.

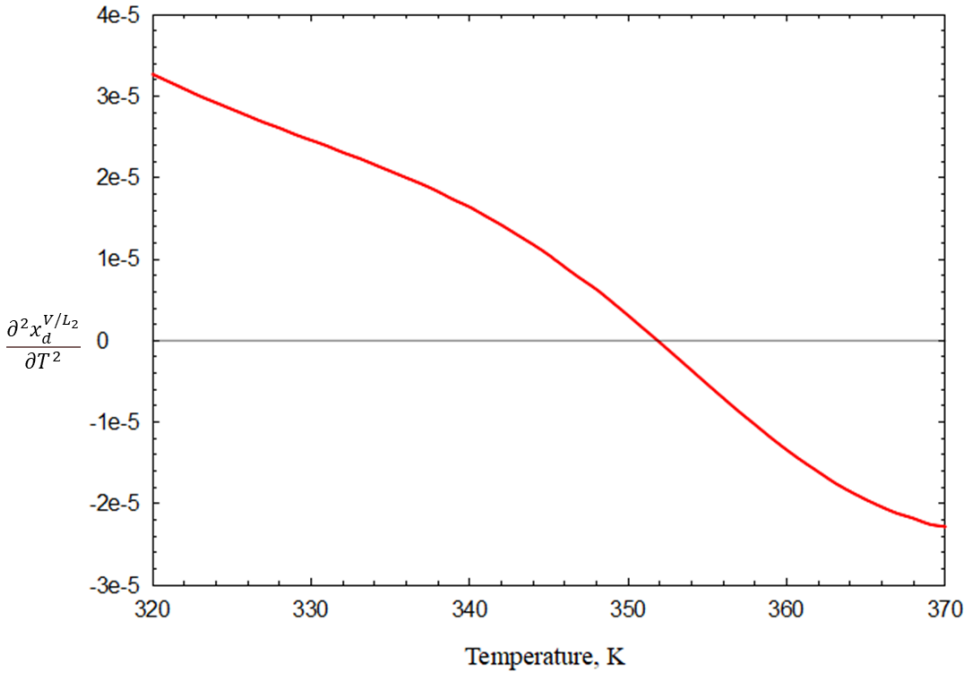

Fig. 5-10 Change of $\frac{\partial^2 x_d^{V/A}}{\partial T^2}$ of Oil G versus temperature at 200 bar.

Figure 5-11 shows the change of $\frac{\partial^2 x_d^{V/L_2}}{\partial P^2}$ with pressure at 313.71 K for BSB Oil with 98 mol% impure CO_2 injection (herein, the impure CO_2 stream contains 95 mol% CO_2 and 5 mol% C_1), whereas Figure 5-12 shows the change of $\frac{\partial^2 x_d^{V/L_2}}{\partial P^2}$ with pressure at 301.48 K for NWE oil with 60 mol% impure CO_2 injection. It can be seen from Figure 5-11 that the solution of Equation (8) is between 80 bar and 85 bar for BSB oil. Using Brent's method (Brent, 1971), we determine the pressure at the VL/LL phase boundary to be 83.5074 bar. Similarly, the VL/LL phase boundary is identified as 97.7841 bar at 301.48 K for NWE Oil with 60 mol% impure CO_2 injection.

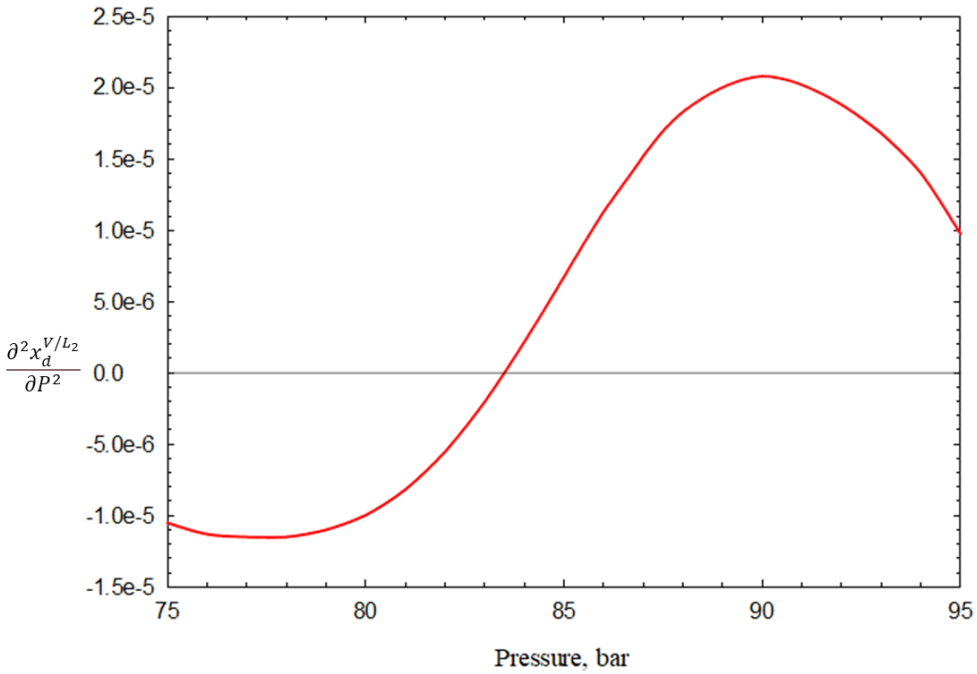

Fig. 5-11 Change of $\frac{\partial^2 x_d^{V/L_2}}{\partial P^2}$ with pressure at 313.71 K for BSB Oil with 98 mol% impure CO_2 injection. The impure CO_2 stream contains 95 mol% CO_2 and 5 mol% C_1.

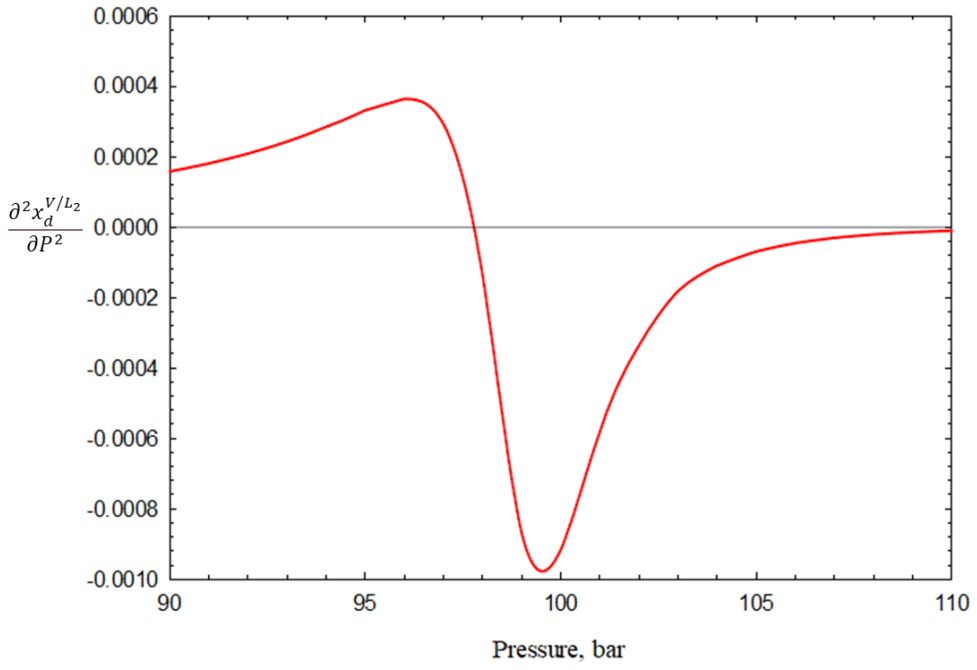

Fig. 5-12 Change of $\frac{\partial^2 x_d^{V/L_2}}{\partial P^2}$ with pressure at 301.48 K of NWE oil with 60 mol% impure CO_2 injection. The impure CO_2 stream contains 95 mol% CO_2 and 5 mol% C_1.

5.4.3 Effect of Different Criteria on the Generation of Phase Diagrams

In this study, we use $\frac{\partial^2 x_d}{\partial T^2} = 0$ to track the VL/LA and VL/LL phase boundaries in the *PT* phase diagrams, whereas we use $\frac{\partial^2 x_d}{\partial P^2} = 0$ to track such phase boundaries in the *Px* phase diagrams. In this section, we use oil sample 1 as an example to examine the effects of different criteria on tracking the VL/LA phase boundaries. Figure 5-13 shows a comparison of the *PT* phase diagrams of oil sample 1 generated using these different criteria. In Figure 5-13, the yellow line shows the VL/LA phase boundary tracked using $\frac{\partial^2 x_d}{\partial T^2} = 0$, whereas the black dots show that tracked using $\frac{\partial^2 x_d}{\partial P^2} = 0$. It can be seen from Figure 5-13 that the phase boundaries tracked by the different criteria are identical. In Figure 5-13, we also draw an isobaric line at 100 bar (i.e., the black dashed line) and an isothermal line at 800 K (i.e., the blue dashed line). We can see from Figure 5-13 that the isothermal line crosses the VL/LA two-phase boundary once, whereas the isobaric line has two intersecting points with the VL/LA two-phase boundary. Therefore, we still recommend using $\frac{\partial^2 x_d}{\partial T^2} = 0$ when tracking the VL/LA and VL/LL phase boundaries as there is only one solution for $\frac{\partial^2 x_d}{\partial T^2} = 0$ in the *PT* phase diagrams but there could be multiple solutions for $\frac{\partial^2 x_d}{\partial P^2} = 0$.

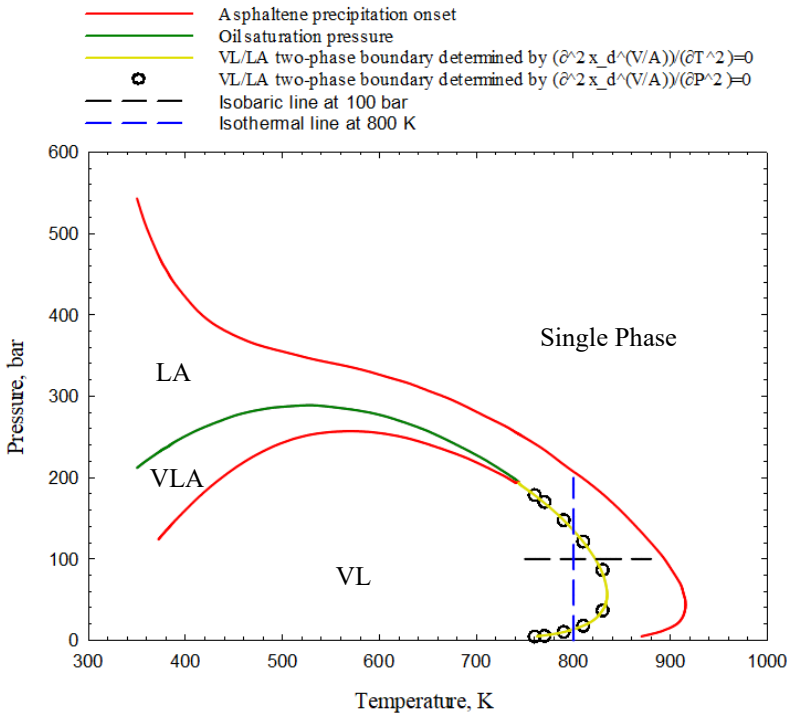

Fig. 5-13 Comparison of the *PT* phase diagrams of oil sample 1 generated by different criteria.

5.5 Conclusions

In this study, we first extend the trust-region-based three-phase VL_1L_2 equilibrium calculation algorithm proposed by Pan *et al.* (2019) to conduct three-phase VLA equilibrium calculations. The calculated phase boundaries are compared with the available experimental data to validate the accuracy of the calculation results. A novel phase boundary tracking method based on Brent's method (Brent, 1971) is then proposed to identify the VL/LL and VL/LA phase boundaries. *PT* and *Px* phase diagrams are generated to test the performances of the multiphase equilibrium calculation algorithm as well as the newly proposed phase boundary tracking method. The calculation results obtained by the three-phase VLA equilibrium calculation algorithm agree well with the experimental data, which proves that the trust-region-based multiphase equilibrium calculation algorithm proposed by Pan *et al.* (2019) can be extended to conduct three-phase VLA equilibrium calculations. The predicted VL/LA two-phase boundaries are smooth and continuous. The VL/LL two-phase

boundary intersects the VL_1L_2 three-phase region at the apex of the VL_1L_2 three-phase boundary, which indicates the continuation of the three-phase region (Bennett and Schmidt, 2017). The calculated VL/LL two-phase boundaries are also compared with those calculated using the thermal expansion coefficient method proposed by Bennett and Schmidt (2017). The comparison indicates that the calculated phase boundaries using the newly proposed phase boundary tracking method agree well with those calculated by Bennett and Schmidt (2017).

Acknowledgments

The authors greatly acknowledge the Discovery Grant from the Natural Sciences and Engineering Research Council of Canada (NSERC) (Grant No.: NSERC RGPIN-2020-04571) to H. Li. Z. Chen, L. Xu, and Y. Zhou greatly acknowledge the financial support provided by the China Scholarship Council (CSC) via three Ph.D. scholarships (No.: 201908180010, No. 201908420225, and No. 202008180027).

References

Angle, C.W., Long, Y., Hamza, H., Lue, L., 2006. Precipitation of asphaltenes from solvent-diluted heavy oil and thermodynamic properties of solvent-diluted heavy oil solutions. *Fuel* 85 (4), 492-506. https://doi.org/10.1016/j.fuel.2005.08.009

Asselineau, L., Bogdanic, G., Vidal, J., 1979. A versatile algorithm for calculating vapour—liquid equilibria. *Fluid Phase Equilibr.* 3 (4), 273-290. https://doi.org/10.1016/0378-3812(79)80002-3

Badamchi-Zadeh, A., Yarranton, H., Maini, B.B., Satyro, M., 2009a. Phase behaviour and physical property measurements for VAPEX solvents: part II. propane, carbon

dioxide and Athabasca bitumen. *J. Can. Pet. Technol.* 48 (03), 57-65. https://doi.org/10.2118/09-03-57

Badamchi-Zadeh, A., Yarranton, H., Svrcek, W., Maini, B., 2009b. Phase behaviour and physical property measurements for VAPEX solvents: Part I. Propane and Athabasca bitumen. *J. Can. Pet. Technol.* 48 (01), 54-61. https://doi.org/10.2118/09-01-54

Bennett, J., Schmidt, K.A., 2017. Comparison of phase identification methods used in oil industry flow simulations. *Energy Fuels* 31 (4), 3370-3379. https://doi.org/10.1021/acs.energyfuels.6b02316

Brent, R.P., 1971. An algorithm with guaranteed convergence for finding a zero of a function. *Comput. J.* 14 (4), 422-425. https://doi.org/10.1093/comjnl/14.4.422

Buenrostro-Gonzalez, E., Lira-Galeana, C., Gil-Villegas, A., Wu, J., 2004. Asphaltene precipitation in crude oils: Theory and experiments. *AIChE. J.* 50 (10), 2552-2570. https://doi.org/10.1002/aic.10243

Chang, Y.B., 1990. Development and application of an equation of state compositional simulator. Ph.D. thesis, the University of Texas at Austin. http://dx.doi.org/10.26153/tsw/7601

Chen, Z., Li, R., Li, H., 2021. An improved vapor-liquid-asphaltene three-phase equilibrium computation algorithm. *Fluid Phase Equilibr.* 537, 1-13. https://doi.org/10.1016/j.fluid.2021.113004

Chen, Z., Li, R., Li, H., 2022a. A new vapor-liquid-asphaltene three-phase equilibrium computation algorithm based on the free-asphaltene assumption. *Fluid Phase Equilibr.* 556, 1-14. https://doi.org/10.1016/j.fluid.2022.113392

Chen, Z., Zhou, Y., Li, H., 2022b. A review of phase behavior mechanisms of CO_2 EOR and storage in subsurface formations.*Ind. Eng. Chem. Res.* 61 (29), 10298-10318. https://doi.org/10.1021/acs.iecr.2c00204

Chueh, P., Prausnitz, J., 1967. Vapor-liquid equilibria at high pressures: Calculation of partial molar volumes in nonpolar liquid mixtures. *AIChE. J.* 13 (6), 1099-1107. https://doi.org/10.1002/aic.690130612

Creek, J.L., 2005. Freedom of action in the state of asphaltenes: Escape from conventional wisdom. *Energy Fuels* 19 (4), 1212-1224. https://doi.org/10.1021/ef049778m

Gosset, R., Heyen, G., Kalitventzeff, B., 1986. An efficient algorithm to solve cubic equations of state. *Fluid Phase Equilibr.* 25 (1), 51-64. https://doi.org/10.1016/0378-3812(86)85061-0

Jamaluddin, A., Creek, J., Kabir, C., McFadden, J., Cruz, D., Manakalathil, J., Joshi, N., Ross, B., 2002. Laboratory techniques to measure thermodynamic asphaltene instability. *J. Can. Pet. Technol.* 41 (07), 44-52. https://doi.org/10.2118/02-07-04

Khan, S., Pope, G., Sepehrnoori, K., 1992. Fluid characterization of three-phase CO_2/oil mixtures, Paper presented at the SPE/DOE Enhanced Oil Recovery Symposium, Tulsa, Oklahoma, April 1992. Paper Number: SPE-24130-MS. OnePetro. https://doi.org/10.2118/24130-MS

Li, C., 1971. Critical temperature estimation for simple mixtures. *Can. J. Chem. Eng.* 49 (5), 709-710. https://doi.org/10.1002/cjce.5450490529

Li, H., 2021. Multiphase equilibria of complex reservoir fluids. Springer.

Li, H., Yang, D., Li, X., 2013. Determination of three-phase boundaries of solvent (s)–CO_2–heavy oil systems under reservoir conditions. *Energy Fuels* 27 (1), 145-153. https://doi.org/10.1021/ef301549a

Li, R., Li, H., 2019. Robust three-phase vapor–liquid–asphaltene equilibrium calculation algorithm for isothermal CO_2 flooding applications. *Ind. Eng. Chem. Res.* 58 (34), 15666-15680. https://doi.org/10.1021/acs.iecr.9b02740

Li, Z., Firoozabadi, A., 2012. General strategy for stability testing and phase-split calculation in two and three phases. *SPE. J.* 17 (04), 1096-1107. https://doi.org/10.2118/129844-PA

Lu, C., Jin, Z., Li, H., Xu, L., 2021. Simple and robust algorithm for multiphase equilibrium computations at temperature and volume specifications. *SPE. J.* 26 (04), 2397-2416. https://doi.org/10.2118/205499-PA

Mohanty, K., Masino, W., Ma, T., Nash, L., 1995. Role of three-hydrocarbon-phase flow in a gas-displacement process. *SPE. Reserv. Eng.* 10 (03), 214-221. https://doi.org/10.2118/24115-PA

Neshat, S.S., Okuno, R., Pope, G.A., 2020. Simulation of solvent treatments for fluid blockage removal in tight formations using coupled three-phase flash and capillary pressure models. *J. Pet. Sci. Eng.* 195 (01), 1-43. https://doi.org/10.1016/j.petrol.2020.107442

Okuno, R., Johns, R.T., Sepehrnoori, K., 2011. Mechanisms for high displacement efficiency of low-temperature CO_2 floods. *SPE. J.* 16 (04), 751-767. https://doi.org/10.2118/129846-PA

Pan, H., Chen, Y., Sheffield, J., Chang, Y.B., Zhou, D., 2015. Phase-behavior modeling and flow simulation for low-temperature CO_2 injection. *SPE. Reserv. Eng.* 18 (02), 250-263. https://doi.org/10.2118/170903-PA

Pan, H., Connolly, M., Tchelepi, H., 2019. Multiphase equilibrium calculation framework for compositional simulation of CO_2 injection in low-temperature reservoirs. *Ind. Eng. Chem. Res.* 58 (5), 2052-2070. https://doi.org/10.1021/acs.iecr.8b05229

Pasad, G., Venkatarathnam, G., 1999. A method for avoiding trivial roots in isothermal flash calculations using cubic equations of state. *Ind. Eng. Chem. Res.* 38 (9), 3530-3534. https://doi.org/10.1021/ie980661t

Pasqualette, M.A., Carneiro, J.N., Johansen, S.T., Løvfall, B.T., Fonseca, R., Ciambelli, J.R., 2020. A numerical assessment of carbon-dioxide-rich two-phase flows with dense phases in offshore production pipelines. *SPE. J.* 25 (02), 712-731. https://doi.org/10.2118/199876-PA

Pedersen, K.S., Christensen, P.L., Shaikh, J.A., Christensen, P.L., 2006. Phase behavior of petroleum reservoir fluids. CRC press.

Peng, D.Y., Robinson, D.B., 1976. A new two-constant equation of state. *Ind. Eng. Chem. Fund.* 15 (1), 59-64. https://doi.org/10.1021/i160057a011

Perschke, D.R., 1988. Equation of state phase behavior modeling for compositional simulation. Ph.D. thesis, the University of Texas at Austin. http://dx.doi.org/10.26153/tsw/7567

Petitfrere, M., Nichita, D.V., 2014. Robust and efficient trust-region based stability analysis and multiphase flash calculations. *Fluid Phase Equilibr.* 362, 51-68. https://doi.org/10.1016/j.fluid.2013.08.039

Poling, B.E., Grens, E.A., Prausnitz, J.M., 1981. Thermodynamic properties from a cubic equation of state: avoiding trivial roots and spurious derivatives. *Ind. Eng. Chem. Process. Des. Dev.* 20 (1), 127-130. https://doi.org/10.1021/i200012a019

Punnapala, S., Vargas, F.M., 2013. Revisiting the PC-SAFT characterization procedure for an improved asphaltene precipitation prediction. *Fuel* 108, 417-429. https://doi.org/10.1016/j.fuel.2012.12.058

PVTsim, 2011. PVT sim 20.0, Calsep A/S: Copenhagen, Denmark.

Schlumberger, 2015. ECLIPSE: Reservoir simulation software, Technical Description, Version 2015.1. Schlumberger: Abingdon, U.K.

Simon, R., Rosman, A., Zana, E., 1978. Phase-behavior properties of CO_2-reservoir oil systems. *SPE. J.* 18 (01), 20-26. https://doi.org/10.2118/6387-PA

Xu, Z., Okuno, R., 2015. Numerical simulation of three-hydrocarbon-phase flow with robust phase identification, Paper presented at the SPE Reservoir Simulation Symposium, Houston, Texas, USA, February 2015. Paper Number: SPE-173202-MS. OnePetro. https://doi.org/SPE-173202-MS

Appendix of Chapter 5

Characterization Results of the Oil Samples Used in the Three-phase VLA Equilibrium Calculations

Oil samples 1 and 2 are shown to have asphaltene precipitation under certain pressure/temperature conditions. Tables A5-1 and A5-2 show the composition of oil samples 1 and 2, respectively. Oil sample 1 is a stock tank oil from the Middle East

region by Jamaluddin *et al.* (2002). The API gravity of this oil sample is 39° API (Jamaluddin *et al.*, 2002). The molecular weights of the oil sample and the C_{7+} fraction are 82.49 g/mol and 228.07 g/mol, respectively (Jamaluddin *et al.*, 2002), the density of the C_{7+} fraction is 0.865 g/cm^3 (Jamaluddin *et al.*, 2002). Oil sample 2 is a live oil sample from Mexico studied by Buenrostro - Gonzalez et al. (Buenrostro - Gonzalez *et al.*, 2004). The C_{7+} component of oil sample 2 has a molecular weight of 334.66 g/mol and a density of 0.8822 g/cm^3 (Buenrostro - Gonzalez *et al.*, 2004).

Table A5- 1 Composition of oil sample 1 (Jamaluddin *et al.*, 2002).

Component	Composition (mol%)
N_2	0.48
CO_2	0.92
C_1	43.43
C_2	11.02
C_3	6.55
i-C_4	0.79
n-C_4	3.70
i-C_5	1.28
n-C_5	2.25
C_6	2.70
C_{7+}	26.88

Table A5- 2 Composition of oil sample 2 (Buenrostro - Gonzalez *et al.*, 2004).

Component	Composition (mol%)
N_2	0.91
CO_2	1.57
H_2S	5.39
C_1	24.02
C_2	10.09
C_3	9.58
i-C_4	1.83
n-C_4	4.83
i-C_5	2.27
n-C_5	2.74
C_6	4.77
C_{7+}	32.00

The oil characterization method proposed by Pedersen *et al.* (2006) is applied in this study. The characterization results for oil samples 1 and 2 are shown in Tables A5-3 and A-4.

Table A5- 3 Characterization results of oil sample 1. The critical properties of the first nine components are taken from the literature (PVTsim, 2011).

Component	Composition (mol%)	T_c (K)	P_c (bar)	V_c (m^3/kmol)	ω	MW (g/mol)
N_2	0.481	126.200	33.94	89.80	0.040	28.014
CO_2	0.922	304.200	73.76	94.00	0.225	44.01
C_1	43.501	190.600	46.00	99.00	0.008	16.043
C_2	11.038	305.400	48.84	148.00	0.098	30.070
C_3	6.561	369.800	42.46	203.00	0.152	44.097
i-C_4	0.791	408.100	36.48	263.00	0.176	58.124
n-C_4	3.706	425.200	38.00	255.00	0.193	58.124
i-C_5	1.282	460.400	33.84	306.00	0.227	72.151
n-C_5	2.254	469.600	33.74	304.00	0.251	72.151
C_6	2.704	507.400	29.69	370.00	0.296	86.178
C_7	2.488	538.119	29.9	446.59	0.338	96.000
C_8	2.257	558.729	27.59	476.11	0.374	107.000
C_9	2.047	582.505	25.16	522.24	0.421	121.000
C_{10}-C_{12}	5.070	622.122	22.00	616.07	0.505	146.458
C_{13}-C_{14}	2.643	669.274	19.15	754.01	0.615	182.135
C_{15}-C_{17}	3.113	715.409	17.21	919.98	0.731	220.660
C_{18}-C_{20}	2.324	760.422	15.85	1102.36	0.846	262.221
C_{21}-C_{23}	1.734	802.703	14.91	1294.39	0.952	303.790
C_{24}-C_{27}	1.648	847.816	14.15	1518.93	1.058	350.513
C_{28}-C_{33}	1.530	910.362	13.39	1860.17	1.181	419.041
C_{34}-C_{42}	1.124	996.391	12.68	2376.67	1.275	519.014
C_{43}-C_{80}	0.692	1135.398	11.45	3547.56	1.020	721.267
C_{43}-C_{80} A	0.089	1423.076	15.48	3547.56	1.274	721.267

Table A5- 4 Characterization results of oil sample 2. The critical properties of the first ten components are taken from the literature (PVTsim, 2011).

Component	Composition (mol%)	T_c (K)	P_c (bar)	V_c (m^3/kmol)	ω	MW (g/mol)
N_2	0.937	126.200	33.94	89.80	0.040	28.014
CO_2	1.617	304.200	73.76	94.00	0.225	44.010
H_2S	5.551	373.200	89.37	98.50	0.100	34.080
C_1	24.740	190.600	46.00	99.00	0.008	16.043
C_2	10.392	305.400	48.84	148.00	0.098	30.070

C_3	9.867	369.800	42.46	203.00	0.152	44.097
iC_4	1.885	408.100	36.48	263.00	0.176	58.124
nC_4	4.975	425.200	38.00	255.00	0.193	58.124
iC_5	2.338	460.400	33.84	306.00	0.227	72.151
nC_5	2.822	469.600	33.74	304.00	0.251	72.151
C_6	4.913	507.400	29.69	370.00	0.296	86.178
C_7	1.312	538.851	30.10	433.59	0.338	96.000
C_8	1.257	559.155	27.69	468.83	0.374	107.000
C_9	1.204	582.660	25.20	519.71	0.421	121.000
C_{10}-C_{16}	7.128	662.330	19.62	751.15	0.603	173.920
C_{17}-C_{22}	4.619	766.814	15.47	1151.31	0.866	268.651
C_{23}-C_{28}	3.572	846.502	13.90	1530.00	1.059	350.742
C_{29}-C_{33}	2.350	915.931	13.02	1900.57	1.195	428.801
C_{34}-C_{40}	2.548	986.513	12.41	2310.52	1.273	511.604
C_{41}-C_{47}	1.888	1065.615	11.93	2800.55	1.268	609.604
C_{48}-C_{80}	3.610	1196.515	11.11	4070.84	0.717	837.328
C_{48}-C_{80} A	0.475	1679.781	11.90	4070.84	1.274	837.328

The model proposed by Chueh and Prausnitz (1967) is adopted in this study to calculate the BIPs,

$$k_{ij} = 1 - \left[\frac{2v_{ci}^{1/6}v_{cj}^{1/6}}{v_{ci}^{1/3}+v_{cj}^{1/3}}\right]^{\theta} \quad \text{(A-1)}$$

where k_{ij} is the BIP between components i and j, v_{ci} and v_{cj} are the critical volumes of components i and j, respectively, and subscripts i and j represent components i and j, respectively. θ is the exponent. In this study, the value of θ is set as 0.0001 when calculating the BIPs between hydrocarbon components, but it is tuned to be 0.1 when calculating the BIPs between the asphaltene component and other components. The BIPs used for oil samples 1 and 2 are listed in Tables A5-5 and A5-6, respectively. In Tables A5-5 and A5-6, the BIPs between N_2, H_2S, and the non-asphaltene components are taken from the literature (PVTsim, 2011).

Table A5- 5 BIPs used for oil sample 1 (PVTsim, 2011).

	N_2	CO_2	C_{43}-C_{80} A

N_2	0	-0.01700	0.08000
CO_2	-0.01700	0	0.10000
C_1	0.03110	0.12000	0.01668
C_2	0.05150	0.12000	0.01332
C_3	0.08520	0.12000	0.01090
i-C_4	0.10330	0.12000	0.00908
n-C_4	0.08000	0.12000	0.00929
i-C_5	0.09220	0.12000	0.00808
n-C_5	0.10000	0.12000	0.00813
C_6	0.08000	0.12000	0.00691
C_7	0.08000	0.10000	0.00583
C_8	0.08000	0.10000	0.00549
C_9	0.08000	0.10000	0.00500
C_{10}-C_{12}	0.08000	0.10000	0.00419
C_{13}-C_{14}	0.08000	0.10000	0.00329
C_{15}-C_{17}	0.08000	0.10000	0.00251
C_{18}-C_{20}	0.08000	0.10000	0.00188
C_{21}-C_{23}	0.08000	0.10000	0.00140
C_{24}-C_{27}	0.08000	0.10000	0.00100
C_{28}-C_{33}	0.08000	0.10000	0.00058
C_{34}-C_{42}	0.08000	0.10000	0.00022
C_{43}-C_{80}	0.08000	0.10000	0
C_{43}-C_{80} A	0.08000	0.10000	0

Table A5- 6 BIPs used for oil sample 2 (PVTsim, 2011).

	N_2	CO_2	H_2S	C_{43}-C_{80} A
N_2	0	-0.01700	0.17700	0.08000
CO_2	-0.01700	0	0.09700	0.10000
H_2S	0.17700	0.09700	0	0.06000
C_1	0.03100	0.07000	0.08000	0.01791
C_2	0.05200	0.07000	0.08300	0.01443
C_3	0.08500	0.07000	0.08800	0.01193
iC_4	0.10300	0.07000	0.04700	0.01003
nC_4	0.08000	0.07000	0.06000	0.01025
iC_5	0.09200	0.07000	0.06000	0.00899
nC_5	0.10000	0.07000	0.06000	0.00903
C_6	0.08000	0.07000	0.06000	0.00775
C_7	0.08000	0.07000	0.06000	0.00679
C_8	0.08000	0.07000	0.06000	0.00633
C_9	0.08000	0.07000	0.06000	0.00576
C_{10}-C_{16}	0.08000	0.07000	0.06000	0.00391
C_{17}-C_{22}	0.08000	0.07000	0.06000	0.00220
C_{23}-C_{28}	0.08000	0.07000	0.06000	0.00132

C_{29}-C_{33}	0.08000	0.07000	0.06000	0.00080
C_{34}-C_{40}	0.08000	0.07000	0.06000	0.00044
C_{41}-C_{47}	0.08000	0.07000	0.06000	0.00019
C_{48}-C_{80}	0.08000	0.07000	0.06000	0
C_{48}-C_{80} A	0.00568	0.00555	0.00542	0

CHAPTER 6 EFFECT OF WATER ON ASPHALTENE-PRECIPITATION BEHAVIOR OF CO_2-CRUDE OIL MIXTURES

A version of this chapter was submitted to *Applied Thermal Engineering* for possible publication on October 21, 2023

Abstract

The asphaltene phase can frequently appear in the CO_2 flooding process due to condition changes and compositional changes in reservoir fluids. The precipitation of asphaltene can become a significant issue since it can cause formation damage and tubing plugging, and, therefore, affect the CO_2 EOR efficiency and CO_2 storage capacity in reservoirs. Meanwhile, water can extensively exist in reservoirs. Since the solubility of CO_2 in water is not negligible under reservoir conditions, the aqueous phase should also be considered during the phase-behavior simulations of the CO_2 flooding process. With the presence of an asphaltene phase and an aqueous phase, four phases (i.e., a vapor phase, a hydrocarbon phase, an asphaltene phase, and an aqueous phase) can coexist at a given thermodynamic equilibrium. In this study, a robust and efficient four-phase vapor-liquid-liquid-aqueous equilibrium calculation algorithm is applied to conduct four-phase vapor-liquid-asphaltene-aqueous equilibrium calculations by assuming asphaltene is a dense liquid phase. The algorithm is first validated by comparing the calculated asphaltene precipitation data with the presence of water against the experimental asphaltene precipitation data documented in the literature. The validation shows that the calculation results agree well with the experimental data, indicating that such algorithm can make reliable predictions of asphaltene precipitation with the presence of water. The validated algorithm is subsequently used to construct pressure-temperature (*PT*) and pressure-composition (*Px*) phase diagrams to study the effect of water on asphaltene precipitation under different pressure/temperature conditions and under the injection of CO_2. We can conclude from the calculated results that although adding water to the reservoir fluid can cause obvious changes in the *PT* phase diagrams, it does not have a noticeable influence on the asphaltene precipitation onsets. However, it can be seen from the

calculated *Px* phase diagrams that the presence of water during the CO_2 flooding process can make asphaltene precipitated more easily. The maximum amount of asphaltene precipitation is decreased by the presence of water due to the fact that a considerable amount of CO_2 is dissolved in the aqueous phase instead of the liquid hydrocarbon phase.

6.1.Introduction

CCUS, which stands for carbon capture, utilization and storage, is an important modern technology that can help mitigate the negative impacts of greenhouse gas emissions on the environment and climate change [1]. CO_2 flooding is a well-established enhanced oil recovery (EOR) technique and has the added benefit of storing the injected CO_2 in the reservoir, which makes it a practical CCUS process [2]. During such a process, CO_2 can be trapped in the reservoir by a variety of mechanisms, including dissolution in oil, solidification onto mineral surfaces, and trapping in the pore spaces [1, 2]. The CO_2 flooding and storage process can be complicated by the phase changes that occur in the reservoir [2]. In addition to the commonly seen vapor phase and liquid phase, other phases can also be present during the CO_2 flooding process. Asphaltene phase is one of the commonly seen third phases that can possibly appear. Asphaltenes are generally defined as the heaviest and most polar components in crude oil, which are insoluble in n-pentane or n-heptane but soluble in aromatic solvents, such as toluene [3-5]. The presence of the asphaltene phase can lead to tubing plugging and formation damage issues, and therefore has become one of the major concerns during the CCUS process [6-8]. Besides, during the CO_2 flooding process, water will be injected into reservoirs for oil recovery and pressure maintenance. If an asphaltene phase and an aqueous phase are present, we can have four phases (i.e., a vapor phase, a hydrocarbon phase, an asphaltene phase, and an aqueous phase) at a given thermodynamic equilibrium.

Asphaltene-inclusive phase behavior models have been a subject of intense research over the past three decades, and two main approaches have been developed: colloidal theory and solubility theory [9]. The colloidal theory assumes that asphaltenes are solid particles stabilized by resins adsorbed on the surface, while the solubility theory assumes that asphaltenes are dissolved in crude oil [10, 11]. Colloidal theory has been

successful in predicting asphaltene precipitation conditions in many cases [12-15], but it has been criticized for assuming polar-polar interactions between asphaltenes and resins, which may not always be appropriate [16-19]. On the other hand, solubility theory has gained popularity in recent years, particularly for its ability to predict asphaltene precipitation using liquid-liquid or solid-liquid equilibria [10]. Regular solution theory and equations of state (EOS) are the two main approaches used in solubility-theory-based asphaltene precipitation models [8]. Regular solution theories [20-24] have been applied by several researchers to predict the onset conditions of asphaltene precipitation [25-35]. However, their accuracy can be compromised when a vapor phase appears [9, 36]. EOS-based models have been particularly useful in accounting for the influences of temperature, pressure, and compositions on phase equilibria, making them suitable for performing vapor-liquid-asphaltene three-phase equilibrium calculations. Therefore, EOS-based models have become popular for predicting asphaltene precipitation behavior.

There are also thermodynamic models that are proposed to capture the phase behavior of water- hydrocarbon mixtures in reservoirs. Among them, the models based on the free-water assumption are one of the most commonly used, in which the aqueous phase is considered as a pure phase that only contains water [37] . The validity of the free-water assumption is backed by the observation that the solubility of hydrocarbon in a water-rich phase is typically around 10^{-4}, which is much lower compared to the solubility of water in a hydrocarbon-rich phase [38]. By using the free-water assumption, the flash calculation algorithm can be greatly simplified. However, it is worth noting that the free-water assumption is no longer valid during the CO_2 flooding process since the solubility of CO_2 is nonnegligible in the aqueous phase under high-

pressure circumstances, and full flash calculations are therefore required to determine the phase behavior of reservoir fluids [39].

Although many efforts have been made to develop three-phase vapor-liquid-asphaltene (VLS) and vapor-liquid-aqueous (VLA) equilibrium calculation algorithms, the effect of water on asphaltene precipitation is still unclear. In 1999, Srivastava *et al.* [40] experimentally investigated the effect of water on the amount of asphaltene precipitation. Their results show that the asphaltene precipitation amount will slightly decrease when water appears [40]. However, the effect of water presence on the asphaltene precipitation onsets is still not clear. Besides, only limited data points are presented to demonstrate the influence of water presence on asphaltene precipitation amount. In order to understand the overall impact of water presence on asphaltene precipitation, we must have a unified thermodynamic model that can be used to perform comprehensive phase-behavior simulations of asphaltene-inclusive fluid mixtures.

In this study, by assuming the asphaltene phase as a high-dense liquid phase, a trust-region-based four-phase equilibrium calculation algorithm is adopted to conduct four-phase vapor-liquid-aqueous-asphaltene (VLAS) equilibrium calculations to study the effect of water on asphaltene precipitation. The algorithm is first validated by the experimental data documented in the literature. The validated algorithm is then applied to generate pressure-temperature (*PT*) and pressure-composition (*Px*) phase diagrams to study the effect of water on asphaltene precipitation onsets under different pressure/temperature/gas-injection conditions. The effect of water on the asphaltene precipitation amount is also investigated using the validated algorithm.

6.2.Mathematical Formulations

6.2.1. Stability test

Stability test is used to determine if a mixture with a feed *Z* will split into two or more phases. Michelsen [41] proposed an efficient algorithm to conduct the stability test by using a tangent-plane distance (TPD) function. The TPD function is given by [41]:

$$TPD(X) = 1 + \sum_{i=1}^{nc} X_i \left[ln\varphi_i(X) + ln(X_i) - ln(z_i) - ln\,\varphi_i(z) - 1\right], i = 1,2,\cdots,n_c \quad (1)$$

where *X* and *z* represent the compositions of the trial phase and the feed, respectively. The subscript i is the component index. $\varphi_i(X)$ and $\varphi_i(z)$ represent the fugacity coefficients of component i in the trial phase and the feed, respectively. n_c is the number of components in the fluid mixture. K_i is the equilibrium ratio of component *i*. Multiple initial K-value estimations [42-44] are applied in this study to ensure the robustness of the algorithm. In addition, the modified trust-region-based algorithm developed by Li *et al.* [45] is used to conduct stability test

6.2.2. Flash Calculations

Flash calculations are conducted to calculate the compositions and phase fractions of individual phases. The convergence of flash calculations will be reached when the equal-fugacity constraint and material balance constraint are satisfied. The equal-fugacity constraint for the four-phase flash calculations can be expressed as:

$$f_{iV} = f_{iL} = f_{iS} = f_{iA} =, i = 1, \ldots, nc \quad (2)$$

where f is fugacity and i is the component index. The subscripts *V*, *L*, *S* and *A* represent the vapor phase, liquid hydrocarbon phase, asphaltene phase, and aqueous phase,

respectively. In this study, the fugacity of different phases is calculated by Peng-Robinson EOS (PR EOS) [46].

By taking the liquid phase as the reference phase, the equilibrium ratios (K) can be defined as [45]:

$$K_{iV} = \frac{V_i}{L_i}, i = 1, \dots, nc \quad (3)$$

$$K_{iS} = \frac{S_i}{L_i}, i = 1, \dots, nc \quad (4)$$

$$K_{iA} = \frac{A_i}{L_i}, i = 1, \dots, nc \quad (5)$$

where V_i, L_i, S_i, A_i, represent the molar fractions of component i in the vapor phase, liquid phase, asphaltene phase, and aqueous phase, respectively. The following material-balance equations need to be satisfied [45]:

$$\sum_{i=1}^{n} V_i = 1 \quad (6)$$

$$\sum_{i=1}^{n} L_i = 1 \quad (7)$$

$$\sum_{i=1}^{n} S_i = 1 \quad (8)$$

$$\sum_{i=1}^{n} A_i = 1 \quad (9)$$

$$\beta_V V_i + \beta_L L_i + \beta_S S_i + \beta_A A_i = Z_i, i = 1, \dots, nc \quad (10)$$

$$\beta_V + \beta_L + \beta_S + \beta_A = 1 \quad (11)$$

where β_V, β_L, β_S, and β_A represent the phase fractions of the vapor phase, liquid phase, asphaltene phase, and aqueous phase, respectively. The Rachford–Rice (RR) equations [47] that are derived based on the material-balance constraints can be then expressed as [45]:

$$RR^V = (V_i - L_i) = \frac{Z_i(K_{iV}-1)}{1+(K_{iV}-1)\beta_V+(K_{iS}-1)\beta_S+(K_{iA}-1)\beta_A} = 0 \quad (12)$$

$$RR^S = (S_i - L_i) = \frac{Z_i(K_{iS}-1)}{1+(K_{iV}-1)\beta_v+(K_{iS}-1)\beta_S+(K_{iA}-1)\beta_A} = 0 \quad (13)$$

$$RR^A = (A_i - L_i) = \frac{Z_i\,(K_{iA}-1)}{1+(K_{iV}-1)\beta_v+(K_{iS}-1)\beta_S+(K_{iA}-1)\beta_A} = 0 \quad (14)$$

Multiple methods have been applied to solve β and K. Successive substitution iteration (SSI) is the conventional method that could be used to solve β and K, but it is linearly convergent for nonideal mixtures [48-50]. Therefore, Pan *et al.* [44] proposed to use the SSI method to provide an initial estimate of equilibrium ratios for higher-order methods (e.g., Newton's method and trust-region method) to achieve the final convergence. This approach is adopted by Li *et al.* [39] to develop a four-phase VLLA equilibrium calculation algorithm. The modified trust-region-based algorithm developed by Li *et al.* [45] is applied in this study to conduct four-phase VLAS equilibrium calculations. The detailed structures and features of the four-phase VLAS equilibrium calculation algorithm can be found in [45].

6.3.Results and Discussion

In this section, the four-phase VLAS equilibrium calculation algorithm is first validated by comparing the calculation results of the asphaltene precipitation amount of two oil samples under CO_2 injection with and without the presence of water. The validated algorithm is then applied to generate *PT* and *Px* phase diagrams of these two oil samples. The effect of water on asphaltene precipitation is studied by predicting asphaltene precipitation amount under different working conditions.

6.3.1. Oil Characterization

6.3.1.1. Oil sample 1

Oil sample 1 is named as fluid W1 by Srivastava *et al.* [40], which is collected from the Weyburn reservoir located in Saskatchewan, Canada. Oil sample 1 has a gravity of 36°API and asphaltene content of 4 wt% [40]. The composition of oil sample 1 is shown in Table 6-1. In this study, we first tune the characterization results based on the experimentally measured asphaltene precipitation amount without the presence of water. The characterized oil samples are used to perform four-phase VLAS equilibrium calculations and predict the asphaltene precipitation amount with the presence of water. The prediction results are compared with the experimental data to validate the accuracy of the four-phase VLAS equilibrium calculation algorithm.

The oil characterization approach developed by Pedersen *et al.* [11] is applied in this study. In Pedersen *et al*.'s method [11], any pseudo-component with a weight greater than C_{49} is divided into two parts: the asphaltene component and the non-asphaltene component. The critical temperature (T_c), critical pressure (P_c), and acentric factor (ω) of the non-asphaltene component can be computed using the following equations [11]:

$$T_{ci} = z_{i\,NA} T_{ci\,NA} + z_{i\,A} T_{ci\,A} \quad (15)$$

$$\frac{1}{P_{ci}} = \frac{(z_{i\,NA})^2}{P_{ci\,NA}} + \frac{(z_{i\,A})^2}{P_{ci\,A}} + \frac{2 \times z_{i\,NA} \times z_{i\,A}}{\sqrt{P_{ci\,NA} * P_{ci\,A}}} \quad (16)$$

$$\omega_i = z_{i\,NA} \omega_{i\,NA} + z_{i\,A} \omega_{i\,A} \quad (17)$$

where $z_{i\,NA}$ and $z_{i\,A}$ are the molar fractions of the non-asphaltene component and the asphaltene component, respectively. The subscripts *A* and *NA* represent the asphaltene component and the non-asphaltene component, respectively. The default values of the

critical temperature, critical pressure, and acentric factor of the asphaltene component are set as 1398.5 K, 14.95 bar, and 1.274 [11]. As recommended by Pedersen *et al*. [11], the critical properties of the asphaltene component and the binary interaction parameters (BIPs) can be tuned to better match the experimental data. For oil sample 1, the critical temperature and critical pressure of the asphaltene component are tuned to be 1125.35 K and 15.30 bar, respectively. The model developed by Chueh and Prausnitz [51] is applied to calculate the BIPs:

$$k_{ij} = 1 - \left[\frac{2v_{ci}^{1/6}v_{cj}^{1/6}}{v_{ci}^{1/3}+v_{cj}^{1/3}}\right]^{\theta} \quad (18)$$

where k_{ij} denotes the BIP between component i and component j, v_{ci} and v_{cj} represent the critical volumes of component i and component j, respectively. θ is the exponent and can be tuned based on experimental data. In this study, we have assigned the value of 0.0001 to the exponent θ while computing the BIPs among hydrocarbon components, and the value of 0.1 between the asphaltene component and the other components to match the experimental data. The oil characterization results and the BIPs used for oil sample 1 are shown in Table 6-2 and Table 6-3, respectively. In Table 6-3, the BIPs between N_2 and the non-asphaltene components are sourced from the literature [52].

Table 6-1 Composition of oil sample 1 [40].

Component	Composition (mol%)
N_2	0.96
CO_2	0.58
H_2S	0.30
C_1	4.49
C_2	2.99
C_3	4.75
i-C_4	0.81
n-C_4	1.92
i-C_5	1.27
n-C_5	2.19
C_{6+}	79.74

Table 6-2 Characterization results of oil sample 1.

Component	Composition (mol%)	T_c (K)	P_c (bar)	V_c (m^3/kmol)	ω	MW (g/mol)
N_2	0.9600	126.20	33.94	89.80	0.04	28.01
CO_2	0.5800	304.20	73.76	94.00	0.22	44.01
H_2S	0.3000	373.20	89.37	98.50	0.10	34.08
C_1	4.4900	190.60	46.00	99.00	0.01	16.04
C_2	2.9900	305.40	48.84	148.00	0.10	30.07
C_3	4.7500	369.80	42.46	203.00	0.15	44.10
i-C_4	0.8100	408.10	36.48	263.00	0.18	58.12
n-C_4	1.9200	425.20	38.00	255.00	0.19	58.12
i-C_5	1.2700	460.40	33.84	306.00	0.23	72.15
n-C_5	2.1900	469.60	33.74	304.00	0.25	72.15
C_6	2.4167	507.40	29.69	370.00	0.30	86.18
C_7	8.3659	540.78	30.62	399.40	0.34	96.00
C_8	7.4610	561.55	28.28	427.91	0.37	107.00
C_9	6.6539	585.47	25.82	474.10	0.42	121.00
C_{10}-C_{11}	11.2264	615.57	23.30	542.80	0.48	140.13
C_{12}-C_{13}	8.9290	653.95	20.73	650.04	0.56	167.60
C_{14}-C_{16}	10.0874	700.76	18.45	811.95	0.67	204.78
C_{17}-C_{18}	5.0374	744.14	16.89	985.01	0.77	243.60
C_{19}-C_{21}	5.6910	778.00	16.02	1134.96	0.84	275.27
C_{22}-C_{24}	4.0367	819.71	15.15	1338.23	0.93	317.01
C_{25}-C_{29}	4.2932	870.73	14.37	1612.36	1.02	370.34
C_{30}-C_{37}	3.0492	906.25	13.42	2073.29	1.12	456.70
C_{38}-C_{80}	1.3572	928.85	11.44	3187.62	1.01	639.01
Asphaltene	1.1348	1125.35	14.95	2908.49	1.16	593.34

Table 6-3 BIPs used for oil sample 1.

	N_2	CO_2	H_2S	A
N_2	0	-0.017	0.177	0.080
CO_2	-0.017	0	0.097	0.310
H_2S	0.177	0.097	0	0.000
C_1	0.031	0.120	0.080	0.015
C_2	0.052	0.120	0.083	0.012
C_3	0.085	0.120	0.088	0.009
i-C_4	0.103	0.120	0.047	0.008
n-C_4	0.080	0.120	0.060	0.008
i-C_5	0.092	0.120	0.060	0.007
n-C_5	0.100	0.120	0.063	0.007
C_6	0.080	0.120	0.050	0.006
C_7	0.080	0.100	0	0.005

C_8	0.080	0.100	0	0.005
C_9	0.080	0.100	0	0.004
C_{10}-C_{11}	0.080	0.100	0	0.004
C_{12}-C_{13}	0.080	0.100	0	0.003
C_{14}-C_{16}	0.080	0.100	0	0.002
C_{17}-C_{18}	0.080	0.100	0	0.002
C_{19}-C_{21}	0.080	0.100	0	0.001
C_{22}-C_{24}	0.080	0.100	0	0.001
C_{25}-C_{29}	0.080	0.100	0	0
C_{30}-C_{37}	0.080	0.100	0	0
C_{38}-C_{80}	0.080	0.100	0	0
Asphaltene	0.080	0.310	0	0

As reported by Srivastava *et al*. [40], the brine/oil volume ratio used in the experiments is 3:7. The density of oil sample 1 is 0.8461 g/cm^3 at 59 ℃, and the molecular weight of oil sample 1 is 230 g/mol. In this study, the density of brine is estimated as 1g/cm^3 and the molecular weight of brine is set as 18.02 g/mol. The composition and properties of oil sample 1 after adding water are shown in Table 6-4.

Table 6-4 The composition and properties of oil sample 1 after adding water.

Component	Composition (mol%)	T_c (K)	P_c (bar)	V_c (m^3/kmol)	ω	MW (g/mol)
H_2O	86.2000	647.30	220.89	56.00	0.34	18.02
N_2	0.1325	126.20	33.94	89.80	0.04	28.01
CO_2	0.0800	304.20	73.76	94.00	0.22	44.01
H_2S	0.0414	373.20	89.37	98.50	0.10	34.08
C_1	0.6196	190.60	46.00	99.00	0.01	16.04
C_2	0.4126	305.40	48.84	148.00	0.10	30.07
C_3	0.6555	369.80	42.46	203.00	0.15	44.10
i-C_4	0.1118	408.10	36.48	263.00	0.18	58.12
n-C_4	0.2650	425.20	38.00	255.00	0.19	58.12
i-C_5	0.1753	460.40	33.84	306.00	0.23	72.15
n-C_5	0.3022	469.60	33.74	304.00	0.25	72.15
C_6	0.3335	507.40	29.69	370.00	0.30	86.18
C_7	1.1545	540.78	30.62	399.40	0.34	96.00
C_8	1.0296	561.55	28.28	427.91	0.37	107.00
C_9	0.9182	585.47	25.82	474.10	0.42	121.00
C_{10}-C_{11}	1.5492	615.57	23.30	542.80	0.48	140.13
C_{12}-C_{13}	1.2322	653.95	20.73	650.04	0.56	167.60

C_{14}-C_{16}	1.3921	700.76	18.45	811.95	0.67	204.78
C_{17}-C_{18}	0.6952	744.14	16.89	985.01	0.77	243.60
C_{19}-C_{21}	0.7854	778.00	16.02	1134.96	0.84	275.27
C_{22}-C_{24}	0.5571	819.71	15.15	1338.23	0.93	317.01
C_{25}-C_{29}	0.5925	870.73	14.37	1612.36	1.02	370.34
C_{30}-C_{37}	0.4208	906.25	13.42	2073.29	1.12	456.70
C_{38}-C_{80}	0.1873	928.85	11.44	3187.62	1.01	639.01
Asphaltene	0.1566	1125.35	14.95	2908.49	1.16	593.34

6.3.1.2. Oil Sample 2

Oil sample 2 is named as fluid W3 by Srivastava *et al*. [40], which is also obtained from the Weyburn reservoir. Oil sample 2 has the API gravity of 31° and an asphaltene content of 4.9 wt% [40]. Table 6-5 shows the composition of oil sample 2. The method proposed by Pedersen *et al*. [11] is also applied to characterize oil sample 2, and the characterization results are shown in Table 6-6. The critical temperature, critical pressure, and acentric factor of the asphaltene component are tuned to be 1398.50 K, 12.20 bar and 1.16 for oil sample 2. The BIPs used for oil sample 2 are shown in Table 6-7.

Table 6-5 Composition of oil sample 2 [40].

Component	Composition (mol%)
N_2	2.07
CO_2	0.74
H_2S	0.12
C_1	7.49
C_2	4.22
C_3	7.85
i-C_4	1.58
n-C_4	4.97
i-C_5	2.01
n-C_5	2.58
C_{6+}	66.37

Table 6-6 Characterization results of oil sample 2.

Component	Composition (mol%)	T_c (K)	P_c (bar)	V_c (m^3/kmol)	ω	MW (g/mol)
N_2	2.0700	126.20	33.94	89.80	0.04	28.01
CO_2	0.7400	304.20	73.76	94.00	0.23	44.01
H_2S	0.1200	373.20	89.37	98.50	0.10	34.08
C_1	7.4900	190.60	46.00	99.00	0.01	16.04
C_2	4.2200	305.40	48.84	148.00	0.10	30.07
C_3	7.8500	369.80	42.46	203.00	0.15	44.10
i-C_4	1.5800	408.10	36.48	263.00	0.18	58.12
n-C_4	4.9700	425.20	38.00	255.00	0.19	58.12
i-C_5	2.0100	460.40	33.84	306.00	0.23	72.15
n-C_5	2.5800	469.60	33.74	304.00	0.25	72.15
C_6	2.1894	507.40	29.69	370.00	0.30	86.18
C_7	6.4072	540.05	30.43	412.25	0.34	96.00
C_8	5.7678	560.75	28.09	441.58	0.37	107.00
C_9	5.1923	584.60	25.63	488.18	0.42	121.00
C_{10}-C_{12}	12.6697	624.25	22.44	583.23	0.50	146.39
C_{13}-C_{14}	6.4794	671.59	19.54	724.32	0.61	182.11
C_{15}-C_{16}	5.2508	709.40	17.86	861.12	0.69	213.58
C_{17}-C_{19}	6.0698	749.42	16.55	1023.90	0.78	249.42
C_{20}-C_{22}	4.4280	790.99	15.53	1211.06	0.87	289.28
C_{23}-C_{26}	4.0997	837.29	14.67	1442.05	0.97	336.46
C_{27}-C_{31}	3.2063	895.20	13.89	1760.00	1.06	399.07
C_{32}-C_{39}	2.2805	904.14	12.93	2217.87	1.14	485.36
C_{40}-C_{80}	1.3229	1007.03	11.32	3358.57	0.96	674.48
Asphaltene	1.0063	1398.50	12.20	2954.54	1.16	607.50

Table 6-7 BIPs used for oil sample 2.

	N_2	CO_2	H_2S	A
N_2	0	-0.017	0.177	0.080
CO_2	-0.017	0	0.097	0.200
H_2S	0.177	0.097	0	0.000
C_1	0.031	0.120	0.080	0.015
C_2	0.052	0.120	0.083	0.012
C_3	0.085	0.120	0.088	0.010
i-C_4	0.103	0.120	0.047	0.008
n-C_4	0.080	0.120	0.060	0.008
i-C_5	0.092	0.120	0.060	0.007
n-C_5	0.100	0.120	0.063	0.007
C_6	0.080	0.120	0.050	0.006
C_7	0.080	0.100	0	0.005

C_8	0.080	0.100	0	0.005
C_9	0.080	0.100	0	0.004
C_{10}-C_{12}	0.080	0.100	0	0.004
C_{13}-C_{14}	0.080	0.100	0	0.003
C_{15}-C_{16}	0.080	0.100	0	0.002
C_{17}-C_{19}	0.080	0.100	0	0.002
C_{20}-C_{22}	0.080	0.100	0	0.001
C_{23}-C_{26}	0.080	0.100	0	0.001
C_{27}-C_{31}	0.080	0.100	0	0
C_{32}-C_{39}	0.080	0.100	0	0
C_{40}-C_{80}	0.080	0.100	0	0
Asphaltene	0.080	0.200	0	0

Similarly, the brine/oil volume ratio is also set as 3:7 during the experiments conducted by Srivastava *et al*. [40]. The density of oil sample 2 is 0.8394 g/cm^3 at 63 ℃, and the molecular weight of oil sample 2 is 215 g/mol. By assuming the density of brine as 1 g/cm^3 and the molecular weight of brine as 18.02 g/mol, we can calculate the mole fraction of water to be 85.64%. Table 6-8 shows the composition and properties of oil sample 2 after the addition of water.

Table 6-8 The composition and properties of oil sample 2 after adding water.

Component	Composition (mol%)	T_c (K)	P_c (bar)	V_c (m^3/kmol)	ω	MW (g/mol)
H_2O	85.6400	647.30	220.89	56.00	0.34	18.02
N_2	0.2973	126.20	33.94	89.80	0.04	28.01
CO_2	0.1063	304.20	73.76	94.00	0.22	44.01
H_2S	0.0172	373.20	89.37	98.50	0.10	34.08
C_1	1.0756	190.60	46.00	99.00	0.01	16.04
C_2	0.6060	305.40	48.84	148.00	0.10	30.07
C_3	1.1273	369.80	42.46	203.00	0.15	44.10
i-C_4	0.2269	408.10	36.48	263.00	0.18	58.12
n-C_4	0.7137	425.20	38.00	255.00	0.19	58.12
i-C_5	0.2886	460.40	33.84	306.00	0.23	72.15
n-C_5	0.3705	469.60	33.74	304.00	0.25	72.15
C_6	0.3144	507.40	29.69	370.00	0.30	86.18
C_7	0.9201	540.78	30.62	399.40	0.34	96.00
C_8	0.8283	561.55	28.28	427.91	0.37	107.00
C_9	0.7456	585.47	25.82	474.10	0.42	121.00
C_{10}-C_{11}	1.8194	615.57	23.30	542.80	0.48	140.13

C_{12}-C_{13}	0.9304	653.95	20.73	650.04	0.56	167.60
C_{14}-C_{16}	0.7540	700.76	18.45	811.95	0.67	204.78
C_{17}-C_{18}	0.8716	744.14	16.89	985.01	0.77	243.60
C_{19}-C_{21}	0.6359	778.00	16.02	1134.96	0.84	275.27
C_{22}-C_{24}	0.5887	819.71	15.15	1338.23	0.93	317.01
C_{25}-C_{29}	0.4604	870.73	14.37	1612.36	1.02	370.34
C_{30}-C_{37}	0.3275	906.25	13.42	2073.29	1.12	456.70
C_{38}-C_{80}	0.1900	928.85	11.44	3187.62	1.01	639.01
Asphaltene	0.1445	1125.35	14.95	2908.49	1.16	593.34

6.3.2. Validation of the Four-Phase VLAS Equilibrium Calculation Algorithm

Figure 6-1 shows the comparison between the calculated asphaltene precipitation amount of oil samples 1 and 2 without the presence of water and the ones measured by Srivastava *et al.* [40]. It can be seen from Figure 6-1 that the calculation results agree reasonably well with the experimental data, which proves that the oil characterization results of the two oil samples are reliable.

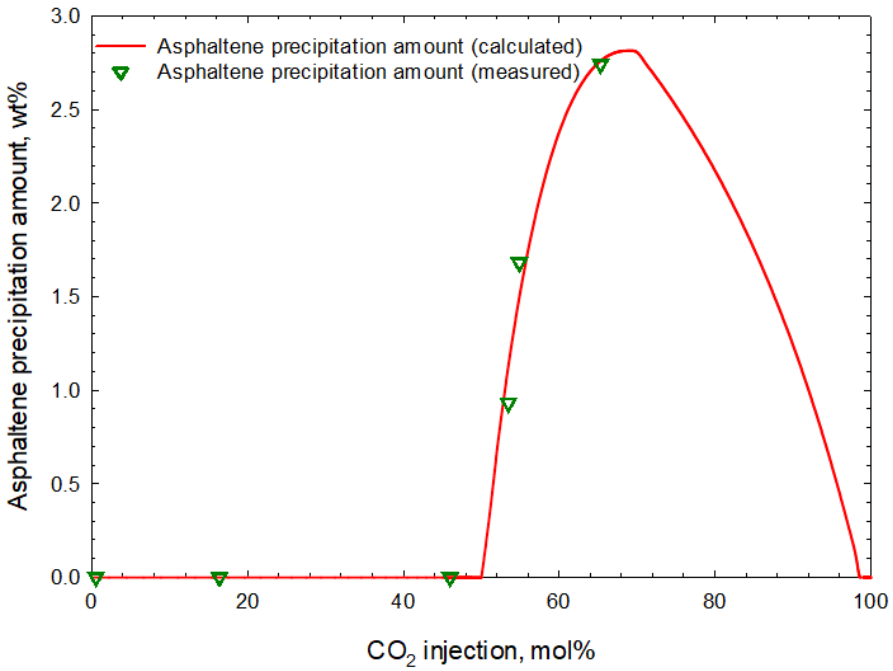

(a)

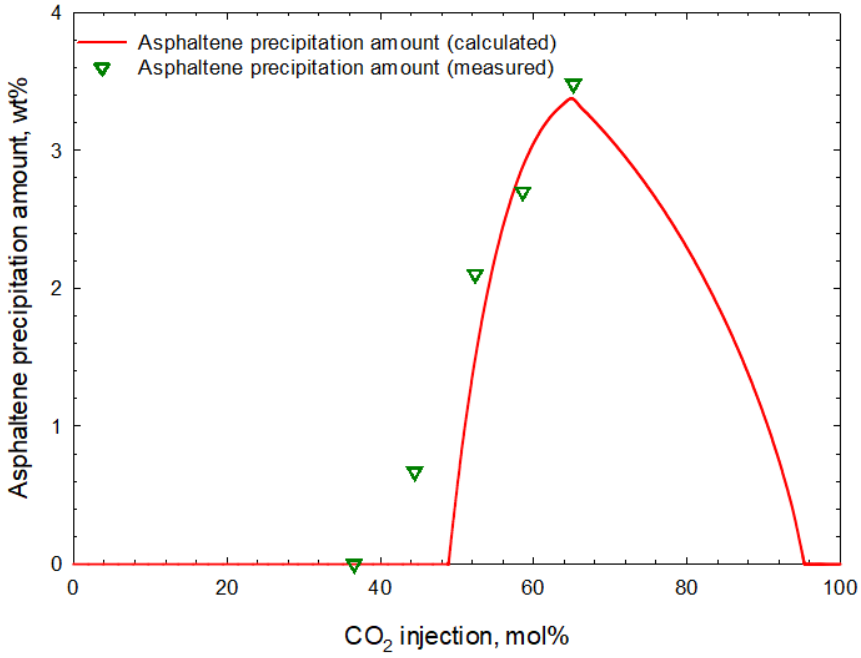

(b)

Fig. 6-1 Comparison between the calculated asphaltene precipitation amount without water and the experimental data: (a) Oil sample 1; (b) Oil sample 2.

The characterized oil samples are subsequently used to predict the asphaltene precipitation amount of oil samples 1 and 2 with the presence of water, and the comparison between the calculated results and the experimental data is presented in Figure 6-2. Good agreement can be seen between the calculated asphaltene precipitation amount and the experimental data for both oil samples, which validates the accuracy of the four-phase VLAS equilibrium calculation algorithm.

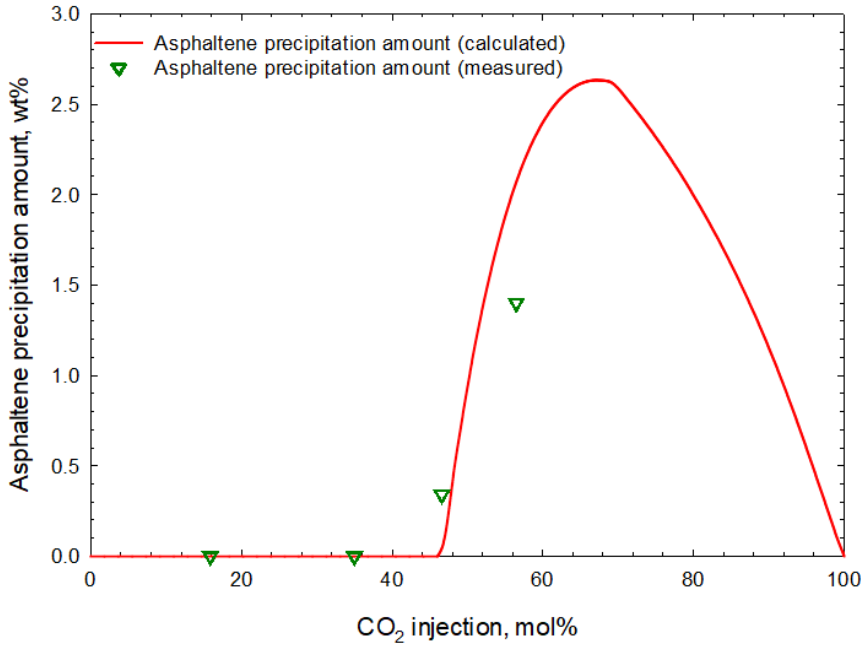

(a)

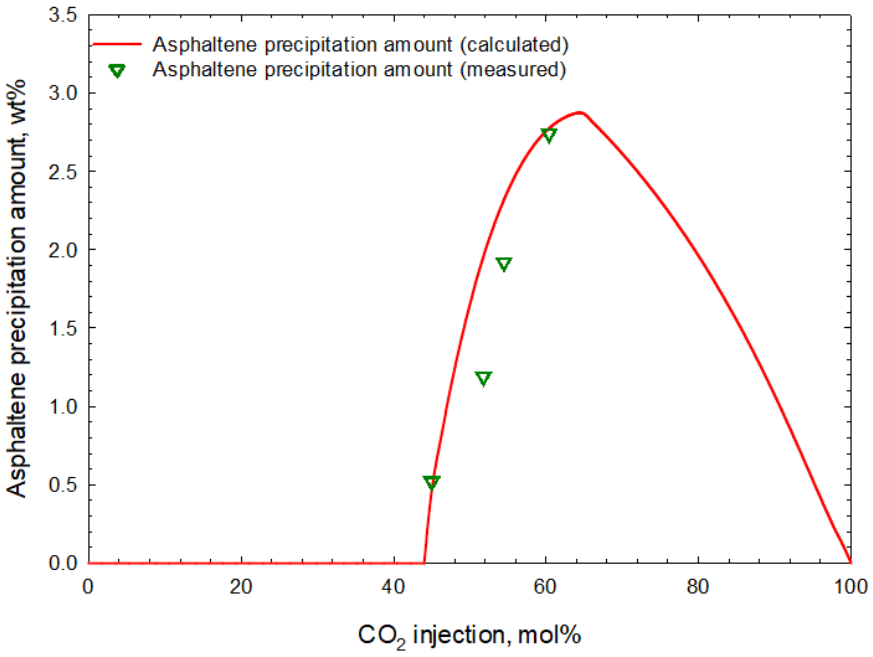

(b)

Fig. 6-2 Comparison between the calculated asphaltene precipitation amount with the presence of water and the experimental data: (a) Oil sample 1 with 86.2 mol% water; (b) Oil sample 2 with 85.64 mol% water.

6.3.3. Effect of Water on Asphaltene Precipitation During the CO_2 Flooding Process

In this part, the tuned fluid models are used to conduct a series of calculations to investigate the effect of water on asphaltene precipitation under different pressure/temperature/gas-injection conditions. Figure 6-3 shows the comparison between the calculated asphaltene precipitation amount with and without water under CO_2 injection conditions. In Figure 6-3, the dashed line represents the asphaltene precipitation amount without water, while the solid line shows the asphaltene precipitation amount with water. It can be observed from Figure 6-3 that the asphaltene precipitation amount of the two oil samples first increases with the increasing amount of CO_2 injection, reaching its maximum value at saturation pressure, and then decreases. It can be also concluded from Figure 6-3 that the maximum asphaltene-precipitation amount of oil samples 1 and 2 is decreased due to the presence of water. This can be attributed to the fact that a considerable amount of CO_2 is dissolved in the aqueous phase instead of the liquid phase. Since the gaseous components, like CO_2, are generally poor solvents for asphaltene, a lower CO_2 concentration in the liquid phase will lead to a lower asphaltene precipitation amount.

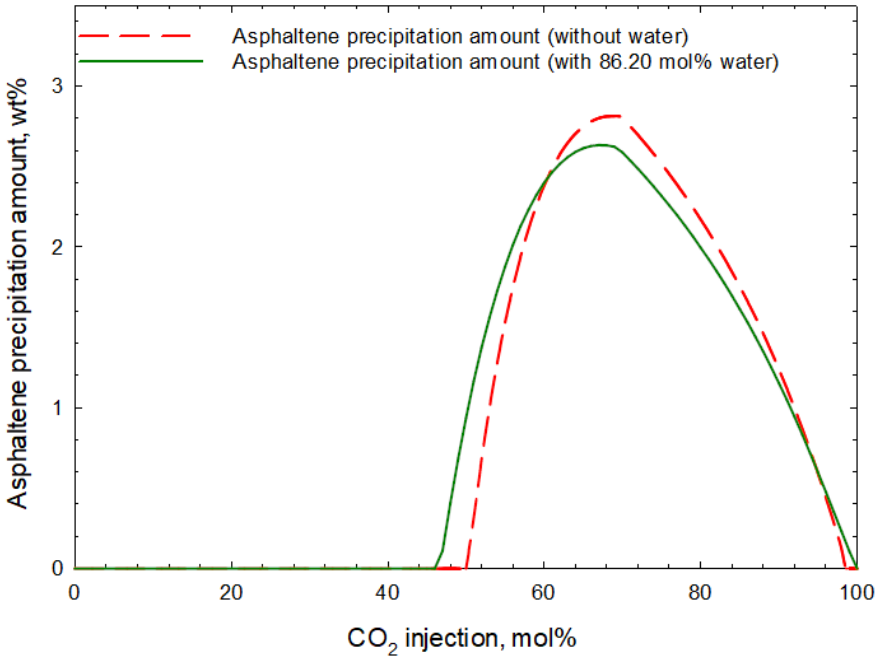

(a)

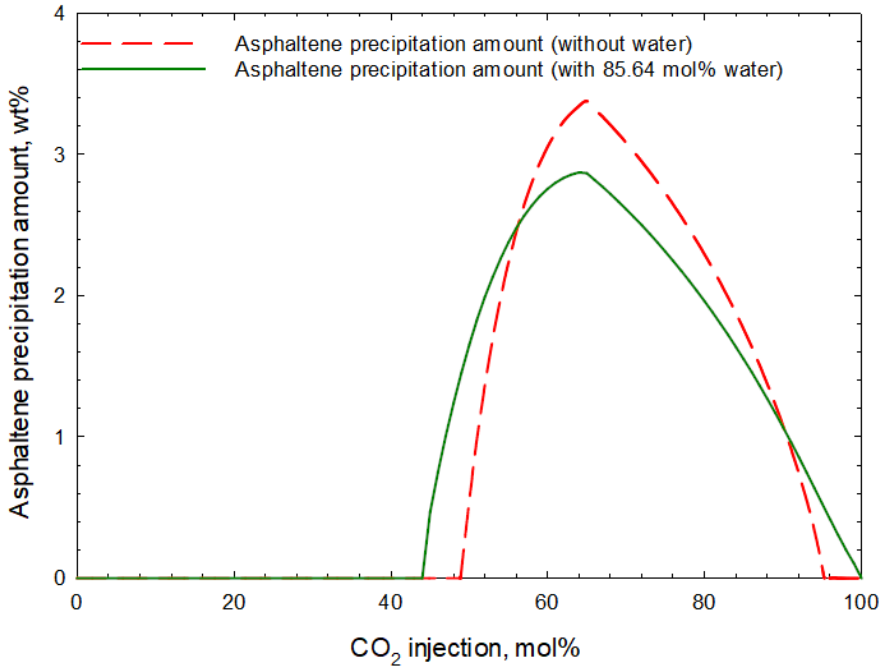

(b)

Fig. 6-3 Comparison between the calculated asphaltene precipitation amount with and without water under CO_2 injection: (a) Oil sample 1; (b) Oil sample 2.

Figure 6-4 compares the change of the precipitated asphaltene amount with pressure in the presence and absence of water at 80 mol% CO_2 concentration. In Figure 6-4, the green solid line shows the asphaltene precipitation amount with the presence of water,

while the red dashed line represents the asphaltene precipitation amount without water. We can see from Figure 6-4 that the asphaltene precipitation amount of the oil samples 1 and 2 with water is larger than that without water at a lower pressure. However, as pressure increases, the asphaltene precipitation amount without water exceeds that with water. This is because the solubility of CO_2 in water increases with pressure, causing a larger amount of CO_2 to be dissolved in the aqueous phase at high pressures and thus leading to a decrease in the asphaltene precipitation amount.

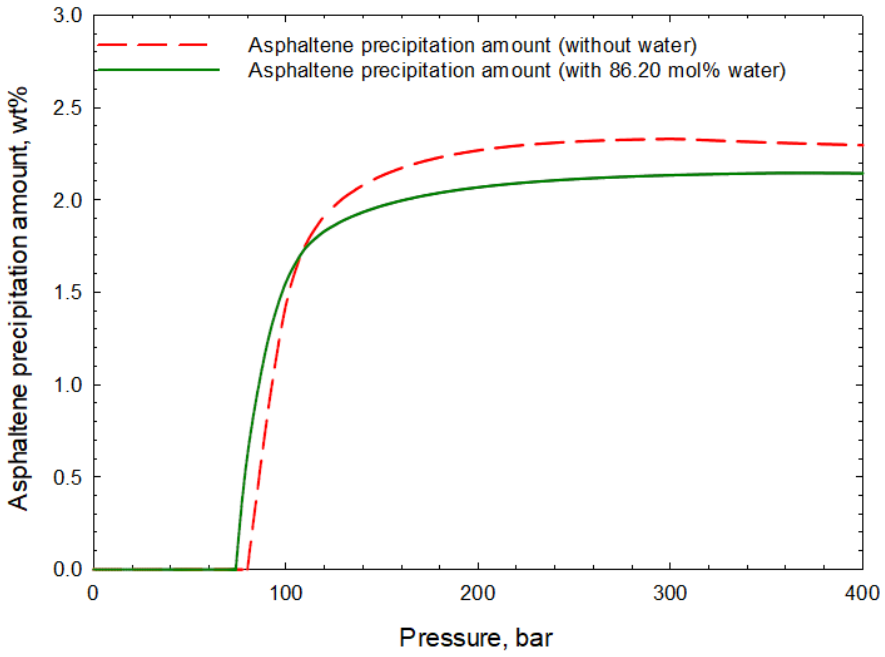

(a)

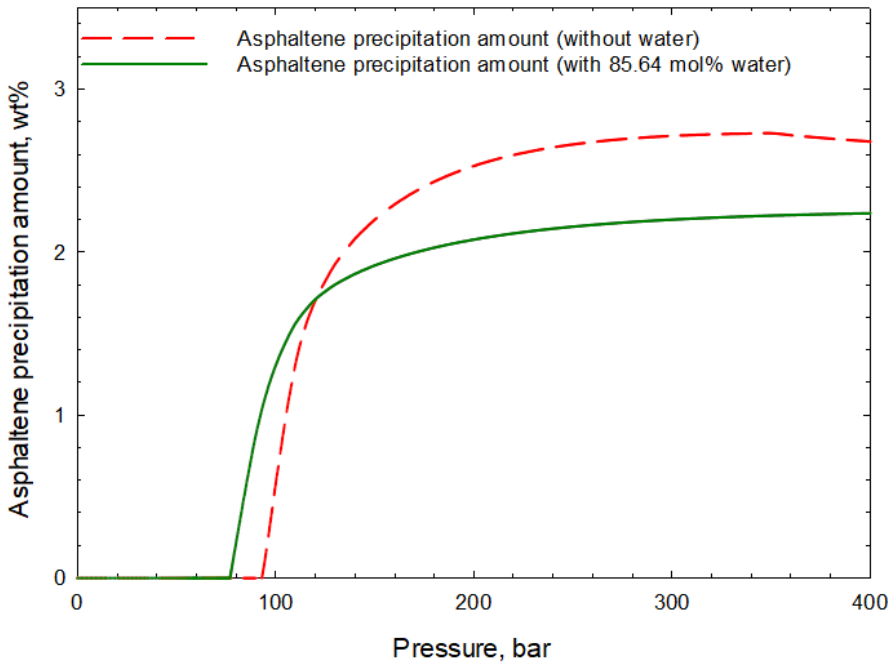

(b)

Fig. 6-4 Comparison between the calculated asphaltene precipitation amount with and without water under 80 mol% CO_2 injection: (a) Oil sample 1; (b) Oil sample 2.

Figure 6-5 compares the *Px* phase diagrams of the oil samples with and without the presence of water. In Figure 6-5, the red dashed line represents the asphaltene precipitation onsets without the presence of water, while the blue solid line shows the asphaltene precipitation onsets with the presence of water. The orange solid line and the green dashed line represent the saturation pressure with and without the presence of water, respectively. It can be observed from Figure 6-5 that the area of asphaltene precipitation in the *Px* phase diagrams is enlarged due to the presence of water, which means the presence of water can make the asphaltene precipitate more easily. We can also see from Figure 6-5 that water does not pose a significant effect on oil saturation pressure with the absence of the asphaltene phase. However, the deviation between the saturation pressure with water and the saturation pressure without water becomes more obvious when asphaltene starts to precipitate. This can be attributed to the fact that the presence of water can greatly affect asphaltene precipitation during CO_2 flooding, which causes nonnegligible changes in the phase compositions and phase fractions.

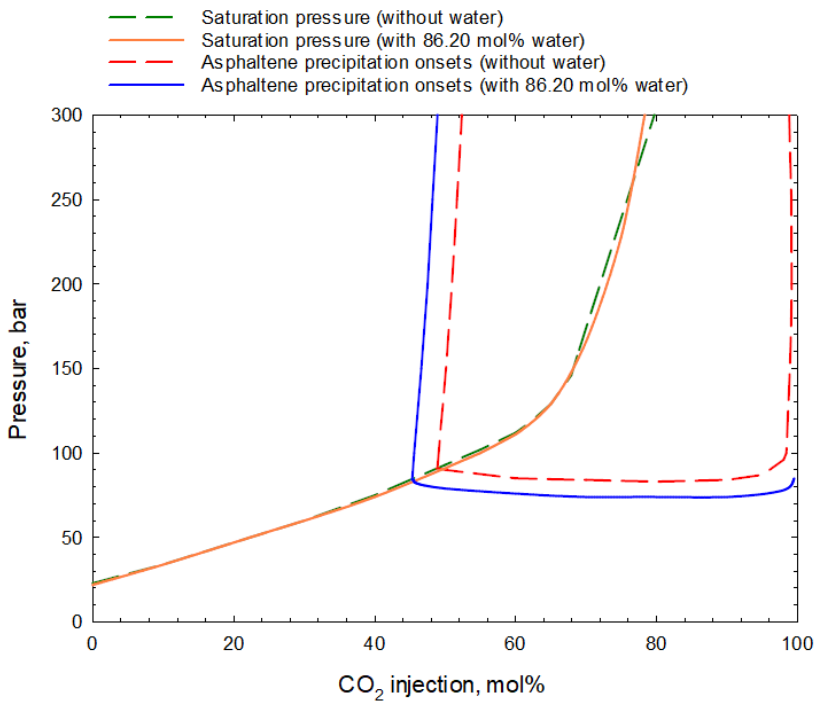

(a)

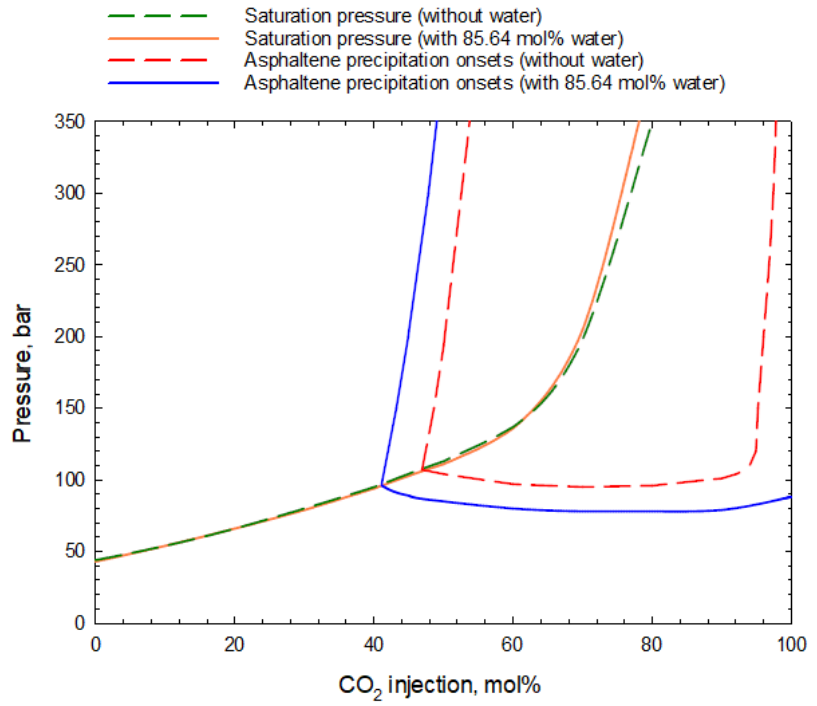

(b)

Fig. 6-5 Comparison between the *Px* phase diagrams with and without water under CO_2 injection: (a) Oil sample 1; (b) Oil sample 2.

Figure 6-6 (a-c) show the *PT* phase diagrams of oil sample 1 with 50% CO_2 injection and 10%, 30% and 50% water injection, respectively. The red line shows the asphaltene precipitation onsets, while the green line represents the oil saturation pressure. The blue line is the aqueous phase boundary. Note that the aqueous phase exists on the left side of the aqueous phase boundary, and disappears on the right side of the aqueous phase boundary. We can see from Figure 6-6 that at lower temperatures and pressures, the system is in a three-phase equilibrium characterized by the coexistence of vapor, liquid, and aqueous phases. As pressure increases, asphaltene phase appears, leading to the formation of a four-phase VLAS equilibrium state. Further elevation in pressure causes the vapor phase to disappear, resulting in a LAS three-phase equilibrium. It can be observed from Figure 6-6 that the VLA three-phase region and the LA two-phase region are expanded with an increasing water content. It can be also seen from Figure 6-6 that the asphaltene precipitation onsets do not vary a lot with a change in water content, which is different from what has been observed from the above *Px* phase diagrams.

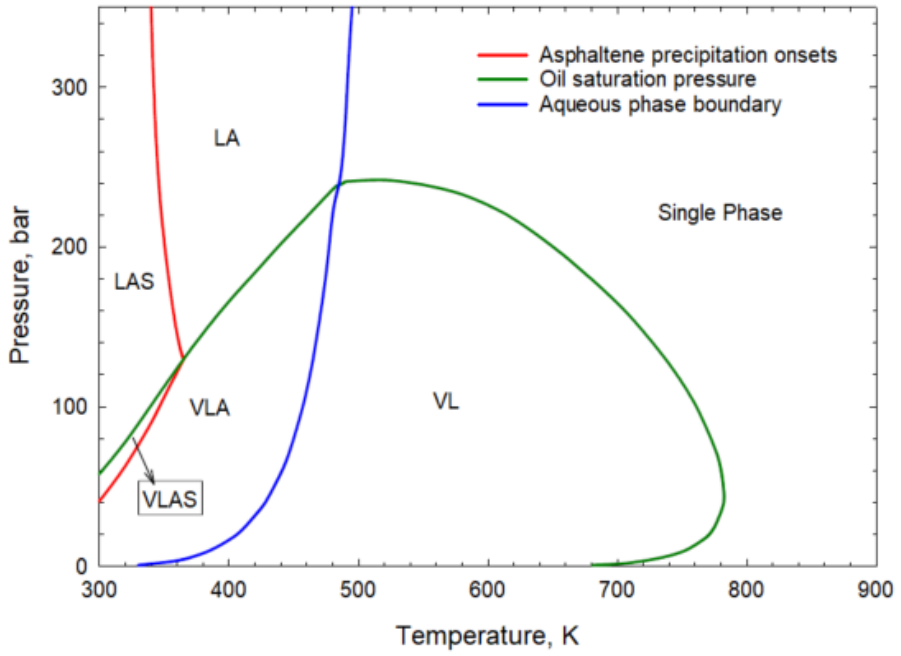

(a)

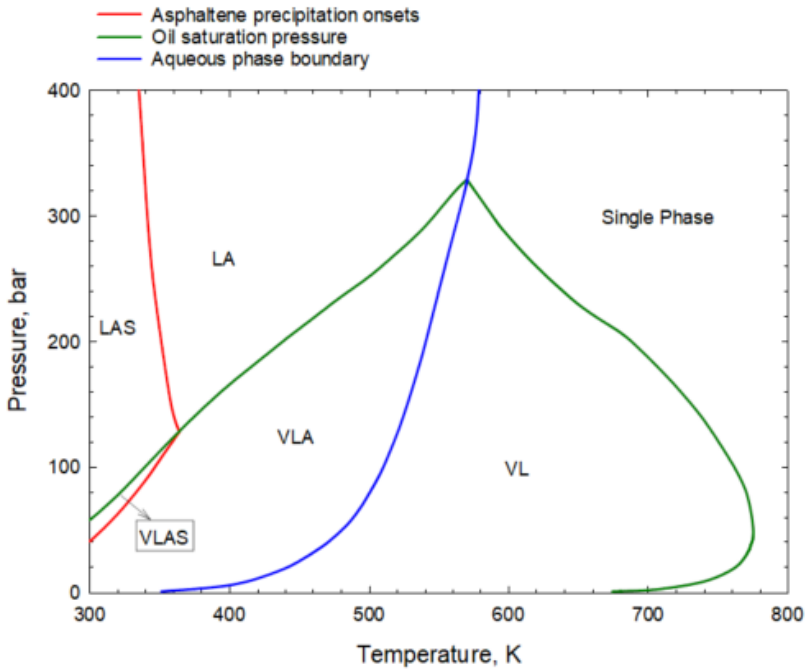

(b)

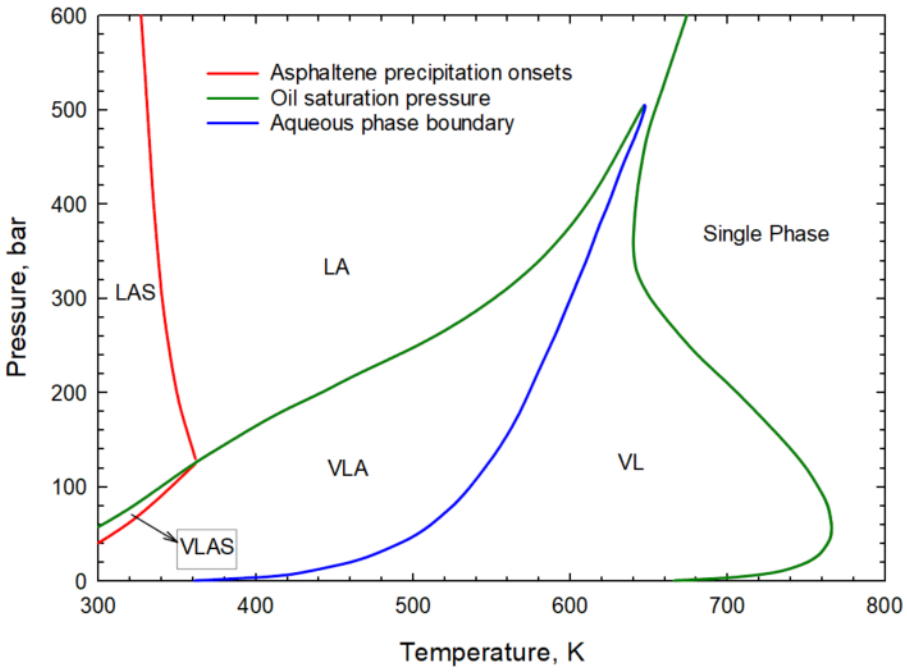

(c)

Fig. 6-6 *PT* phase diagrams of oil sample 1 with 50% CO_2 injection and (a) 10% water injection; (b) 30% water injection; (c) 50% water injection.

In Figure 6-6, the asphaltene phase only appears at the low-temperature region. However, it has been reported by several modeling studies [53-55] that the asphaltene precipitation can also occur at the high-temperature region of the *PT* phase diagrams.

In order to reveal the different topographies of the *PT* phase diagrams that can take into account both the presence of the aqueous phase and the asphaltene phase, the characterization results of oil sample 1 are adjusted. The adjusted compositions and BIPs are shown in Tables 6-9 and 6-10 and the calculated *PT* phase diagrams are shown in Figure 6-7. Note that the phase boundary between the VL two-phase region and the LS two-phase region is identified by the phase boundary tracking method proposed by Chen *et al.* [56]. Different from the *PT* phase diagrams shown in Figure 6-6, in which the asphaltene phase only appears at the low-temperature region, the *PT* phase diagrams depicted in Figure 6-7 show two areas of asphaltene precipitation. We can conclude from Figure 6-7 that although the change in water content does not pose any significant effects on the asphaltene precipitation onsets at the low-temperature region, obvious shifts can be observed on the asphaltene precipitation onsets at the high-temperature side. This is because the compositions of the vapor phase and the liquid phase can vary a lot at high temperatures due to the increasing water content.

Table 6-9 Adjusted composition and properties of oil sample 1.

Component	Composition (mol%)	T_c (K)	P_c (bar)	V_c (m^3/kmol)	ω	MW (g/mol)
N_2	0.9962	126.20	33.94	89.80	0.04	28.01
CO_2	0.6019	304.20	73.76	94.00	0.22	44.01
H_2S	0.3113	373.20	89.37	98.50	0.10	34.08
C_1	4.6594	190.60	46.00	99.00	0.01	16.04
C_2	3.1028	305.40	48.84	148.00	0.10	30.07
C_3	4.9292	369.80	42.46	203.00	0.15	44.10
i-C_4	0.8406	408.10	36.48	263.00	0.18	58.12
n-C_4	1.9925	425.20	38.00	255.00	0.19	58.12
i-C_5	1.3179	460.40	33.84	306.00	0.23	72.15
n-C_5	2.2726	469.60	33.74	304.00	0.25	72.15
C_6	3.5055	507.40	29.69	370.00	0.30	86.18
C_7	7.4596	539.14	30.18	428.46	0.34	96.00
C_8	6.7226	559.81	27.86	457.61	0.37	107.00
C_9	6.0584	583.64	25.42	503.78	0.42	121.00
C_{10}-C_{12}	14.8147	623.26	22.25	597.88	0.50	146.40
C_{13}-C_{14}	7.5977	670.56	19.37	737.33	0.60	182.11

C_{15}-C_{16}	6.1706	708.34	17.71	872.46	0.69	213.58
C_{17}-C_{19}	7.1524	748.34	16.40	1033.20	0.78	249.43
C_{20}-C_{22}	5.2350	789.89	15.39	1217.94	0.87	289.29
C_{23}-C_{26}	4.8652	836.16	14.54	1445.88	0.97	336.48
C_{27}-C_{31}	3.8236	894.05	13.76	1759.55	1.06	399.10
C_{32}-C_{40}	3.4069	974.39	13.03	2240.37	1.14	490.43
C_{41}-C_{80}	1.9242	1114.00	11.90	3411.24	0.99	688.83
Asphaltene	0.2391	1452.32	15.95	3411.24	1.16	688.83

Table 6-10 BIPs used for adjusted oil sample 1.

	N_2	CO_2	H_2S	A
N_2	0	-0.017	0.177	0.000
CO_2	-0.017	0	0.097	0.080
H_2S	0.177	0.097	0	0.100
C_1	0.031	0.120	0.080	0.000
C_2	0.052	0.120	0.083	0.016
C_3	0.085	0.120	0.088	0.013
i-C_4	0.103	0.120	0.047	0.011
n-C_4	0.080	0.120	0.060	0.009
i-C_5	0.092	0.120	0.060	0.009
n-C_5	0.100	0.120	0.063	0.008
C_6	0.080	0.120	0.050	0.008
C_7	0.080	0.100	0	0.007
C_8	0.080	0.100	0	0.006
C_9	0.080	0.100	0	0.005
C_{10}-C_{12}	0.080	0.100	0	0.005
C_{13}-C_{14}	0.080	0.100	0	0.004
C_{15}-C_{16}	0.080	0.100	0	0.003
C_{17}-C_{19}	0.080	0.100	0	0.003
C_{20}-C_{22}	0.080	0.100	0	0.002
C_{23}-C_{26}	0.080	0.100	0	0.001
C_{27}-C_{31}	0.080	0.100	0	0.001
C_{32}-C_{39}	0.080	0.100	0	0.001
C_{40}-C_{80}	0.080	0.100	0	0
Asphaltene	0.080	0.100	0	0

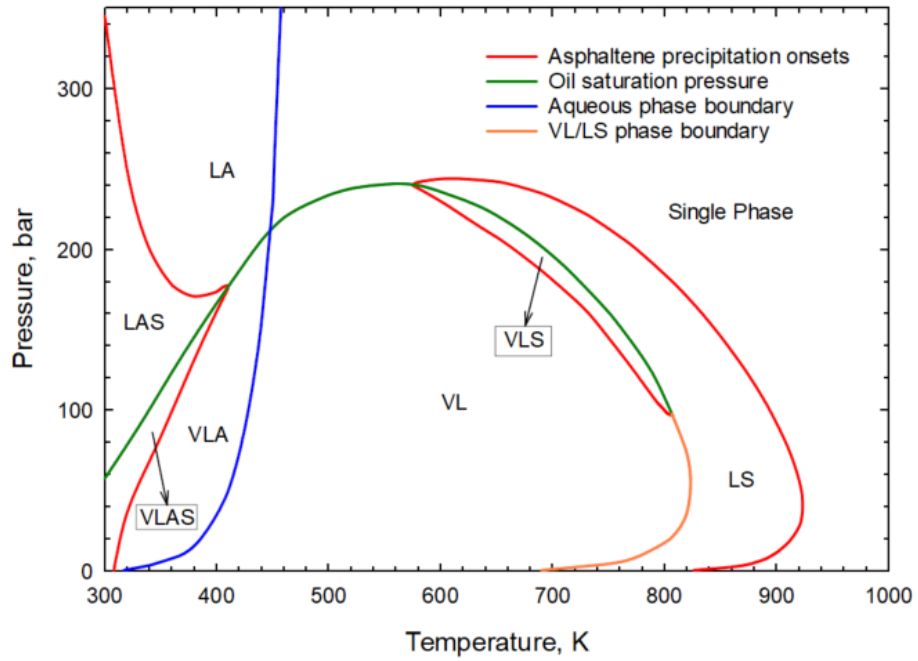
Asphaltene precipitation onsets
Oil saturation pressure
Aqueous phase boundary
VL/LS phase boundary
LA
Single Phase
LAS
VLS
VL
VLA
LS
VLAS
Pressure, bar
Temperature, K
0
100
200
300
300
400
500
600
700
800
900
1000

(a)

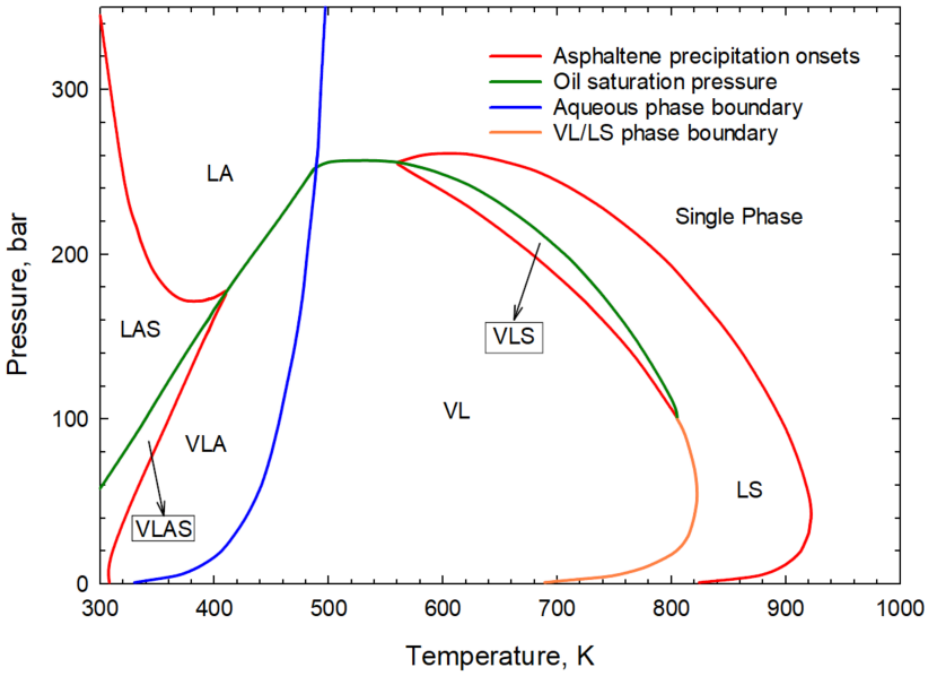
Asphaltene precipitation onsets
Oil saturation pressure
Aqueous phase boundary
VL/LS phase boundary
LA
Single Phase
LAS
VLS
VL
VLA
LS
VLAS
Pressure, bar
Temperature, K
0
100
200
300
300
400
500
600
700
800
900
1000

(b)

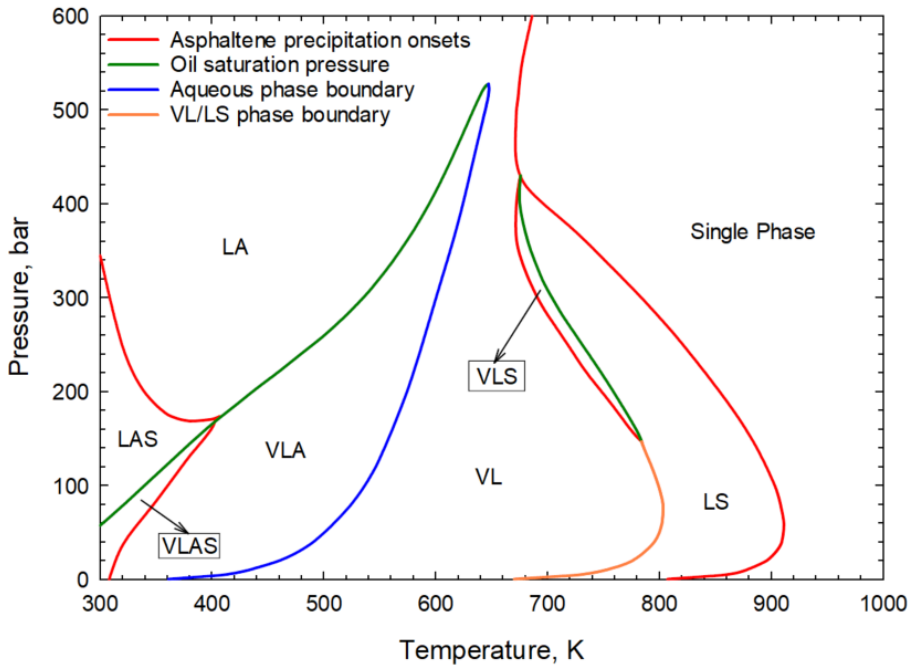

(c)

Fig. 6-7 *PT* phase diagrams of the adjusted oil sample 1 with 50% CO_2 injection and (a) 5% water injection; (b) 10% water injection; (c) 50% water injection.

6.4.Conclusions

A trust-region based four-phase VLLA equilibrium calculation algorithm is applied to conduct four-phase VLAS equilibrium calculations to study the effect of water on asphaltene precipitation. The algorithm is first validated by comparing the calculation results of the asphaltene precipitation amount with and without the presence of water under CO_2 injections. The validated algorithm is then applied to calculate the asphaltene precipitation amount at different pressures and generate *PT* and *Px* phase diagrams. The following conclusions can be drawn based on the results obtained in this study:

• A reasonably good agreement can be seen between the results calculated by the four-phase VLAS equilibrium calculation algorithm and the experimental data, which indicates that such an algorithm together with the oil characterization method by

Pedersen *et al.* [11] can be used to reliably predict asphaltene precipitation phenomena with the presence of water.

- The maximum asphaltene precipitation amount is decreased due to the presence of water. This is because a considerable amount of CO_2 is dissolved in the aqueous phase instead of the liquid phase, and the gaseous components like CO_2 are generally poor solvents for asphaltene. A decrease of CO_2 content in the liquid phase will lead to increased solubility of the asphaltene component in the liquid phase, and therefore reduce the precipitated asphaltene amount.
- The asphaltene precipitation amount of the oil samples tested in this study with water is larger than that without water at a lower pressure. However, as pressure increases, the asphaltene precipitation amount without water exceeds that with water. This can be attributed to the fact that the solubility of CO_2 in water increases with pressure, causing a larger amount of CO_2 to be dissolved in the aqueous phase.
- The area of asphaltene precipitation in the *Px* phase diagrams is enlarged due to the presence of water, which indicates that the presence of water can make the asphaltene phase precipitate more easily.
- Water does not pose significant effects on oil saturation pressures in the *Px* phase diagrams with the absence of the asphaltene phase, but the deviation between the saturation pressures with and without the presence of water will become more obvious after asphaltene starts to precipitate. This can be attributed to that the presence of water significantly influences asphaltene precipitation during the CO_2 injection process, leading to notable alterations in phase compositions and fractions.
- It can be concluded from the calculated *PT* phase diagrams that the VLA three-phase region and the LA two-phase region are expanded with an increasing water content.

However, the asphaltene precipitation onsets at the low-temperature region do not change much with an increasing water content.

•In the *PT* phase diagrams where asphaltene precipitation is observed at both the low-temperature region and the high-temperature region, noticeable shifts in the asphaltene precipitation onsets due to water presence are evident on the high-temperature side. This is caused by the significant variations in the compositions of the vapor phase and the liquid phase at high temperatures due to an increasing water content.

Acknowledgments

The authors greatly acknowledge a Discovery Grant from the Natural Sciences and Engineering Research Council of Canada (NSERC) (Grant No.: NSERC RGPIN-2020-04571) to H. Li. Z. Chen also greatly acknowledges the financial support provided by the China Scholarship Council (CSC) via a Ph.D. scholarship (No.: 201908180010). Y. Zhou greatly acknowledges the financial support provided by the China Scholarship Council (CSC) via a Ph.D. scholarship (No. 202008180027). R. Li greatly acknowledges the financial support provided by National Natural Science Foundation of China (Grant No. 52004040). Q. Wang greatly acknowledges the financial support provided by National Natural Science Foundation of China (Grant No. 52074344).

References

[1]Cao C, Liu H, Hou Z, Mehmood F, Liao J, Feng W. A review of CO_2 storage in view of safety and cost-effectiveness. Energies 2020; 13 (3): 600. https://doi.org/10.3390/en13030600

[2]Chen Z, Zhou Y, Li H. A review of phase behavior mechanisms of CO_2 EOR and storage in subsurface formations. *Ind. Eng. Chem. Res.* 2022; 61 (29): 10298-10318. https://doi.org/10.1021/acs.iecr.2c00204

[3]Hirschberg A, deJong LN, Schipper B, Meijer J. Influence of temperature and pressure on asphaltene flocculation. *SPE J.* 1984;24(03):283-293. https://doi.org/10.2118/11202-PA

[4]Speight J. Petroleum Asphaltenes-Part 1: Asphaltenes, resins and the structure of petroleum. *Oil Gas Sci. Technol.* 2004; 59 (5): 467-477. https://doi.org/10.2516/ogst:2004032

[5]Vargas FM, Garcia-Bermudes M, Boggara M, Punnapala S, Abutaqiya M, Mathew N, *et al.* On the development of an enhanced method to predict asphaltene precipitation. Presented at Offshore Technology Conference, Houston, TX, May 5-8, 2014; SPE 2014; Paper No. OTC-25294-MS.

[6]Chen Z, Li R, Li H. A new vapor-liquid-asphaltene three-phase equilibrium computation algorithm based on the free-asphaltene assumption. *Fluid Phase Equilib.* 2022; 556: 113392. https://doi.org/10.1016/j.fluid.2022.113392

[7]Creek JL. Freedom of action in the state of asphaltenes: Escape from conventional wisdom. *Energy Fuels* 2005; 19 (4): 1212-1224. https://doi.org/10.1021/ef049778m

[8]Punnapala S, Vargas FM. Revisiting the PC-SAFT characterization procedure for an improved asphaltene precipitation prediction. *Fuel* 2013; 108: 417-429. https://doi.org/10.1016/j.fuel.2012.12.058

[9]Chen Z, Li R, Li H. An improved vapor-liquid-asphaltene three-phase equilibrium computation algorithm. *Fluid Phase Equilib.* 2021; 537: 113004. https://doi.org/10.1016/j.fluid.2021.113004

[10]Ting PD, Hirasaki GJ, Chapman WG. Modeling of asphaltene phase behavior with the SAFT equation of state. *Pet. Sci. Technol.* 2003; 21 (3-4): 647-661. https://doi.org/10.1081/LFT-120018544

[11]Pedersen KS, Christensen PL, Shaikh JA. Phase behavior of petroleum reservoir fluids. CRC press; 2014.

[12]Leontaritis KJ, Mansoori GA. Asphaltene flocculation during oil production and processing: A thermodynamic collodial model. Presented at SPE International

Symposium on Oilfield Chemistry, San Antonio, TX, Feb. 4-6, 1987; SPE 1987; Paper No. SPE-16258-MS.

[13]Pan H, Firoozabadi A. A thermodynamic micellization model for asphaltene precipitation: Part 1: Micellar size and growth. Presented at Annual Technical Conference and Exhibition of the Society of Petroleum Engineers, Denver, CO, Oct. 6-9, 1996; SPE 1996; Paper No. SPE-36741-PA.

[14]Victorov AI, Firoozabadi A. Thermodynamic micellizatin model of asphaltene precipitation from petroleum fluids. *AIChE J.* 1996; 42 (6): 1753-1764. https://doi.org/10.1002/aic.690420626

[15]Wu J, Prausnitz JM, Firoozabadi A. Molecular-thermodynamic framework for asphaltene-oil equilibria. *AIChE J.* 1998; 44 (5): 1188-99. https://doi.org/10.1002/aic.690440516

[16]Boek ES, Yakovlev DS, Headen TF. Quantitative molecular representation of asphaltenes and molecular dynamics simulation of their aggregation. *Energy Fuels* 2009; 23 (3): 1209-1219. https://doi.org/10.1021/ef800876b

[17]Buckley J, Hirasaki G, Liu Y, Von Drasek S, Wang J, Gill B. Asphaltene precipitation and solvent properties of crude oils. *Pet. Sci. Technol.* 1998; 16 (3-4): 251-285. https://doi.org/10.1080/10916469808949783

[18]Czarnecki J, Tchoukov P, Dabros T. Possible role of asphaltenes in the stabilization of water-in-crude oil emulsions. *Energy Fuels* 2012; 26 (9): 5782-5786. ttps://doi.org/10.1021/ef300904a

[19]Goual L. Impedance spectroscopy of petroleum fluids at low frequency. *Energy Fuels* 2009; 23 (4): 2090-2094. https://doi.org/10.1021/ef800860x

[20]Flory PJ. Thermodynamics of high polymer solutions. *J. Chem. Phys.* 1941; 9 (8): 660660. https://doi.org/10.1063/1.1750971

[21]Hildebrand JH. Solubility. III. Relative values of internal pressures and their practical application. *J. Am. Chem. Soc.* 1919; 41 (7): 1067-1080. https://doi.org/10.1021/ja02228a004

[22]Huggins ML. Solutions of long chain compounds. *J. Chem. Phys.* 1941; 9 (5): 440-440. https://doi.org/10.1063/1.1750930

[23] Scatchard G. Equilibria in non-electrolyte solutions in relation to the vapor pressures and densities of the components. *Chem. Rev.* 1931; 8 (2): 321-333. https://doi.org/10.1021/cr60030a010

[24] Scott RL, Magat M. The thermodynamics of high-polymer solutions: I. The free energy of mixing of solvents and polymers of heterogeneous distribution. *J. Chem. Phys.* 1945; 13 (5): 172-177. https://doi.org/10.1063/1.1724018

[25] Alboudwarej H, Akbarzadeh K, Beck J, Svrcek WY, Yarranton HW. Regular solution model for asphaltene precipitation from bitumens and solvents. *AIChE J.* 2003; 49 (11): 2948-2956. https://doi.org/10.1002/aic.690491124

[26] Andersen SI, Speight JG. Thermodynamic models for asphaltene solubility and precipitation. *J. Pet. Sci. Eng.* 1999; 22 (1-3): 53-66. https://doi.org/10.1016/S0920-4105(98)00057-6

[27] Cimino R, Correra S, Sacomani P, Carniani C. Thermodynamic modelling for prediction of asphaltene deposition in live oils. Presented at SPE International Symposium on Oilfield Chemistry, San Antonio, TX, Feb. 14-17, 1995; SPE 1995; Paper No. SPE-28993-MS.

[28] Correra S, Merino-Garcia D. Simplifying the thermodynamic modeling of asphaltenes in upstream operations. *Energy Fuels* 2007; 21 (3): 1243-1247. https://doi.org/10.1021/ef060371m

[29] De Boer R, Leerlooyer K, Eigner M, Van Bergen A. Screening of crude oils for asphalt precipitation: theory, practice, and the selection of inhibitors. *SPE Prod. Facil.* 1995; 10 (01): 55-61. https://doi.org/10.2118/24987-PA

[30] Gonzalez DL, Vargas FM, Mahmoodaghdam E, Lim F, Joshi N. Asphaltene stability prediction based on dead oil properties: Experimental evaluation. *Energy Fuels* 2012; 26 (10): 6218-27. https://doi.org/10.1021/ef300837y

[31] Kawanaka S, Park SJ, Mansoori GA. Organic deposition from reservoir fluids: a thermodynamic predictive technique. *SPE Reserv. Eng.* 1991; 6 (02): 185-192. https://doi.org/10.2118/17376-PA

[32] Kraiwattanawong K, Fogler HS, Gharfeh SG, Singh P, Thomason WH, Chavadej S. Thermodynamic solubility models to predict asphaltene instability in live crude oils. *Energy Fuels* 2007; 21 (3): 1248-1255. https://doi.org/10.1021/ef060386k

[33] Wang J, Buckley J. A two-component solubility model of the onset of asphaltene flocculation in crude oils. *Energy Fuels* 2001; 15 (5): 1004-1012. https://doi.org/10.1021/ef0100121

[34] Wang J, Buckley J, Burke N, Creek J. A practical method for anticipating asphaltene problems. *SPE Prod. Facil.* 2004; 19 (03): 152-160. https://doi.org/10.2118/87638-PA

[35] Yarranton HW, Masliyah JH. Molar mass distribution and solubility modeling of asphaltenes. *AIChE J.* 1996; 42 (12): 3533-3543. https://doi.org/10.1002/aic.690421222

[36] Vargas FM, Gonzalez DL, Hirasaki GJ, Chapman WG. Modeling asphaltene phase behavior in crude oil systems using the perturbed chain form of the statistical associating fluid theory (PC-SAFT) equation of state. *Energy Fuels* 2009; 23 (3): 1140-1146. https://doi.org/10.1021/ef8006678

[37] Lapene A, Nichita DV, Debenest G, Quintard M. Three-phase free-water flash calculations using a new Modified Rachford–Rice equation. *Fluid Phase Equilib.* 2010; 297 (1): 121-28. https://doi.org/10.1016/j.fluid.2010.06.018

[38] Tang Y, Saha S. An efficient method to calculate three-phase free-water flash for water-hydrocarbon systems. *Ind. Eng. Chem. Res.* 2003; 42 (1): 189-197. https://doi.org/10.1021/ie010785x

[39] Li S, Xu L, Li H. Four-phase flash calculation algorithm based on the free-water assumption. *Ind. Eng. Chem. Res.* 2022; 61 (10): 3742-3753. https://doi.org/10.1021/acs.iecr.1c04912

[40] Srivastava R, Huang S, Dong M. Asphaltene deposition during CO_2 flooding. *SPE Prod. Facil.* 1999; 14 (04): 235-245. https://doi.org/10.2118/59092-PA

[41] Michelsen ML. The isothermal flash problem. Part I. Stability. *Fluid Phase Equilib.* 1982; 9 (1): 1-19. https://doi.org/10.1016/0378-3812(82)85001-2

[42] Michelsen ML. The isothermal flash problem. Part II. Phase-split calculation. *Fluid Phase Equilib.* 1982; 9 (1): 21-40. https://doi.org/10.1016/0378-3812(82)85002-4

[43] Li Z, Firoozabadi A. Initialization of phase fractions in Rachford–Rice equations for robust and efficient three-phase split calculation. *Fluid Phase Equilib.* 2012; 332: 21-27. https://doi.org/10.1016/j.fluid.2012.06.021

[44] Pan H, Connolly M, Tchelepi H. Multiphase equilibrium calculation framework for compositional simulation of CO_2 injection in low-temperature reservoirs. *Ind. Eng. Chem. Res.* 2019; 58 (5): 2052-2070. https://doi.org/10.1021/acs.iecr.8b05229

[45] Li S, Xu L, Li H. A robust four-phase equilibrium calculation algorithm based on the scaled trust-region method for water/hydrocarbon mixtures. *To be Submitted to Chemical Engineering Science*.

[46] Peng D-Y, Robinson DB. A new two-constant equation of state. *Ind. Eng. Chem. Fundam.* 1976; 15 (1): 59-64. https://doi.org/10.1021/i160057a011

[47] Rachford Jr HH, Rice J. Procedure for use of electronic digital computers in calculating flash vaporization hydrocarbon equilibrium. *J. Pet. Technol.* 1952; 4 (10): 19-23. https://doi.org/10.2118/952327-G

[48] Ammar M, Renon H. The isothermal flash problem: new methods for phase split calculations. *AIChE J.* 1987; 33 (6): 926-939. https://doi.org/10.1002/aic.690330606

[49] Mehra RK, Heidemann RA, Aziz K. An accelerated successive substitution algorithm. *Can. J. Chem. Eng.* 1983; 61 (4): 590-596. https://doi.org/10.1002/cjce.5450610414

[50] Pan H, Firoozabadi A. Fast and robust algorithm for compositional modeling: part II-two-phase flash computations. *SPE J.* 2003; 8 (04): 380-391. https://doi.org/10.2118/87335-PA

[51] Chueh P, Prausnitz J. Vapor-liquid equilibria at high pressures: Calculation of partial molar volumes in nonpolar liquid mixtures. *AIChE J.* 1967; 13 (6): 1099-1107. https://doi.org/10.1002/aic.690130612

[52]PVTsim Nova 5; Calsep A/S: Copenhagen, Denmark, 2020.

[53]Agger CS, Sørensen H. Algorithm for constructing complete asphaltene pt and px phase diagrams. *Ind. Eng. Chem. Res.* 2018; 57 (1): 392-400. https://doi.org/10.1021/acs.iecr.7b04246

[54]Cismondi M. Phase envelopes for reservoir fluids with asphaltene onset lines: An integral computation strategy for complex combinations of two-and three-phase behaviors. *Energy Fuels* 2018; 32 (3): 2742-2748. https://doi.org/10.1021/acs.energyfuels.7b02790

[55]Benelli FE, Pisoni GO, Cismondi-Duarte M. A classification of phase envelopes for reservoir fluids with asphaltene onset lines: Exploring topology transitions based on compositional changes. *Fluid Phase Equilib.* 2023; 575: 113914. https://doi.org/10.1016/j.fluid.2023.113914

[56] Chen Z, Xu L, Zhou Y, Li R, Li H. A robust and efficient algorithm for vapor-liquid-equilibrium/liquid-liquid-equilibrium (VLE/LLE) phase boundary tracking. *Chem. Eng. Sci.* 2023; 266: 118286. https://doi.org/10.1016/j.ces.2022.118286

CHAPTER 7 CONCLUSIONS, CONTRIBUTIONS, AND RECOMMENDATIONS

7.1 Conclusions and Scientific Contributions to the Literature

This dissertation begins with a comprehensive review of the phase behavior mechanisms related to CO_2 storage in subsurface formations. Advanced three-phase VLS equilibrium calculation algorithms with improved robustness and efficiency, grounded in both the solid and free-asphaltene assumptions, are formulated in this thesis. In addition, algorithms designed to precisely track the VL/LL and VL/LS two-phase boundaries in *PT* and *Px* phase diagrams are introduced. Eventually, a VLLA four-phase equilibrium calculation algorithm is adopted to undertake VLAS four-phase equilibrium calculations as well as investigate the impact of water on asphaltene precipitation. Key findings from this thesis research are summarized below.

Chapter 2:

The interactions between CO_2 and formation fluids play a crucial role in determining the effectiveness of CO_2 trapping mechanisms and storage efficiency. In Chapter 2, we present a thorough review of the phase behavior mechanisms related to CO_2 storage in various subsurface formations, examining both experimental findings and modeling approaches. Generally, increasing salt concentrations result in lower CO_2 solubility, indicating that a saline aquifer with lower salt concentration may facilitate increased CO_2 storage via solubility trapping. In comparison to aquifer storage sites, oil reservoirs typically offer better sealing qualities due to the existence of cap rocks. Depleted reservoirs, due to their lower reservoir pressures and CO_2's heightened solubility in oil, stand out as prominent storage sites. Their well-characterized nature also simplifies CO_2 storage evaluations. CO_2 injection into low-temperature oil reservoirs can lead to

three-phase $VL_{CO2}L_{HC}$ equilibria and four-phase $VL_{CO2}L_{HC}A$ equilibria, with high CO_2 concentrations observed in both the CO_2-riched phase and liquid hydrocarbon phase. This suggests that residual oil in the depleted reservoir can contribute to substantial CO_2 storage following the CO_2 flooding process.

Chapter 3:

In this study, a novel three-phase VLS equilibrium calculation algorithm is proposed to enhance the accuracy and robustness of predicting asphaltene precipitation phenomena during oil production processes. The performance of this algorithm is thoroughly evaluated using three oil samples, demonstrating excellent agreement between the prediction results and experimental observations across diverse pressure/temperature conditions. By calibrating the algorithm with measured asphaltene onset data, accurate predictions of phase boundaries and asphaltene precipitation quantities can be made with different injectants. Notably, the molar volume of the asphaltene component plays a significant role in determining the lower boundary of asphaltene precipitation in the *PT* phase diagram, with larger molar volumes corresponding to lower asphaltene precipitation boundaries. Moreover, pressure and temperature exert significant effects on asphaltene precipitation. At a fixed temperature, the amount of asphaltene precipitation initially increases, reaches a maximum value, and then decreases with increasing pressure. At a certain pressure, the asphaltene precipitation amount decreases with rising temperature, along with a reduction in the region of asphaltene precipitation occurrence. The algorithm demonstrates convergence to correct results for all the tested conditions and enables the generation of comprehensive *PT* and *Px* diagrams, holding great promise for diverse applications.

Chapter 4:

In this work, a modified three-phase VLS equilibrium calculation algorithm is proposed, incorporating the newly introduced free-asphaltene assumption. The algorithm's performance is assessed using four different oil samples. It can be concluded from the results that our algorithm together with the free-asphaltene assumption can accurately capture asphaltene precipitation phenomena. Upon calibration with the measured asphaltene precipitation onsets, the algorithm enables the prediction of phase boundaries with different injectants. Comparatively, calculations under the free-asphaltene assumption demonstrate better alignment with experimental data than those using the solid assumption. However, further validation is required, particularly at high-temperature regions, to determine which assumption offers more precise asphaltene precipitation predictions. Additionally, phase envelopes derived from the free-asphaltene assumption closely mirror those from the liquid assumption, underscoring the viability of the free-asphaltene assumption.

Chapter 5:

In this chapter, we have adopted the three-phase VL_1L_2 equilibrium calculation algorithm based on the trust region method introduced by Pan *et al.* (2019) to perform three-phase VLS equilibrium calculations. The accuracy of our calculation results has been validated by comparing the phase boundaries obtained with the available literature data. To detect the VL/LL and VL/LS phase boundaries, we have devised a novel phase boundary detection technique based on Brent's method (Brent, 1971). *PT* and *Px* phase diagrams are generated to assess the performance of our new algorithms. It can be observed that the results yielded by the three-phase VLS equilibrium calculation algorithm align well with the experimental data. Notably, the predicted VL/LS and the VL/LL two-phase boundaries demonstrate smooth behavior. The calculated VL/LS and VL/LL two-phase boundary intersects with the three-phase region at the apex of the

VL_1L_2 three-phase boundary, providing evidence for the extension of the three-phase region (Bennett and Schmidt, 2017). Furthermore, we have compared our prediction results with the VL/LL two-phase boundaries determined by Bennett and Schmidt (2017). This comparison reveals a good agreement.

Chapter 6:

In this study, a trust-region-based algorithm is employed to perform four-phase VLAS equilibrium calculations and investigate the impact of water on asphaltene precipitation. The algorithm is first validated by comparing asphaltene precipitation amounts with and without the presence of water during CO_2 injections, and the validated algorithm is utilized to calculate asphaltene precipitation amounts at different pressures and generate *PT* and *Px* phase diagrams. The obtained results demonstrate a strong agreement between the asphaltene precipitation amounts yielded by the four-phase VLAS equilibrium calculation algorithm and experimental data, indicating the algorithm and the oil characterization method can be used to reliably predict asphaltene precipitation with the presence of water. It can be also concluded that the maximum asphaltene precipitation amount decreases due to the presence of water, which is attributed to a significant amount of CO_2 being dissolved in the aqueous phase rather than the liquid phase, and gaseous components like CO_2 generally being poor solvents for asphaltene. Comparing oil samples tested with and without water, the asphaltene precipitation amount is higher at low pressures when water is present. However, as the pressure increases, the amount of asphaltene precipitation without water surpasses that with water. This behavior can be attributed to an increased solubility of CO_2 in water at higher pressures, leading to a larger amount of CO_2 dissolving in the aqueous phase. Moreover, the presence of water enlarges the area of asphaltene precipitation in the *Px*

phase diagrams, indicating that water facilitates easier precipitation of the asphaltene phase.

7.2 Suggested Future Work

- The multiphase equilibrium calculations algorithms and the phase-boundary tracking algorithms developed in this thesis should be implemented in a compositional reservoir simulator for simulating the multiphase flow in reservoirs and wellbores. These newly proposed algorithms have the potential to significantly enhance the predictive accuracy of compositional simulations in reservoirs and wellbores, ultimately contributing to the optimization of the engineering design of EOR and CCUS projects.
- It is pointed out in **Chapter 2** that despite of the existence of numerous experimental studies on measuring the solubilities of CO_2 in water, there is still a lack of comprehensive experimental program that measures the solubility of CO_2 in sulfate and mixed-salt brine solutions. These additional experimental data are crucial for the development and validation of thermodynamic models specifically designed for CO_2/brine mixtures.
- Thermodynamic models focused on predicting the solubilities of CO_2 in brine using the φ-φ approach are currently limited in their ability to account for the impact of specific salt types. Consequently, there is a need for the development of a universal φ-φ-approach-based model that can accurately predict the solubility of CO_2 in various types of brine solutions.
- In **Chapters 3 and 4**, we compare the predicted onset of asphaltene precipitation based on various assumptions. The results highlight the necessity for conducting additional experiments to validate which assumption yields the

most accurate asphaltene precipitation predictions, especially at high temperatures.

- High-pressure microfluidic experiments should be conducted to reveal the asphaltene precipitation behavior in pore spaces. Such visual experiments can be possibly used to not only measure the onset of asphaltene precipitation but also the amount of precipitated asphaltene.
- Miscible CO_2 injection has been established as a highly effective method for enhancing oil recovery in light to medium oil reservoirs. The determination of the oil-CO_2 minimum miscibility pressure (MMP) holds significant importance in the design and implementation of CO_2 injections. Nevertheless, the existing MMP prediction models fail to account for the influence of both water and asphaltene on MMP. Consequently, there is a pressing need for an accurate oil-CO2 MMP modeling framework that takes into consideration the presence of both asphaltene phase and aqueous phase, offering valuable insights for the industry.

References

Bennett, J., Schmidt, K.A., 2017. Comparison of phase identification methods used in oil industry flow simulations. Energy & Fuels 31, 3370-3379.

Brent, R.P., 1971. An algorithm with guaranteed convergence for finding a zero of a function. The Computer Journal 14, 422-425.

Brusilovsky, A.I., 1992. Mathematical simulation of phase behavior of natural multicomponent systems at high pressures with an equation of state. SPE Reservoir Engineering 7, 117-122.

Hustad, O.S., Browning, D.J., 2010. A fully coupled three-phase model for capillary pressure and relative permeability for implicit compositional reservoir simulation. SPE Journal 15, 1003-1019.

Jin, Z., Firoozabadi, A., 2016. Thermodynamic modeling of phase behavior in shale media. SPE Journal 21, 190-207.

Lashgari, H.R., Sun, A., Zhang, T., Pope, G.A., Lake, L.W., 2019. Evaluation of carbon dioxide storage and miscible gas EOR in shale oil reservoirs. Fuel 241, 1223-1235.

Moortgat, J., Firoozabadi, A., 2013. Three-phase compositional modeling with capillarity in heterogeneous and fractured media. SPE Journal 18, 1150-1168.

Pan, H., Connolly, M., Tchelepi, H., 2019. Multiphase equilibrium calculation framework for compositional simulation of CO_2 injection in low-temperature reservoirs. Industrial & Engineering Chemistry Research 58, 2052-2070.

Wang, Y., Yan, B., Killough, J., 2013. Compositional modeling of tight oil using dynamic nanopore properties, SPE Annual Technical Conference and Exhibition. OnePetro.

Yu, W., Lashgari, H.R., Wu, K., Sepehrnoori, K., 2015. CO_2 injection for enhanced oil recovery in Bakken tight oil reservoirs. Fuel 159, 354-363.

BIBLIOGRAPHY

Aasen, A., Hammer, M., Skaugen, G., Jakobsen, J.P., Wilhelmsen, Ø., 2017. Thermodynamic models to accurately describe the PVTxy-behavior of water/carbon dioxide mixtures. Fluid Phase Equilibria 442, 125-139.

Abutaqiya, M.I., Sisco, C.J., Khemka, Y., Safa, M.A., Ghloum, E.F., Rashed, A.M., Gharbi, R., Santhanagopalan, S., Al-Qahtani, M., Al-Kandari, E., 2020. Accurate modeling of asphaltene onset pressure in crude oils under gas injection using Peng-Robinson equation of state. Energy & Fuels 34, 4055-4070.

Abutaqiya, M.I., Sisco, C.J., Vargas, F.M., 2019a. A linear extrapolation of normalized cohesive energy (LENCE) for fast and accurate prediction of the asphaltene onset pressure. Fluid Phase Equilibria 483, 52-69.

Abutaqiya, M.I., Sisco, C.J., Wang, J., Vargas, F.M., 2019b. Systematic investigation of asphaltene deposition in the wellbore and near-wellbore region of a deepwater oil reservoir under gas injection. Part 1: thermodynamic modeling of the phase behavior of polydisperse asphaltenes. Energy & Fuels 33, 3632-3644.

Ahmadi, K., Johns, R.T., 2011. Multiple-mixing-cell method for MMP calculations. SPE Journal 16, 733-742.

Akinfiev, N.N., Diamond, L.W., 2003. Thermodynamic description of aqueous nonelectrolytes at infinite dilution over a wide range of state parameters. Geochimica et Cosmochimica Acta 67, 613-629.

Akinfiev, N.N., Diamond, L.W., 2010. Thermodynamic model of aqueous CO_2-H_2O-NaCl solutions from- 22 to 100° C and from 0.1 to 100 MPa. Fluid Phase Equilibria 295, 104-124.

Al-Ajmi, M.F., Alomair, O.A., Elsharkawy, A.M., 2009. Planning miscibility tests and gas injection projects for four major Kuwaiti reservoirs, Kuwait International Petroleum Conference and Exhibition. OnePetro.

Al Ghafri, S.Z., Maitland, G.C., Trusler, J.M., 2014. Experimental and modeling study of the phase behavior of synthetic crude oil+CO_2. Fluid Phase Equilibria 365, 20-40.

Alboudwarej, H., Akbarzadeh, K., Beck, J., Svrcek, W.Y., Yarranton, H.W., 2003. Regular solution model for asphaltene precipitation from bitumens and solvents. AIChE Journal 49, 2948-2956.

Alston, R., Kokolis, G., James, C., 1985. CO_2 minimum miscibility pressure: a correlation for impure CO_2 streams and live oil systems. SPE Journal 25, 268-274.

Ammar, M., Renon, H., 1987. The isothermal flash problem: new methods for phase split calculations. AIChE Journal 33, 926-939.

Anderko, A., Pitzer, K.S., 1993. Equation-of-state representation of phase equilibria and volumetric properties of the system NaCl-H_2O above 573 K. Geochimica et Cosmochimica Acta 57, 1657-1680.

Andersen, S.I., Speight, J.G., 1999. Thermodynamic models for asphaltene solubility and precipitation. Journal of Petroleum Science and Engineering 22, 53-66.

Angle, C.W., Long, Y., Hamza, H., Lue, L., 2006. Precipitation of asphaltenes from solvent-diluted heavy oil and thermodynamic properties of solvent-diluted heavy oil solutions. Fuel 85, 492-506.

Arya, A., Liang, X., Von Solms, N., Kontogeorgis, G.M., 2016a. Modeling of asphaltene onset precipitation conditions with cubic plus association (CPA) and

perturbed chain statistical associating fluid theory (PC-SAFT) equations of state. Energy & Fuels 30, 6835-6852.

Arya, A., Liang, X., von Solms, N., Kontogeorgis, G.M., 2017a. Modeling of asphaltene precipitation from crude oil with the cubic plus association equation of state. Energy & Fuels 31, 2063-2075.

Arya, A., Liang, X., von Solms, N., Kontogeorgis, G.M., 2017b. Prediction of gas injection effect on asphaltene precipitation onset using the cubic and cubic-plus-association equations of state. Energy & Fuels 31, 3313-3328.

Arya, A., von Solms, N., Kontogeorgis, G.M., 2015. Determination of asphaltene onset conditions using the cubic plus association equation of state. Fluid Phase Equilibria 400, 8-19.

Arya, A., von Solms, N., Kontogeorgis, G.M., 2016b. Investigation of the gas injection effect on asphaltene onset precipitation using the cubic-plus-association equation of state. Energy & Fuels 30, 3560-3574.

Asselineau, L., Bogdanic, G., Vidal, J., 1979. A versatile algorithm for calculating vapour-liquid equilibria. Fluid Phase Equilibria 3, 273-290.

Austegard, A., Solbraa, E., De Koeijer, G., Mølnvik, M.J., 2006. Thermodynamic models for calculating mutual solubilities in H_2O-CO_2-CH_4 mixtures. Chemical Engineering Research and Design 84, 781-794.

Avlonitis, D., Danesh, A., Todd, A., 1994. Prediction of VL and VLL equilibria of mixtures containing petroleum reservoir fluids and methanol with a cubic EoS. Fluid Phase Equilibria 94, 181-216.

Bachu, S., 2008. CO_2 storage in geological media: Role, means, status and barriers to deployment. Progress in Energy and Combustion Science 34, 254-273.

Badamchi-Zadeh, A., Yarranton, H., Maini, B.B., Satyro, M., 2009a. Phase behaviour and physical property measurements for VAPEX solvents: part II. propane, carbon dioxide and Athabasca bitumen. Journal of Canadian Petroleum Technology 48, 57-65.

Badamchi-Zadeh, A., Yarranton, H., Svrcek, W., Maini, B., 2009b. Phase behaviour and physical property measurements for VAPEX solvents: Part I. Propane and Athabasca bitumen. Journal of Canadian Petroleum Technology 48, 54-61.

Bamberger, A., Sieder, G., Maurer, G., 2000. High-pressure (vapor+liquid) equilibrium in binary mixtures of (carbon dioxide+ water or acetic acid) at temperatures from 313 to 353 K. The Journal of Supercritical Fluids 17, 97-110.

Behbahani, T.J., Ghotbi, C., Taghikhani, V., Shahrabadi, A., 2011. Experimental investigation and thermodynamic modeling of asphaltene precipitation. Scientia Iranica 18, 1384-1390.

Bennett, J., Schmidt, K.A., 2017. Comparison of phase identification methods used in oil industry flow simulations. Energy & Fuels 31, 3370-3379.

Bermejo, M.D., Martín, A., Florusse, L.J., Peters, C.J., Cocero, M.J., 2005. The influence of Na_2SO_4 on the CO_2 solubility in water at high pressure. Fluid Phase Equilibria 238, 220-228.

Beygi, M.R., Delshad, M., Wheeler, M.F., Pope, G.A., 2016. Aqueous Phase Relative Permeability from a Unified Thermodynamics-Petrophysics-Geochemistry-Electrolyte Model, SPE Western Regional Meeting. OnePetro.

Blencoe, J.G., Naney, M.T., Anovitz, L.M., 2001. The CO_2-H_2O system: III. A new experimental method for determining liquid-vapor equilibria at high subcritical temperatures. American Mineralogist 86, 1100-1111.

Boek, E.S., Yakovlev, D.S., Headen, T.F., 2009. Quantitative molecular representation of asphaltenes and molecular dynamics simulation of their aggregation. Energy & Fuels 23, 1209-1219.

Brent, R.P., 1971. An algorithm with guaranteed convergence for finding a zero of a function. The Computer Journal 14, 422-425.

Buckley, J., Hirasaki, G., Liu, Y., Von Drasek, S., Wang, J., Gill, B., 1998. Asphaltene precipitation and solvent properties of crude oils. Petroleum Science and Technology 16, 251-285.

Buenrostro-Gonzalez, E., Lira-Galeana, C., Gil-Villegas, A., Wu, J., 2004. Asphaltene precipitation in crude oils: theory and experiments. AIChE Journal 50, 2552-2570.

Cao, C., Liu, H., Hou, Z., Mehmood, F., Liao, J., Feng, W., 2020. A review of CO_2 storage in view of safety and cost-effectiveness. Energies 13, 600.

Carroll, J.J., Slupsky, J.D., Mather, A.E., 1991. The solubility of carbon dioxide in water at low pressure. Journal of Physical and Chemical Reference Data 20, 1201-1209.

Chabab, S., Théveneau, P., Corvisier, J., Coquelet, C., Paricaud, P., Houriez, C., El Ahmar, E., 2019. Thermodynamic study of the CO_2-H_2O-NaCl system: Measurements of CO_2 solubility and modeling of phase equilibria using Soreide and Whitson, electrolyte CPA and SIT models. International Journal of Greenhouse Gas Control 91, 102825.

Chaback, J., Harmon, R., Grigg, R., 1989. Discussion of vapor-density measurement for estimating minimum miscibility pressure. SPE Reservoir Engineering 4, 253-254.

Chang, Y.-B., 1990. Development and application of an equation of state compositional simulator. The University of Texas at Austin.

Chang, Y.-B., Coats, B.K., Nolen, J.S., 1996. A compositional model for CO_2 floods including CO_2 solubility in water, Permian Basin Oil and Gas Recovery Conference. OnePetro.

Chapman, W.G., Gubbins, K.E., Jackson, G., Radosz, M., 1990a. New reference equation of state for associating liquids. Industrial & Engineering Chemistry Research 29, 1709-1721.

Chapoy, A., Mohammadi, A., Chareton, A., Tohidi, B., Richon, D., 2004. Measurement and modeling of gas solubility and literature review of the properties for the carbon dioxide-water system. Industrial & Engineering Chemistry Research 43, 1794-1802.

Chen, Z., Li, R., Li, H., 2021. An improved vapor-liquid-asphaltene three-phase equilibrium computation algorithm. Fluid Phase Equilibria 537, 113004.

Chen, Z., Li, R., Li, H., 2022a. A new vapor-liquid-asphaltene three-phase equilibrium computation algorithm based on the free-asphaltene assumption. Fluid Phase Equilibria, 113392.

Chen, Z., Xu, L., Zhou, Y., Li, R., Li, H., 2023. A robust and efficient algorithm for vapor-liquid-equilibrium/liquid-liquid-equilibrium (VLE/LLE) phase boundary tracking. Chemical Engineering Science 266, 118286.

Chen, Z., Zhou, Y., Li, H., 2022b. A review of phase behavior mechanisms of CO_2 EOR and storage in subsurface formations. Industrial & Engineering Chemistry Research 61, 10298-10318.

Chueh, P., Prausnitz, J., 1967. Vapor-liquid equilibria at high pressures: Calculation of partial molar volumes in nonpolar liquid mixtures. AIChE Journal 13, 1099-1107.

Cimino, R., Correra, S., Sacomani, P., Carniani, C., 1995. Thermodynamic modelling for prediction of asphaltene deposition in live oils, SPE International Symposium on Oilfield Chemistry. OnePetro.

Connolly, M., Pan, H., Tchelepi, H., 2019. Three-phase equilibrium computations for hydrocarbon-water mixtures using a reduced variables method. Industrial & Engineering Chemistry Research 58, 14954-14974.

Correra, S., Merino-Garcia, D., 2007. Simplifying the thermodynamic modeling of asphaltenes in upstream operations. Energy & Fuels 21, 1243-1247.

Creek, J.L., 2005. Freedom of action in the state of asphaltenes: Escape from conventional wisdom. Energy & Fuels 19, 1212-1224.

Cronquist, C., 1978. Carbon dioxide dynamic miscibility with light reservoir oils, Fourth Annual US DOE Symposium, Tulsa, 28-30.

Crovetto, R., 1991. Evaluation of solubility data of the system CO_2-H_2O from 273 K to the critical point of water. Journal of Physical and Chemical Reference Data 20, 575-589.

Czarnecki, J., 2009. Stabilization of water in crude oil emulsions. Part 2. Energy & Fuels 23, 1253-1257.

Czarnecki, J., Tchoukov, P., Dabros, T., 2012. Possible role of asphaltenes in the stabilization of water-in-crude oil emulsions. Energy & Fuels 26, 5782-5786.

Darabi, H., Shirdel, M., Kalaei, M.H., Sepehrnoori, K., 2014. Aspects of modeling asphaltene deposition in a compositional coupled wellbore/reservoir simulator, SPE Improved Oil Recovery Symposium. OnePetro.

Darwish, N., Hilal, N., 2010. A simple model for the prediction of CO_2 solubility in H_2O-NaCl system at geological sequestration conditions. Desalination 260, 114-118.

De Boer, R., Leerlooyer, K., Eigner, M., Van Bergen, A., 1995. Screening of crude oils for asphalt precipitation: theory, practice, and the selection of inhibitors. SPE Production & Facilities 10, 55-61.

Deng, K., Lin, Y., Ning, H., Liu, W., Singh, A., Zhang, G., 2018. Influences of temperature and pressure on CO_2 solubility in saline solutions in simulated oil and gas well environments. Applied Geochemistry 99, 22-30.

Dicharry, R.M., Perryman, T., Ronquille, J., 1973. Evaluation and design of a CO_2 miscible flood project-SACROC unit, Kelly-Snyder field. Journal of Petroleum Technology 25, 1309-1318.

Dindoruk, B., Johns, R., Orr, F.M., 2021. Measurement and modeling of minimum miscibility pressure: a state-of-the-art review. SPE Reservoir Evaluation & Engineering 24, 367-389.

Dong, M., Huang, S., Dyer, S.B., Mourits, F.M., 2001. A comparison of CO_2 minimum miscibility pressure determinations for Weyburn crude oil. Journal of Petroleum Science and Engineering 31, 13-22.

dos Santos, P.F., André, L., Ducousso, M., Lassin, A., Contamine, F., Lach, A., Parmentier, M., Cézac, P., 2021. An improved model for CO_2 solubility in aqueous Na^+-Cl-SO_4^{2-} systems up to 473.15 K and 40 MPa. Chemical Geology 582, 120443.

Drummond Jr, S.E., 1981. Boiling and mixing of hydrothermal fluids: chemical effects on mineral precipitation. The Pennsylvania State University.

Duan, Z., Møller, N., Greenberg, J., Weare, J.H., 1992. The prediction of methane solubility in natural waters to high ionic strength from 0 to 250 °C and from 0 to 1600 bar. Geochimica et Cosmochimica Acta 56, 1451-1460.

Duan, Z., Sun, R., 2003. An improved model calculating CO_2 solubility in pure water and aqueous NaCl solutions from 273 to 533 K and from 0 to 2000 bar. Chemical Geology 193, 257-271.

Duan, Z., Sun, R., Zhu, C., Chou, I.-M., 2006. An improved model for the calculation of CO_2 solubility in aqueous solutions containing Na^+, K^+, Ca^{2+}, Mg^{2+}, Cl^-, and SO_4^{2-}. Marine Chemistry 98, 131-139.

Eakin, B., Mitch, F., 1988. Measurement and correlation of miscibility pressures of reservoir oils, SPE Annual Technical Conference and Exhibition. OnePetro.

Emera, M.K., Sarma, H.K., 2005. Use of genetic algorithm to estimate CO_2-oil minimum miscibility pressure-a key parameter in design of CO_2 miscible flood. Journal of Petroleum Science and Engineering 46, 37-52.

Enick, R.M., Klara, S.M., 1990. CO_2 solubility in water and brine under reservoir conditions. Chemical Engineering Communications 90, 23-33.

Ennis-King, J., Paterson, L., 2002. Engineering aspects of geological sequestration of carbon dioxide, SPE Asia Pacific Oil and Gas Conference and Exhibition. OnePetro.

Eshraghi, S.E., Rasaei, M.R., Zendehboudi, S.J., 2016. Optimization of miscible CO_2 EOR and storage using heuristic methods combined with capacitance/resistance and Gentil fractional flow models. Journal of Natural Gas Science and Engineering 32, 304-318.

Fazelipour, W., 2011. Predicting asphaltene precipitation in oilfields via the technology of compositional reservoir simulation, SPE International Symposium on Oilfield Chemistry. OnePetro.

Flory, P.J., 1941. Thermodynamics of high polymer solutions. The Journal of Chemical Physics 9, 660-660.

Flory, P.J., 1942. Thermodynamics of high polymer solutions. The Journal of Chemical Physics 10, 51-61.

Freed, D.E., Mullins, O.C., Zuo, J.Y., 2010. Theoretical treatment of asphaltene gradients in the presence of GOR gradients. Energy & Fuels 24, 3942-3949.

Fussell, L.T., 1979. A technique for calculating multiphase equilibria (includes associated papers 8734 and 8746). SPE Journal 19, 203-210.

Gardner, J., Orr, F., Patel, P., 1981. The effect of phase behavior on CO_2-flood displacement efficiency. Journal of Petroleum Technology 33, 2067-2081.

Ghomian, Y., 2008. Reservoir simulation studies for coupled carbon dioxide sequestration and enhanced oil recovery. The University of Texas at Austin.

Glaso, O., 1985. Generalized minimum miscibility pressure correlation (includes associated papers 15845 and 16287). SPE Journal 25, 927-934.

Gonzalez, D.L., Hirasaki, G.J., Creek, J., Chapman, W.G., 2007a. Modeling of asphaltene precipitation due to changes in composition using the perturbed chain statistical associating fluid theory equation of state. Energy & Fuels 21, 1231-1242.

Gonzalez, D.L., Hirasaki, G.J., Creek, J., Chapman, W.G., 2007b. Modeling of asphaltene precipitation due to changes in composition using the perturbed chain statistical associating fluid theory equation of state. Energy & Fuels 21, 1231-1242.

Gonzalez, D.L., Mahmoodaghdam, E., Lim, F., Joshi, N., 2012a. Effects of gas additions to deepwater Gulf of Mexico reservoir oil: Experimental investigation of asphaltene precipitation and deposition, SPE Annual Technical Conference and Exhibition. OnePetro.

Gonzalez, D.L., Ting, P.D., Hirasaki, G.J., Chapman, W.G., 2005. Prediction of asphaltene instability under gas injection with the PC-SAFT equation of state. Energy & Fuels 19, 1230-1234.

Gonzalez, D.L., Vargas, F.M., Hirasaki, G.J., Chapman, W.G., 2008. Modeling study of CO_2-induced asphaltene precipitation. Energy & Fuels 22, 757-762.

Gonzalez, D.L., Vargas, F.M., Mahmoodaghdam, E., Lim, F., Joshi, N., 2012. Asphaltene stability prediction based on dead oil properties: Experimental evaluation. Energy & Fuels 26, 6218-6227.

Gonzalez Rodriguez, D.L., 2008. Modeling of asphaltene precipitation and deposition tendency using the PC-SAFT equation of state. Rice University.

Gosset, R., Heyen, G., Kalitventzeff, B., 1986. An efficient algorithm to solve cubic equations of state. Fluid Phase Equilibria 25, 51-64.

Goual, L., 2009. Impedance spectroscopy of petroleum fluids at low frequency. Energy & Fuels 23, 2090-2094.

Graue, D.J., Zana, E., 1981. Study of a possible CO_2 flood in Rangely Field. Journal of Petroleum Technology 33, 1312-1318.

Gross, J., Sadowski, G., 2001a. Perturbed-chain SAFT: An equation of state based on a perturbation theory for chain molecules. Industrial Engineering Chemistry Research 40, 1244-1260.

Gross, J., Sadowski, G., 2001b. Perturbed-chain SAFT: An equation of state based on a perturbation theory for chain molecules. Industrial & Engineering Chemistry Research 40, 1244-1260.

Haynes, S., Alston, R., 1990. Study of the mechanisms of carbon dioxide flooding and applications to more efficient EOR projects, SPE/DOE Enhanced Oil Recovery Symposium. OnePetro.

Henry, R.L., Metcalfe, R.S., 1983. Multiple-phase generation during carbon dioxide flooding. SPE Journal 23, 595-601.

Henry, W., 1803. III. Experiments on the quantity of gases absorbed by water, at different temperatures, and under different pressures. Philosophical Transactions of the Royal Society of London, 29-274.

Hildebrand, J.H., 1919. Solubility. III. Relative values of internal pressures and their practical application. Journal of the American Chemical Society 41, 1067-1080.

Hill, P.G., 1990. A unified fundamental equation for the thermodynamic properties of H_2O. Journal of Physical and Chemical Reference Data 19, 1233-1274.

Hirschberg, A., deJong, L.N., Schipper, B., Meijer, J., 1984. Influence of temperature and pressure on asphaltene flocculation. SPE Journal 24, 283-293.

Holm, L., Josendal, V., 1974. Mechanisms of oil displacement by carbon dioxide. Journal of Petroleum Technology 26, 1427-1438.

Holm, L., O'Brien, L., 1971. Carbon dioxide test at the Mead-Strawn Field. Journal of Petroleum Technology 23, 431-442.

Holm, L.W., Josendal, V.A., 1982. Effect of oil composition on miscible-type displacement by carbon dioxide. SPE Journal 22, 87-98.

Holm, W.L., 1987. Evolution of the carbon dioxide flooding processes. Journal of Petroleum Technology 39, 1337-1342.

Hou, S.-X., Maitland, G.C., Trusler, J.M., 2013. Phase equilibria of (CO_2+ H_2O+ NaCl) and (CO_2+ H_2O+ KCl): Measurements and modeling. The Journal of Supercritical Fluids 78, 78-88.

Huang, E.T., Tracht, J.H., 1974. The displacement of residual oil by carbon dioxide, SPE Improved Oil Recovery Symposium. OnePetro.

Huang, S.H., Radosz, M., 1990. Equation of state for small, large, polydisperse, and associating molecules. Industrial & Engineering Chemistry Research 29, 2284-2294.

Huggins, M.L., 1941. Solutions of long chain compounds. The Journal of Chemical Physics 9, 440-440.

Huron, M.-J., Vidal, J., 1979. New mixing rules in simple equations of state for representing vapour-liquid equilibria of strongly non-ideal mixtures. Fluid Phase Equilibria 3, 255-271.

Husodo, W., Sudibjo, R., Walsh, B.W., 1985. Laboratory experiment on CO_2 injection.

IEA., 2019. Energy Technology Perspectives, Scenarios and Strategies to 2050.

Iglauer, S., 2018. Optimum storage depths for structural CO_2 trapping. International Journal of Greenhouse Gas Control 77, 82-87.

Imai, M., Pan, H., Connolly, M., Tchelepi, H., Kurihara, M., 2019. Reduced variables method for four-phase equilibrium calculations of hydrocarbon-water-CO_2 mixtures at a low temperature. Fluid Phase Equilibria 497, 151-163.

Jacob, R., Saylor, B.Z., 2016. CO_2 solubility in multi-component brines containing NaCl, KCl, $CaCl_2$ and $MgCl_2$ at 297 K and 1-14 MPa. Chemical Geology 424, 86-95.

Jacobson, H., 1972. Acid gases and their contribution to miscibility. Journal of Canadian Petroleum Technology 11, 56-59.

Jamaluddin, A., Creek, J., Kabir, C., McFadden, J., D'cruz, D., Manakalathil, J., Joshi, N., Ross, B., 2002a. Laboratory techniques to measure thermodynamic asphaltene instability. Journal of Canadian Petroleum Technology 41, 44-52.

Jamaluddin, A., Joshi, N., Iwere, F., Gurpinar, O., 2002b. An investigation of asphaltene instability under nitrogen injection, SPE International Petroleum Conference and Exhibition in Mexico. OnePetro.

Jamaluddin, A., Nighswander, J., Kohse, B.F., El Mahdi, A., Binbrek, M., Hogg, P., 2000. Experimental and theoretical assessment of the asphaltene precipitation

characteristics of the Sahil field under a proposed miscible gas injection scheme, SPE Abu Dhabi International Petroleum Exhibition and Conference. OnePetro.

Jaubert, J.-N., Avaullee, L., Souvay, J.-F., 2002. A crude oil data bank containing more than 5000 PVT and gas injection data. Journal of Petroleum Science and Engineering 34, 65-107.

Jaubert, J.-N., Wolff, L., Neau, E., Avaullee, L., 1998. A very simple multiple mixing cell calculation to compute the minimum miscibility pressure whatever the displacement mechanism. Industrial & Engineering Chemistry Research 37, 4854-4859.

Jessen, K., Michelsen, M.L., Stenby, E.H., 1998. Global approach for calculation of minimum miscibility pressure. Fluid Phase Equilibria 153, 251-263.

Johns, R.T., Dindoruk, B., Orr, F., 1993. Analytical theory of combined condensing/vaporizing gas drives. SPE Advanced Technology Series 1, 7-16.

Johns, R.T., Orr, F.M., 1996. Miscible gas displacement of multicomponent oils. SPE Journal 1, 39-50.

Kalorazi, B.T., 1995. Gas hydrate equilibria in the presence of electrolyte solutions. Heriot-Watt University.

Kawanaka, S., Park, S.J., Mansoori, G.A., 1991. Organic deposition from reservoir fluids: a thermodynamic predictive technique. SPE Reservoir Engineering 6, 185-192.

Kesler, M.G., Lee, B.I., 1976. Improve prediction of enthalpy of fractions. Hydrocarbon Process 55, 153-158.

Khan, S., Pope, G., Sepehrnoori, K., 1992. Fluid characterization of three-phase CO_2/oil mixtures, SPE/DOE Enhanced Oil Recovery Symposium. OnePetro.

Kohse, B.F., Nghiem, L.X., Maeda, H., Ohno, K., 2000. Modelling phase behaviour including the effect of pressure and temperature on asphaltene precipitation, SPE Asia Pacific Oil and Gas Conference and Exhibition. OnePetro.

Kontogeorgis, G.M., Voutsas, E.C., Yakoumis, I.V., Tassios, D.P., 1996. An equation of state for associating fluids. Industrial & Engineering Chemistry Research 35, 4310-4318.

Kord, S., Ayatollahi, S., 2012. Asphaltene precipitation in live crude oil during natural depletion: Experimental investigation and modeling. Fluid Phase Equilibria 336, 63-70.

Kosinski, J.J., Anderko, A., 2001. Equation of state for high-temperature aqueous electrolyte and nonelectrolyte systems. Fluid Phase Equilibria 183, 75-86.

Kraiwattanawong, K., Fogler, H.S., Gharfeh, S.G., Singh, P., Thomason, W.H., Chavadej, S., 2007. Thermodynamic solubility models to predict asphaltene instability in live crude oils. Energy & Fuels 21, 1248-1255.

Kraska, T., Gubbins, K.E., 1996. Phase equilibria calculations with a modified SAFT equation of state. 1. Pure alkanes, alkanols, and water. Industrial & Engineering Chemistry Research 35, 4727-4737.

Lake, L.W., Johns, R., Rossen, B., Pope, G.A., 2014. Fundamentals of enhanced oil recovery. Society of Petroleum Engineers.

Lapene, A., Nichita, D.V., Debenest, G., Quintard, M., 2010. Three-phase free-water flash calculations using a new modified Rachford-Rice equation. Fluid Phase Equilibria 297, 121-128.

Lara Cruz, J., Neyrolles, E., Contamine, F.o., Cézac, P., 2020. Experimental study of carbon dioxide solubility in sodium chloride and calcium chloride brines at 333.15 and 453.15 K for pressures up to 40 MPa. Journal of Chemical & Engineering Data 66, 249-261.

Lebowitz, J.L., Helfand, E., Praestgaard, E., 1965. Scaled particle theory of fluid mixtures. The Journal of Chemical Physics 43, 774-779.

Lee, B.I., Kesler, M.G., 1975. A generalized thermodynamic correlation based on three-parameter corresponding states. AIChE Journal 21, 510-527.

Lee, I., 1979. Effectiveness of carbon dioxide displacement under miscible and immiscible conditions. Technical Report.

Leekumjorn, S., Risum, R. B., Sørensen, H., Krejbjerg, K., 2020. Asphaltene modeling with cubic and more complex equations of state, Abu Dhabi International Petroleum Exhibition & Conference. OnePetro.

Leibovici, C.F., Nichita, D.V., 2008. A new look at multiphase Rachford-Rice equations for negative flashes. Fluid Phase Equilibria 267, 127-132.

Leontaritis, K.J., Mansoori, G.A., 1987. Asphaltene flocculation during oil production and processing: A thermodynamic collodial model, SPE International Symposium on Oilfield Chemistry. OnePetro.

Li, C., 1971. Critical temperature estimation for simple mixtures. The Canadian Journal of Chemical Engineering 49, 709-710.

Li, H., 2021. Multiphase equilibria of complex reservoir fluids: an equation of state modeling approach. Springer Nature.

Li, H., Qin, J., Yang, D., 2012. An improved CO_2-oil minimum miscibility pressure correlation for live and dead crude oils. Industrial & Engineering Chemistry Research 51, 3516-3523.

Li, H., Yang, D., Li, X., 2013. Determination of three-phase boundaries of solvent (s)-CO_2-heavy oil systems under reservoir conditions. Energy & Fuels 27, 145-153.

Li, R., Li, H., 2019a. A modified multiple-mixing-cell algorithm for minimum miscibility pressure prediction with the consideration of the asphaltene-precipitation effect. Industrial & Engineering Chemistry Research 58, 15332-15343.

Li, R., Li, H., 2019b. Robust three-phase vapor-liquid-asphaltene equilibrium calculation algorithm for isothermal CO_2 flooding applications. Industrial & Engineering Chemistry Research 58, 15666-15680.

Li, R., Li, H.A., 2018. New two-phase and three-phase Rachford-Rice algorithms based on free-water assumption. The Canadian Journal of Chemical Engineering 96, 390-403.

Li, S., Xu, L., Li, H., 2022. Four-phase flash calculation algorithm based on the free-water assumption. Industrial & Engineering Chemistry Research 61, 3742-3753.

Li, S., Xu, L., Li, H., 2023. A robust four-phase equilibrium calculation algorithm based on the scaled trust-region method for water/hydrocarbon mixtures. To be submitted to Chemical Engineering Science.

Li, X., Yang, D., 2013. Determination of mutual solubility between CO_2 and water by using the Peng-Robinson equation of state with modified alpha function and binary interaction parameter. Industrial & Engineering Chemistry Research 52, 13829-13838.

Li, Y.K., Nghiem, L.X., 1986. Phase equilibria of oil, gas and water/brine mixtures from a cubic equation of state and Henry's law. The Canadian Journal of Chemical Engineering 64, 486-496.

Li, Z., Firoozabadi, A., 2012a. General strategy for stability testing and phase-split calculation in two and three phases. SPE Journal 17, 1096-1107.

Li, Z., Firoozabadi, A., 2012b. Initialization of phase fractions in Rachford-Rice equations for robust and efficient three-phase split calculation. Fluid Phase Equilibria 332, 21-27.

Liao, C., Liao, X., Zhao, X., Ding, H., Liu, X., Liu, Y., Chen, J., Lu, N., 2014. Comparison of different methods for determining key parameters affecting CO_2 storage capacity in oil reservoirs. International Journal of Greenhouse Gas Control 28, 25-34.

Liu, Y., Hou, M., Yang, G., Han, B., 2011. Solubility of CO_2 in aqueous solutions of NaCl, KCl, $CaCl_2$ and their mixed salts at different temperatures and pressures. The Journal of Supercritical Fluids 56, 125-129.

Lu, C., Jin, Z., Li, H., Xu, L., 2021b. Simple and robust algorithm for multiphase equilibrium computations at temperature and volume specifications. SPE Journal 26, 2397-2416.

Lucas, M.A., Borges, G.R., da Rocha, I.C., Santos, A.F., Franceschi, E., Dariva, C., 2016. Use of real crude oil fractions to describe the high pressure phase behavior of crude oil in carbon dioxide. The Journal of Supercritical Fluids 118, 140-147.

Mader, U., 1991. H_2O-CO_2 mixtures: A review of PVTX data and an assessment from a phase-equilibrium point of view. Canadian Mineralogist 29, 767-790.

Malik, Q.M., Islam, M., 2000. CO_2 Injection in the Weyburn field of Canada: optimization of enhanced oil recovery and greenhouse gas storage with horizontal wells, SPE/DOE improved oil recovery symposium. OnePetro.

Mather, A.E., Franck, E.U., 1992. Phase equilibria in the system carbon dioxide-water at elevated pressures. The Journal of Physical Chemistry 96, 6-8.

Mathias, P.M., Copeman, T.W., 1983. Extension of the Peng-Robinson equation of state to complex mixtures: evaluation of the various forms of the local composition concept. Fluid Phase Equilibria 13, 91-108.

Mehra, R.K., Heidemann, R.A., Aziz, K., 1982. Computation of multiphase equilibrium for compositional simulation. SPE Journal 22, 61-68.

Mehra, R.K., Heidemann, R.A., Aziz, K., 1983. An accelerated successive substitution algorithm. The Canadian Journal of Chemical Engineering 61, 590-596.

Melhem, G.A., Saini, R., Goodwin, B.M., 1989. A modified Peng-Robinson equation of state. Fluid Phase Equilibria 47, 189-237.

Memon, A., Qassim, B., Al-Ajmi, M., Kumar Tharanivasan, A., Gao, J., Ratulowski, J., Al-Otaibi, B., Khan, R.A., 2012. Miscible gas injection and asphaltene flow assurance fluid characterization: a laboratory case study for a black oil reservoir, SPE EOR Conference at Oil and Gas West Asia. OnePetro.

Metcalfe, R., Fussell, D., Shelton, J., 1973. A multicell equilibrium separation model for the study of multiple contact miscibility in rich-gas drives. SPE Journal 13, 147-155.

Metcalfe, R., Yarborough, L., 1974. Discussion of mechanisms of oil displacement by carbon dioxide. Journal of Petroleum Technology 26, 1436-1437.

Metcalfe, R.S., 1982. Effects of impurities on minimum miscibility pressures and minimum enrichment levels for CO_2 and rich-gas displacements. SPE Journal 22, 219-225.

Michelsen, M., 1994. Calculation of multiphase equilibrium. Computers & Chemical Engineering 18, 545-550.

Michelsen, M.L., 1982a. The isothermal flash problem. Part I. Stability. Fluid Phase Equilibria 9, 1-19.

Michelsen, M.L., 1982b. The isothermal flash problem. Part II. Phase-split calculation. Fluid Phase Equilibria 9, 21-40.

Mohanty, K., Masino, W., Ma, T., Nash, L., 1995. Role of three-hydrocarbon-phase flow in a gas-displacement process. SPE Reservoir Engineering 10, 214-221.

Mohebbinia, S., Sepehrnoori, K., Johns, R.T., 2013. Four-phase equilibrium calculations of carbon dioxide/hydrocarbon/water systems with a reduced method. SPE Journal 18, 943-951.

Mohebbinia, S., Sepehrnoori, K., Johns, R.T., Korrani, A.K.N., 2017a. Simulation of asphaltene precipitation during gas injection using PC-SAFT EOS. Journal of Petroleum Science Engineering 158, 693-706.

Mohebbinia, S., Sepehrnoori, K., Johns, R.T., Korrani, A.K.N., 2017b. Simulation of asphaltene precipitation during gas injection using PC-SAFT EOS. Journal of Petroleum Science and Engineering 158, 693-706.

Møller, N., 1988. The prediction of mineral solubilities in natural waters: A chemical equilibrium model for the Na-Ca-Cl-SO_4-H_2O system, to high temperature and concentration. Geochimica et Cosmochimica Acta 52, 821-837.

Mullins, O.C., 2010. The modified Yen model. Energy & Fuels 24, 2179-2207.

Mullins, O.C., Sheu, E.Y., Hammami, A., Marshall, A.G., 2007. Asphaltenes, heavy oils, and petroleomics. Springer Science & Business Media.

Nascimento, F.b.P., Souza, M.M., Costa, G.M., Vieira de Melo, S.A., 2018. Modeling of the asphaltene onset pressure from few experimental data: A comparative evaluation of the Hirschberg method and the cubic-plus-association equation of state. Energy & Fuels 33, 3733-3742.

Nasrabadi, H., Moortgat, J., Firoozabadi, A., 2013. A new three-phase multicomponent compositional model for asphaltene precipitation using CPA-EOS, SPE Reservoir Simulation Symposium. OnePetro.

Nasrabadi, H., Moortgat, J., Firoozabadi, A., 2016. New three-phase multicomponent compositional model for asphaltene precipitation during CO_2 injection using CPA-EOS. Energy & Fuels 30, 3306-3319.

Nellensteyn, F., 1938. The colloidal structure of bitumens. The Science of Petroleum 4, 401.

Neshat, S.S., Okuno, R., Pope, G.A., 2020. Simulation of solvent treatments for fluid blockage removal in tight formations using coupled three-phase flash and capillary pressure models. Journal of Petroleum Science and Engineering 195, 107442.

Nghiem, L., Hassam, M., Nutakki, R., George, A., 1993a. Efficient modelling of asphaltene precipitation, SPE Annual Technical Conference and Exhibition. OnePetro.

Nghiem, L., Heidemann, R., 1982. General acceleration procedure for multiphase flash calculation with application to oil-gas-water systems, Proceedings of the 2nd European Symposium on Enhanced Oil Recovery, 303-316.

Nghiem, L.X., Li, Y.-K., 1984. Computation of multiphase equilibrium phenomena with an equation of state. Fluid Phase Equilibria 17, 77-95.

Nguele, R., Ghulami, M.R., Sasaki, K., Said-Al Salim, H., Widiatmojo, A., Sugai, Y., Nakano, M., 2016a. Asphaltene aggregation in crude oils during supercritical gas injection. Energy & Fuels 30, 1266-1278.

Ni, H., Boon, M., Garing, C., Benson, S.M., 2019. Predicting CO_2 residual trapping ability based on experimental petrophysical properties for different sandstone types. International Journal of Greenhouse Gas Control 86, 158-176.

Okuno, R., Johns, R., Sepehrnoori, K., 2010a. A new algorithm for Rachford-Rice for multiphase compositional simulation. SPE Journal 15, 313-325.

Okuno, R., Johns, R.T., Sepehrnoori, K., 2011. Mechanisms for high displacement efficiency of low-temperature CO_2 floods. SPE Journal 16, 751-767.

Orr, F., Jensen, C., 1984. Interpretation of pressure-composition phase diagrams for CO_2/crude-oil systems. SPE Journal 24, 485-497.

Orr, F., Yu, A., Lien, C., 1981. Phase behavior of CO_2 and crude oil in low-temperature reservoirs. SPE Journal 21, 480-492.

Orr Jr, F., Taber, J.J., 1981. Displacement of oil by carbon dioxide. Final report. New Mexico Institute of Mining and Technology, Socorro (USA).

Pan, H., Chen, Y., Sheffield, J., Chang, Y.-B., Zhou, D., 2015. Phase-behavior modeling and flow simulation for low-temperature CO_2 injection. SPE Reservoir Evaluation & Engineering 18, 250-263.

Pan, H., Connolly, M., Tchelepi, H., 2019. Multiphase equilibrium calculation framework for compositional simulation of CO_2 injection in low-temperature reservoirs. Industrial & Engineering Chemistry Research 58, 2052-2070.

Pan, H., Firoozabadi, A., 1998. A thermodynamic micellization model for asphaltene precipitation: Part I: Micellar size and growth. SPE Production & Facilities 13, 118-127.

Pan, H., Firoozabadi, A., 2003. Fast and robust algorithm for compositional modeling: part ii-two-phase flash computations. SPE Journal 8, 380-391.

Pang, W., Li, H.A., 2017. An augmented free-water three-phase Rachford-Rice algorithm for CO_2/hydrocarbons/water mixtures. Fluid Phase Equilibria 450, 86-98.

Panuganti, S.R., Tavakkoli, M., Vargas, F.M., Gonzalez, D.L., Chapman, W.G., 2013. SAFT model for upstream asphaltene applications. Fluid Phase Equilibria 359, 2-16.

Panuganti, S.R., Vargas, F.M., Chapman, W.G., 2012a. Modeling reservoir connectivity and tar mat using gravity-induced asphaltene compositional grading. Energy & Fuels 26, 2548-2557.

Panuganti, S.R., Vargas, F.M., Gonzalez, D.L., Kurup, A.S., Chapman, W.G., 2012b. PC-SAFT characterization of crude oils and modeling of asphaltene phase behavior. Fuel 93, 658-669.

Pasad, G., Venkatarathnam, G., 1999. A method for avoiding trivial roots in isothermal flash calculations using cubic equations of state. Industrial & Engineering Chemistry Research 38, 3530-3534.

Pasqualette, M.d.A., Carneiro, J.N., Johansen, S.T., Løvfall, B.T., Fonseca, R., Ciambelli, J.R., 2020. A numerical assessment of carbon-dioxide-rich two-phase flows with dense phases in offshore production pipelines. SPE Journal 25, 712-731.

Pedersen, K.S., Christensen, P.L., Shaikh, J.A., 2014. Phase behavior of petroleum reservoir fluids. CRC press.

Pedersen, K.S., Fredenslund, A., Thomassen, P., 1989. Properties of oils and natural gases. Gulf Publishing Company.

Peng, D.-Y., Robinson, D.B., 1976. A new two-constant equation of state. Industrial & Engineering Chemistry Fundamentals 15, 59-64.

Pérez-Salado Kamps, Á., Meyer, E., Rumpf, B., Maurer, G., 2007. Solubility of CO_2 in aqueous solutions of KCl and in aqueous solutions of K_2CO_3. Journal of Chemical & Engineering Data 52, 817-832.

Perschke, D.R., 1988. Equation of state phase behavior modeling for compositional simulation. The University of Texas at Austin.

Petitfrere, M., Nichita, D.V., 2014. Robust and efficient trust-region based stability analysis and multiphase flash calculations. Fluid Phase Equilibria 362, 51-68.

Pitzer, K.S., 1973. Thermodynamics of electrolytes. I. Theoretical basis and general equations. The Journal of Physical Chemistry 77, 268-277.

Poling, B.E., Grens, E.A., Prausnitz, J.M., 1981. Thermodynamic properties from a cubic equation of state: avoiding trivial roots and spurious derivatives. Industrial & Engineering Chemistry Process Design and Development 20, 127-130.

Punnapala, S., Vargas, F.M., 2013. Revisiting the PC-SAFT characterization procedure for an improved asphaltene precipitation prediction. Fuel 108, 417-429.

PVT sim Nova, 2019. Calsep A/S: Copenhagen, Denmark.

PVTsim, 2011. PVT sim 20.0, Calsep A/S: Copenhagen, Denmark.

Qin, X., Wang, P., Sepehrnoori, K., Pope, G.A., 2000. Modeling asphaltene precipitation in reservoir simulation. Industrial & Engineering Chemistry Research 39, 2644-2654.

Rachford, H.H., Rice, J., 1952. Procedure for use of electronic digital computers in calculating flash vaporization hydrocarbon equilibrium. Journal of Petroleum Technology 4, 327-328.

Rajan Babu, N., Lin, P.-H., Abutaqiya, M.I., Sisco, C.J., Wang, J., Vargas, F.M., 2018. Systematic investigation of asphaltene deposition in the wellbore and near-wellbore region of a deepwater oil reservoir under gas injection. Part 2: computational fluid dynamics modeling of asphaltene deposition. Energy & Fuels 33, 3645-3661.

Rathmell, J., Stalkup, F., Hassinger, R., 1971. A laboratory investigation of miscible displacement by carbon dioxide, Fall meeting of the society of petroleum engineers of AIME. OnePetro.

Redlich, O., Kwong, J.N., 1949. On the thermodynamics of solutions. V. An equation of state. Fugacities of gaseous solutions. Chemical Reviews 44, 233-244.

Riazi, M., 1980. Simplify property predictions. Hydrocarbon Process 59, 115-116.

Risnes, R., Dalen, V., 1984. Equilibrium calculations for coexisting liquid phases. SPE Journal 24, 87-96.

Scatchard, G., 1931. Equilibria in Non-electrolyte Solutions in Relation to the Vapor Pressures and Densities of the Components. Chemical Reviews 8, 321-333.

Schlumberger, 2015. ECLIPSE: Reservoir Simulation Software, Technical Description, Version 2015.1. Schlumberger: Abingdon, U.K.

Scott, R.L., Magat, M., 1945. The thermodynamics of high-polymer solutions: I. The free energy of mixing of solvents and polymers of heterogeneous distribution. The Journal of Chemical Physics 13, 172-177.

Sebastian, H., Wenger, R., Renner, T., 1985. Correlation of minimum miscibility pressure for impure CO_2 streams. Journal of Petroleum Technology 37, 2076-2082.

Seifert, D.J., Qureshi, A., Zeybek, M., Pomerantz, A.E., Zuo, J.Y., Mullins, O.C., 2012. Heavy oil and tar mat characterization within a single oil column utilizing novel asphaltene science, SPE Kuwait International Petroleum Conference and Exhibition. OnePetro.

Shelton, J., Yarborough, L., 1977a. Multiple phase behavior in porous media during CO_2 or rich-gas flooding. Journal of Petroleum Technology 29, 1171-1178.

Shokir, E.M.E.-M., 2007. CO_2-oil minimum miscibility pressure model for impure and pure CO_2 streams. Journal of Petroleum Science and Engineering 58, 173-185.

Simon, R., Rosman, A., Zana, E., 1978. Phase-behavior properties of CO_2-reservoir oil systems. SPE Journal 18, 20-26.

Simoncelli, A.P., Goméz, W., Charin, R.M., Fleming, F.P., Ndiaye, P.M., Tavares, F.W., 2020. Phase behavior of systems with high CO_2 content: Experiments and thermodynamic modeling. Fluid Phase Equilibria 515, 112574.

Soave, G., 1972. Equilibrium constants from a modified Redlich-Kwong equation of state. Chemical Engineering Science 27, 1197-1203.

Soreide, I., 1989. Improved phase behavior predictions of petroleum reservoir fluids from a cubic equation of state. The Norwegian Institute of Technology.

Søreide, I., Whitson, C.H., 1992. Peng-Robinson predictions for hydrocarbons, CO_2, N_2, and H_2S with pure water and NaCI brine. Fluid Phase Equilibria 77, 217-240.

Speight, J., 2004. Petroleum Asphaltenes-Part 1: Asphaltenes, resins and the structure of petroleum. Oil & Gas Science and Technology 59, 467-477.

Spence, A.P., Watkins, R.W., 1980. The effect of microscopic core heterogeneity on miscible flood residual oil saturation, SPE Annual Technical Conference and Exhibition. OnePetro.

Springer, R.D., Wang, Z., Anderko, A., Wang, P., Felmy, A.R., 2012. A thermodynamic model for predicting mineral reactivity in supercritical carbon dioxide: I. Phase behavior of carbon dioxide-water-chloride salt systems across the H_2O-rich to the CO_2-rich regions. Chemical Geology 322, 151-171.

Spycher, N., Pruess, K., 2005. CO_2-H_2O mixtures in the geological sequestration of CO_2. II. Partitioning in Chloride Brines at 12-100 °C and up to 600 bar. Geochimica et Cosmochimica Acta 69, 3309-3320.

Spycher, N., Pruess, K., 2010. A phase-partitioning model for CO_2-brine mixtures at elevated temperatures and pressures: application to CO_2-enhanced geothermal systems. Transport in Porous Media 82, 173-196.

Spycher, N., Pruess, K., Ennis-King, J., 2003. CO_2-H_2O mixtures in the geological sequestration of CO_2. I. Assessment and calculation of mutual solubilities from 12 to 100 °C and up to 600 bar. Geochimica et Cosmochimica Acta 67, 3015-3031.

Srivastava, R., Huang, S., Dong, M., 1999. Asphaltene deposition during CO_2 flooding. SPE Production & Facilities 14, 235-245.

Srivastava, R., Huang, S., Dong, M., 2000. Laboratory investigation of Weyburn CO_2 miscible flooding. Journal of Canadian Petroleum Technology 39, 41-51.

Stalkup, F.I., 1987. Displacement behavior of the condensing/vaporizing gas drive process, SPE Annual Technical Conference and Exhibition. OnePetro.

Stryjek, R., Vera, J., 1986. PRSV: An improved Peng-Robinson equation of state for pure compounds and mixtures. The Canadian Journal of Chemical Engineering 64, 323-333.

Sun, Q., Ampomah, W., Kutsienyo, E.J., Appold, M., Adu-Gyamfi, B., Dai, Z., Soltanian, M.R., 2020. Assessment of CO_2 trapping mechanisms in partially depleted oil-bearing sands. Fuel 278, 118356.

Sun, R., Dubessy, J., 2010. Prediction of vapor-liquid equilibrium and PVTx properties of geological fluid system with SAFT-LJ EOS including multi-polar contribution. Part I: Application to H_2O-CO_2 system. Geochimica et Cosmochimica Acta 74, 1982-1998.

Sun, R., Dubessy, J., 2012. Prediction of vapor-liquid equilibrium and PVTx properties of geological fluid system with SAFT-LJ EOS including multi-polar contribution. Part II: Application to H_2O-NaCl and CO_2-H_2O-NaCl System. Geochimica et Cosmochimica Acta 88, 130-145.

Sun, X., Wang, Z., Li, H., He, H., Sun, B., 2021. A simple model for the prediction of mutual solubility in CO_2-brine system at geological conditions. Desalination 504, 114972.

Sun, Z., 2021. Phase behavior modeling for carbon dioxide/brine mixtures. MSc Thesis. University of Alberta.

Taber, J., 1994. A study of technical feasibility for the utilization of CO_2 for enhanced oil recovery. The Utilization of Carbon Dioxide from Fossil Fuel Fired Power Stations, 134-204.

Takenouchi, S., Kennedy, G.C., 1964. The binary system H_2O-CO_2 at high temperatures and pressures. American Journal of Science 262, 1055-1074.

Tang, Y., Saha, S., 2003. An efficient method to calculate three-phase free-water flash for water- hydrocarbon systems. Industrial & Engineering Chemistry Research 42, 189-197.

Tavakkoli, M., Chen, A., Vargas, F.M., 2016. Rethinking the modeling approach for asphaltene precipitation using the PC-SAFT Equation of State. Fluid Phase Equilibria 416, 120-129.

Thakur, G., Lin, C., Patel, Y., 1984. CO_2 minitest, little knife field, ND: a case history, SPE Enhanced Oil Recovery Symposium. OnePetro.

Ting, P.D., Hirasaki, G.J., Chapman, W.G., 2003. Modeling of asphaltene phase behavior with the SAFT equation of state. Petroleum Science and Technology 21, 647-661.

Tong, D., Trusler, J.M., Vega-Maza, D., 2013. Solubility of CO_2 in aqueous solutions of CaCl2 or MgCl2 and in a synthetic formation brine at temperatures up to 423 K and pressures up to 40 MPa. Journal of Chemical & Engineering Data 58, 2116-2124.

Tsivintzelis, I., Kontogeorgis, G.M., Michelsen, M.L., Stenby, E.H., 2011. Modeling phase equilibria for acid gas mixtures using the CPA equation of state. Part II: Binary mixtures with CO_2. Fluid Phase Equilibria 306, 38-56.

Twu, C.H., Bluck, D., Cunningham, J.R., Coon, J.E., 1991. A cubic equation of state with a new alpha function and a new mixing rule. Fluid Phase Equilibria 69, 33-50.

Valderrama, J.O., 1990. A generalized Patel-Teja equation of state for polar and nonpolar fluids and their mixtures. Journal of Chemical Engineering of Japan 23, 87-91.

Valtz, A., Chapoy, A., Coquelet, C., Paricaud, P., Richon, D., 2004. Vapour-liquid equilibria in the carbon dioxide-water system, measurement and modelling from 278.2 to 318.2 K. Fluid Phase Equilibria 226, 333-344.

Vargas, F.M., Garcia-Bermudes, M., Boggara, M., Punnapala, S., Abutaqiya, M., Mathew, N., Prasad, S., Khaleel, A., Al Rashed, M., Al Asafen, H., 2014. On the development of an enhanced method to predict asphaltene precipitation, Offshore Technology Conference. OnePetro.

Vargas, F.M., Gonzalez, D.L., Hirasaki, G.J., Chapman, W.G., 2009. Modeling asphaltene phase behavior in crude oil systems using the perturbed chain form of the statistical associating fluid theory (PC-SAFT) equation of state. Energy & Fuels 23, 1140-1146.

Victorov, A.I., Firoozabadi, A., 1996. Thermodynamic micellizatin model of asphaltene precipitation from petroleum fluids. AIChE Journal 42, 1753-1764.

Waals, V.d., 1873. On the continuity of the gaseous and liquid states. Universiteit Leiden.

Wang, J., Buckley, J., 2001. A two-component solubility model of the onset of asphaltene flocculation in crude oils. Energy & Fuels 15, 1004-1012.

Wang, J., Buckley, J., Burke, N., Creek, J., 2004a. A practical method for anticipating asphaltene problems. SPE Production & Facilities 19, 152-160.

Wang, J., Buckley, J., Burke, N., Creek, J., 2004b. A practical method for anticipating asphaltene problems (includes associated papers 104235 and 105396). SPE Production & Facilities 19, 152-160.

Wang, Y., Orr Jr, F.M., 1997. Analytical calculation of minimum miscibility pressure. Fluid Phase Equilibria 139, 101-124.

Whitson, C.H., 1983. Characterizing hydrocarbon plus fractions. SPE Journal 23, 683-694.

Whitson, C.H., Michelsen, M.L., 1989. The negative flash. Fluid Phase Equilibria 53, 51-71.

Wilson, G., 1968. A modified redlich-kwong eos, application to general physical data calculations, paper no. 15c, AIChE 65th National Meeting.

Won, K., 1986. Thermodynamics for solid solution-liquid-vapor equilibria: wax phase formation from heavy hydrocarbon mixtures. Fluid Phase Equilibria 30, 265-279.

Wong, D.S.H., Sandler, S.I., 1992. A theoretically correct mixing rule for cubic equations of state. AIChE Journal 38, 671-680.

Wu, J., Prausnitz, J.M., Firoozabadi, A., 1998. Molecular-thermodynamic framework for asphaltene-oil equilibria. AIChE Journal 44, 1188-1199.

Xu, L., Li, H., 2021. A modified multiple-mixing-cell method with sub-cells for MMP determinations. Energies 14, 7846.

Xu, Z., Okuno, R., 2015. Numerical simulation of three-hydrocarbon-phase flow with robust phase identification, SPE Reservoir Simulation Symposium. OnePetro.

Xue, G., Datta-Gupta, A., Valko, P., Blasingame, T., 1997. Optimal transformations for multiple regression: application to permeability estimation from well logs. SPE Formation Evaluation 12, 85-94.

Yan, W., Michael, L.M., Erling, H.S., 2011a. On application of non-cubic EoS to compositional reservoir simulation, SPE EUROPEC/EAGE Annual Conference and Exhibition. OnePetro.

Yarranton, H.W., Masliyah, J.H., 1996. Molar mass distribution and solubility modeling of asphaltenes. AIChE Journal 42, 3533-3543.

Yasunishi, A., Tsuji, M., Sada, E., 1979. Solubility of carbon dioxide in aqueous mixed-salt solutions. ACS Publications.

Yeheng, S., Guangzhong, L., Yanfang, W., 2006. A method of state equation for determining minimum miscible pressure of CO_2. Petroleum Geology and Recovery Efficiency.

Yellig, W., Metcalfe, R., 1980. Determination and prediction of CO_2 minimum miscibility pressures (includes associated paper 8876). Journal of Petroleum Technology 32, 160-168.

Yuan, H., Johns, R.T., 2005. Simplified method for calculation of minimum miscibility pressure or enrichment. SPE Journal 10, 416-425.

Zanganeh, P., Dashti, H., Ayatollahi, S., 2015. Visual investigation and modeling of asphaltene precipitation and deposition during CO_2 miscible injection into oil reservoirs. Fuel 160, 132-139.

Zendehboudi, S., Khan, A., Carlisle, S., Leonenko, Y., 2011. Ex situ dissolution of CO_2: A new engineering methodology based on mass-transfer perspective for enhancement of CO_2 sequestration. Energy & Fuels 25, 3323-3333.

Zhang, L., Chen, P., Pan, S., Liu, F., Pauchard, V., Pomerantz, A.E., Banerjee, S., Yao, N., Mullins, O.C., 2021. Structure-dynamic function relations of asphaltenes. Energy & Fuels 35, 13610-13632.

Zhao, H., Dilmore, R.M., Lvov, S.N., 2015a. Experimental studies and modeling of CO_2 solubility in high temperature aqueous $CaCl_2$, $MgCl_2$, Na_2SO_4, and KCl solutions. AIChE Journal 61, 2286-2297.

Zhao, H., Fedkin, M.V., Dilmore, R.M., Lvov, S.N., 2015b. Carbon dioxide solubility in aqueous solutions of sodium chloride at geological conditions: Experimental results

at 323.15, 373.15, and 423.15 K and 150 bar and modeling up to 573.15 K and 2000 bar. Geochimica et Cosmochimica Acta 149, 165-189.

Zhao, H., Lvov, S.N., 2016. Phase behavior of the CO_2-H_2O system at temperatures of 273-623 K and pressures of 0.1-200 MPa using Peng-Robinson-Stryjek-Vera equation of state with a modified Wong-Sandler mixing rule: an extension to the CO_2-CH_4-H_2O system. Fluid Phase Equilibria 417, 96-108.

Zuo, J.Y., Elshahawi, H., Mullins, O.C., Dong, C., Zhang, D., Jia, N., Zhao, H., 2012. Asphaltene gradients and tar mat formation in reservoirs under active gas charging. Fluid Phase Equilibria 315, 91-98.

Zuo, J.Y., Mullins, O.C., Freed, D., Elshahawi, H., Dong, C., Seifert, D.J., 2013. Advances in the Flory-Huggins-Zuo equation of state for asphaltene gradients and formation evaluation. Energy & Fuels 27, 1722-1735.

Zuo, Y. X., Chu, J. Z., Ke, S. L., Guo, T. M., 1993. A study on the minimum miscibility pressure for miscible flooding systems. Journal of Petroleum Science and Engineering 8, 315-328.